POST-TRANSLATIONAL MODIFICATION OF CHEMOKINES: IMPLICATIONS FOR THEIR BIOLOGICAL FUNCTION

SARAH THOMPSON

A thesis submitted in partial fulfilment of the requirements for the degree of Doctor of Philosophy

Institute of Cellular Medicine, Newcastle University, UK

September 2018

ABSTRACT

Chemokines mediate a targeted immune response by orchestrating the migration of leukocytes to sites of injury. CXCL8 is a neutrophil-recruiting chemokine implicated in the pathology of many diseases. Ischaemia-reperfusion Injury (IRI) induces oxidative stress, and the reactive nitrogen species (RNS) peroxynitrite ($ONOO^-$). Our group has shown that post-translational nitration of chemokines by peroxynitrite can affect function and detectability. These modified chemokines (if non-functional) could pose a natural mechanism for the regulation of inflammation.

I have shown that nitration of CXCL8 by peroxynitrite reduces its ability to induce neutrophil migration in chemotaxis assays *in vitro* and murine intraperitoneal chemotaxis assays *in vivo*, through inhibition of both G-protein coupled receptor (GPCR) signalling and glycosaminoglycan (GAG) binding. I have used N-loop mutant and nitrated mutant versions of CXCL8 (Y13F) and CXCL1 (L15Y) to assess the importance of tyrosine residues in nitration. In both cases nitration impairs chemokine function.

In collaboration with Bio-Rad, I have developed a novel antibody which has shown specificity for nitrated CXCL8 over wild type CXCL8 in initial validation studies, and a detection limit of 1-10ng/ml. This antibody has facilitated the detection of naturally occurring nitrated CXCL8 in a bronchoalveolar lavage sample from a pneumonia patient. Pending further optimisation, this antibody could be incorporated into an ELISA assay to measure nitrated CXCL8 in biological fluids.

I have demonstrated that CXCL8 and 3-nitrotyrosine (a marker of $ONOO^-$ activity) production can be differentially upregulated in response to different stressing agents in breast cancer and cardiovascular cell lines *in vitro*. This indicates that the potential for CXCL8 to be nitrated naturally is likely to vary between health and disease states, and also between specific tissues and types of stress.

Characterising the expression and function of wild type and nitrated chemokines could lead to the development of techniques measuring these molecules as biomarkers to indicate the severity of IRI, or their use as anti-inflammatory therapies.

CONTENTS

LIST OF FIGURES

LIST OF ABBREVIATIONS

Aa	Amino acids
ACKR	Atypical chemokine receptor
APS	Ammonium persulfate
AP-1	Activator protein 1
ATP	Adenosine triphosphate
BAL	Bronchoalveolar lavage
BSA	Bovine serum albumin
CMC	Carboxymethyl cellulose
DC	Dendritic cell
DNA	Deoxyribonucleic acid
ECM	Extracellular matrix
eNOS	Endothelial nitric oxide synthase
ER	Endoplasmic reticulum
ER+/-	Oestrogen receptor positive/negative
FAK	Focal adhesion kinase
FBS	Foetal bovine serum
fMLP	N-Formyl-Methionyl-Leucyl-Phenylalanine
GAGs	Glycosaminoglycans
Gal	Galactose
GalNac	N-acetylgalactosamine
GAPDH	Glyceraldehy 3 phosphate dehydrogenase
GlucA	D-glucuronic acid
GlucNac	N-acetylglucosamine
GPCRs	G-protein coupled receptors
GPX	Glutathione peroxidase
GTPase	Guanosine triphosphatase
HBSS	Hanks' balanced salt solution
HER2	Human epidermal growth factor receptor 2
HIF-1	Hypoxia-inducible factors
H_2O_2	Hydrogen peroxide

HClO	Hypochlorous acid
HPLC	High performance liquid chromatography
HRP	Horseradish peroxidase
HSP90	Heat shock protein 90
IdurA	Iduronic acid
ILC	Innate lymphoid cell
IP_3	Inositol 1, 4, 5-triphosphate
iNOS	Inducible nitric oxide synthase
IRI	Ischaemia-reperfusion injury
LPS	Lipopolysaccharide
MDSC	Myeloid-derived suppressor cells
MALDI-TOF	Matrix-associated laser desorption/ionisation time-of-flight
MAPK	Mitogen-activated protein kinase
MI	Myocardial infarction
MMP	Matrix metalloproteinase
MPO	Myeloperoxidase
mPTP	Mitochondrial permeability transition pore
MS	Mass spectrometry
NET	Neutrophil extracellular trap
NADPH	Nictotinamide adenine dinucleotide phosphate oxidase
NFκB	Nuclear factor κB
nNOS	Neural nitric oxide synthase
NOS	Nitric oxide synthase
N_2O_3	Nitrous anhydride
NK	Natural killer cell
NO	Nitric oxide
OCl^-	Hypochlorite
OD	Optical density
OH^-	Hydroxyl anion
$ONOO^-$	Peroxynitrite
O_2^-	Superoxide anion

PAD	Peptidylarginine deaminase
PARP	Poly (ADP-ribose) polymerase
PBS	Phosphate buffered saline
PCR	Polymerase chain reaction
PI3K	Phosphoinositide 3-kinase
PKC	Protein kinase C
PMN	Polymorphonuclear leukocyte
PMS	Phenazine methosulfate
PP2A	Protein phosphatase type 2A
PR+/-	Progesterone receptor postivie/negative
PSGL-1	P-selection glycoprotein ligand-1
RF	Radio frequency
RNS	Reactive nitrogen species
ROS	Reactive oxygen species
RU	Resonance units
SFM	Serum-free media
SLE	Systemic lupus erythematosus
SOD	Superoxide dismutase
SPR	Surface plasmon resonance
STAT3	Signal transducer and activator of transcription 3
TEMED	Tetramethylethylenediamine
TFA	Trifluoroacetic acid
Tfh	T follicular helper cell
Th	T helper cell
TLR	Toll-like receptor
Treg	Regulatory T cell
TSG-6	TNF-stimulated gene/protein-6
TTR	Transthyretin
VAD	Ventricular assist device
VAP	Ventillator-associated pneumonia

XOD	Xanthine oxidase
XTT	Tetrazolium salt
Xyl	Xylose
3NT	3-nitrotyrosine

ACKNOWLEDGEMENTS

Firstly, I would like to thank the British Heart Foundation charity and all its donors for my funding, without their support my research would not have been possible.

I would like to sincerely thank my supervisors Professor Simi Ali, Professor Neil Sheerin and Professor John Kirby for their guidance and advice throughout my studies.

My greatest thanks go out to all the members of the Applied Immunobiology and Transplantation group, who have all offered me support (moral as well as scientific!), through the trying times of this project. Special thanks to Katie Cooke for her technical assistance, but also for always keeping my spirits up.

I am also grateful to all the core facility staff at Newcastle University, particularly those in Flow Cytometry, BioImaging and the Comparative Biology Centre for their technical knowledge and expertise.

Special thanks are due to Professor Krishna Rajarathnam and his group in the University of Texas Medical Branch for their extensive knowledge on CXCL8 and provision of nitrated CXCL8. I would like to express my gratitude to Professor Paul Proost and the Laboratory of Molecular Immunology for making me feel so welcome and supported during my research visit to their laboratory in Leuven, Belgium. Their expertise in mass spectrometry and proteomics was invaluable.

Finally I would like to thank my family and Christopher for their continual support, encouragement and belief in me throughout everything I have done to date, and this project in particular.

1 INTRODUCTION

1.1 BACKGROUND TO THIS STUDY

Chemokines regulate states of health and disease by orchestrating the migration of leukocytes to sites of inflammation or injury. This study looks at how chemokine function is regulated, focusing on post-translational nitration of the chemokine CXCL8 in particular.

1.2 CHEMOKINES

Chemokines are small positively charged chemoattractant cytokines that have developed as part of the immune system to direct the migration of leukocytes towards areas of inflammation or damage. Leukocytes will migrate along a chemokine gradient from areas of low chemokine concentration to areas of high chemokine concentration. This gradient is achieved by the dynamic immobilisation of chemokines on glycosaminoglycans (GAGs) present on the surfaces of cells and within the extracellular matrix. Chemokines interact with leukocytes through binding to their G-protein coupled receptors (GPCRs). Chemokines can be grouped into four major subfamilies depending upon the location and arrangement of the N-terminal cysteine residues; C, CC, CXC and CX_3C. The chemokine system is complex, with multiple chemokines binding the same receptor and the multiple receptors being activated by the same chemokine. The system is non-redundant, however, partly due to its complex regulation.

1.2.1 Chemokine Structure

Most chemokines share a common basic structure with some variations. Shown in Figure 1-1 is the basic structure with four cysteines, although it is worth noting that some chemokines have two or six cysteines. The first and third cysteines form a disulphide bridge, as do the second and fourth, and is it these disulphide bonds that give the chemokines a globular 3D shape, and arrange the N-terminus as a loop, the centre as 3 anti-parallel β-sheets, and the C-terminus as an α-helix [1].

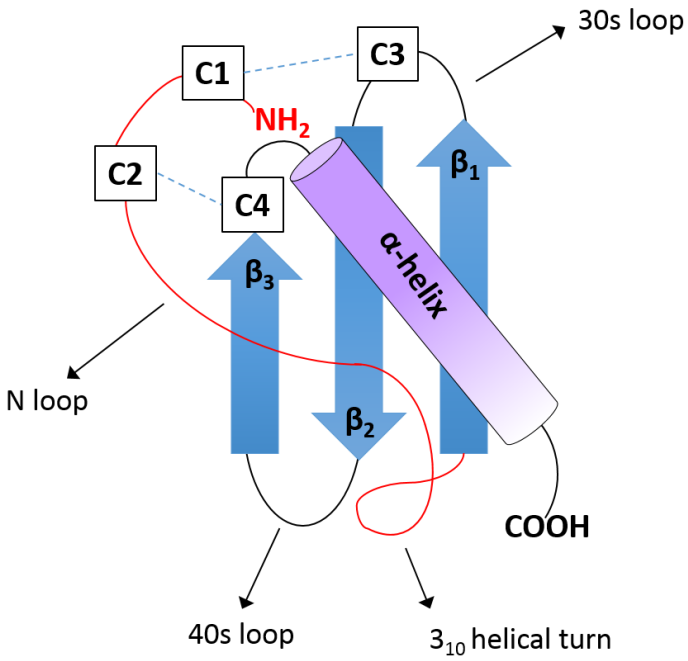

Figure 1-1. Diagrammatic representation of the structure of a typical chemokine. A flexible N-terminus is connected by the N loop to 3 anti-parallel β-sheets in the centre of the molecule, which ends in an α-helix in the C-terminus. This structure is achieved by the formation of disulphide bonds between cysteine1 – cysteine3 and cysteine2 – cysteine4.

1.2.2 G-protein Coupled Receptor Signalling

Chemokines mediate their effects through binding to GPCRs present on the surfaces of leukocytes. These receptors all share a similar fold structure: an extra-cellular N-terminal domain, seven transmembrane-spanning segments, three extracellular loops, three cytoloops, and a C-terminal segment, as shown in Figure 1-2. Disulphide bonds form between two cysteine residues in extracellular loops 1 and 2, and between cysteine residues in the N-terminal domain and exoloop 3. The α-helix and β-strands function as a scaffold, and could be exchanged between different chemokines without impairing function [2]. Receptor binding occurs between the chemokine N-loop and receptor N-domain residues, and between the chemokine N-terminal and receptor extracellular loop residues [2]. The receptors are classified as C, CC and CXC as the chemokines are, but with the "L" for ligand replaced by "R" for receptor.

The chemokine system is complex, and although some receptor-ligand interactions are specific, such as CCL20-CCR6, often multiple chemokines bind the same receptor (CCL3/4/5/7/8 all bind CCR1) and one chemokine can bind multiple receptors (CCL7 can bind CCR1/2/3/5) as shown below in Table 1. Despite this promiscuity, the system is non-redundant, although its complexity and ability to compensate could be the reason

that many therapeutics designed to target a single chemokine or receptor have largely been unsuccessful.

Binding of chemokine ligands to their receptors leads to a signalling cascade involving $G\alpha_{i/o}$, $G\alpha_s$, $G\alpha_{q/11}$ or $G\alpha_{12/13}$, which ultimately leads to calcium flux and cell migration (chemotaxis) [3]. Chemokines can also signal through other pathways involving β-arrestin (though this is dependent on the ligand and cell type involved) [4]. Chemokine-GPCR signalling can be involved in many homeostatic processes. For example, B and T cell migration to, and organisation within, the lymphoid organs during maturation in the case of CCL25-CCR9 and CCL19/CCl21-CCR7 signalling [5,6]. CXCL12-CXCR4 signalling mediates the migration of haematopoietic precursor cells to the bone marrow during embryogenesis, as well as the development of organs such as the heart and brain in mice [7,8]. Chemokines can also regulate angiogenesis, both physiological ad pathological, as occurs during chronic inflammation. CXCL1/5/8/12, CCL1/2/11 and CXC3CL1 are pro-angiogenic *in vitro*, whereas CXCL4/9/10, and CCL21 are anti-angiogenic *in vitro* [6].

In addition to homeostatic roles and as mentioned previously, chemokines also mediate inflammation by signalling through GPCRs to recruit leukocytes to sites of injury or insult in a range of diseases. Increased levels of CX3CL1-CX3CR1and CCL1-CCR8 signaling have been implicated in the pathology of atopic dermatitis [9]. CXCR4 and CCR5 are known co-receptors that, along with CD4, facilitate infection by the HIV virus in humans [10]. CXCL4/9/10/11 signaling promotes tumour invasiveness in CXCR3-expressing cells in prostate cancer, lymphoma and leukaemia, and this signalling system has also been linked to inflammatory arthritis, diabetes, organ transplant rejection and systemic sclerosis [11]. Alterations to receptor-ligand interactions can also alter normal signalling and cause disease, for example mutations in CXCR4 lead to neutrophil retention in the bone marrow causing WHIM syndrome [12], and a polymorphism in the CX3CR1 gene has been linked to atherosclerosis [13].

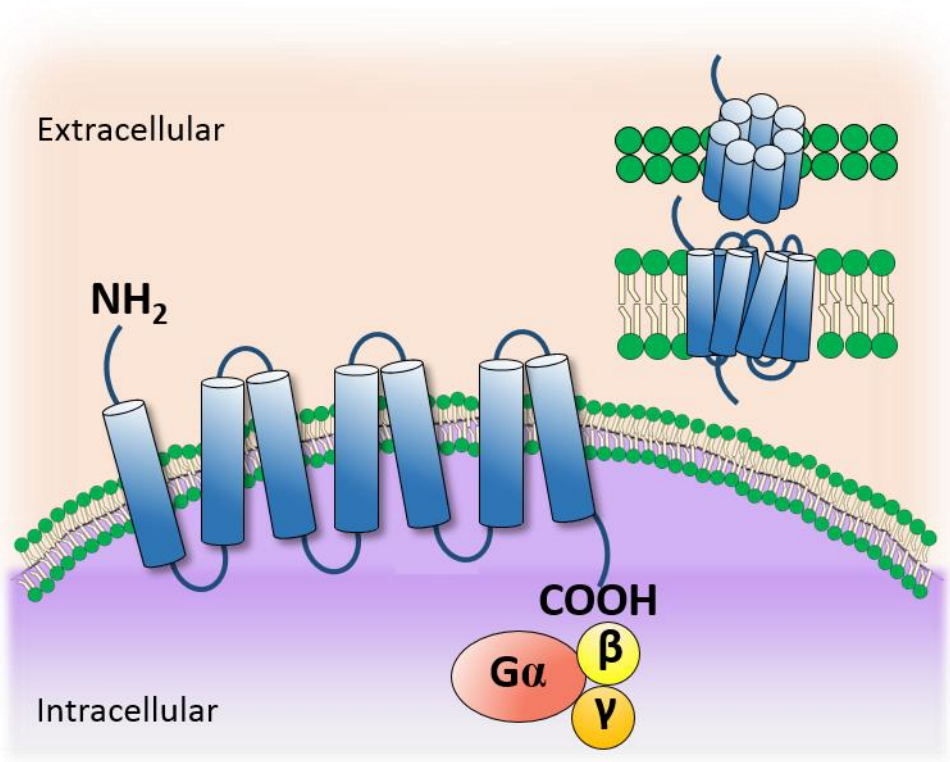

Figure 1-2. Diagrammatic representation of the structure of a typical chemokine receptor. Shown are the 7 trans-membrane spanning loops of the receptor, its orientation within the cell membrane, and association with a G-protein through which it signals.

1.2.3 Atypical Chemokine Receptors

As well as their typical GPCRs, chemokines can also bind atypical chemokine receptors 1-4 (ACKRs 1-4) [14]. As shown Table 1, the same variations in ligand-receptor binding specificity apply to ACKRs as they do to GPCRs, for example, ACKR2 can bind to 12 different CC chemokines. Chemokine binding affinity for ACKRs also varies, for example, CXCL12 has a stronger affinity for ACKR3 than for its typical GPCR CXCR4 [15].

Upon ligand binding, these receptors do not induce downstream signalling due to their inability to couple to G-proteins, but instead act as chemokine scavengers and are thought to modulate the immune response [16,17]. Indeed, ACKR1 expressed on the surface of erythrocytes is thought to act as a "buffer" of inflammatory chemokines in the circulation, preventing large fluctuations in free chemokine concentration. If chemokines are cleared from the blood by other methods ACKR1-bound chemokines can be released back into the circulation to compensate for this, and if there are high chemokine concentrations in the circulation, then scavenging of these chemokines by ACKR1 will ensure that excessive circulating chemokine concentrations do not result in leukocyte desensitisation and chemokine receptor downregulation [15,18]. ACKR-mediated

activation of the β-arrestin pathway can lead to chemokine-receptor complex internalisation and dissociation within endosomes, followed by intracellular degradation of the chemokines in lysosomes [15]. The ACKR can then be translocated back to the cell surface to scavenge more chemokine ligand. In the case of polarised cells, binding to ACKR1 (but not ACKR2 or ACKR3) can also lead to the transport of chemokines to the opposite side of the cell monolayer [15,17].

ACKRs can form homodimers and heterodimers to mediate their own biological function, as well as that of typical chemokine receptors. For example, ACKR3 homodimers can heterodimerise with CXCR4, which modulates the signalling of CXCL12 through it [19].

ACKRs play many roles in physiological processes, such as blood clotting in mice [20], in parasitic infections such as malaria where ACKR1 acts as a cell entry factor for the parasite *Plasmodium vivax* [21], and in diseases like cancer where ACKR2 is reported to have anti-tumour functions [22] and ACKR3 is reported to promote tumour survival and metastasis [15]. This broad range of functions can be carried out through binding to chemokines as well as other molecules, and ACKRs are clearly key regulators of chemokine biology.

Family & Name	Other Names	Typical Receptors	Atypical Receptors	Main Immune function
C				
XCL1	SCM-1α, Lymphotactin A	XCR1		Cross-presentation by CD8+ DCs
XCL2	SCM-1β, Lymphotactin B	XCR1		
CC				
CCL1	1-309	CCR8/11	ACKR1	Th2 cell and Treg cell trafficking
CCL2	MCP-1	CCR2/4	ACKR1/2	Inflammatory monocyte trafficking
CCL3	MIP-1α	CCR1/4/5	ACKR2	Macrophage and NK cell migration, T cell-DC interations
CCL4	MIP-1β	CCR1/5/8	ACKR2	
CCL5	RANTES	CCR1/3/4/5	ACKR1/2	
CCL7	MCP-3	CCR1/2/3/4	ACKR1/2	Monocyte mobilisation
CCL8	MCP-2	CCR1/2/3/5/11	ACKR2	Th2 response
CCL9/10	MIP-1γ	CCR1		Mediates hepatobiliary excretion
CCL11	Eotaxin	CCR3	ACKR1/2	Eosinophil and basophil migration
CCL12	MCP-5	CCR2		Monocyte/macrophage chemoattractant
CCL13	MCP-4	CCR1/2/3/11	ACKR1/2	Th2 response
CCL14	HCC-1	CCR1	ACKR1/2	
CCL15	HCC-2	CCR1/3		
CCL16	HCC4-LEC	CCR1		
CCL17	TARC	CCR4	ACKR1/2	Th2 responses, Th2 cell migration, Treg cell homing, homing to the lungs and skin
CCL18	PARC, DCCK1	Unknown		Th2 responses, AAM marker, homing to the skin

CCL19	ELC, Exodus-3, MIP-3β	CCR7	ACKR4	T cell and DC homing to lymph nodes
CCL20	LARC, Exodus-1, MIP-3α	CCR6		Th17 responses, B cell and DC homing to gut-associated lymphoid tissue
CCL21	SLC, 6Ckine, Exodus-6	CCR7	ACKR4	T cell and DC homing to lymph nodes
CCL22	MDC	CCR4	ACKR2	Th2 response, Th2 and Treg cell migration
CCL23	MPIF-1, Ckβ8	CCR1		
CCL24	Eotaxin-2, MPFIF-2, Ckβ6	CCR3		Eosinophil and basophil migration
CCL25	TECK	CCR9	ACKR4	T cell homing to gut, thymocyte migration
CCL26	Eotaxin-3, MIP-4α	CCR3		Eosinophil and basophil migration
CCL27	CTAC, ILC	CCR2/3/10		T cell homing to skin
CCL28	MEC	CCR3/10		T cell and IgA plasma cell homing to skin
CXC				
CXCL1	Gro-α	CXCR1/2	ACKR1	Neutrophil trafficking
CXCL2	Gro-β, MIP-2α	CXCR2	ACKR1	
CXCL3	Gro-γ, MIP-2β	CXCR2	ACKR1	
CXCL4	PF-4	CXCR3		Pro-coagulant
CXCL5	ENA-78	CXCR2	ACKR1	Neutrophil trafficking
CXCL6	GCP-2	CXCR1/2	ACKR1	
CXCL7	NAP-2	CXCR2		
CXCL8	Interleukin 8, NAP-1	CXCR1/2	ACKR1	
CXCL9	MIG	CXCR3		Th1 and CD8 T cell trafficking, NK cell trafficking
CXCL10	IP10	CXCR3		
CXCL11	I-TAC	CXCR3	ACKR1/3	
CXCL12	SDF-1	CXCR4	ACKR3	Bone marrow homing

CXCL13	BCA-1	CXCR5		B cell and Tfh cell positioning
CXCL14	BRAK, Bolekine	Unknown		Macrophage homing to the skin
CXCL15	Lungkine	Unknown		Neutrophil recruitment to the lung
CXCL16	SRPSOX	CXCR6		NK Cell and ILC migration and survival
CXCL17	DMC, VCC1	CXCR8		Monocyte/dendritic cell chemoattractant
CX_3C				
CX3CL1	Fractalkine, Neurotaxin	CX3CR1		NK cell, monocyte and T cell migration

Table 1-1. Members of the chemokine families, their receptors and primary functions within the immune system. This list was adapted from Griffith, Sokol and Luster (2014) [23] and other sources [24-26]. Abbreviations: DC = dendritic cell, ILC = innate lymphoid cell, NK = natural killer cell, Tfh = T follicular helper cell, Th = T helper cell, Treg = regulatory T cell.

1.2.4 Glycosaminoglycan Binding

GAGs are linear polysaccharides (consisting of repeating disaccharides that can range in length from one unit to over a hundred units), the majority of which are bound to a core protein through covalent interactions, therefore forming a glycoprotein [27]. N-linked glycosylation accompanies protein synthesis in the endoplasmic reticulum and refers to glycoproteins where the interaction between the sugar residues and the core protein occurs at the amide nitrogen group within asparagine. O-linked glycosylation occurs through the step-wise addition of sugar residues to the core protein post-translationally, where the interactions occur at the oxygen on serine/threonine side chains [28,29]. GAGs can be classified into five groups; heparin/heparan sulphate, chondroitin sulphate, dermatan sulphate, keratin sulphate and hyaluronic acid, the latter being a non-sulphated GAG which forms non-covalent attachments to proteins [30]. The structures of these GAGs are shown below in Figure 1-3. The highly acidic and negatively charged O-linked GAGs such as chondroitin sulphate, dermatan sulphate, heparin or heparan sulphate bind to basic residues in chemokines (usually lysine, arginine and histidine, which can be arranged in the form of a BBXB or (B)BXX(X/B)BXXB(B) motif) through electrostatic and hydrogen bonds [29,31,32]..

GAGs such as heparan sulphate are present on the surface of endothelial cells and within the extracellular matrix (ECM), where they bind and immobilise chemokines dynamically. It is thought that transient binding of chemokines between GAGs and GPCRs creates an equilibrium of free/GAG bound/GPCR bound chemokine monomers/dimers localised to the site of injury [27,33,34]. This state of equilibrium is highest in concentration at the site of injury, and becomes more diffuse further away, thereby creating a "trail of breadcrumbs" effect to direct leukocyte migration [35,36]. Immobilisation of chemokines on GAGs also assists their presentation to leukocytes in tissues [37,38], and prevents their degradation [39,40]. The interactions between chemokines, GAGs and chemokine receptors are shown diagrammatically in Figure1-4, using a neutrophil, CXCL8 and CXCR1/CXCR2 as a simplified example system.

GAG binding has been shown to be essential for chemotactic function *in vivo*, as chemokine mutants with a retained ability to bind GPCRs, but an impaired ability to bind GAGs were unable to induce leukocyte migration [32]. GAG heterogeneity is an important contributing factor to the fine-tuning and regulation of chemokine functionality, as the exact composition of GAGs and thus selective affinity for certain chemokines depends on cell type and location [41]. This heterogeneity occurs at many levels, from differences in GAGs expressed by different tissues (and the ability of cells to modulate their GAG expression in response to stimuli), amounts of soluble versus matrix-bound GAGs within the vicinity, the polysaccharide chain lengths of these GAGs, and their varying patterns of sulphation all contribute to chemokine binding specificity [27,29,36,42,43]. Generally, however, longer GAGs have higher affinity for chemokines (due to their length enabling them to interact with multiple GAG-binding epitopes present within chemokine oligomers), and as most chemokines are basic they tend to have higher affinities for GAGs with high sulphate content such as heparan sulphate, although the distribution of sulphate groups also affects affinity [27].

CXCL4/11 and CCL5/21 have high affinities for GAGs, while CCL2 and CXCL8 have intermediate affinity and CCL3/4 have low affinity. Different chemokine oligomers have varying affinities for GAGs [44], and GAG binding is known to stabilize chemokine oligomers, therefore oligomerisation and GAG-binding are described as mutually re-enforcing processes[27]. CXCL11, CXCL12, CCL2 and CCL5 all showed a decreased binding affinity for 2-O-desulphated heparin in comparison to wild type heparin, but CXCL4 showed equal affinity for both [44]. Naturally, the interactions between free and bound

chemokine monomers/dimers/oligomers with soluble and immobilised GAGs will in turn affect the ability of the chemokines within this localised area to interact with their respective GPCRs in what is a greatly complex and dynamic situation.

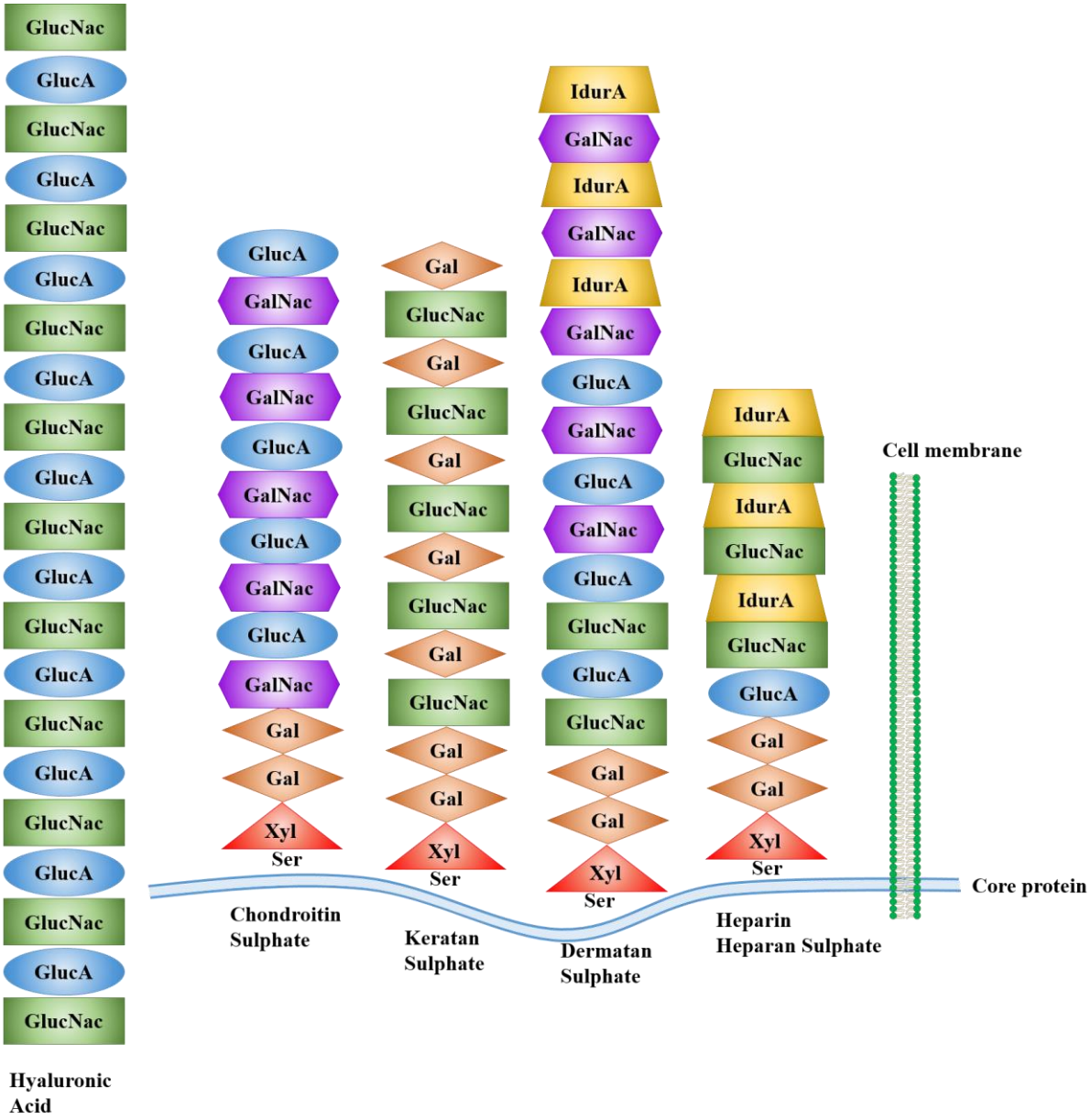

Figure 1-3. The structures of glycosaminoglycans (GAGs). Heparin/heparan sulphate, dermatan sulphate, keratin sulphate and chondroitin sulphate are connected to a transmembrane protein within the extracellular matrix (ECM) by a serine residue (O-linked GAGs are shown as examples). Hyaluronic acid is not linked to a protein core. Abbreviations: Xyl = xylose, Gal = galactose, GlucA = D-glucuronic acid, GlucNac = N-acetylglucosamine, GalNac = N-acetylgalactosamine, IdurA = iduronic acid. This figure was adapted from [45].

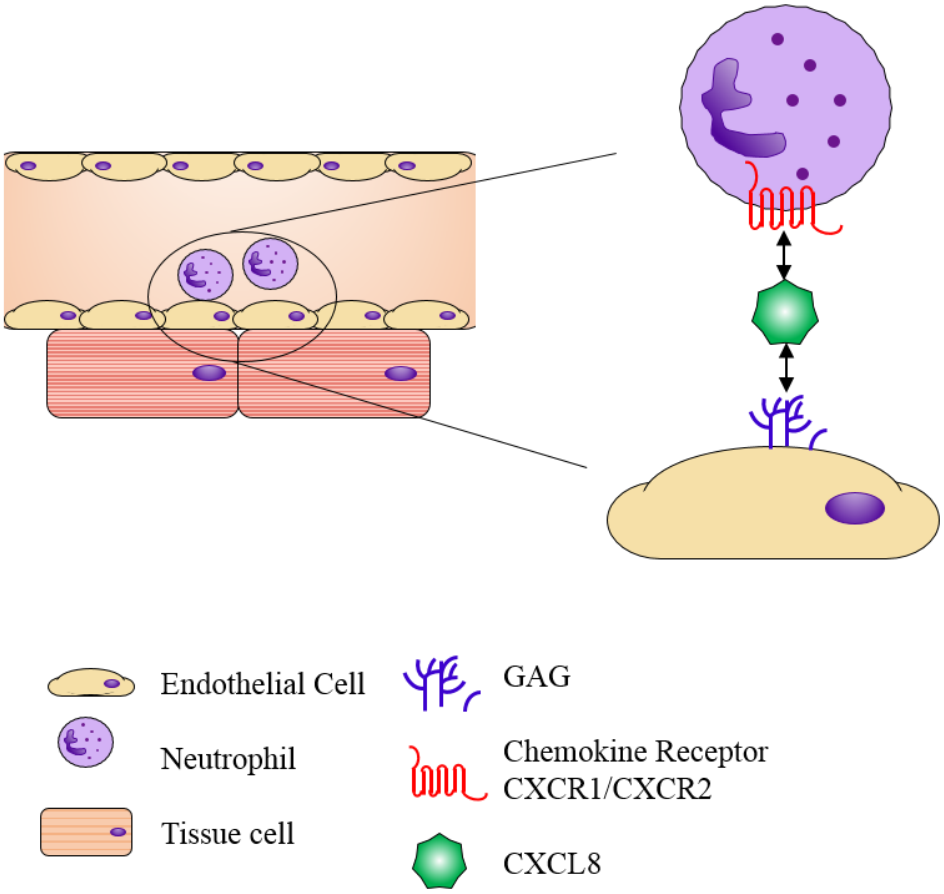

Figure 1-4. Chemokine function is mediated through glycosaminoglycan (GAG) and G-protein coupled receptor (GPCR) binding. Diagrammatic representation of the dynamic interaction and on/off binding of chemokines with both GAGs present on endothelial cells (via the chemokine C-terminal region), and with the GPCR present on the leukocyte surface (via the chemokine N-terminal region).

1.2.5 Chemokine Multimerisation and Structural Function

Many chemokines exist as multimers both at high concentrations *in vitro* and during interactions with GAGs at sites of inflammation *in vivo* [32,46]. The affinity that a given chemokine has for its GPCR and for GAGs is largely affected by its oligomerisation state as mentioned previously, although it is generally accepted that all chemokines are active as monomers in terms of GPCR activation [47]. This has been demonstrated for CCL2/3/4/5 [48-50] and CXCL1/7/8/10 [51,5253]. In the case of CC chemokines, dimers are unable to bind to GPCRs due to essential GPCR-binding residues being located within the dimer interface (thus they are not accessible to the GPCR) [54], however dimerised CXC chemokines are still able to bind to their GPCRs, albeit with affinities different than those of their monomeric forms [46,55]. CXC-type dimers are globular in structure, and are formed by interactions between the β1 strands in the two monomers, whereas CC-type dimers are more elongated in nature, and are formed by interactions between the two short N-terminal β-strands in the two monomers [56].

Some chemokines primarily exist as monomers such as CCL7, whereas others form tetramers such as CXCL4, and polymers such as CCL5 [27]. CCL7 is still able to bind to GAGs with high affinity despite its inability to oligomerise, (CCL7 lacks a conserved proline residue necessary for the dimerization of CC chemokines), due to its high numbers of GAG-binding epitopes, in contrast to chemokines such as CCL2, which has fewer GAG-binding epitopes but readily oligomerises [27,57]. Oligomerisation-deficient CXCL4 and CCL5 mutants showed reduced binding to heparin and heparan sulphate in surface plasmon resonance experiments than their wild type counterparts, which where able to oligomerise upon the immobilised GAGs [44].

As well as forming homodomers and multimers, chemokines can also form heterodimers, as has been shown for CCL3-CCL4, CCL2-CCL8 [58], CXCL4-CXCL8 [59] and CXCL4-CCL5 *in vitro* and *in vivo* [60,61], and as with homodimerisation, heterodimerisation modulates the biological activity of chemokines. Interactions with GAGS have been shown to promote the formation of, and stabilise chemokine hetero-oligomerisation as well as homo-oligomerisation .[62,63]

Monomers, dimers and multimers exist in a dynamic equilibrium, although the relative amounts of these different structural forms depends upon the chemokine in question (some form strong and stable oligomers whereas others have weaker interactions and

exist as monomers/dimers), the tissue microenvironment i.e. GPCRs/GAGs present, as well as the chemical environment i.e. pH, ionic strength and buffer type [56].

In addition to chemokine multimerisation, GPCRs themselves can also multimerise both with other GPCRs and non-chemokine receptors, which also alters signalling. Homodimers have been detected in the cases of CCR2/5, CXCR1/2/4 and ACKR1, and heterodimers have been detected in the cases of CCR2-CCR5, CXCR1-CXCR2, CXCR4-CCR2, CXCR4-CXCR7, CXCR4-CCR5 and ACKR1-CCR5 [64]. Inflammation induces oligomerisation of CCR7, which facilitates an oligomer-specific Src kinase signalling pathway leading to enhances chemotaxis [65].

1.2.6 Regulation of Chemokine Function

Regulating the function of chemokines is essential in order to create adequate but not excessive inflammation after injury, to facilitate optimum healing. As eluded to above, this regulation is complex and involves many aspects of chemokine biology, including the actual production of chemokines (affected by epigenetic modifications), the concentration and therefore oligomeric state of the chemokine (i.e. monomers/dimers/oligomers (both hetero and homo), as this will affect chemokine affinity for GAG and GPCR binding), tissue microenvironment, length/composition/sulphation patterns of GAGs, and receptor signalling bias [30,66]. For example, CCL19 and CCL21 both signal through CCR7, but CCL19 is known to exist mainly as a soluble unbound monomer whereas CCL21 binds with high affinity to GAGs unless cleaved, but shows enhanced CCR7 signalling when heterodimerised with CXCL13 [44,56,67]. CCL3 and CCL5 are both ligands of CCR1 and CCR5, and homo-oligomerisation of both has been linked to GAG binding, however these chemokines differ in their affinities for GAGs, with CCL3 having a low and CCL5 having a high affinity [44,56,68]. In addition, and as mentioned above, CCL3 heterodimerises with CCL4, and CCL5 heterodimerises with CXCL4 [56]. Another novel aspect of chemokine biology that can regulate function is post-translational modification, such as nitration, citrullination, phosphorylation and glycosylation. This project will focus on post-translational nitration of CXCL8 as a model CXC chemokine.

1.3 POST-TRANSLATIONAL MODIFICATION OF CHEMOKINES

Post-translational modification is emerging as a critical aspect of chemokine biology in terms of regulating function. The modifications themselves, as well as their causes and subsequent effects on biological activity vary and must be studied on an individual basis. Post-translational modifications have been shown to affect chemokine function in terms of GAG and receptor binding abilities which in turn affects their ability to induce migration of leukocytes, as well as their detectability by antibodies raised against their wild type un-modified counterparts. This project will focus on nitration, although other types of post-translational modification are discussed briefly.

1.3.1 Truncation and Cleavage

Enzymatic modifications of chemokines can involve cleavage by a range of enzymes including matrix metalloproteinases (MMPs), CD26 and cathepsin G. The expression of MMPs is closely linked to inflammation, with MMP-8 being released by neutrophils, and MMP-12 by macrophages. These enzymes (and others) can cleave chemokines, as well as mediate tissue remodelling and ECM degradation [69].

In some cases, cleavage of chemokines by MMPs can enhance function, with the resulting molecule being more chemotactically active. This is the case for the cleavage of CXCL5 by MMP-8, and CXCL8 by MMP-1/MMP-8/MMP-9 [70-72]. In other cases however, cleavage can abrogate function, such as the N-terminal cleavage of CXCL8 by MMP-12 (due to disruption of the ELR motif which is essential for function), or the C-terminal cleavage of CXCL9/CXCL10 by MMP-8/MMP-9 (likely due to disrupted GAG binding/oligomerisation) [73,74]. Enzymatic cleavage of chemokines to reduce function is also used as a method of immune evasion by bacteria including *Streptococcus pyogenes*. The bacterial enzyme *Streptococcus pyogenes* cell envelope proteinase (*Spy*CEP) cleaves chemokines such as CXCL8 at the C-terminus, which prevents the chemokines from inducing neutrophil recruitment and thus allows the bacteria to disseminate [75].

1.3.2 Citrullination

Enzymes can also mediate single residue modifications such as the citrullination of arginine residues by peptidylarginine deaminase (PAD) enzymes [76]. Citrullination results in a 1Da increase in mass per residue affected, and in a loss of the basic charge of

the arginine residue, which is therefore likely to impact negatively on its ability to form hydrogen bonds and participate in ionic interactions. This in turn compromises chemokine structure and function. This is thought to be one reason that citrullination of all chemokines tested to date, including CXCL10, CXCL11, CXCL12 and CXCL8 [76-78], reduces chemotactic ability and could therefore be described as an "anti-inflammatory" post-translational modification.

1.4 POST-TRANSLATIONAL NITRATION BY PEROXYNITRITE

The reactive species peroxynitrite ($ONOO^-$) is produced from the spontaneous reaction of nitric oxide (NO) and the superoxide anion (O_2^-), which will be discussed later in more detail. Peroxynitrite has a very short half-life of around 10ms at physiological pH, during which it will modify any proteins within a 20μm range of its production [79]. Peroxynitrite has been shown to nitrate both free and protein-bound tyrosine residues to form 3-nitrotyrosine (3NT), alter tryptophan via oxidation, nitration and nitrosation at many positions on the core phenol ring, and oxidise thiol groups present in cysteine and methionine residues to form sulfoxide groups [80-82]. Peroxynitrite can also modify histidine to create a histidyl radical, and lysine to produce N6-(Carboxymethyl)lysine [83,84]. Some examples of these modifications are shown diagrammatically in Figure 1-5. 3NT has been shown to be a detectable footprint of nitrative stress and peroxynitrite activity (due to peroxynitrite itself having such a short half-life) [85], and has been documented in plasma samples from many human diseases [81].

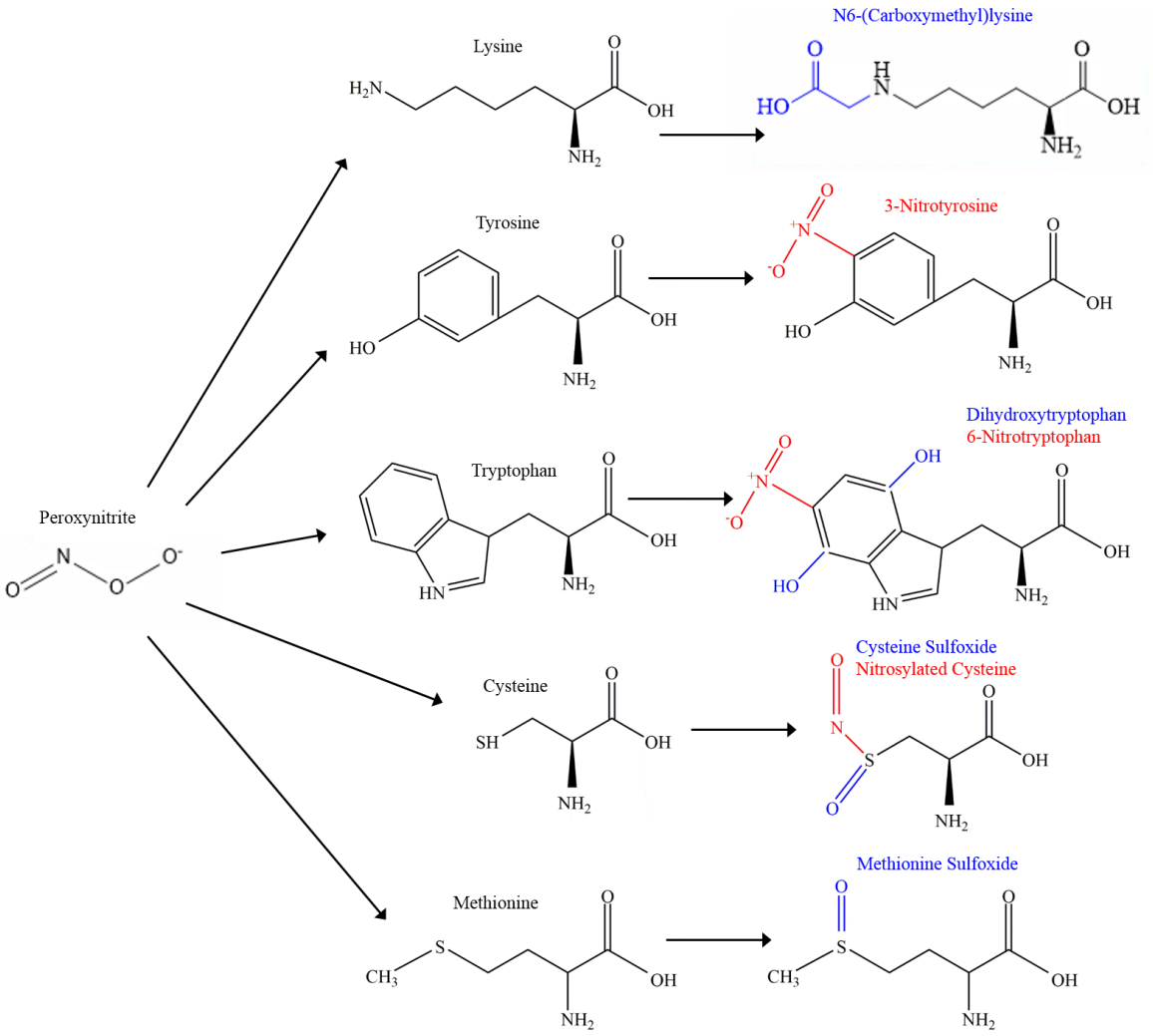

Figure 1-5. Peroxynitrite (ONOO-)-mediated modifications of amino acids. Peroxynitrite-mediated nitration (red) of tyrosine to form 3-nitrotyrosine, tryptophan to form (e.g.) 6-nitrotryptophan, and cysteine to form nitroslyated cysteine. Peroxynitrite-mediated oxidation (blue) on tryptophan to form dihydroxytryptophan, on thiol groups of methionine and cysteine to form sulfoxide groups which can then form disulphide bonds. Lysine can also be modified by peroxynitrite to form N(Carboxymethyl)lysine, and histidine can be converted to a histidyl radical (not shown).

1.4.1 Nitration, Ischaemia-Reperfusion Injury and Oxidative Stress

Organ transplantation is a model scenario in which to study the nitration of chemokines and other proteins, due to the ischaemia-reperfusion injury (IRI) which occurs when the donor organ is isolated from circulation and is then reperfused upon transplantation into the recipient. IRI is associated with delayed graft function and rejection in kidney transplantation [86] and graft dysfunction in liver, lung and heart transplantation [87-89]. IRI features in a number of other conditions including acute coronary syndrome/acute heart failure after cardiopulmonary bypass in the heart, acute kidney injury as a result of

vascular surgery, acute lung injury as a result of thoracic surgery, and stroke in the brain [86].

During the ischaemic phase of IRI, the shift from aerobic to anaerobic metabolism (due to a lack of oxygen), leads to the depletion of adenosine triphosphate (ATP) and calcium overload within cells, which in turn results in mitochondrial damage involving the opening of the mitochondrial permeability transition pore (mPTP) during reperfusion, the generation of reactive oxygen and nitrogen species (ROS and RNS respectively) [86,90,91], and ultimately cell death. The most common ROS/RNS are, non-radicals such as hypochlorous acid (HClO) and hydrogen peroxide (H_2O_2), and radicals (a molecule containing a spin-unpaired electron in the outer shell) including the superoxide anion, peroxynitrite and the hydroxyl anion ($OH^{\cdot}$) [92,93]. It is the imbalance between the formation and release of these reactive substances, and anti-oxidative mechanisms such as scavengers, which prevent excessive stress and damage [90,94,95], that causes the oxidative stress that is a key feature of IRI.

As reactive species themselves, the precursors of peroxynitrite; NO and O_2^-, are both known to be increased during oxidative stress and inflammation [96-98]. NO is produced by a range of enzymes, including endothelial NO synthase (eNOS), neural NO synthase (nNOS) and inducible NO synthase (iNOS), which are widely expressed by many cell types including endothelial cells and cardiomyocytes [99-101]. NO acts as a vasodilator and inhibitor of platelet aggregation and is therefore beneficial at low concentrations [102]. O_2^- is produced by many enzymes including nicotinamide adenine dinucleotide phosphate (NADPH) oxidase, which is present within the mitochondria of all cells, and xanthine oxidase (XOD), which is also widely expressed by polymorphonuclear cells, endothelial and epithelial cells [103]. It is also released during the neutrophil oxidative burst. Both NO and O_2^- can be detrimental if present in excess either as themselves, or through the formation of secondary molecules. NO itself can inhibit enzymes that have transition metal components or produce free radical intermediates as part of their catalytic cycles, such as cytochrome P450 [81]. NO can form nitrous anhydride, (N_2O_3) when autooxidised, which mediates DNA and protein damage [99,104]. Two superoxide molecules can undergo spontaneous dismutation to form H_2O_2 [105], and as aforementioned, NO and O_2^- can react together to produce peroxynitrite [81,106,107]. A simplified version of this complex pathway is shown diagrammatically below in Figure 1-6. Upregulation of XOD, NADPH and NOS enzymes occurs during IRI as, therefore, will the production of peroxynitrite [86].

Peroxynitrite elicits many damaging effects, including DNA strand breaks, lipid peroxidation and increasing MMP2 activity [108]. Peroxynitrite is also responsible for the activation of poly (ADP-ribose) polymerase (PARP) which alters metabolism and increases energy consumption, thereby depleting intracellular ATP stores leading to cell dysfunction and death [81,109,110]. In addition, peroxynitrite can inhibit natural anti-oxidative mechanisms such as the superoxide dismutase enzyme (SOD) and glutaredoxin, which leads to positive feedback loops of intracellular oxidant generation, and therefore exacerbation of injury [98,111]. Peroxynitrite has therefore unsurprisingly been implicated in the pathology of many diseases [112] as well as in organ transplantation. These include neutrophil –induced myocardial IRI [113], cardiac allograft rejection post-transplant [114], kidney diseases such as acute tubular necrosis [115], osteoarthritis [116], interstitial lung disease [117], type II diabetes mellitus and Fabry disease [118].

As production of both peroxynitrite and chemokines are upregulated during periods of oxidative stress, nitration of chemokines would therefore be more likely to occur during oxidative stress and inflammation.

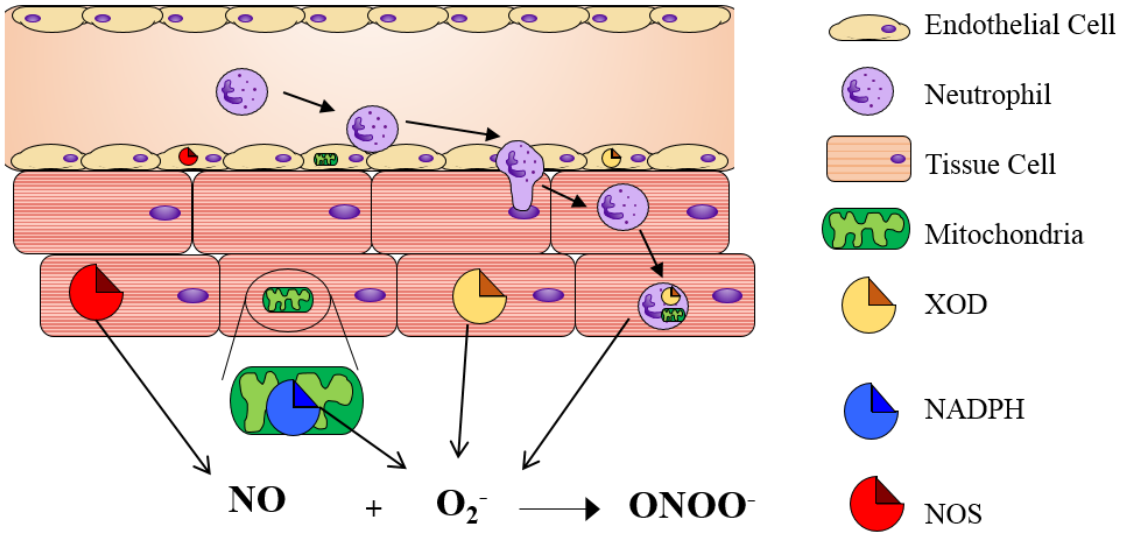

Figure 1-6. Diagrammatic representation of the formation of peroxynitrite (ONOO-). Shown are the sources and production of nitric oxide (NO) by nitric oxide synthase enzymes (NOS), the superoxide anion (O_2^-) by nicotinamide adenine dinucleotide phosphate oxidase (NADPH) /xanthine oxidase (XOD), and the reaction of the two to form peroxynitrite.

1.4.2 Functional Consequences of Chemokine Nitration

Nitration of chemokines is a non-silent modification, which affects biological function. Nitration of CCL2 and CCL5 by incubation with peroxynitrite has been shown to reduce their ability to induce monocyte and eosinophil chemotaxis respectively [119], whereas nitration of CCL2 by tumour-derived reactive nitrogen species (RNS) was shown to impair CD8+ T cell, but not myeloid cell, recruitment. This is thought to be due to nitration partially reducing the ability of CCL2 to bind to its GPCR CCR2, as this receptor is present at much lower concentrations on the surface of CD8+ T cells than on myeloid cells, which express far greater amounts [120]. Nitrated CCL2 has also been shown to have impaired binding to both heparin and heparan sulphate in comparison to wild type CCL2 [121], so the reduction in migratory capacity in this case is likely due to a combination of impaired GPCR and GAG binding. CXCL12 was unable to induce lymphocyte chemotaxis *in vitro* or *in vivo* when nitrated, despite the fact that this modification does not affect the ability of CXCL12 to bind GAGs. It was, however, found that while nitration does not inhibit the binding of CXCL12 to its GPCR CXCR4, it does prevent the chemokine from inducing downstream signalling once bound [122]. In the case of CXCL12 therefore, the inability to induce migration is a likely a result of nitration impairing GPCR activation solely. Incubation with peroxynitrite also impaired the ability of CCL3 to recruit neutrophils and monocytes [123] and of CCL11 to recruit eosinophils [124].

In some cases, as for CCL2 and CXCL12, nitration has also been shown to prevent the detection of chemokines by antibodies raised against their wild type un-modified counterparts. This is presumably due to epitope modification by the added NO_2 group(s), which prevents the antibody from recognising the modified chemokine [95,120]. This therefore limits the biological relevance of chemokines as biomarkers if only wild type chemokine is detectable in samples. The number of different modified versions of chemokines present within biological samples, and the ratios they are present in, could be a more accurate profile of the inflammatory situation, and could prove to be a more accurate indicator of health/disease than just measuring unmodified chemokines alone.

1.4.3 Functional Consequences of Protein Nitration

Any proteins present within the vicinity of peroxynitrite production (besides chemokines) are also susceptible to nitration. Nitration of tyrosine residues may alter protein signal transduction *in vivo* through interference with tyrosine phosphorylation,

which is an important aspect of many signalling cascades [125]. Nitration of proteins is thought to be the main cause of pathology in acute and chronic alcoholic fatty liver injury models, due to the nitration altering their functionality [126-128]. Nitration of Complex I (NADH ubiquinone oxidoreductase) and Complex V (ATP synthase) decreases protein function leading to decreased energy production, nitration of SOD1, SOD2, and glutathione peroxidase (GPX) decreases their antioxidant abilities [128]. Nitration of some liver proteins is also thought, but not confirmed, to contribute to pathology by increasing their functions, such as nitration of heat shock protein 90 (HSP90) leading to its conversion to a toxic product, and nitration of protein phosphatase type 2A (PP2A) leading to increased vascular permeability [128]. Nitration of glutathione *S*-transferase 1 (GST-1), however, increases the protein's antioxidant functionality, and is an example of protein nitration increasing function in a beneficial manner [128]. Peroxynitrite-mediated nitration of specific proteins in particular have been correlated with various other diseases, such as Apolipoprotein A1/ Glyceraldehy 3-phosphate dehydrogenase (GAPDH) in cardiovascular disease, Apolipoprotein B100 in atherosclerosis, creatine kinase in myocardial infarction, and Tau protein in Alzheimer's disease [129].

Nitration of proteins also has the potential to be immunogenic, as suggested by the increased levels of anti-3NT antibodies detected in the plasma of patients with acute lung injury [130], the serum of patients with systemic lupus erythematosus (SLE), and the synovial fluid of arthritis patients [129].

1.4.4 Protein Denitration

The denitration of proteins has been observed in many experimental settings *in vitro*, although its exact mechanisms *in vivo* are yet to be determined [125]. Nitratase activity has been detected in rat heart and brain homogenates [131], isolated platelets [132], isolated mitochondria[133] and activated macrophages [134], and is usually determined by an inverse correlation between 3-nitrotyrosine-positive proteins and free nitrate groups [135]. This likely means that nitration is alterable, and the proportions of nitrated and denitrated proteins, including chemokines, could be actively regulated to fine-tune protein signalling and function.

1.5 CXCL8

This project will study CXCL8 as a model CXC chemokine. CXCL8 is a potent neutrophil chemoattractant protein released by many cell types (both leukocytic and non-leukocytic) in response to a wide range of stimuli including cytokines, microbial products and hypoxia [1,136]. CXCL8 has also been shown to act on other cell types such as lymphocytes and fibroblasts, and is known to promote leukocyte degranulation [137] and angiogenesis [138]. CXCL8 is therefore implicated in both acute and chronic inflammation [139]. The primary amino acid sequence of CXCL8 is shown in Figure 1-7A, as well as the 3D structures of monomeric CXCL8 (Figure 1-7B), and dimeric CXCL8 (Figure 1-7B) with some key amino acids highlighted. The biological significance of some of these highlighted amino acid residues are described in more detail in Figure 1-8.

While mice do not express the CXCL8 gene, they do express MIP2 and KC, which are known functional homologues of CXCL8 and signal through the same receptor, both inducing neutrophil chemotaxis [139,140]. KC and MIP2 share 43% and 53% amino acid sequence homology with CXCL8 respectively (protein BLAST) [140]. Despite the differences in their sequences, conserved regions between the three chemokines include the ERL motif, which is necessary for GPCR binding, and key basic residues at positions 20, 60, 64, 67 and 68 which are involved in GAG binding [140]. It is likely due to these similarities in key functional regions that human CXCL8 can be administered in murine *in vivo* models and successfully induce the recruitment of murine neutrophils [46,55,140].

1.5.1 CXCL8 and GCPR Signalling

CXCL8 signals via both CXCR1 and CXCR2 present on the surface of neutrophils, with a higher affinity for CXCR1. Distinct parts of the CXCL8 3D structure are responsible for activating the different receptors; the N-loop is responsible for CXCR1 activation, whereas the N-terminus is responsible for CXCR2 activation [141]. The ELR motif of CXCL8 is known to be necessary but not sufficient for receptor binding and activation [142-145], and other residues such as tyrosine 13 (Y13) [142,146-148] and leucine 49 (L49) [142] are also known to be important for GPCR signalling as shown in Figure 1-8. Disulphide residues present within CXCL8 have been shown to be important in receptor binding, as modifying (without deleting) these disulphides results in reduced receptor binding affinities –demonstrating that they do mediate function in the folded protein [2]. After ligand binding, the receptor becomes phosphorylated, and the CXCL8 receptor-ligand complex is rapidly internalised and recycled back to the cell surface [149]. CXCR2 is internalised more rapidly than CXCR1, but its recycling back to the cell surface occurs more slowly [150].

A range of signalling pathways can be activated downstream of CXCL8 binding, including PI3K, MAPK, PKC and FAK, and CXCL8 is known to activate transcription factors such as AP-1, HIF-1, STAT3 and NFκB [150]. CXCR1 has been shown to mediate both the neutrophil's cytotoxic microbicidal effects and facilitate the oxidative burst, as both of these functions are impaired when cells are stimulated with CXCL8 in the presence of CXCR1, (but not CXCR2) blocking antibodies [151-153].

Chemotaxis in response to large quantities of CXCL8 (i.e. in an inflammatory situation) has been shown to be mediated largely by CXCR1, as blocking CXCR1 (particularly the N-terminus) either abolished [154] or reduced [155] chemotactic function. Other studies have suggested that CXCR2 does in fact also play a role in neutrophil chemotaxis, however this is generally in induction of chemotaxis in response to picomolar concentrations of CXCL8 [156,157]. Both receptors are reported to mediate granule enzyme release [152].

CXCL8 can also bind the atypical chemokine receptor ACKR1 which is present on the surface of erythrocytes and facilitates the clearance of CXCL8, therefore preventing its ability to induce migration of neutrophils and thus reducing inflammation [77].

1.5.2 CXCL8 and GAG Binding

The dimeric form of CXCL8 is the higher affinity GAG ligand, but binds the receptor with a lower affinity than the monomer – possibly negatively regulating receptor function [2]. H18, K20, R60, K64, K67 and R68 are core GAG-binding residues (red in Figure 1-8) present in GAG binding sites of both the monomer and dimer. K15, R47, K23 and K54 are secondary GAG-binding residues located around the core residues (dark blue in Figure 1-8) [158,159]. K64A, K67A and R68A CXCL8 mutants showed reduced ability to bind to GAGs such as heparin and heparan sulphate, and a reduced ability to induce chemotaxis [151].

1.5.3 CXCL8 Multimerisation and Function

Unbound CXCL8 is detectable in serum/blood samples, and is known to be present at low concentrations (pg/ml) during normal conditions, and to increase during inflammation. What is not reliably measurable is the concentration of bound CXCL8 immobilised on GPCRs or GAGs. As CXCL8 concentrations increase both temporally and spatially during inflammation, it is likely that CXCL8 is actually present as a dynamic mix of monomers/dimers/multimers that varies in composition over time and space [160]. This is supported by data showing that at high concentrations in both solution and crystallised state, CXCL8 has been detected as a homodimer [161], however at lower concentrations in the nanomolar range (assumed to be more physiologically relevant), CXCL8 exists as a monomer [162].

Studying CXCL8 monomers/dimers has been attempted in a number of studies using disulphide-linked dimers and induced monomers. Monomeric CXCL8 is known to be active in terms of mediating GPCR signalling; a "forced monomer" analogue of CXCL8 (created by methylating L25) was shown to be functional in terms of GPCR binding and neutrophil activation, and was 10 to 100-fold more active than an R26C non-dissociating dimer mutant [52,160,163]. This data is supported by a later study conducted by Leong *et al.*, who found that a range of disulphide-linked CXCL8 variants could bing CXCR1 and CXCR2, but with lower affinities than wild type CXCL8 [164], and a study showing a different monomeric CXCL8 analogue (a V27P/E29P mutant) was as active as wild type CXCL8 in functional studies [165]. Another study, however, showed that a different disulphide-linked CXCL8 dimer was as equally active as wild type CXCL8 in terms of inducing calcium release in neutrophils [166]. These discrepancies could be due to the

disulphides being introduced at different positions in the different studies. The consequences of artificially introducing disulphides to create dimers is not fully understood, although data shows that the R26C disulphide-linked dimer is similar to the wild type CXCL8 dimer in terms of dimer interface and NMR-analysed 3D structure [47]. More recent studies have shown that in a mix of CXCL8 monomers and dimers only the monomer preferentially binds to CXCR1, and binding of CXCL8 to CXCR1 has been shown to cause dimer dissociation [163,167,168]. The observed attenuation of neutrophil recruitment observed at very high CXCL8 concentrations could be attributed to the chemokine dimerising and therefore having a reduced affinity for GPCRs at these concentrations [47].

Monomeric and dimeric CXCL8 also regulate GPCR function differently. For CXCR1 monomeric CXCL8 shows greater activity in terms of mediating receptor phosphorylation, desensetisation and β–arrestin-mediated internalisation, whereas for CXCR2 monomeric and dimeric CXCL8 show similar activity in regulating these functions [160]. The differences in binding affinities between the CXCL8 monomer and dimer can likely be attributed to differences in the C-terminal helical residues, which are unstructured in the monomer and structured in the dimer and altered binding properties of the N-loop residues [47,169,170]. The latter is likely due to a general reduction in flexibility observed in the dimer, as the N-terminal and N-loop regions that mediate GPCR binding are located away from the dimer interface [47]. CXCL8 has also been shown to form a heterodimer with CXCL4, which enhances the signalling capabilities of both chemokines [59].

As it has been shown that heparin-bound CXCL8 monomers and dimers are unable to bind to CXCR1/CXCR2 [34], it is hypothesised that CXCL8 exists as a dynamic "cloud" of bound (to GPCRs or GAGs) and free CXCL8 monomers/dimers/multimers (both homo and hetero), which fine-tunes the immune response,. The ratio of these components within the "cloud" will be affected by chemokine concentration, GPCR expression and homo/heterodimerisation, GAG composition/length/sulphation patterns as well as the chemical microenvironment described previously. Simplistically, while both CXCL8 monomers and dimers bind GAGS and GPCRs, due to different affinities it is likely that the dimer preferentially exists in GAG-bound form, and the monomer in the free/GPCR-bound form [34]. The dynamic conversion of free CXCL8 monomers to dimers and vice

versa means that that the overall CXCL8 "cloud" composition is also dynamic and in constant flux [34].

1.5.4 Post-Translational Modifications of CXCL8

Several N-terminal processed forms of CXCL8 are produced by proteolytic cleavage after secretion from peripheral blood monocytes, leukocytes and endothelial cells. In general, CXCL8 (amino acids 6-77) is the most common form [2,171]. As mentioned previously, cleavage of CXCL8 by MMP-1/MMP-8/MMP-9 increases the chemotactic ability of CXCL8, whereas cleavage by MMP-12 abrogates function. Citrullination of CXCL8 has been shown to reduce its ability to induce neutrophil migration into the mouse peritoneum *in vivo*, impair its ability to bind heparin, and also prevents its enzymatic cleavage into more active forms [76]. Citrullinated CXCL8 was shown to have an enhanced ability to induce neutrophil mobilisation from the bone marrow into the circulation, where the chemokine itself also persists as citrullination prevents it from binding to ACKR1 and thus protects it from erythrocyte scavenging [172]. This is likely one explanation for the lack of recruitment to the mouse peritoneum seen, as both the neutrophils and the chemokine will remain in the circulation due to impaired GAG binding of the latter. Naturally occurring citrullination could occur as a mechanism by which the numbers of blood neutrophils are kept constant at a time of injury or inflammation when many are recruited out of the blood and into tissues [172].

Peroxynitrite is also known to activate the NF-κβ pathway leading to CXCL8 production and neutrophil recruitment [100]. Production of CXCL8 in the same vicinity as peroxynitrite means nitration of CXCL8 is also highly likely to occur. A study conducted by Sato *et al*, has shown that incubation of CXCL8 with peroxynitrite inhibits its ability to recruit neutrophils *in vitro* [173]. As tyrosine residues are targets of peroxynitrite-mediated modification (to form 3-nitrotyrosine), and the sole tyrosine residue at position 13 within CXCL8 has a functional role in GPCR signalling, it is likely that nitration of CXCL8 could affect is ability to signal through CXCR1/CXCR2. CXCL8's GAG-binding capacity could also be affected by peroxynitrite, through the modification of lysine residues that are essential for CXCL8-GAG interactions. This project aims to characterise how nitration affects CXCL8's biological activity and detectability.

1.5.5 Targeting CXCL8 Therapeutically

Targeting the function of CXCL8 is an attractive therapeutic concept, and has been researched in a number of studies. Regulating chemokine function could be achieved through targeting many different aspects of chemokine biology, including GPCR signalling (through inhibitors/antagonists/blocking antibodies), the chemokine itself (through antibodies), and GAG binding (through competitors/synthetic non-GAG binding mutants).

1.5.5.1 Targeting CXCL8 Production

Treatment of primary blood neutrophils with sirolimus (Rapamycin) and its derivative everolimus, which are selective mTOR inhibitors, decreased the ability of the cells to produce CXCL8 and VEGF, and could therefore possibly inhibit excessive neutrophil recruitment in *in vivo* transplant cases [174].

Neutralizing monoclonal antibodies raised against CXCL8 have successfully decreased necrosis in rabbit myocardial IRI [175], and rat intestinal IRI [176]. Peptides synthesised from chemokine receptor sequences have been shown to bind and inhibit chemokines including CXCL8 [177,178].

1.5.5.2 Targeting of GPCRs

In mouse studies, genetically targeting CXCR2 through gene knockout out ($CXCR2^{-/-}$), reduced (but did not abrogate) neutrophil migration into the mouse peritoneum in response to a thioglycollate injection [179], and reduced neutrophil migration in a murine urinary tract infection model which resulted in pyelonephritis [180]. This suggests that while CXCR2 is largely responsible for neutrophil migration in mice, another mechanism must exist to compensate for its loss. In a mouse cardiac allograft rejection model, hearts transplanted into a $CXCR2^{-/-}$ recipient mouse showed reduced leukocyte infiltration and expression of pro-inflammatory cytokines [181], and $CXCR2^{-/-}$ mice showed smaller infarct sizes and fewer infiltrating immune cells than wild type mice in a myocardial infarction model [182]. SB656933 is a compound designed to specifically inhibit CXCR2 signalling that is currently in phase I clinical trials to treat chronic obstructive pulmonary disease [183]. Danirixin is another CXCR2-specific antagonist, which was shown to inhibit LPS-induced neutrophil migration to rat lungs *in vivo* [184].

Several small peptides derived from the CXCR1 binding portions of CXCL8 (residues 8-21) have also been shown to reduce the adhesion of THP-1 cells (a monocyte-like cell line) to HMEC-1 cells in vitro by binding to CXCR1 and thus preventing the interactions between CXCR1 and CXCL8 [185].

Reparixin is a small molecular weight non-competitive allosteric CXCR1 and CXCR2 inhibitor, which has been shown to be highly effective in decreasing CXCL8-mediated neutrophil chemotaxis in several IRI models. It is now currently in phase II clinical trials for primary and delayed graft function treatment, in lung and kidney transplant patients [183]. Reparixin has also been shown to improve survival of pancreatic islet allografts in both mice and humans [186], as well as reduce damage in post-ischemic rat intestine [187] , brain [188] , liver [189] and kidney transplant [190].Targeting the CXCL8/CXCR1/CXCR2 axis is an area of focus in many other disease states including type 1 diabetes [191], neurological damage post-stroke [192], arthritis [193,194], and cancers [195].

1.5.5.3 Targeting GAG Binding

The interactions between CXCL8 and GAGs can be targeted to modulate inflammation. This occurs naturally, as the anti-inflammatory TNF-stimulated gene/protein-6 (TSG-6) causes a reduction in neutrophil recruitment by directly interacting with the GAG-binding domain of CXCL8. This prevents the formation of haptotactic CXCL8 gradients on GAGs and, by extension, neutrophil recruitment and inflammation [151].

Small, synthesised chemokine peptides have been used to compete with wild type chemokines for binding on GAGs. A CXCL9 C-terminal peptide has been shown to bind heparin and heparan sulphate (as well as other GAGs), thus competing with a range of chemokines, including CXCL8, resulting in a reduction in neutrophil migration [196]. These small peptides, or variants of them, could in theory exist naturally as a result of chemokine cleavage by proteinases as mentioned previously.

Heparin and other GAG mimetics have been administered in mouse models of arthritis, traumatic brain injury, and LPS treatment, and were shown to reduce inflammation by the same principle of disrupting pre-formed chemokine gradients [197-199]. Although this beneficial effect was found to be dependent upon dosage and administration time [200], and would likely affect a large range of heparin-binding proteins rather than chemokines or a single chemokine specifically.

Non-GAG-binding mutants of many chemokines have also been created with the idea that these mutants could be administered to occupy receptor-binding sites on leukocytes, where they would prevent GAG-associated chemokines from binding and thereby reduce leukocyte recruitment. This was shown to be the case for CCL5, CCL7 and CXCL12 [201,202], but not for CXCL11 [203]. For CXCL8 non-GAG binding mutants could prevent migration of neutrophils to the peritoneum but not the lung [55,140]. This emphasises the need to study each chemokine on an individual basis and avoid generalisation.

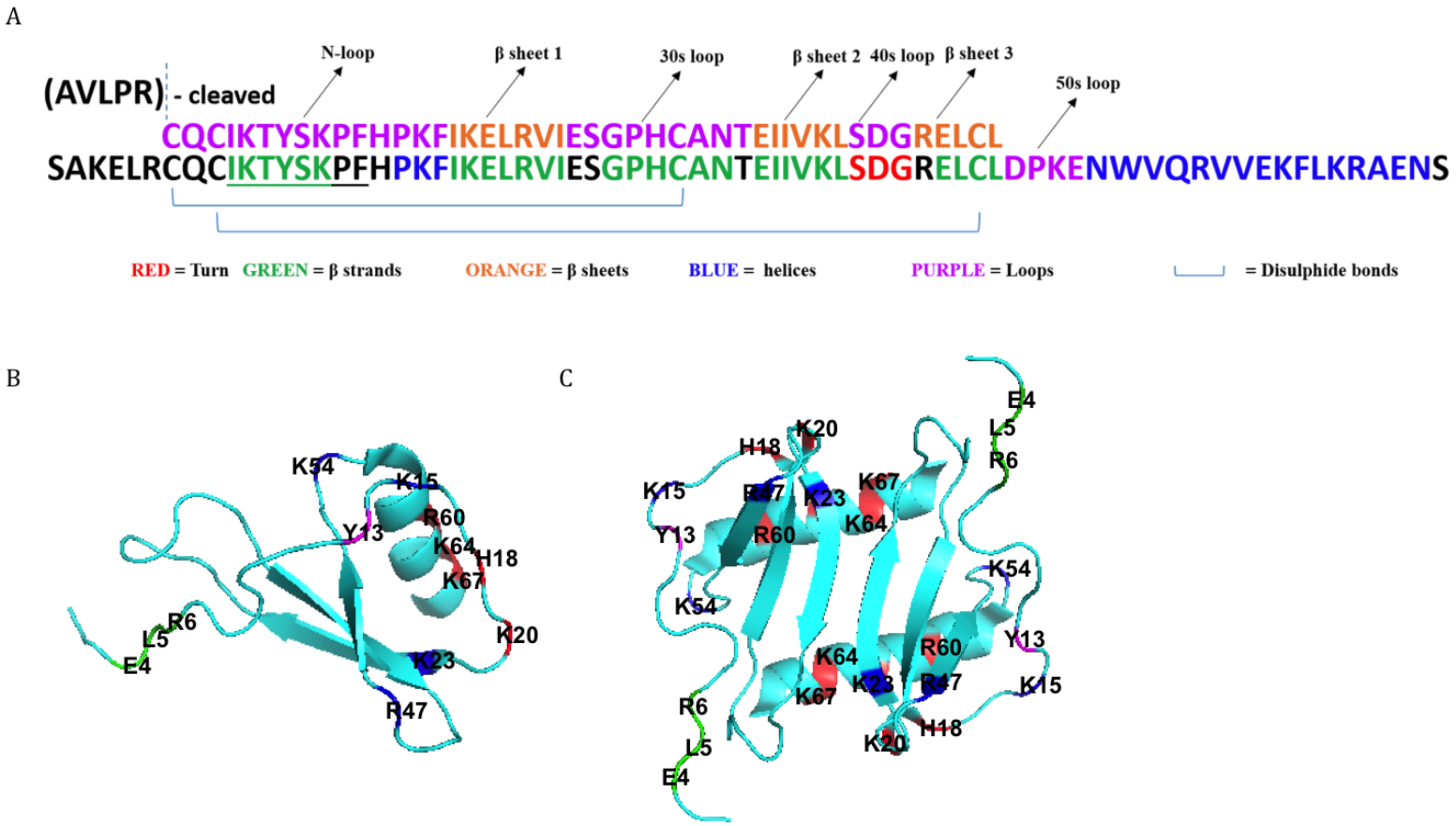

Figure 1-7. Different structural regions within the peptide sequence of CXCL8. A) The full-length chemokine (1-77 amino acids) is shown, as well as the more common and active form (6-77 amino acids), which is produced due to cleavage of the first 5 amino acids (AVLPR). Loop regions within the chemokine are shown in purple, β strands in green, β sheets in orange, helices in blue, the turn in red, and blue brackets indicate disulphide bonds. B) Monomeric 3D structure of CXCL8 (PyMOL), with tyrosine 13 (Y13) highlighted in magenta C) Dimeric 3D structure of CXCL8 (PyMOL). GPCR binding residues are highlighted in green, core GAG binding residues in red, secondary GAG binding residues in dark blue, and tyrosine 13 (Y13) in magenta.

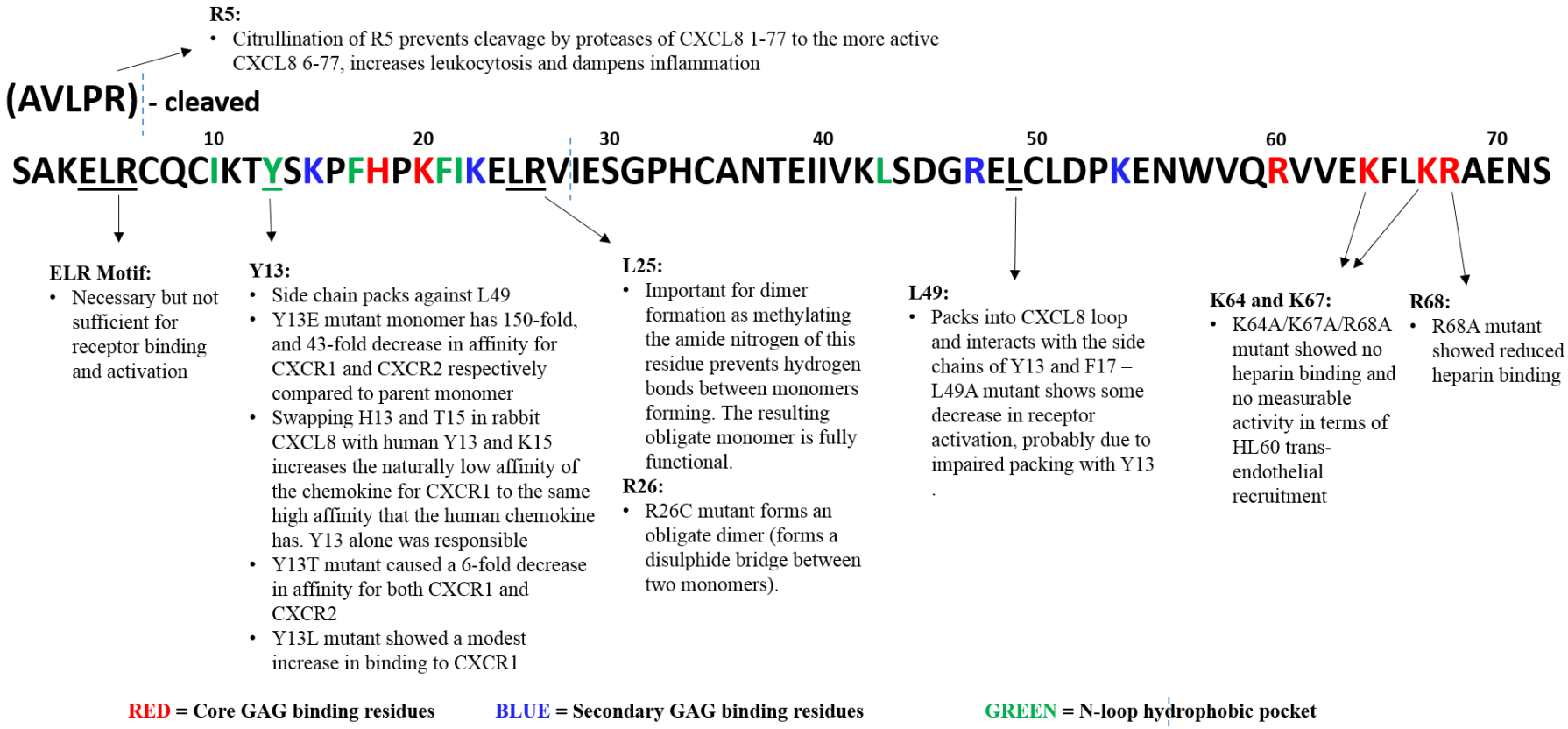

Figure 1-8. Functional roles of some key residues within the peptide sequence of CXCL8.

1.6 NEUTROPHILS

Neutrophils, or polymorphonuclear leukocytes (PMN) are essential components of the innate immune system. They are produced in the bone marrow, where they mature in response to a combination of cytokines, then they emigrate into the circulation as the most abundant leukocyte present in human blood, from which they are recruited rapidly to sites of inflammation [204]. Neutrophils are undoubtedly a major component of acute inflammatory responses, but evidence is now suggesting they play complex roles beyond pathogen elimination, that can affect the adaptive immune system and chronic inflammation [205].

CXCL8 is the most potent neutrophil chemoattractant and activator [136,206], and upon binding to G_i-coupled receptor on the neutrophil surface (CXCR1/CXCR2), elicits calcium flux and MMP-9 release. MMP-9, as mentioned previously, can cleave CXCL8 to its more active form, thereby creating a positive feedback loop of CXCL8-dependant neutrophil recruitment [1]. Activation of neutrophils by chemokines or bacterial products can also extend their lifespan beyond the usual 8 hours (under normal conditions), to ensure an adequate immune response within the site of inflammation, although this can inadvertently lead to the damage of healthy host cells [207].

1.6.1 Chemotaxis and Transmigration

This study will focus on neutrophil migration along chemotactic gradients of CXCL8 specifically (through its binding to CXCR1/CXCR2 GPCRs expressed on the surface of neutrophils) however it should be noted that there is a complex interplay between many chemoattractant molecules and their receptors that contributes to neutrophil chemotaxis and biological function. These include endogenously released molecules such as leukotriene B4, platelet activating factor, and complement-derived C5a and C3a, other chemokines such as CXCL1/2/3/5/6/7/12 and CCL3/5/6/7/9 or bacterial chemoattractants during infection, such as N-Formyl-Methionyl-Leucyl-Phenylalanine (fMLP) (through binding to FPR1), which is presented by GAGs on the surface of endothelial cells [208,209]. Neutrophil migration from the bone marrow into the circulation, the circulation into tissue, and then to the inflammatory site within the tissue, is tightly

regulated by temporal and spatial cascades consisting of complex mixes of many of these signalling molecules simultaneously [209].

Initial interactions between the neutrophil and the endothelial cells involves the activated endothelial cells translocating Wiebel-Palade bodies storing P-selectin/E-selectin to their surface membrane where these selectins are then expressed, and can interact with selectin ligands (such as P-selectin glycoprotein ligand-1 (PSGL-1)), which are expressed by neutrophils. This creates tethering and slow rolling of the neutrophil along the endothelial cell layer. Neutrophils will then upregulate the expression and clustering of β2-integrins (such as the CD11a/CD18 and CD11b/CD18 complexes), which will interact with integrin ligands (adhesion molecules ICAM-1, VCAM-1 and PECAM-1) on the endothelial cells. This facilitates the arrest and firm adhesion of the neutrophil on the endothelium and allows ICAM-1-CD11b/CD18-mediated crawling to occur. This crawling then leads to the transmigration of the neutrophil from the circulation into the tissue. This can occur transcellularly (i.e. though an endothelial cell itself), or more preferentially paracellularly (i.e. between endothelial cells) through interactions with PECAM-1, which is expressed at intercellular endothelial junctions. The neutrophil must then cross the basement membrane, aided by MMPs and other proteinases, before passing between pericytes and travelling further along the chemotactic gradient to the precise location of injury or inflammation [210,211]. This process is summarised in Figure 1-9 below.

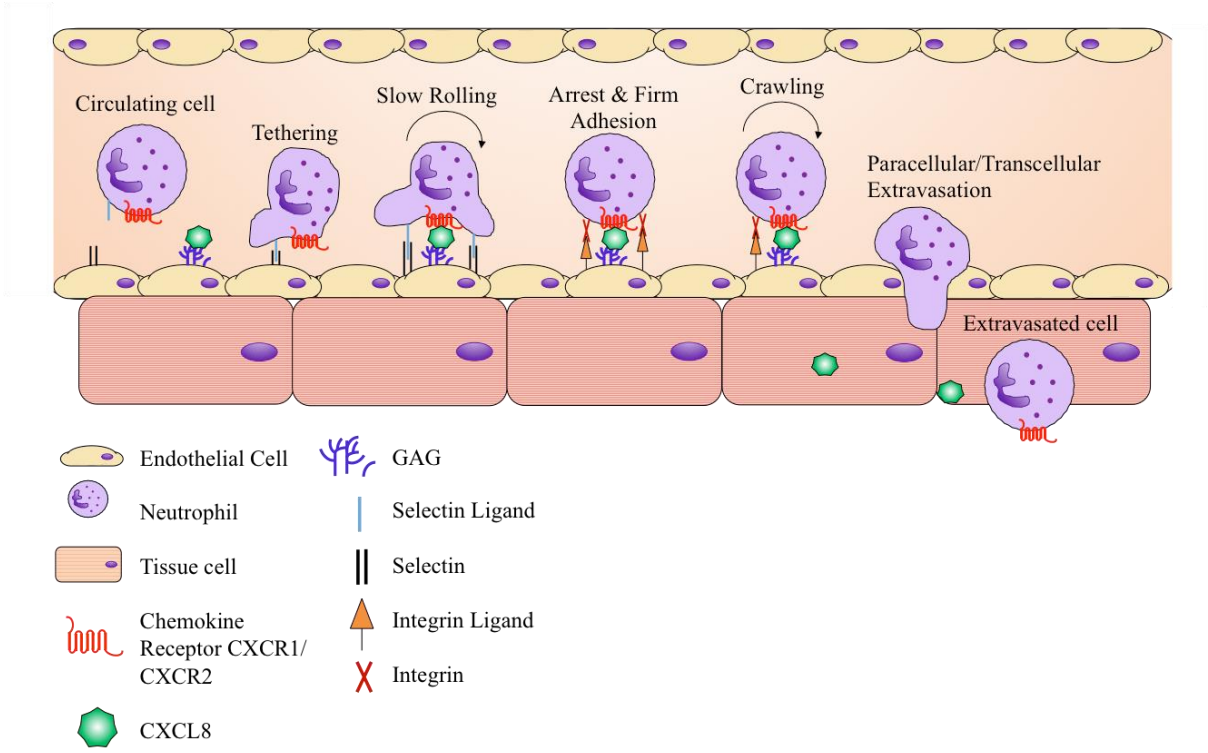

Figure 1-9. Neutrophil trans-migration into tissue from the circulation. Neutrophil tethering and slow rolling is mediated by interactions between selectins (P-selection/E-selectin) expressed by endothelial cells and selection ligands (PSGL-1) present on neutrophils. Arrest and firm adhesion, and crawling of the neutrophil is then mediated by its upregulation of integrin complexes (CD11a/CD18 and CD11b/CD18), which interact with integrin ligands (ICAM-1, VCAM-1, PECAM-1) on the endothelial cells. The neutrophil can then extravasate by paracellular or transcellular migration into the tissue.

1.6.2 Degranulation

Neutrophils mediate their anti-pathogenic functions by the release of a range of anti-microbial proteins and enzymes into membrane-bound phagosomes where bacteria/pathogens have been engulfed [204]. Neutrophils can also release substances stored in pre-formed granules (or synthesised in response to stimuli) through exocytosis in a process called degranulation, which is regulated by a range of signalling molecules within neutrophils including guanosine triphosphatases (GTPases), β-arrestins, src kinases and phospholipids [204], this process is summarised diagrammatically in Figure 1-10. Four types of granules have been identified in neutrophils. Primary (or azurophilic) granules contain elastase, myeloperoxidase (MPO), defensins, heparanase, collagenase, alkaline phosphatase, lactoferrin and a range of lysozymes amongst others [212]. Secondary and tertiary granules both contain lactoferrin and MMP-9, but can be distinguished from each other by their densities when

centrifuged in gradient media [213]. The fourth type of granules are secretory vesicles, which are known to contain human plasma [204].

1.6.3 Oxidative Burst

The neutrophil oxidative burst is an essential aspect of the neutrophil's anti-microbial function and involves the rapid production of ROS. This is mediated by the NADPH oxidase enzyme, which as described above, converts oxygen to the super oxide anion O_2^- [214] . This superoxide anion radical can then go on to from other ROS such as H_2O_2, the hydroxyl radical (OH^-), and HClO [215]. The enzyme MPO, which is released from primary granules during degranulation also contributes to the ROS produced. MPO oxidises halides to form hypohalous acids such as HClO mentioned above, and hypochlorite (OCl^-), as well as other classic peroxidase substrates through reactions with H_2O_2 [216].

When neutrophils are inactive/quiescent, these multiprotein oxidase complexes are segregated into cytosolic and membrane compartments, but upon activation of the cells, these complexes translocate and assemble at the cell surface membranes to facilitate this oxidative burst, in a manner dependent on protein kinase C (PKC) [215,217] .

The way in which the ROS produced during the neutrophil oxidative burst damages invading microorganisms is unclear. Both H_2O_2 and O_2^- can oxidize 4FE-4S clusters present in many proteins, and also damage any enzymes containing iron as a non-redox co-factor through Fenton's chemistry. H_2O_2 can also react with cysteine residues, and OH^- can damage many biological molecules including DNA [218] .

Many of these secreted substances, while being anti-pathogenic, do not distinguish between self and non-self and can damage normal healthy tissue cells [204]. They include O_2^-, H_2O_2, and HClO– which is a strong oxidising agent and can alter the balance between proteases and anti-proteases, thereby contributing further to cellular damage and dysfunction [219-221]. Thus neutrophils are essential components of IRI and oxidative stress due to their close proximity to endothelial cells and tissue epithelial cells which they can damage during tissue infiltration, and other leukocytes which they may influence/polarise [105,222-233].

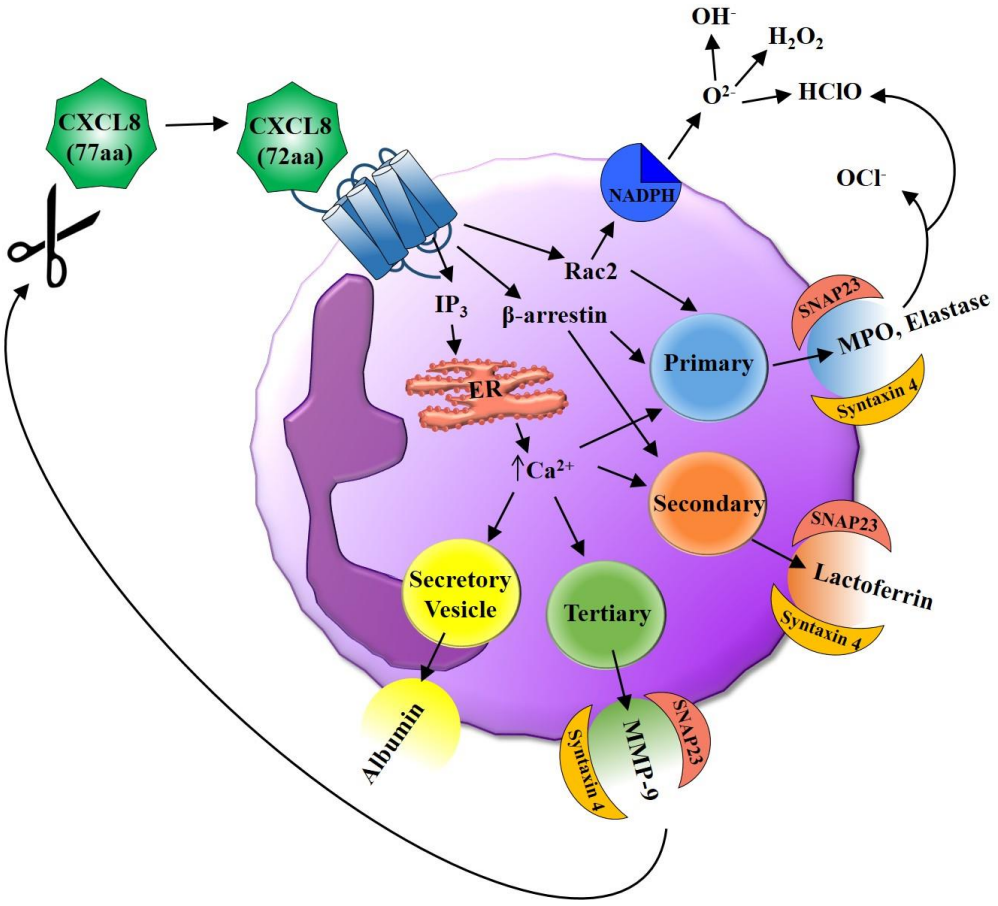

Figure 1-10. Neutrophil degranulation and oxidative burst. The binding of CXCL8 to its receptors CXCR1/CXCR2 on the surface of the neutrophil induces transduction of the signal through G-proteins. This can lead to either the coupling of β-arrestin to both the receptor and primary/secondary granules leading to their translocation and exocytosis, or can lead to signalling through IP_3 resulting in an increase in intracellular calcium and the subsequent mobilisation of primary/secondary/tertiary granules or secretory vesicles. The neutrophil oxidative burst, which comprises of the production of reactive oxygen species (ROS) including OH-, HClO, OCl- and H_2O_2 by NADPH oxidase and MPO is also shown. Abbreviations: aa = amino acids, ER = endoplasmic reticulum, IP_3 = inositol 1, 4, 5-triphosphate, MMP-9 = matrix metalloprotease-9, MPO = myeloperoxidase, NADPH = nicotinamide adenine dinucleotide phosphate oxidase.

1.6.4 Neutrophil Extracellular Traps (NETs)

Neutrophil activation by CXCL8, microbes, bacteria, viruses, yeast or parasites can also can also induce a novel anti-pathogenic function known as neutrophil extracellular traps, or NETs [234]. These NETs comprise of anti-microbial granules concentrated in a web of extracellular fibres composed of deoxyribonucleic acid (DNA) and histones [204,219]. Three models for the production of NETS, or NETosis, have been described. Suicidal NETosis involves activation of the cell, decondensation of chromatin, and ROS-mediated loss of the nuclear membrane, then formation of NETs through the translocation of

elastase and MPO from granules to the nucleus. Vital NETosis occurs through cell activation via toll-like receptors (TLRs) or the complement receptor for C3, occurs independently of ROS, and the loss of DNA does not affect the neutrophil lifespan. The final model is a variation of vital NETosis that occurs in response to neutrophil stimulation by C5a or LPS, is ROS-dependant, and involves the release of mitochondrial DNA as opposed to nuclear DNA. The NETs are then released from the cells through lysis or membrane pores [234].

NETosis has been implicated in the pathology of a range of diseases including systemic lupus erythematosus [235], rheumatoid arthritis [236,237], type 1 diabetes mellitus [238] and ulcerative colitis [239] amongst others.

1.6.5 Resolution of Inflammation

Neutrophils can also contribute to the resolution of inflammation. Ageing neutrophils express higher levels of CXCR4, which traffics them back to the bone marrow for clearance, and also inhibits the release of further neutrophils out of the bone marrow and into the circulation. Neutrophils can also be cleared in the intestinal tract, and within the liver circulation by Kupffer cells (resident macrophages) in a process involving a balance of IL-17, IL23 and C-GSF. Upon apoptosis, neutrophils enhance their own clearance and phagocytic destruction by macrophages through self-opsonisation with molecules such as phosphatidylserine and altered lipids [240], and inhibit the recruitment of more neutrophils by releasing lactoferrin and annexin A1 [241]. Phagocytosis of these dying neutrophils by macrophages stimulates them to release TGF-β, IL-10 and resolvins, all of which act to promote fibrosis and reduce inflammation [242,243].

Neutrophil activity is a double-edged sword; infections occur if the neutrophil response is deficient or absent as in neutropoenic conditions, but excessive recruitment or degranulation is also detrimental, as is the case in conditions such as asthma, septic shock and inflammatory arthritis [204], therefore the function of CXCL8 in recruiting these cells must be tightly regulated. We aim to study how post-translational nitration of CXCL8 affects neutrophil function.

1.7 THE ROLE OF CXCL8 AND NEUTROPHILS IN INFLAMMATION AND DISEASE

Increases in CXCL8 expression, both circulating and localised to specific tissue, have been reported and implicated in the pathophysiology of many diseases. CXCL8's primary function is the recruitment of neutrophils to sites of damage and inflammation, thereby facilitating neutrophil involvement in multiple pathologies.

1.7.1 Respiratory Diseases

CXCL8 secreted by airway smooth muscle cells has been shown to drive steroid-resistant neutrophilic airway inflammation in asthma patients [244] and cystic fibrosis patients [245]. CXCL8 production has been linked to the inflammation driving chronic obstructive pulmonary disease [246], and cigarette smoke was shown to stimulate CXCL8 production by neutrophils [247]. The levels of CXCL8 detectible in bronchoalveolar lavage samples from patients suffering from acute respiratory distress syndrome as a result of tuberculosis also directly correlated with disease severity [248].

1.7.2 Neurological Diseases

CXCL8 is implicated in the pathology of neuroinflammation and neurodegeneration within the central nervous system. CXCL8 expression is increased in HIV-1 positive patient serum, plasma, cerebrospinal fluid and brain lysates in comparison to controls [249-252]. Sources of the CXCL8 produced during HIV infection include astrocytes, microglia and human brain microvascular endothelial cells [253]. Actrocytes, microglia and neurons also produce CXCL8 in response to amyloid-β, hence CXCL8's elevated expression in Alzheimer's disease [254,255]. CXCL8 has also been detected in the cerebrospinal fluid and serum from multiple sclerosis patients during periods of relapse [256].

In all cases, CXCL8 mediates the recruitment of neutrophils and monocytes across the blood-brain barrier, where they potentiate inflammation.

1.7.3 Organ Transplantation

Serum levels of CXCL8 have been shown to be elevated in cardiac transplant patients 5 minutes post-reperfusion in comparison to those of elective cardiac surgery patients [257].

This CXCL8 is thought to be produced by cardiac endothelial cells due to the extended period of hypothermic ischaemia experienced during transplant surgery.

1.7.4 Cancers

CXCL8 is often implicated in the pathogenesis of many cancers. It has been shown to be a major chemoattractant for myeloid-derived suppressor cells (MDSCs) [258,259], and N2-like immunosuppressive tumour-associated neutrophils [260] , which migrate into the tumour environment and inhibit T-cell anti-tumour responses . CXCL8 also induces granulocytic neutrophil-like GrMDSCs to release NETs, which are implicated in thrombus formation and metastasis [261,262]. CXCL8 derived from tumour-associated macrophages has been linked to progression and metastasis in papillary thyroid carcinoma [263] and endometrial carcinoma [264] .

Increased expression of CXCL8 has been linked to worse prognosis and outcomes in cases of hepatocellulcar carcinoma (due to its activation of AKT/mTOR/STAT3 pathways which lead to disease progression and metastasis) [265], and in colorectal cancer (due to its promotion of angiogenesis and inhibition of anoikis/apoptosis) [266]. Similar patterns have been observed in lung cancer, prostate cancer, renal cell carcinoma, pancreatic cancer, gastric cancer, ovarian cancer and lymphomas [267] .

1.8 HYPOTHESIS

As the production of peroxynitrite and its precursor molecules increase during inflammation, and as most of the studies performed to date have shown that nitration of chemokines impairs their ability to recruit leukocytes, we hypothesise that chemokine nitration (and nitration of CXCL8 specifically), is anti-inflammatory, and occurs during times of stress/injury where it acts as a negative regular of inflammation to dampen the immune response.

Simply attempting to measure levels of wild type chemokines does not reflect the complexity of the chemokine system, and may not give an accurate portrayal of the inflammatory situation [268]. The heterogeneous nature of post-translational modifications emphasises the need for better understanding of these signalling molecules and their variants, with some modifications enhancing/abrogating function, and others preventing detection using conventional methods.

1.9 SPECIFIC AIMS OF THIS STUDY

Better understanding of the presence and function of post-translationally nitrated chemokines is essential if their potential as therapeutic agents or biomarkers is to be actualized.

1. Characterise the biological activity of chemokines and variants in vitro and in vivo ~ I aimed to use wild type, nitrated, mutant and nitrated mutant versions of CXCL8 in trans-filter, trans-endothelial and *in vivo* chemotaxis models to assess chemotactic function. I aimed to assess GAG binding and GPCR signalling properties of these chemokine variants, via surface plasmon resonance (SPR) and calcium flux assays respectively.

2. Develop a method to detect nitrated CXCL8 ~ I aimed to develop an antibody to detect nitrated CXCL8 specifically, and to use this antibody to develop an ELISA to measure the levels of wild type and nitrated CXCL8 in serum samples from patients with a range of diseases. I also aimed to use this antibody to detect wild type and nitrated CXCL8 in tissue biopsies from these patients using immunofluorescence staining.

3. Determine how stress affects CXCL8 production and nitration ~ I aimed to examine how different stresses affect the gene and protein expression of CXCL8 in different cell types. I aimed to purify and analyse the CXCL8 produced via mass spectrometry for post-translational modifications.

2 MATERIALS AND METHODS

2.1 LABORATORY PROCEDURE

All experiments and laboratory work was carried out according to the Control of Substances Hazardous to Health (COSHH) and BioCOSHH regulations, and according to the University Safety Policy and Newcastle University's "Safe Working with Biological Hazards" and "Safe Working with Chemicals in the Laboratory" guidelines. Cell culture work was performed according to the regulations for the containment of class II pathogens. Any animal work was approved by the Home Office UK and was carried out under project license number 66/4497, protocol number 19b2/19b4. All human tissue samples accessed were covered under REC reference number 11/NE/0352.

2.2 NITRATION OF CHEMOKINES

Our collaborator Professor Krishna Rajarathnam (University of Texas, Medical Branch), kindly provided us with nitrated and non-nitrated CXCL8 and CXCL1 variants. These included Y13F CXCL8 and L15Y CXCL1. For the nitrated CXCL8, Y13F CXCL8, CXCL1 and L15Y CXCL1 the chemokines at concentrations of 1mg/ml were incubated with 1mM peroxynitrite for 15 minutes at 37°C, then dialysed overnight against water. A sample was tested using matrix-associated laser desorption/ionisation time-of-flight (MALDI-TOF) mass spectrometry to ensure nitration was successful. NMR analysis was also performed by the group to ensure that incubation with peroxynitrite had not damaged the 3D structures of the molecules. These chemokine variants were received from our collaborator as lyophilised powder, resuspended to 1µg/ml in sterile PBS and immediately stored in 2µl aliquots at -80°C. Each aliquot was defrosted once only for use.

Nitrated CXCL8 was also created in collaboration with Professor Paul Proost (Laboratory of Microbiology and Immunology, Rega Institute, KU Leuven). This was achieved by three consecutive incubations of 1mg/ml recombinant CXCL8 (72aa) with 2mM, 2mM and 4nM peroxynitrite for 1 minute each at room temperature. A sample

was tested using ion trap mass spectrometry (methods will be discussed later in section 3.2.7), to confirm that >90% of the sample was nitrated.

2.3 CELL CULTURE

2.3.1 General Principles

All media (if complete) was supplemented with 5-15% Foetal Bovine Serum (FBS), 2mM L-Glutamine, 100 U penicillin and 0.1mg/ml streptomycin. Serum-free media consisted of 0.1% BSA in RPMI-1640, with 2mM L-Glutamine, 100 U penicillin and 0.1mg/ml streptomycin. Cells were cultured at 37°C with 5% $C0_2$.

2.3.2 C1 and C4 Hybridomas

Abmart provided two colonies (C1 and C4) of mouse hybridoma cells producing an antibody raised against wild type and nitrated human CXCL8 peptides. The sequences of these peptides are shown below. Cells were grown in complete DMEM Ham's F-12 with 1ng/ml IL-6 and 5% normal or charcoal IgG-stripped FBS.

C1 peptide: Ac-QCIKTY(NO_2)SKP-NH_2

C4 peptide: Ac-IKTY(NO_2)SKPFHPC-N

2.3.3 HMEC-1 Cells

HMEC-1 cells are a human microvascular endothelial cell line [269], and were grown in complete MCDB-131 media (ThermoFischer Scientific) (15% FBS) supplemented with 10ng/ml EGF and 1µg/ml hydrocortisone. Cell morphologies in culture are shown below in Figure 2-1.

2.3.4 AC10 Cells

AC10 cells are primary human ventricular cardiomyocytes fused with simian virus 40-transformed human fibroblasts [270]. These cells were all grown in complete DMEM media (ThermoFischer Scientific) with 12% FBS. Cell morphologies in culture are shown below in Figure 2-1.

2.3.5 MCF-7 Cells

MCF-7s are epithelial breast cancer cells derived from a pleural effusion from an invasive ductal carcinoma. They are oestrogen and progesterone receptor positive and human epidermal growth factor receptor 2 (HER2) negative [271]. These cells were all grown in complete DMEM media without phenol red (ThermoFischer Scientific), with 8mM L-Glutamine, and with 10% FBS. Cell morphologies in culture are shown below in Figure 2-1.

2.3.6 MDA-MB-231 Cells

MDA-MB-231 cells are also epithelial breast cancer cells derived from a pleural effusion from an invasive ductal carcinoma. They are oestrogen and progesterone receptor negative and HER2 negative, therefore they are representative of triple negative breast cancer [272]. These cells were all grown in complete DMEM media without phenol red (ThermoFischer Scientific), with 8mM L-Glutamine, and with 10% FBS. Cell morphologies in culture are shown below in Figure 2-1.

2.3.7 Primary Human Neutrophils

Primary neutrophils were isolated from healthy donor blood using a Percoll gradient (performed by Professor John Simpson's group), and were rested for 1 hour in serum-free RPMI at 37˚C and 5% CO_2 before being used in any experiments [273].

2.3.8 Mycoplasma Testing and Treatment

MycoAlert™ Mycoplasma Detection Kit (Lonza) was used to test for the presence of mycoplasma in cultured cells – following the manufacturer's instructions. Results were read on a luminometer, values of <0.9 were considered negative for contamination, for values of 0.9-1.2 it was recommended that cells were quarantined for 24h then retested, and values of >1.2 were classed as positive for contamination. MycoZap™ Mycoplasma Elimination Reagent (Lonza) was used to treat infected C4 cells as per kit instructions.

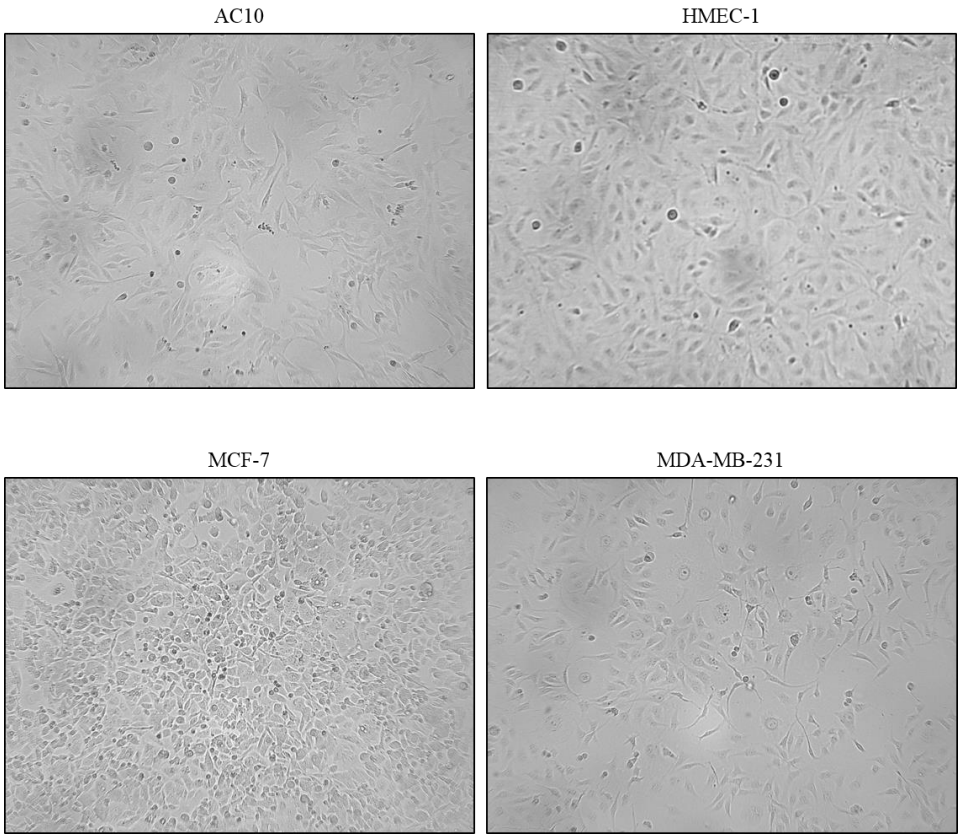

Figure 2-1. Cell morphologies. The morphologies of AC10, HMEC-1, MCF-7 and MDA-MB-231 cells in culture. Images taken at 10x magnification.

2.4 FLOW CYTOMETRY

2.4.1 General Principles

Flow cytometry is a technique that measures light scattering and often emission from fluorochromes, to analyse single cells as they pass through a laser in a fluid stream.

The way light is reflected and refracted by cells is dependent upon their size and internal structure. Optical detectors measure this light, and convert it into electrical pulses in order to give information on the physical characteristics of the cells. Forward Scatter (FSC) is a parameter calculated from light scattered in the forward direction of the laser and is related to cell size and shape. Side Scatter (SSC) is calculated based on light scattered in a direction perpendicular to the beam of the laser, and is related to the granularity/contents of the cell. Combining these two parameters can help identify cell types.

Cells can also be labelled with dyes or fluorochrome-conjugated antibodies to detect markers expressed on the surface of the cell. Stimulating fluorochromes at specific wavelengths causes excitation, which results in the emission of lower energy and longer wavelength light. This emitted light is detected and split by wavelength into individual colours. Ideally, a panel of fluorochromes should be selected so that their emission/excitation wavelengths are sufficiently separated to allow the detection of each fluorochrome individually, as if not there is a chance that the signal of one fluorochrome will be artificially increased by photons from the peripheral spectrum of another fluorochrome. In addition, fluorochromes can emit a spectrum that will activate different detectors to different extents (as opposed to a single wavelength). Compensatrion algorithms can be applied in order to minimise this – and for these experiments OneComp eBeads (Affymetrix) were used [274].

2.4.2 Counting Cells

This method was used to count the number of neutrophils migrated during *in vitro* chemotaxis assays. CountBright Absolute Counting Beads (Life Technologies) were brought to room temperature and vortexed. 8µl of beads (or 8000 beads) was then added to 200µl of cell suspension from each sample in flow cytometry tubes (BD Falcon) and vortexed. Samples were analysed using a FACS Canto II flow cytometer with 1000 bead events set as the stopping gate. Calculations were performed as per the bead manufacturer's instructions to determine total number of migrated cells per µl as a ratio to beads, which was extrapolated out to calculate the percentage of the total number of cells that had migrated.

2.4.3 Cell Characterisation

This method was used to assess adhesion molecule expression by HMEC-1 cells following TNF-α treatment, and to characterise the murine cells migrated during *in vivo* chemotaxis assays. Following centrifugation, cells were resuspended in 100µl of flow cytometry buffer (PBS + 2% BSA). Samples were incubated for 1 hour at 4˚C with antibodies to detect cell surface markers (all directly conjugated to fluorophores, see Table 2-2) at concentrations recommended by the manufacturers. Cells were washed twice by centrifugation in flow cytometry buffer. Cells were then stained with a live/dead marker. For the air pouch model, the cells were then stained with DAPI at 10% of sample volume and analysed using a FACS Canto II flow cytometer. For the

intraperitoneal recruitment model, the cells were stained with Sytox Red (1µl added per tube and incubated for 15 minutes room temperature) and then analysed and counted on the BD Accuri C6 flow cytometer.

In order to perform compensation, one drop of OneComp eBeads (Affymetrix) was added to 100µl containing each antibody individually. Compensation values were calculated using the FACSDiva wizard and were then applied to all samples as part of gating and analysis using FlowJo V10 software, and the gating strategy used to characterise murine cells is shown in Figure 2-2 as an example.

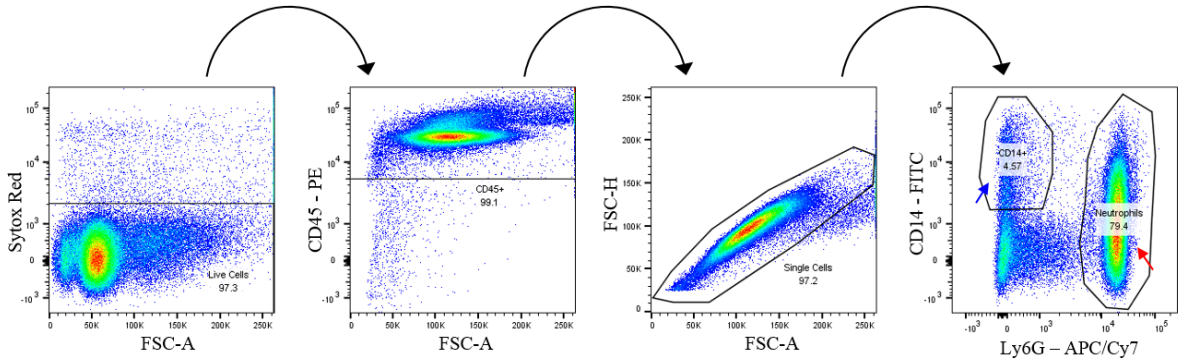

Figure 2-2. Cell characterisation gating strategy. Sequential gating strategy used to analyse *in vivo* peritoneal lavage samples. The monocyte gate is indicated by the blue arrow, and the neutrophil gate by the red arrow.

2.5 Western Blotting

2.5.1 General Principles

This method involves the use of antibodies to detect a target protein in a sample. The sample is denatured and loaded onto an SDS gel to be separated by size (recipes shown in Table 2-1). The proteins are then transferred from the gel onto a nitrocellulose membrane and detected by chemiluminescence using a primary antibody, secondary antibody and an appropriate enzyme-substrate combination.

2.5.2 Cell Treatment and Lysis

This method was used to detect ERK phosphorylation as another downstream result of GPCR activation in primary human neutrophils stimulated with CXCL8 or CXCL8 variants.

Primary human neutrophils were isolated as described previously, then resuspended in serum-free RPMI ($2x10^6$ cells in 1ml per treatment tube) and rested for 1 hour at 37˚C prior to treatment. Cells were then treated and placed immediately on ice. Cells were then centrifuged at 400xg for 5 minutes, washed with ice-cold PBS, and each pellet was resuspended in 200µl cell lysis buffer (10ml CellLytic M (Sigma)) plus 1x PhosSTOP™ phosphatase inhibitor tablet (Roche) and 1x cOmplete™ protease inhibitor tablet (Roche)) on ice for 10 minutes with intermittent vortexing. The CelLytic M lysis/extraction reagent contains a low percentage of a mild detergent for minimal interference with protein interactions and biological activity. The detergent can be dialyzed out as needed and is supplied in a bicine buffer which is suitable for evaluation of biological activity. The supplier withholds the identity of the detergent. After incubation cells were centrifuged at 15000xg for 10 minutes at 4˚C, DNA and cell debris was pelleted, and the lysate supernatant containing the protein was removed and stored at -20˚C.

2.5.3 Protein Quantification - Bicinchoninic Acid (BCA) Assay

To quantify the total protein in the lysates, a Bicinchoninic Acid (BCA) assay kit (ThermoFisher Scientific) was used. This assay is based on the Biuret reaction (where peptide bonds reduce Cu^{2+} to Cu^{1+} in an alkaline solution), and forms a purple colour as the BCA chelates with Cu^{1+}. The absorbance at 562nm can then be measured on a spectrophotometer using a range of protein standards to calculate the protein concentrations of each lysate.

BSA standard concentrations (0, 125, 250, 500, 1000, 2000µg/ml) were diluted in lysis buffer and added in triplicate to a 96 well plate (10µl per well). Neat sample lysates, and lysates diluted 1/5 in lysis buffer were also added to the plate in duplicate. Reaction buffer was prepared as per the manufacturer's instructions and 200µl was added to each well and incubated at 37˚C for 30 minutes before the absorbance at 562nm (with wavelength correction) is measured on a Synergy plate reader using Gen5 software (BioTek). The unknown protein concentration of the samples is then calculated using a standard curve created from the BSA standard concentrations and nonlinear regression.

2.5.4 SDS-PAGE Gel Electrophoresis

Sodium dodecyl sulphate - polyacrylamide gel electrophoresis (SDS-PAGE) is a method used to separate protein molecules according by size as they move through a porous acrylamide gel [275]. Samples (either cell lysates, human serum, or other patient sample types) were mixed with 15µl 4x loading buffer with β-mercaptoethanol (Bio-Rad) and lysis buffer to a total volume of 60µl. Due to the addition of β-mercaptoethanol to the samples, all experiments were performed under reducing conditions. The volume of each sample used was calculated using the concentration measured in the BCA assay so as to load the maximum amount of protein (equivalent in all samples) onto the gel. Samples were then denatured by heating in a T100™ Thermocycler (Bio-Rad) at 99˚C for 10 minutes. This destroys the tertiary structure of the proteins by breaking the disulphide bonds, allowing the SDS in the gel (recipe for making the gels is described in Table 2-1) to associate with the resulting polypeptide chains so that charge is proportional to protein size. The samples were then loaded into the wells of the gel, along with a well containing 8µl of PageRuler™ protein ladder (ThermoFisher Scientific). When an electrical charge is applied to the gel (in a tank with electrophoresis buffer (25mM Tris, 250mM glycine, 0.1% SDS)), these proteins will then migrate through the gel towards the anode, with smaller proteins running faster than large proteins. Gels were run at 180v for 45 minutes – 1 hour.

Resolving Gel (10%, 10ml)	**Resolving Gel (18%, 10ml)**	**Stacking Gel (5%, 3ml)**
4ml dH_2O	1.25ml dH_2O	4.1ml dH_2O
3.3ml 30% Acrylamide	6ml 30% Acrylamide	1ml 30% Acrylamide
2.5ml 1.5M Tris-HCl pH 8.8	2.5ml 1.5M Tris-HCl pH 8.8	750µl 0.5M Tris-HCl pH 6.8
100µl 10% SDS	100µl 10% SDS	60µl 10% SDS
100µl 10% APS	100µl 10% APS	60µl 10% APS
4µl Electran (TEMED)	10µl Electran (TEMED)	6µl Electran (TEMED)

Table 2-1. Recipes for a 10% or 18% resolving gel and 5% stacking gel.

For examining the protein composition of samples, protocols for silver staining (section 2.5.5) or coomassie blue staining (section 2.5.6) were performed.

For immunoblotting, following gel electrophoresis proteins were transferred from the gel onto a nitrocellulose membrane with 0.2µM pores (Trans-Blot® Turbo# Mini Nitrocellulose Transfer Packs, Bio-Rad) using a 10 minute dry transfer method and the Trans-Blot® Turbo™ Transfer System (Bio-Rad) as per the manufacturer's instructions.

2.5.5 Silver Staining

This method was used to test the protein composition of lung samples (listed below) (which were run through SDS-PAGE Gel Electrophoresis as described above, but using a pre-cast Novex™ 16% Tris-Glycine WedgeWell™ Mini Gel (ThermoFisher Scientific), along with a well containing 5µl of Mark12™ Unstained Standard (ThermoFisher Scientific) protein standard. Protein components were separated by size, then visualised in comparison to a range of standard protein size markers using a silver stain. The gel was stained using the SilverQuest™ Silver Staining Kit (ThermoFisher Scientific) as per the manufacturer's instructions. Briefly, the gel was incubated in fixing solution for a minimum of 1 hour, washed with 30% ethanol for 10 minutes and incubated in a sensitising solution for 10 minutes. The gel was then washed with 30% ethanol followed by MilliQ ultrapure water for 10 minutes each, stained for 15 minutes, washed with MilliQ water for 20-60 seconds, then developed for 4-8 minutes before being stopped by the addition of a stopping solution. After a final wash in MilliQ water, the gel was imaged.

- 2x bronchoalveolar lavage samples from lung transplant patients
- 2x bronchoalveolar lavage samples from ventilator-associated pneumonia patients
- 1x bronchoalveolar lavage sample from a patient with inhaled chemical burns
- 2x samples from primary nasal musosa/polyp cell secretomes
- 2x samples of perfusate from *ex vivo* perfused lungs

2.5.6 Coomassie® Blue Staining

Similarly to silver staining above, this protocol was used to visualise protein bands on a gel. Gels were placed in Coomassie® Blue solution (0.1% Coomassie® R-250 in 40% ethanol, 10% acetic acid (ThermoFisher Scientific)) and microwaved for 1 minute, then placed on an orbital shaker for 15 minutes at room temperature. The gel was rinsed in deionised water, then placed in de-staining solution (10% ethanol and 7.5% acetic acid) and microwaved for 1 minute, followed by orbital shaking again until the desired staining was achieved.

2.5.7 Immunoblotting

Following transfer, the membrane (now with transferred proteins) was rinsed in PBS and placed in block solution (5% BSA in TBS+0.1% Tween-20) for 1 hour at room temperature on an orbital shaker. The membrane was then incubated with primary antibodies diluted in blocking solution overnight at 4˚C, again on an orbital shaker. The membrane was then washed 3x for 5 minutes each in TBS+0.1% Tween-20, and incubated with relevant secondary antibodies (HRP-conjugated or biotinylated) diluted in block solution for 1 hour at room temperature. If a biotinylated secondary antibody was used, the membrane was washed 3 times and incubated with streptavidin-HRP (R&D Systems) diluted in block solution at 1/40 for 30 minutes at room temperature. Following 3 more washes, membranes were incubated with ECL chemiluminescent substrate (SuperSignal West PicoSubstrate, Thermo Scientific) for 5 minutes and signal was detected using film (Kodak) developed in ready-made developer and fixer (Tentenal, Germany).

2.5.8 Dot Blots

This method was used to test the specificity of antibodies, and is similar to a Western blot except that protein is directly pipetted onto a nitrocellulose membrane with 0.2µM pores (Bio-Rad) in 2µl dots, and left to air dry for 30 minutes. The protocol for detection and development then continues as described in section 2.5.7.

2.6 IMMUNOHISTOCHEMISTRY AND IMMUNOFLUORESCENCE

2.6.1 General Principles

Immunohistochemistry involves the use of antibodies against specific markers to detect cell types/expression of antigens in fixed/frozen tissue or cells. Immunohistochemistry uses enzymes such as horseradish peroxidase or alkaline phosphatase which metabolise substrates and give off a colour in order to indicate the presence of the marker, whereas immunofluorescence relies on detection using fluorochromes conjugated to antibodies.

2.6.2 Immunofluorescence

Samples were fixed in 4% PFA overnight, then embedded in paraffin and cut into 4µm sections using standard microtomy. Following de-paraffinisation in xylene (2x 5 minute

immersions) and rehydration through graded ethanol (99%, 95%, 70%, H_2O), antigen retrieval was performed using 10mM Citrate buffer pH 6 or Tris EDTA pH 8 in a pressurised environment for 2 minutes, or by incubation in 0.05% Trypsin solution with 0.1% calcium chloride for 10 minutes in a water bath at 37˚C. Slides were then washed and blocked for 30 minutes in a 20% solution of the serum of the secondary antibody species diluted in PBS. Slides were then incubated overnight at 4˚C or 1 hour at room temperature with primary antibody, washed 3 times for 5 minutes each in PBS+0.1% Tween-20, and incubated for 2 hours at room temperature with secondary antibody. Following a further 3 washes, slides were incubated in 0.1% Sudan Black B in 70% EtOH to reduce any tissue autofluorescence, washed 3 times, mounted with VECTASHIELD Antifade Mounting Medium with DAPI (Vectorlabs), and sealed with nail polish. Slides were stored wrapped in foil at 4˚C. All antibodies were diluted in PBS, details can be found in Table 2-2. Images were taken using a Zeiss AxioImager with Apotome enabled or Nikon A1 Upright confocal microscope.

Frozen sections or chamber slides were fixed in ice-cold methanol for 5 minutes at -20˚C, then protocol carried out as normal from the addition of the serum block.

2.6.3 Immunohistochemistry – Haematoxylin and Eosin Staining

For paraffin-embedded tissue sections, the same de-paraffinisation and rehydration protocol described in section 2.6.2 was followed. Slides were incubated in Haematoxylin for 1 minute and 20 seconds, then washed for 1 minute in running tap water. Slides were then "blued" briefly in Scotts' tap water before being washed again in running tap water for a further 2 minutes. Slides were then stained with Eosin for 30 seconds, before being briefly washed and rapidly dehydrated through graded ethanol (70%, 95%, 99%). Slides were then cleared in xylene and mounted in DPX.

2.7 Enzyme-Linked Immunosorbent Assays (ELISA)

2.7.1 General Principles

An enzyme-linked immunosorbent assay (ELISA) is a widely used method of detecting and quantifying specific proteins in a sample. The principle involves the sample being bound to the wells of a plate (if using a direct method) or to a capture antibody, which is bound to the plate (if using a sandwich method). The bound protein is detected using

another antibody, and the reaction developed using an enzyme, which produces a colour as it metabolises its substrate. The optical density of this colour change can then be measured by spectrophotometry. The optical density of a range of protein standards (known concentrations) is used to create a standard curve, from which the concentrations of the protein of interest in the samples are derived in relation to their optical densities.

2.7.2 ELISA Protocol

For a sandwich ELISAs, Immulon HB4X plate (ThermoFisher Scientific) were coated with a capture antibody diluted in coating buffer (15mMNa_2CO_3, 35mM$NaHCO_3$, pH9.6) overnight at room temperature, and then blocked for 1 hour at room temperature with 5% BSA in PBS + 0.05% Tween20 to prevent non-specific interactions. Samples and standards were added to the plate and incubated at room temperature for 2 hours, followed by incubation with a detection antibody at room temperature for 2 hours. The detection antibody was either directly conjugated to horseradish peroxidase (HRP) enzyme or biotinylated. If a biotinylated antibody was used, the plate was then incubated with streptavidin-HRP (1/40, R&D Systems). The plate was washed with PBS + 0.05% Tween20 between each of these steps, and unless specified otherwise all reagents used were added to the plate in dilutent solution (a 1/10 dilution of block solution in wash solution). The reaction was then developed using TMB or OPD substrate solution (R&D Systems), and stopped when the colour intensity was deemed optimal by adding 1M H_2SO_4. The optical density of the plate was then read at 450nm for TMB development, or 492nm for OPD development, both with wavelength correction on a Synergy plate reader using Gen5 software (BioTek).

For a direct ELISAs, a capture antibody was not used, as the sample were directly coated onto the plate (diluted in coating buffer) and incubated overnight at 4°C. The detection protocol then proceeds from the blocking step as described above.

2.8 RNA ISOLATION AND COMPLIMENTARY DNA SYNTHESIS

In order to minimise contamination, all reagents used were RNase free, and only sterile filter tips and sterile autoclaved tubes were used.

2.8.1 RNA Isolation and Analysis

RNA was isolated from the cells using RNeasy Pro Kit (Qiagen) as per the manufacturer's instructions. The RNA collected was then run on a 1% agarose gel (50ml tris-acetate-EDTA (TAE) buffer, 0.5g agrose and 0.5µg/ml ethidium bromide) (TAE buffer contains 40mM Tris, 20mM acetic acid and 1mM EDTA at pH8.0). The gel was then visualised on an AlphaImager (Alpha Innotech) to check RNA integrity.

2.8.2 cDNA Synthesis

Complimentary DNA (cDNA) was then synthesised from 1µg of RNA from each sample, using a Tetro cDNA Synthesis Kit (Bioline), as per the manufacturer's instructions. The reaction mix was placed in a T100™ Thermocycler (Bio-Rad), which was run at 45°C for 30 minutes, then 85°C for 5 minutes and finally 4°C for 15 minutes.

2.9 Real-time Quantitative Reverse Transcription Polymerase Chain Reaction (RT-qPCR)

2.9.1 General Principles

Polymerase Chain Reaction (PCR) is a semi-quantitative technique used to amplify the quantity of a specific gene of interest within a sample by using primers specific for this gene, which can then be visualised and compared to a "housekeeping" endogenous control gene by gel electrophoresis.

Real-time quantitative PCR (RT-qPCR) is quantitative, as DNA products are detected as they are produced by means of a fluorescent signal generated by primer/probes. These primer/probes have a fluorescent reporter dye attached to the 5' end, and a fluorescence quencher attached to the 3' end. In its intact state, the fluorescent signal of the primer/probe is quenched, but during the elongation steps of the PCR reaction, the reporter dye is cleaved away from the quencher by the polymerase enzyme, meaning its signal is detectable, and will increase with each cycle in proportion to the amount of PCR product created.

Firstly an initiation step takes place in order to activate the polymerase enzyme, then the reaction progresses as a series of repeated cycles each containing the same series of steps involving heating/cooling as shown in Figure 2-3. The denaturing step involves

breaking of the hydrogen bonds within the cDNA to create single-stranded cDNA, the annealing step then involves the binding of the primer/probes to their target genes on the single-stranded cDNA template, and the elongation step then involves the polymerase enzyme synthesising a new DNA strand.

Each cycle consists of two phases; an exponential amplification phase where the production doubles, then a plateau phase whereby exhausted resources mean that the production levels off. The threshold cycle (Ct) value (which is defined as the cycle number where the level of fluorescence detected passes a defined threshold) is key for quantifying gene expression. A low Ct value means that few cycles were required in order to pass the fluorescence threshold, meaning there was a large amount of this cDNA product already present in the sample, i.e. gene expression was high. A high Ct value would indicate low gene expression.

2.9.2 Protocol

A reaction mix was created (a 20µl total volume containing 1µl cDNA, 1µl TaqMan® primer/probe, 10µl of SensiFast Probe Hi-ROX Mix (Bioline), 8µl sterile water) and run on a StepOnePlus real-time PCR machine (Applied Biosystems). Running steps were:

- 95°C for 20 seconds to activate the polymerase

- 95°C for a further 1 second to denature the cDNA

- 60°C for 20 seconds to facilitate annealing and elongation.

These steps were repeated for 40 cycles.

2.9.3 Analysis

The data was analysed by using the Ct values reported from the RT-qPCR reaction to calculate ΔCt (mean target gene Ct – mean endogenous control gene Ct), ΔΔCt (treated sample ΔCt – control sample ΔCt), and therefore fold change in gene expression ($2^{-\Delta\Delta Ct}$).

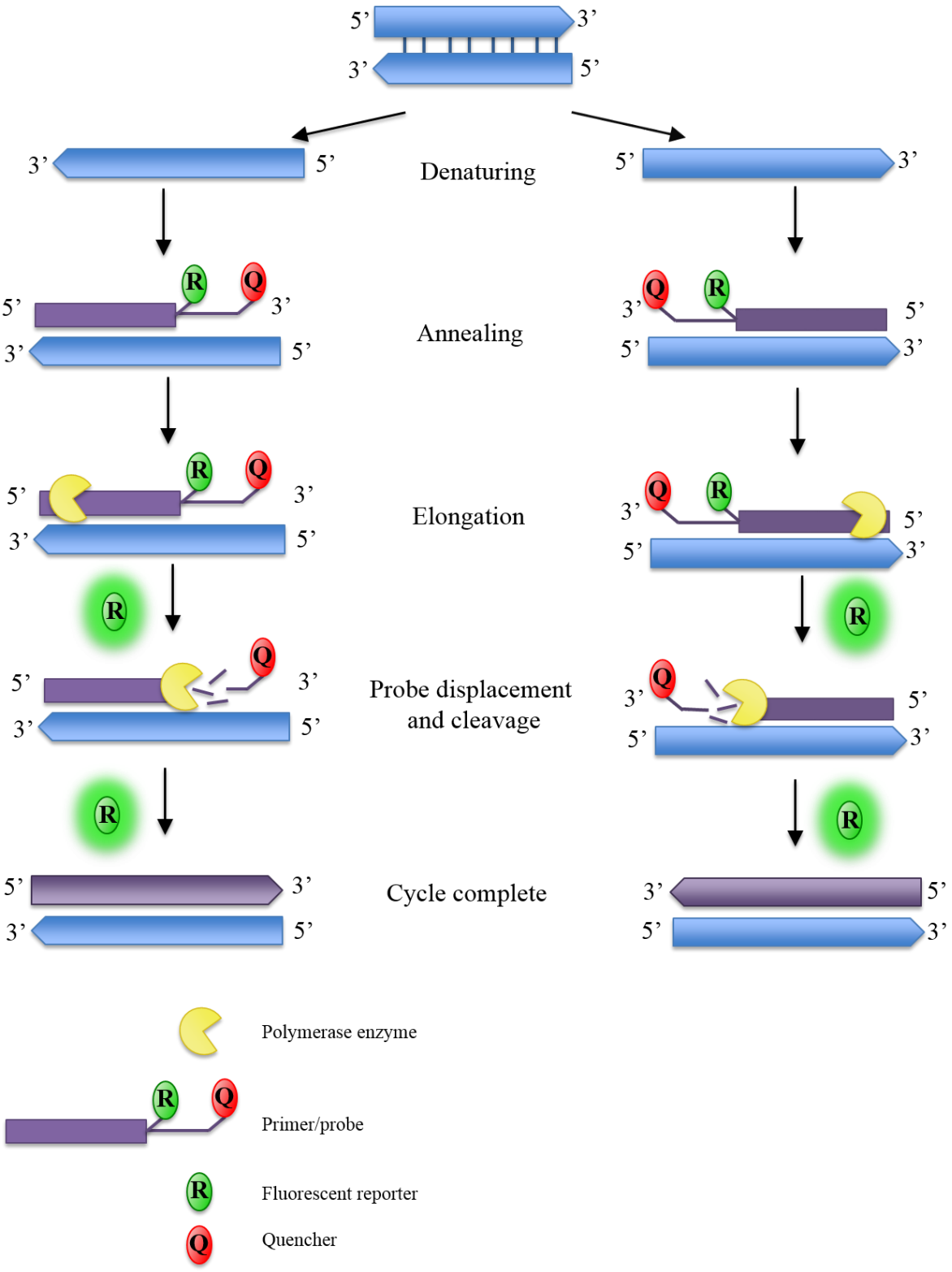

Figure 2-3. RT-qPCR with TaqMan® primer/probes. Denaturing of the DNA is followed by annealing of the primer/probes to the single-stranded cDNA. The polymerase enzyme then extends the strand, using the cDNA template strand, and in the process cleaves the probe allowing the fluorescent reporter to move away from the quencher, thus allowing its signal to be detected. The fluorescence detected is proportional to the amount of PCR product synthesised.

2.10 ANTIBODIES USED

Antibodies used in ELISAs, Western blots, dot blots, flow cytometry and immunofluorescence are shown below in Table 2-2.

Method	Company	Product Code	Antibody Type	[Working]
IF	Collaborator		10-E4 clone Anti-human Heparan Sulphate	1/100 (polyclonal)
IF	Immunoreagents	GtxRb-003-D550NHSX	Goat anti-rabbit-DyLight®550 conjugated secondary	5µg/ml
IF	Immuno reagents	GtxRt-003-E488NHSX	Goat anti-rat-DyLight®488 conjugated secondary antibody	5µg/ml
IF	Immuno reagents	GtxMs-003-E488NHSX	Goat anti-mouse-DyLight®488 conjugated secondary antibody	5µg/ml
IF, ELISA/ Blot	Millipore	06-284	Anti-3-Nitrotyrosine polyclonal	1µg/ml, 2µg/ml
IF, ELISA/ Blot	Abcam	Ab61392	Anti-3-Nitrotyrosine monoclonal	1µg/ml, 10µg/ml
IF	Biolegend	127623	Anti-mouse-Ly6G	1µg/ml
IF, ELISA/Blot	Life Technologies	AHC0881	Anti-human-CXCL8	0.2µg/ml, 1µg/ml
Western Blot	ThermoFisher Scientific	36-8800	Anti-human-pERK1/2	1/5000 (polyclonal)
Western Blot	-	-	Serum from Primary Billiary Cirrhosis patients (containing antibodies against pyruvate dehydrogenase complex 2 (PDC-E2)	1/5000
Western Blot	Sigma	AP112P	Anti-human-HRP secondary antibody	1/5000
ELISA/Blot	Sigma	M-8144	Anti-mouse-IgG1	1/1000
ELISA/Blot	Sigma	M-8269	Anti-mouse-IgG2a	1/1000
ELISA/Blot	Sigma	M-8394	Anti-mouse-IgG2b	1/1000
ELISA/Blot	Sigma	M-9924	Anti-mouse IgG3	1/1000
ELISA/Blot	Sigma	A3673	Anti-mouse IgG-HRP secondary antibody	1/5000
ELISA/Blot	Sigma	A6154	Anti-rabbit-HRP secondary antibody	1/5000
ELISA/Blot	Sigma	A5420	Anti-goat-HRP secondary antibody	1/5000
ELISA/Blot	Bio-Rad	MCA1396B	Biotinylated anti-histidine6 secondary antibody	1µg/ml
Chemotaxis	Abcam	Ab89251	Anti-huamn-CXCR1	20µM
Chemotaxis	Abcam	Ab10401	Anti-human-CXCR2	20µM
Flow Cytometry	Abcam	Ab25603	PE conjugated anti-mouse-CD45	0.2µg /100µl
Flow Cytometry	eBioscience	11-0141-82	FITC conjugated Anti-mouse-CD14	0.5µg/100µl

Flow Cytometry	Biolegend	127623	APC-Cy7 conjugated Anti-mouse-Ly6G	0.5µg/100µl
Flow Cytometry	Biolegend	353105	PE conjugated Anti-human ICAM-1	0.5µg/100µl
Flow Cytometry	Biolegend	305805	PE conjugated Anti-human VCAM	0.5µg/100µl
Flow Cytometry	ThermoFisher Scientific	12-4714-42	Isotype control mouse IgG1k-PE	0.5µg/100µl
Rega Institute ELISA protocol	Collaborator	#4576	Goat anti-human CXCL8	1/300
Rega Institute ELISA protocol	R&D	MAB208	Mouse anti-human CXCL8	2µg/ml
Rega Institute ELISA protocol	Jackson Immuno	115-035-146	Goat anti-mouse-HRP	1/2500

Table 2-2. Details of antibodies used throughout this project.

2.11 STATISTICAL ANALYSIS

Results are shown as means ± standard error of the mean. "N" denotes the number of experimental replicates performed, and "n" denotes the number of technical replicates within each experimental replicate. Statistical analysis was performed using a One Way ANOVA with Tukey's post-hoc correction test GraphPad Prism 5.0 software. Values of < 0.05 were considered to be significant. p=<0.05: *, p=<0.01: **, p=<0.0001: ***, p=<0.00001: ****. Stars directly above samples indicate statistical difference from the negative control, stars on brackets indicate statistical difference between two samples.

3 CHARACTERISING THE BIOLOGICAL FUNCTION OF NITRATED CXCL8

3.1 INTRODUCTION

One of the reasons that very few therapeutics designed to target chemokines have been successful is thought to be the known degree of redundancy within the chemokine system. Another is that we have an incomplete understanding of how chemokines are regulated and function in an *in vivo* inflammatory environment, which is likely to differ from observed behaviour in reductionist *in vitro* experimental settings. Detecting chemokines by immunoassays such as ELISAs, or by immunohistochemistry in tissue sections, merely indicates the presence of the protein, and does not reflect the actual biological activity of that protein within the given environment.

As mentioned previously in section 1.3, chemokines can be altered by a range of post-translational modifications. Some modifications have been shown to enhance function (such as CXCL8 truncation [70]), some to abrogate function (such as CXCL12 nitration[122]), and some modified chemokines can antagonise their wild type counterparts. A truncated form of CCL5 (3-68aa) is a 10-fold less potent inducer of monocyte and eosinophil chemotaxis than full length CCL5 [276], and was shown to be detectable in all serum samples in a cohort of 297 type 2 diabetes patients, making up ~15% of the total CCL5 detected [277]. High levels of CXCL10 have been associated with viral persistence in hepatitis C patients [278], and it has been discovered that this is because the CXCL10 detected is actually the truncated form of the chemokine, which antagonises the wild type molecule [279,280]. The amount of citrullinated CXCL5 present in the serum and synovial fluid of rheumatoid arthritis patients has also been correlated with disease activity, possibly due to this modification increasing the capacity of the chemokine to recruit monocytes [281].

Clearly, analysing only the expression of wild type chemokines does not accurately reflect the global inflammatory situation or the contribution of an individual chemokine (in all its varying forms) to this response.

Understanding the function of these modified chemokines, how they interact with their wild type counterparts, and under what circumstances these modifications are likely to occur, is essential for utilising these molecules as potential biomarkers, and developing new therapeutic interventions to effectively target the chemokine system. As evidenced, this is applicable to a range of diseases; autoimmune conditions such as rheumatoid arthritis, metabolic conditions such as type 2 diabetes, and viral infection.

One method of modification is nitration by peroxynitrite, as is hypothesised to occur during oxidative stress and ischaemia-reperfusion injury as described in section 1.4. Briefly, the spontaneous reaction of the superoxide anion O_2^- and NO (production of both is known to increase during inflammation [96-98]) forms peroxynitrite, which mediates oxidative damage [108,109,111] and is implicated in the pathology of many diseases [112]. Peroxynitrite can also post-translationally nitrate proteins within the vicinity of its production. In the case of chemokines studied to date, such as CCL2, CCL5 and CXCL12, this nitration appears to have anti-inflammatory consequences, reducing the chemotactic ability of these molecules [119,122]. This chapter will focus on post-translational nitration of CXCL8 by peroxynitrite, and will examine the consequences this modification has on the biological function of CXCL8.

3.1.1 Specific Aims

Focusing on peroxynitrite-mediated nitration of CXCL8, this chapter aimed to examine and assess:

- The ability of nitrated CXCL8 to induce neutrophil chemotaxis *in vitro* and *in vivo*
- The ability of nitrated CXCL8 to induce GPCR signalling in neutrophils
- The ability of nitrated CXCL8 to bind GAGs
- On which residues within CXCL8 nitration occurs

3.2 SPECIFIC MATERIALS AND METHODS

3.2.1 Chemotaxis Assays

3.2.1.1 General Principles

Chemotaxis assays test the ability of a chemokine to induce the chemotactic migration of cells. These assays can be performed in a variety of ways; *in vitro* in the form of trans-filter/bare membrane assays or trans-endothelial (where a layer of endothelial cells is grown on the filter of a cell culture insert for cells of interest to migrate through), and *in vivo* in mice through the injection of a chemotactic agent into an isolated compartment that cells can migrate into and be retrieved from, such as the peritoneum or a pre-formed air pouch on the back.

3.2.1.2 In Vitro Trans-filter Chemotaxis

24 well companion plates (BD Falcon) were blocked by adding 1ml of 2% BSA (diluted in PBS and sterile filtered through a 0.2µm filter) to each well, and incubating overnight at 4°C. This prevents chemokines binding to the surface of the plate, which would reduce the availability of said chemokine to induce chemotaxis. The use of FBS as a blocking agent should be avoided, as any bovine chemokines present in this could affect reliability of data collected.

Relevant chemokine solution at 10nM, 20nM or 30nM diluted in serum-free RPMI (0.1% BSA in RPMI-1640 + pen/strep + L-glut) in a total volume of 600µl was added to each well of the plate in triplicate, then a cell culture insert with 3µM pores (BD Falcon) was carefully inserted into the well to avoid trapping air bubbles. Serum-free RPMI only with no chemokine added was used as a negative control. After 1 hour of resting in serum-free RPMI at 37˚C, 500µl of neutrophil cell suspension (300,000 cells per well diluted in serum-free RPMI) was gently pipetted into each insert, and the plates incubated at 37°C with 5% CO_2 for 1.5 hours to allow cells to migrate. The experimental set-up is shown in Figure 3-1A. The number of cells that had migrated through the filter and into the well below was counted using flow cytometry as described in section 2.4.2.

Chemokines used included CXCL8, CXCL1 (R&D), as well as mutant and nitrated chemokines generated by our collaborator Dr Krishna Rajarathnam. These included

nitrated CXCL8, Y13F mutant CXCL8, nitrated Y13F mutant CXCL8, nitrated CXCL1, L15Y mutant CXCL1 and nitrated L15Y mutant CXCL1. The amino acid sequences of these chemokines are shown below, with mutated residues highlighted in red.

CXCL8:

SAKELRCQCIKTYSKPFHPKFIKELRVIEDGPHCANTEIIVKLSDGRELCLDPKENWVQRVVEKFLKRAENS

Y13F CXCL8:

SAKELRCQCIKTFSKPFHPKFIKELRVIEDGPHCANTEIIVKLSDGRELCLDPKENWVQRVVEKFLKRAENS

CXCL1:

ASVATELRCQCLQTLQGIHPKNIQSVNVKSPGPHCAQTEVIATLKNGRKACLNPASPIVKKIIEKMLNSDKSN

L15Y CXCL1:

ASVATELRCQCLQTYQGIHPKNIQSVNVKSPGPHCAQTEVIATLKNGRKACLNPASPIVKKIIEKMLNSDKSN

For trans-filter assays using neutralising antibodies, neutrophils were incubated with 20μM anti-CXCR1 or anti-CXCR2 or both for 30 minutes (incubation was trialled at 37°C, room temperature and 4°C in 3 separate experimental runs). Both antibodies are described as suitable for GPCR neutralization studies according to their datasheets provided by Abcam.

3.2.1.3 In Vitro Trans-endothelial Chemotaxis

72 hours prior to the assay, cell culture inserts were seeded with $2x10^5$ HMEC-1 cells in 1ml complete MCDB-131 media, and incubated at 37°C with 5% CO_2. It is important to place media in the insert only (not in the well underneath) to discourage cells from growing in a "double monolayer" both above and below the filter. When cells were deemed to be 80% confluent, 5ng/ml of TNF-α was added to the culture media in the insert and incubated overnight. This creates a pro-inflammatory environment, encouraging the upregulation of adhesion molecules such as ICAM-1 and VCAM by the endothelial monolayer. Confluency of the monolayer was closely monitored – if endothelial cells are underconfluent, migratory cells can pass through gaps in the monolayer, and if they are overconfluent this can inhibit migration. On the day the assay was performed, the endothelial monolayer was washed once in serum-free RPMI, then the plate was set up, incubated and analysed as described in section 3.2.1.2. The experimental set-up is shown in Figure 3-1B. After the incubation, inserts were removed

and stained with haematoxylin and eosin to check the HMEC-1 monolayer confluency as described in section 2.6.3.

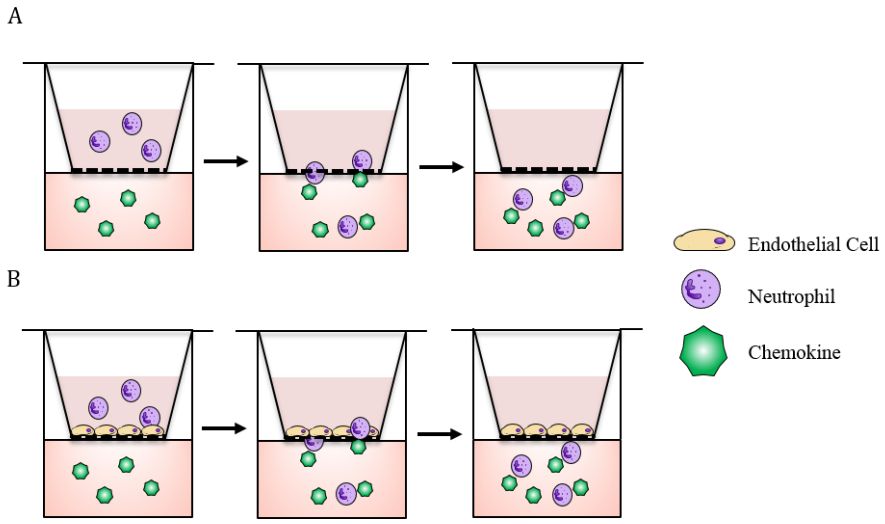

Figure 3-1. Chemotaxis assay experimental set-up. Diagrammatic representation of A) a trans-filter chemotaxis assay and B) a trans-endothelial chemotaxis assay.

3.2.1.4 In Vitro Ibidi® µ- Slide Chemotaxis

24 hours prior to the assay, Ibidi® µ-slides Chemotaxis (ibiTreat), plugs (Ibidi®) and serum-free RPMI were placed in an incubator at 37°C with 5% CO_2 in order to allow gases to equilibrate and minimise the formation of air bubbles as the assay is set up.

On the day of the assay, primary neutrophils were isolated and rested as described previously in section 2.3.7. The assay was then set-up according to Ibidi®'s Application Note 17, following instructions for "2D chemotaxis experiments without gel". Briefly, $3x10^6$ neutrophils/ml were seeded into the central channel which was then sealed using the plugs provided, and a gradient of 30nM (highest concentration) CXCL8 or nitrated CXCL8 was created, and the chambers either side of the channel were sealed (Figure 3-2A). This exposes the neutrophils to a linear chemokine gradient across the channel. A negative control experimental chamber was then set up using serum-free RPMI only (no gradient), and controls using 30nM CXCL8 or nitrated CXCL8 on both sides of the channel were also set up to test for chemokinesis as opposed to chemotaxis (Figure 3-2B). The slides were then imaged every 2 minutes for 3 hours using a Nikon TiE Multi-Modality microscope with a 10x phase contrast lense, and images analysed using Fiji's manual tracking plug-in by tracking 40 individual randomly chosen cells through all images. An example of an image with 40 randomly selected cells for tracking in shown below in Figure 3-2C. These tracks were then imported in to Ibidi®'s Chemotaxis and

Migration Tool, where they were animated and analysed for parameters including velocity, directness, Euclidean distance and forward migration index.

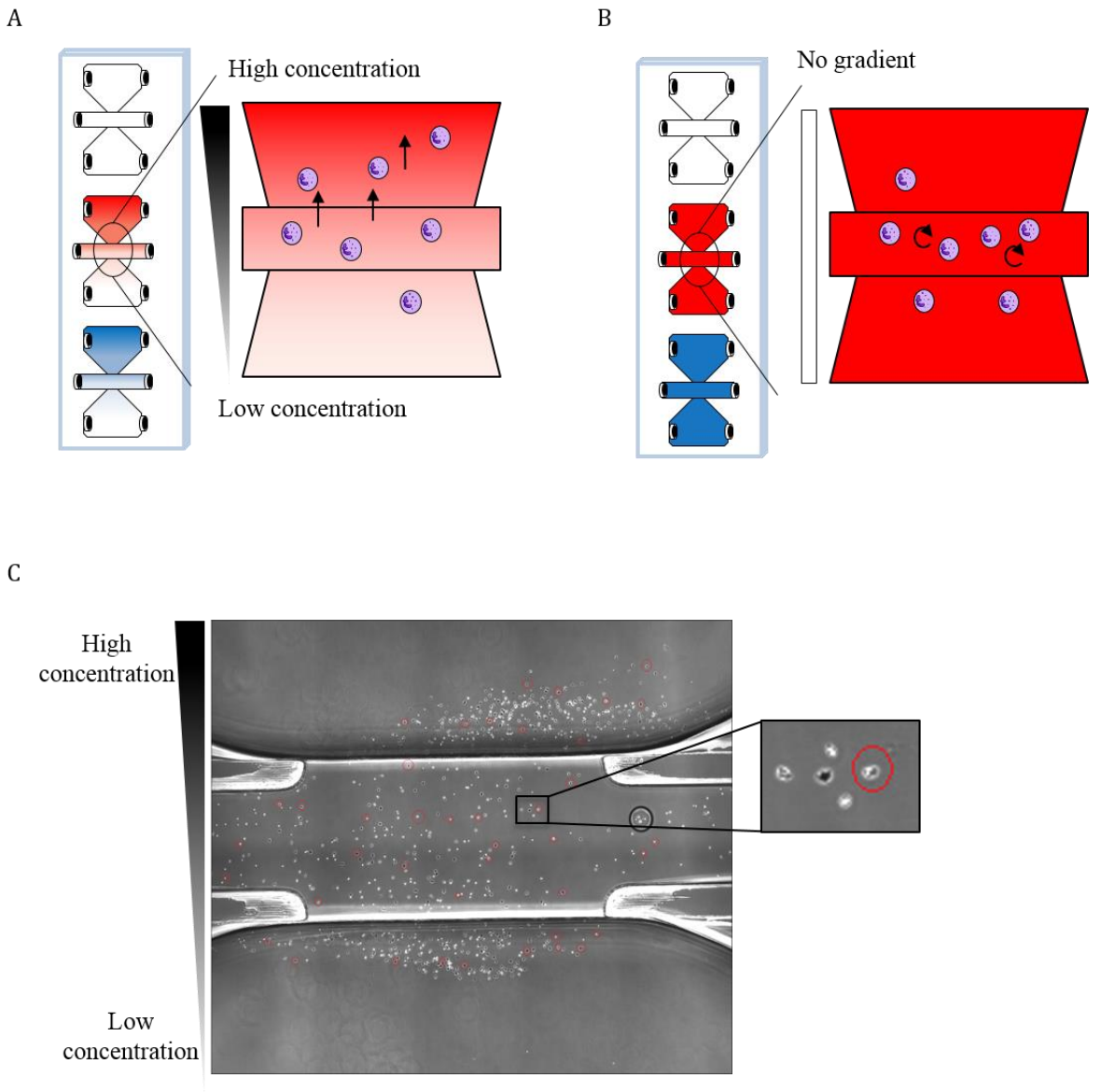

Figure 3-2. Diagrammatic representation of the experimental set up using Ibidi®'s µ-slide Chemotaxis equipment and analysis of images performed using FIJI. Experimental set-ups showing a negative control containing serum-free RPMI (white) in both chambers, and A) 30nM gradient of wild type CXCL8 (red) and nitrated CXCL8 (blue) created by adding serum-free RPMI to one chamber and chemokine to the other, or B) no gradient with 30nM of wild type CXCL8 (red) or nitrated CXCL8 (blue) in both chambers, with neutrophils around the central channel and arrows indicating the direction of cell movement towards the area of highest concentration. Images of each of the three experiments per slide are taken every 2 minutes for 3 hours using a 10x phase contrast lens on a Nikon TiE Multi-Modality microscope, and an example image opened in FIJI with 40 cells randomly selected for tracking (red circles) is shown in C). Each cell is tracked through all images, and tracks are then uploaded and analysed using Ibidi®'s Chemotaxis and Migration Tool.

3.2.2 *In Vivo* Murine Air Pouch Recruitment

3.2.2.1 General Principles

The aim of this model is to create a stable fluid-filled subcutaneous pouch on the back of a mouse, which mimics a synovial joint cavity. This pouch can then be injected with a chemotactic agent, then later flushed out and the contents analysed. This creates a sealed environment into which cells can migrate and be retrieved from.

3.2.2.2 Air Pouch Chemotaxis

Female 7-8 week old BALBC female mice were used in this study.

Stable, fluid-filled air pouches were created on the backs of the mice by injecting 3ml of sterile air subcutaneously under general anaesthetic (isoflurane) on the first day. On the second, fourth and fifth day, 1ml of sterile air is injection to top up the pouch as shown in Figure 3-3.

On the sixth day, the mice were split into groups and 500µl sterile PBS with 0.5% carboxymethylcellulose (CMC) ± chemokine was injected subcutaneously into the air pouch. For optimisation experiments concentrations of 0.1µg, 1µg and 3µg wild type CXCL8 were used, and for the final experiment 1µg of wild type CXCL8 or nitrated CXCL8 was administered. The initial CXCL8 concentrations tested were based on successful neutrophil recruitment observed in response to 0.1-10µg of CXCL8 administered in a murine *in vivo* recruitment experiment conducted by our collaborator Professor Krishna Rajarathnam [55].

Mice were then left for 4 hours to allow cells to migrate into the air pouch. After mice were sacrificed via intraperitoneal Euthatal injection, pouches were lavaged twice with 1ml sterile PBS + 3mM EDTA each time. The lavage samples were then centrifuged at 500xg for 5 minutes, and resuspended in 125µl flow cytometry buffer (PBS + 2% BSA). TALI total cell counts were performed on 25µl of each sample, and the remaining 100µl was stained with fluorescently conjugated primary antibodies for 1 hour at 4˚C, and analysed using the FACS Canto II flow cytometer. Samples were analysed using FlowJo v10 software as described in section 2.4.3.

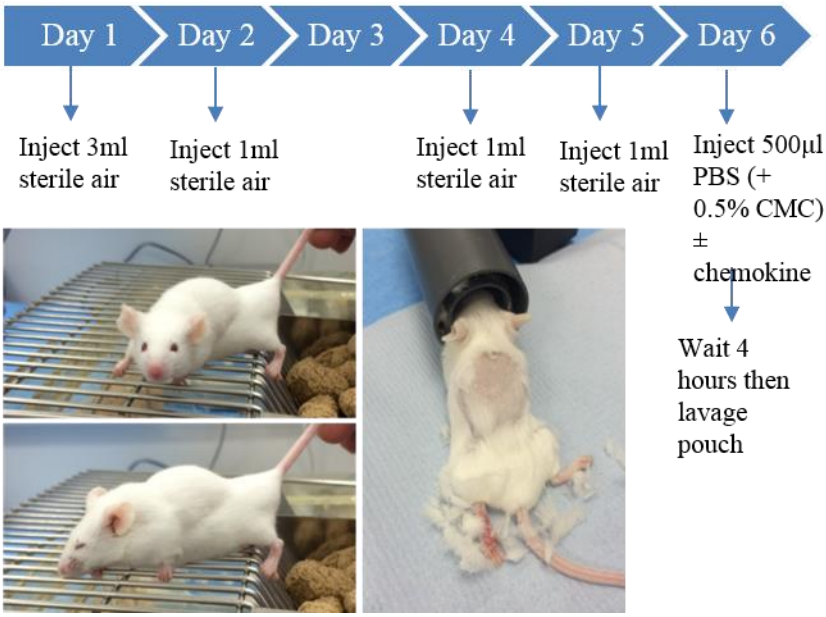

Figure 3-3. Murine air pouch model. Schematic diagram of the generation of a stable fluid-filled pouch on the back of a mouse through a series of injections of sterile air.

3.2.3 *In Vivo* Murine Intraperitoneal Recruitment

3.2.3.1 General Principles

This model was used to replace the air pouch recruitment model. The aim was to use the peritoneum as a naturally occurring sealed cavity, which cells can migrate to and be harvested from. This model should encompass less basal inflammation than the air pouch model, due to the lack of repeated injections and separation of the skin needed to create the pouch.

3.2.3.2 Intraperitoneal Chemotaxis

Female 7-8 week old BALBC female mice were used in this study. On the day of the assay, mice were split into groups to receive injections of 500µl of sterile clinical grade saline ± chemokine into the peritoneum. Mice were then left for 6 hours to allow cells to migrate into the peritoneum. After mice were culled via cervical dislocation under anaesthesia, pouches were lavaged three times with 1ml sterile PBS + 3mM EDTA each time. The lavage samples were then centrifuged at 500xG for 5 minutes, and resuspended in 100µl flow cytometry buffer, stained with fluorescently conjugated primary antibodies for 1 hour at 4˚C and analysed using the BD Accuri c6 flow cytometer as described in section 2.4.3. Data was analysed using FlowJo v10 software.

3.2.4 Calcium Flux Assays

3.2.4.1 General Principles

This technique was used to measure the release of intracellular calcium stores as a result of GCPR activation in primary human neutrophils stimulated with CXCL8 or CXCL8 variants. This method involves the loading of primary neutrophils with Indo-1 AM in order to measure cellular calcium levels. Indo-1 is excited by the UV laser and its emission changes depending upon whether it is bound to calcium (~420nm) or free (~510nm). Measuring the ratio of these two wavelengths upon addition of a stimulant can inform whether or not the stimulant activates receptor signalling through changes in intracellular calcium concentration. Ionomycin (an ionophoric antibiotic) is used as a positive control to raise intracellular calcium levels by allowing transfer of calcium across the cell membrane.

3.2.4.2 Measuring Calcium Flux in Neutrophils

Primary neutrophils were isolated and rested as described previously. Cells were washed in HBSS supplemented with 1mM $CaCl_2$, 1mM $MgCl_2$ and 1% FBS (v/v), and resuspended to $1x10^7$ cells/ml. Cells were then stained with 3μM Indo-1 (ThermoFisher Scientific) for 30 minutes at 37˚C and washed twice in supplemented HBSS by centrifugation at 400xg for 5 minutes. Cells were resuspended and split into individual testing tubes, each containing $3x10^6$ cells in 1ml of supplemented HBSS, and rested in a 37 ˚C waterbath for 30 minutes before analysis using a Fortessa X20 flow cytometer. A baseline reading at both wavelengths was recorded for 1 minute, before the tube was removed and PBS (for the negative control tube) or 30nM chemokine (CXCL8, nitrated CXCL8, Y13F CXCL8, nitrated Y13F CXCL8), was added. Fluorescence was recorded for a further 5 minutes, then the tube was removed again and 2mM Ionomycin was added and the response recorded for a further 2 minutes. Ratio of 420nm emission to 510nm emission was calculated using FlowJo v10 software.

3.2.5 Flow-Based Adhesion Assays - Cellix™ VenaFlux

3.2.5.1 General Principles

Assays were performed using a Cellix™ machine to determine how primary blood neutrophils adhere to an HMEC-1 cell monolayer under flow conditions, after

stimulation with CXCL8 or the variants described in the chemotaxis assays above. This experimental set up involves an 8-channel chip (Vena8 Endothelial+ Biochips, Cellix™ Ltd.) attached to a remotely controlled pump system by a set of needles connected to tubes as shown below in Figure 3-4. Prior to the assay, the chips can be coated with either a ligand of interest, or an adherent cell type. A suspension of test cells, such a neutrophils or monocytes, can then be added to the chip, and flown across by the pump in order to allow the imaging and measurement of adhering cells.

3.2.5.2 Assay Protocol

The day before the assay, Venaflux chip channels were coated with fibronectin at 100µg/ml (10µl per channel) overnight, then 250,000 HMEC-1s (previously stimulated with varying concentrations TNF-α overnight) were seeded onto each of the chip's 8 channels and left to adhere for 1 hour at 37°C. Unstimulated HMEC-1s were used as a negative control.

HMEC-1 monolayers were then treated with a range of concentrations of CXCL8, or CXCL8 variants in duplicate for 1 hour at room temperature. Controls received media only without chemokine. Neutrophils isolated from healthy donor blood were purified, rested for 1 hour in serum-free RPMI at 37˚C, and stained with 1mM $DiOC_6(3)$ then 300,000 were pipetted onto each channel in the chip in succession, flown over the chip at 0.5 dyne/cm^2, and adherent cells were visualised using the Cellix™ machine. Adherent cells were counted from 5 sequential images per position and 5 positions per channel, using ImageJ software, and averages were calculated.

A

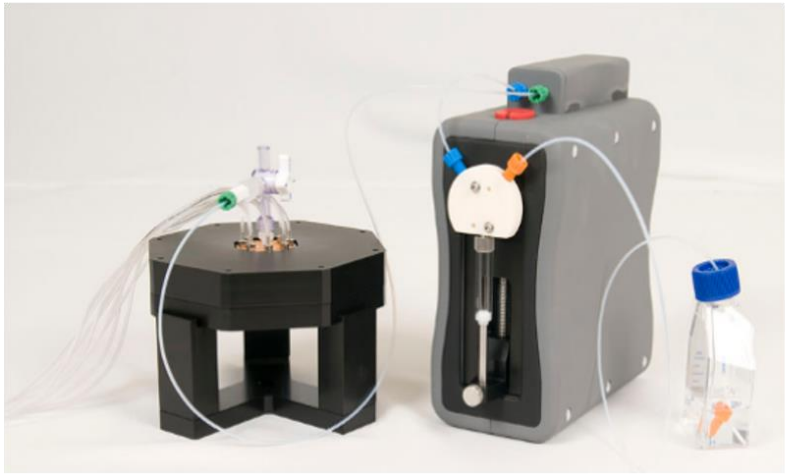

B

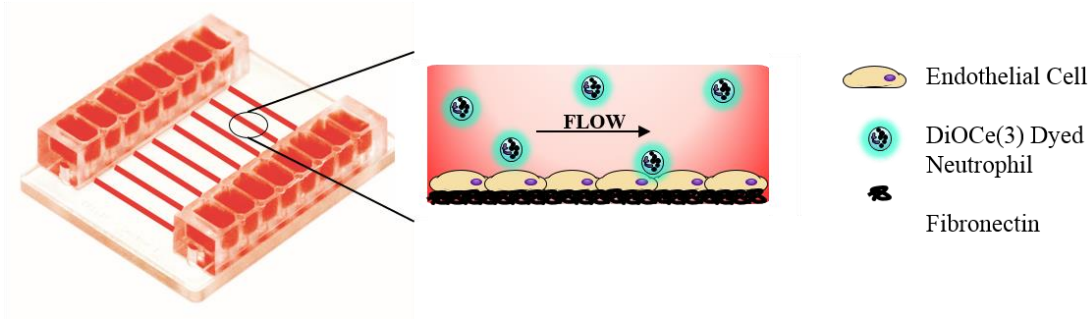

Figure 3-4. Cellix™ assay experimental set-up. A) Cellix™ microfluidics Mirus Evo pump and 8-tube multiflow. B) Vena 8 Endothelial+ chip, showing the 8 channels coated with fibronectin followed by a layer of endothelial cells. Fluorescent neutrophils dyed with DiOCe(3) are then flown across the channel and images taken periodically in order to count the number of adherent neutrophils.

3.2.5.3 Assay Optimisation

The assay was set up as described previously in section 3.2.5.2, assessing the optimum method of detaching HMEC-1 cells from flasks (PBS + 3mM EDTA, Trypsin or Accutase), and the optimum concentration of TNF-α to treat HMEC-1s with after seeding onto the chip (1-10ng/ml) which was assessed by ICAM-1 and VCAM upregulation (assessed by flow cytometry following the basic protocol described in section 2.4.3) and CXCL8 production (assessed by R&D's IL8 Duoset ELISA Kit).

I also tested seeding the chip by growing HMEC-1 cells overnight on the chip under flow conditions using the KimaPump, with a flow rate of 200µl/minute for 2 minutes, followed by 1 minute of no flow in repeated cycles.

The final protocol involved detachment of HMEC-1s using PBS + 3mM EDTA, followed by static growth on the chip then treatment with 5ng/ml TNF-α overnight.

3.2.5.4 Neutrophil Adhesion to a Chemokine-Treated HMEC-1 Monolayer

The day before the assay, Venaflux chip channels were coated with fibronectin and seeded with HMEC-1s (previously stimulated with TNF-α overnight, or unstimulated as a negative control) were seeded onto the chip and left to adhere for 1 hour at 37°C.

HMEC-1 monolayers were treated with a range of concentrations of wild type CXCL8, nitrated CXCL8, Y13F mutant CXCL8 or nitrated Y13F mutant CXCL8 in duplicate for 1 hour at room temperature. Controls received media only. Neutrophils were isolated, flown across each channel in turn, imaged, and the number of adherent cells counted as described above.

3.2.5.5 Immunofluorescence – Heparan Sulphate

Immunofluorescence was performed on HMEC-1 cells seeded onto chamber slides and frozen, following detachment from flasks using PBS+3mM EDTA, Accutase or Trypsin. This was done to visualise the extent of GAG degradation resulting from each of the detachment methods, and was performed as described in section 2.6.2. Briefly, an anti-human heparan sulphate primary antibody (10-E4 clone donated by Laura Ferreras) was used at 1/100 and detected with a goat anti-mouse-Dylight488 secondary antibody. Chamber slides were imaged using a Zeiss AxioImager microscope.

3.2.6 Surface Plasmon Resonance

3.2.6.1 General Principles

Surface plasmon resonance (SPR), performed using Biacore Systems, is a reproducible technique used to study the interactions between molecules without the need for labelling. Firstly the ligand is immobilized onto the surface of the sensorchip (a glass slide coated with a 50nm layer of gold), and then the analyte is flown over the surface. Binding of the analyte to the ligand on the sensorchip surface generates a response, which is proportional to the bound mass, and can be sensitive to changes in the order of picograms per mm^2. As binding events are monitored in real time a range of interaction characteristics can be determined. The gold coating on the sensorchip acts as an electrically conducting surface, and upon binding, electron charge density waves (plasmons) are generated, reducing the polarised light reflected at a specific angle (the resonance angle) in proportion to the mass bound to the surface. The interface must be

in conditions of total internal reflection for SPR to occur. Alterations in binding can therefore be read out in resonance units (RU) [282]. This is shown diagrammatically below in Figure 3-5A.

SA sensorchips (pre-coated with streptavidin), and a running buffer of HBS-P (10mM HEPES pH7.4, 150mM NaCl, 0.005% P20) were used for these experiments. Unless stated all reagents are from GE Healthcare.

3.2.6.2 Heparin Immobilization

Biotinylated heparin was kindly provided by Dr Hugues Lortat-Jacob (Institut de Biologie Structurale, Grenoble, France). Briefly, 1mM heparin (9kDa; Sigma) is dissolved in PBS and incubated with 10mM biotin-LC-hydrazide for 24hr at room temperature. The biotinylated heparin is then dialysed against water to remove any free biotin in the solution. It is essential that GAGs such as heparin are non-biotinylated at the reducing end in order for them to be correctly presented on the surface of the sensorchip. Biotinylated heparin was diluted to a concentration of 16μg/ml in 300mM NaCl and injected using the Biacore Wizard until a target of 200RU was reached.

3.2.6.3 SPR Protocol

Following immobilization of heparin onto the sensorchip surface, SPR was then performed to compare the ability of CXCL8, nitrated CXCL8, Y13F CXCL8 and nitrated Y13F CXCL8 (all at 5-1000nM), to bind to the heparin. Chemokines were flown across the chip at 30μl/min for 2 minutes followed by a 300 second dissociation phase (Figure 3-5B). RU from a flow cell coated with streptavidin only (no biotinylated heparin) was subtracted from the results from the heparin-coated flow cells and analysis was performed using BIAevaluation 4.1 software.

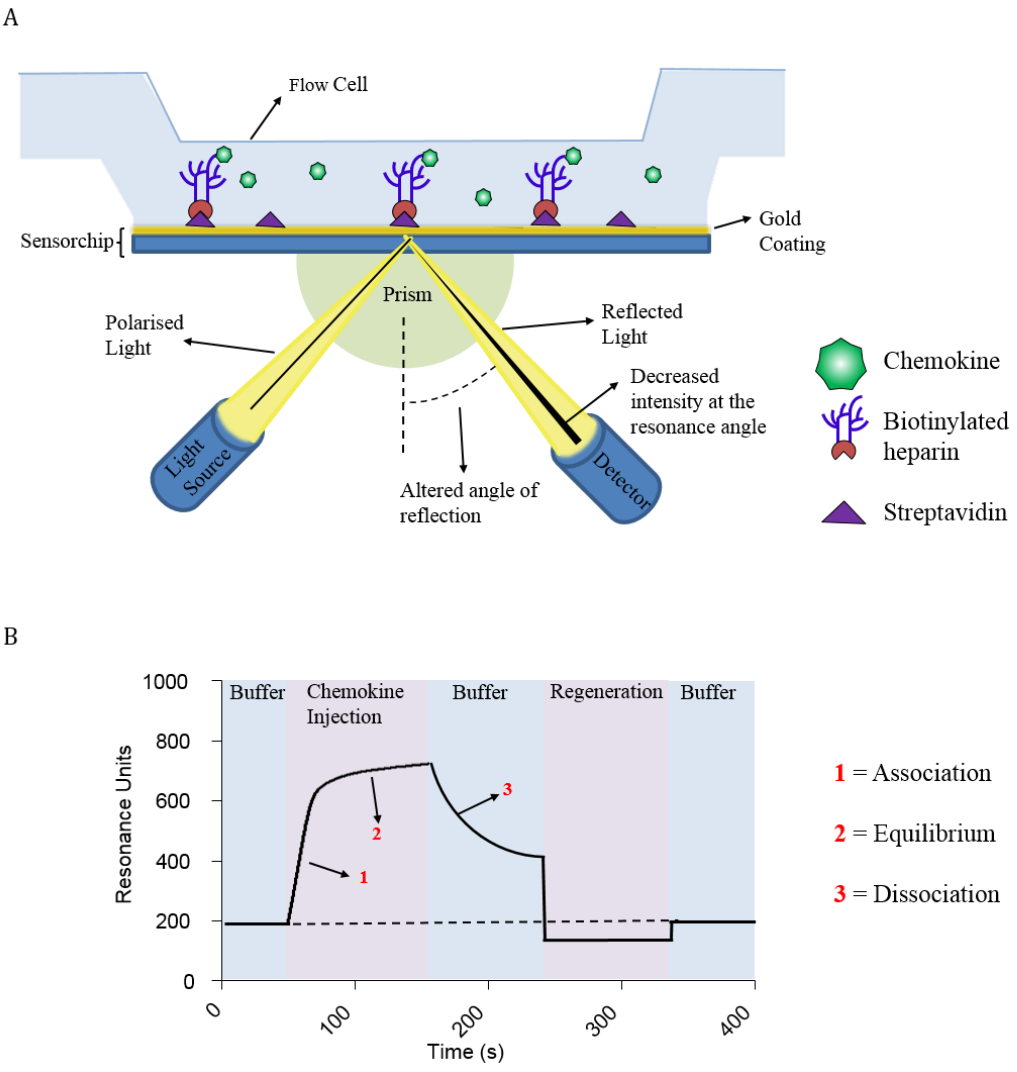

Figure 3-5. The principles of surface plasmon resonance. A) Diagrammatic representation of a surface plasmon resonance (SPR) experiment. The ligand (biotinylated heparin) is flown across the gold-coated sensorchip, where it is immobilised through the interactions between the biotin on the heparin molecules and the streptavidin already pre-coated onto the chip surface. The analyte (chemokine) is them flown across the chip where, if it binds to the immobilized heparin, it will cause a shift in the refractive index and change the SPR angle. B) Diagram of a typical sonogram, showing the change in resonance unit (RU) during analyte binding (association) and dissociation. The more the analyte binds, the higher the RU.

3.2.7 Ion Trap Mass Spectrometry

3.2.7.1 General Principles

Mass spectrometry is a technique, which uses the ratio of mass/charge (m/z) of a compound to determine its molecular mass. Samples are diluted in acid and injected manually or through an attached HPLC system (with 50% outlet diverted into the mass spectrometer), into a small diameter needle at high voltage, which sprays the sample into droplets. The proteins within these droplets are positively charged (due to binding

protons from the acid), and so travel towards the instrument, which is negatively charged. High temperatures and a flow of heated nitrogen cause the droplets to evaporate during the spray. Ions are then held in a 3-dimensional multipolar field within the ion trap by a repelling potential, and through collisions with helium ions also present within the trap (this causes the ions to lose kinetic energy and focuses them in the centre of the trap). The radio frequency (RF) of the ion trap is then increased and ions are ejected out according to their m/z. The mass to charge ratio of each ion is recorded as it hits the detector [283]. This is shown diagrammatically below in Figure 3-6. Usually chemokines (if diluted in 0.1% TFA or 0.1% acetic acid) will produce ions carrying 5 – 15 protons.

This technique was used to assess the nitration of CXCL8 after peroxynitrite incubation, and to analyse the chemokine variants Y13F CXCL8 and nitrated Y13F CXCL8.

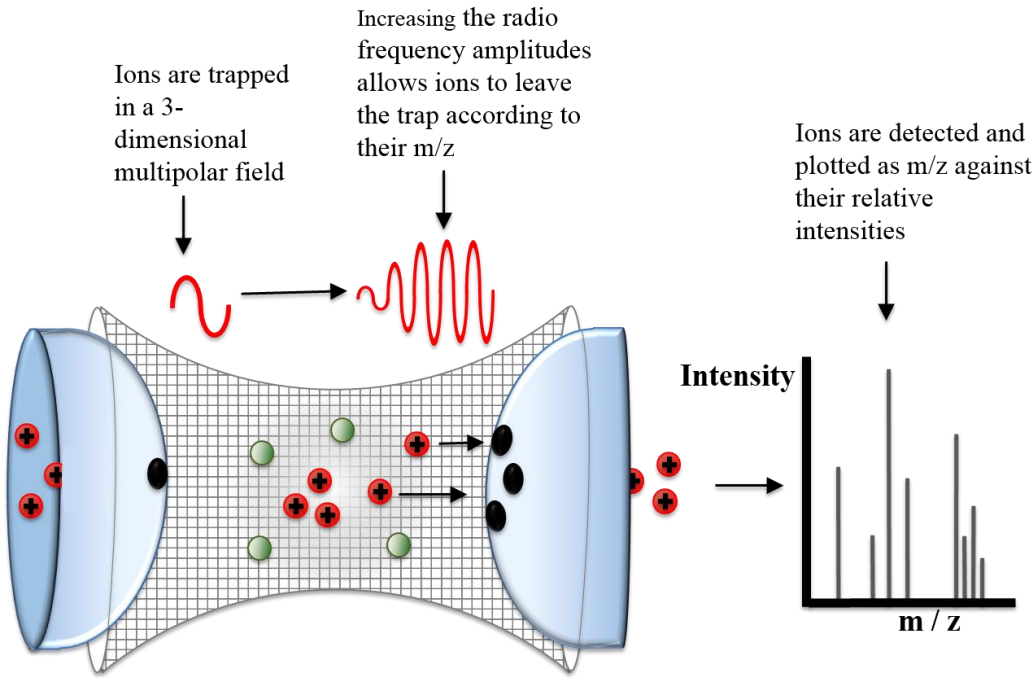

Figure 3-6. The principles of ion trap mass spectrometry. Positively charged protein ions (red circles) are held in the ion trap containing helium ions (green) by a 3-dimensional multipolar field. As the relative frequency of the ion trap is increased, ions will begin to move out of the trap according to their m/z, where they will then be detected and their relative intensities plotted.

3.2.7.2 ZipTip® Preparation of Samples for Manual Injection

Any salts, detergents and contaminants must be removed from the samples before they can be manually injected into the mass spectrometer. This is done through ZipTip® purification (Merck Millipore). ZipTips are 2-20µl pipette tips with a small reverse phase C4 chromatography column within the tip.

Firstly, the tip must be prepared before the sample can be purified. This is done by pipetting up, then ejecting out into a waste tube, 10µl of 50% acetonitrile (repeat 10 times), then 0.1% TFA (repeat 10 times). The entire volume of the sample should then be pipetted up (where the proteins will bind to the column within the tip), and then ejected out into the waste tube. Contaminants are then removed from the sample by pipetting up and ejecting out 10µl of 0.1% acetic acid 10 times, then 10µl of 10% acetonitrile in 0.1% TFA 10 times. The sample is then eluted from the column by pipetting up 10µl of 50% acetonitrile in 0.1% TFA twice, each time ejecting into a clean tube.

3.2.7.3 Sample Running – Mass Spectrometry (MS)

The sample can then be manually injected into the mass spectrometer (Esquire LC, Bruker Daltonics, Germany).

Using Bruker's mass spectrometer software, the sample is set to run at 2µl/minute, at a tune of 1500m/z (as this was found to be optimal for CXCL8), while scanning for peaks from 500-2200m/z. The machine will display a range of ion peaks, plotting m/z on the x-axis and relative intensity on the y-axis. Data should be acquired from the start.

3.2.7.4 Sample Running – Mass Spectrometry/Mass Spectrometry (MS2)

MS2 involves selecting only one individual ion, (± 4Da), and retaining this ion within the ion trap while excluding all others. This is usually the most abundant ion i.e. the ion with the highest relative intensity. The kinetic energy of the ion trap is then increased to increase collisions between the protein ions and helium ions in order to fragment them. This kinetic energy intensity is controlled by an "Amp" setting, which was set to 0.9-1.0 for CXCL8, as this was found to be the optimal setting to cleave the protein at the aspartic acid (D)-proline (P) bond creating two daughter fragments. Setting this value

too low will prevent fragmentation, and setting it too high will result in multiple cleavages at many sites.

The most abundant peaks selected for fragmentation were the 1198.3 peak for wild type CXCL8, the 1204.7 peak for CXCL8 with one nitration. We also attempted to fragment a 1210 peak for nitrated CXCL8, which would be indicative of a molecule with two nitrations. A range of calculated ions for both wild type and nitrated CXCL8, and their m/z values are shown in Table 3-1.

Fragmentation of the 1198.3 or 1204.7 ions at the D-P bond produces a C-terminal fragment and an N-terminal fragment. We could then analyse the m/zs of these fragments to determine at which part of the chemokine contains the nitrated residue.

	Wild Type CXCL8 (72aa)	Nitrated CXCL8 (one nitration) (72aa)
Equation	(m+z)/z	(m+z)/z
Molecular Mass	8381	8381 + 45 = 8426
Ion +3 protons	(8381+3)/3 = 2794.6	(8426+3)/3 = 2809.7
Ion +4 protons	2096.4	2107.5
Ion +5 protons	1677.2	1686.2
Ion +6 protons	1397.8	1405.3
Ion +7 protons	1198.3	1204.7
Ion +8 protons	1048.625	1054.25
Ion +9 protons	932.2	937.2
Ion +10 protons	839.1	843.6

Table 3-1.Mass spectrometry CXCL8 and nitrated CXCL8 ions. Different possible ions of wild type CXCL8 and nitrated CXCL8 and their m/z values. The most abundant ions are in red.

3.3 RESULTS

3.3.1 Assessing the Ability of CXCL8 and CXCL8 Variants to Induce Neutrophil Chemotaxis *in Vitro*

In order to determine the effect that nitration, loss of tyrosine (Y) 13, and nitration without the presence of Y13 had on the ability of CXCL8 to induce neutrophil chemotaxis *in vitro*, trans-filter chemotaxis assays were performed to assess the percentage of 300,000 neutrophils that would migrate through the insert into the well of the plate below in response to 10nM, 20nM or 30nM of CXCL8, nitrated CXCL8, Y13F CXCL8 and nitrated Y13F CXCL8. The results in Figure 3-7A show that wild type CXCL8 induces chemotaxis at all concentrations tested ($p=0.00001$ at 10nM, 20nM and 30nM), whereas the nitrated CXCL8 has almost no chemotactic function at any of the concentrations tested. The Y13F mutant showed equal if not higher levels of chemotaxis induction than the wild type molecule, and the nitrated Y13F mutant showed a reduction in the induction of chemotaxis when compared to the non-nitrated Y13F chemokine ($p=0.00001$ at 10nM and 20nM, and $p=0.0001$ at 30nM). In order to assess migration in a slightly more physiologically relevant model, experiments were repeated with neutrophils migrating through a confluent monolayer of HMEC-1 endothelial cells grown on the filter. This mimics neutrophils infiltrating tissue by migrating through the wall of a blood vessel. The results shown in Figure 3-7B demonstrate that the nitrated chemokine is also unable to induce chemotaxis through an endothelial monolayer. Interestingly, the ability of the Y13F mutant CXCL8 to induce chemotaxis appears to be impaired when cells must cross an endothelial barrier than through the filter alone, although the nitration of this mutant reduces chemotactic ability further, as it did in trans-filter assays.

As tyrosine is one of the key residues targeted by peroxynitrite, we aimed to assess how nitration would affect CXCL1 – which signals through CXCR2 (like CXCL8) but does not contain any tyrosine residues naturally. We also aimed to see how introducing a tyrosine into this chemokine artificially through the use of an L15Y mutant CXCL1 variant, and then nitrating it, would affect function.

Trans-filter chemotaxis assays were performed as described for CXCL8 and its variants; migration of primary blood neutrophils in response to 10nM, 20nM or 30nM of wild type CXCL1, nitrated CXCL1, L15Y mutant CXCL1, and nitrated L15Y CXCL1 was assessed and migrated cells counted using flow cytometry. As with CXCL8, nitration of CXCL1 abolished chemotactic function, however unlike CXCL8 the same effect was observed for the nitrated L15Y mutant (see Figure 3-8A). This suggests that tyrosine is not the only target for peroxynitrite, and that other residues must be present within CXCL1 which are targets for peroxynitrite and essential for the induction of chemotaxis. As CXCL1 does not contain any tryptophan residues, this is likely to be a cysteine or histidine residue, or a combination of multiple residues which further analysis would be needed to confirm. The L15Y mutant CXCL1 could still induce some degree of chemotaxis of neutrophils, although this was reduced in comparison to the values observed for the wild type CXCL1. As with CXCL8, these experiments were repeated in trans-endothelial chemotaxis assays. However, as shown in Figure 3-8B, the percentage of neutrophils that migrated in response to each chemokine varied more so than in the trans-filter assays, and none were found to be significant in comparison to the negative control group.

Chemotaxis assays were also performed *in vitro* using Ibidi® μ-slide chemotaxis assays, using time-lapse microscopic analysis to assess neutrophil migration in response to a gradient of 30nM wild type or nitrated CXCL8, in order to assess the neutrophil response as the cells are actually migrating.

The trajectory plots and analysis in Figure 3-9 show that neutrophils migrated towards wild type CXCL8 with a greater forward migration index, velocity, directness and Euclidean distance than both the negative control and the same concentration of nitrated CXCL8. No difference in any measurement was found between the negative control and nitrated CXCL8.

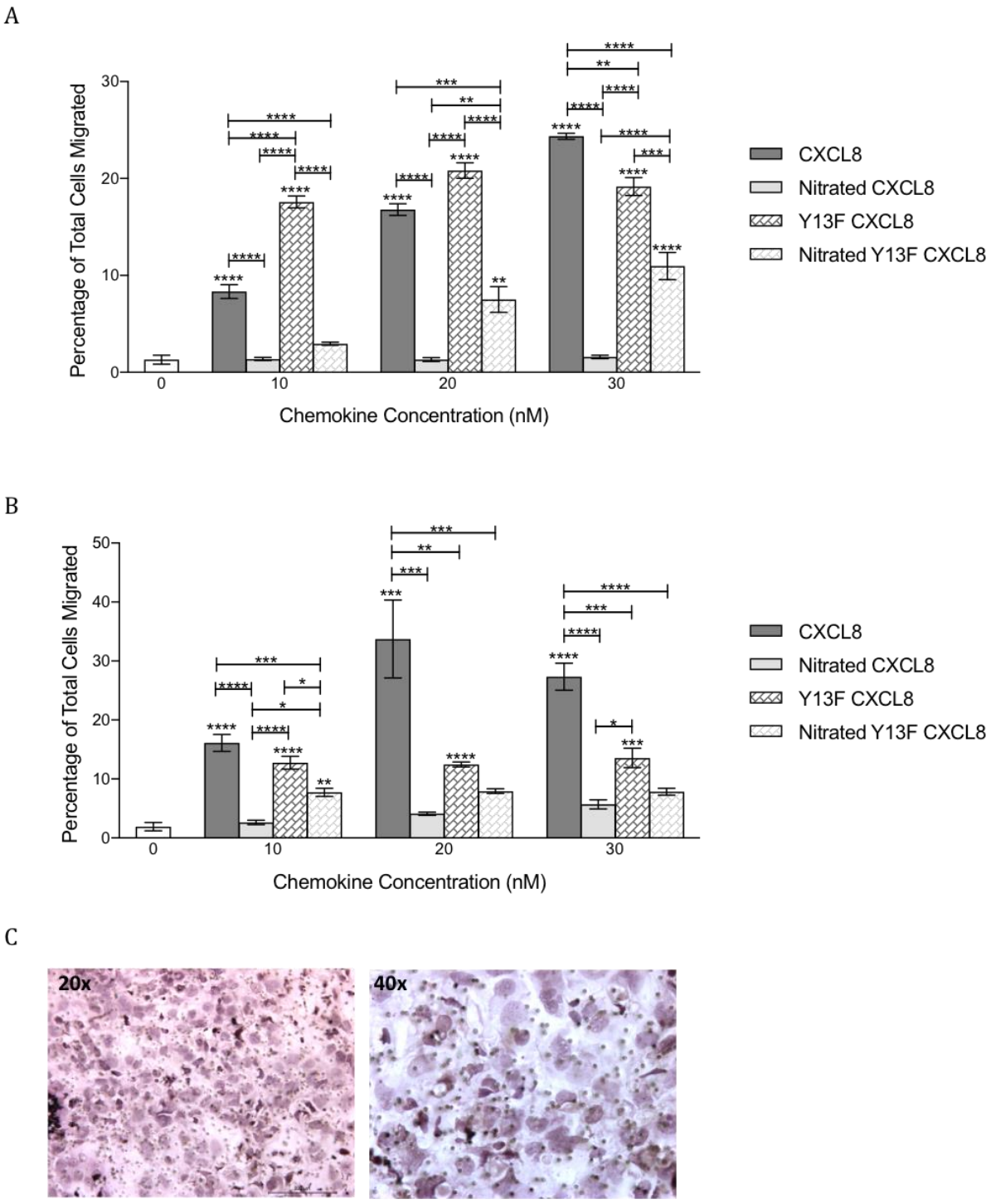

Figure 3-7. Ability of wild type CXCL8, nitrated CXCL8, Y13F CXCL8 and nitrated Y13F CXCL8 to induce neutrophil migration *in vitro*. A) Trans-filter chemotaxis assay, and B) Trans-endothelial chemotaxis assay, showing percentage of total neutrophils that migrated through a bare filter in response to 10nM, 20nM or 30nM of wild type CXCL8, nitrated CXCL8, Y13F mutant CXCL8, and nitrated Y13F mutant CXCL8. C) Images taken at 20x and 40x show the confluent layer of HMEC-1 cells stained with haematoxylin. Data shown in A) is combined from N=2, in B) is combined from N=3, and in C) is representative N=3 experimental replicates (using neutrophils isolated from different blood donors), each with n=3 technical replicates. Statistical analysis was performed using a One Way ANOVA with Tukey's post-test for each concentration individually.

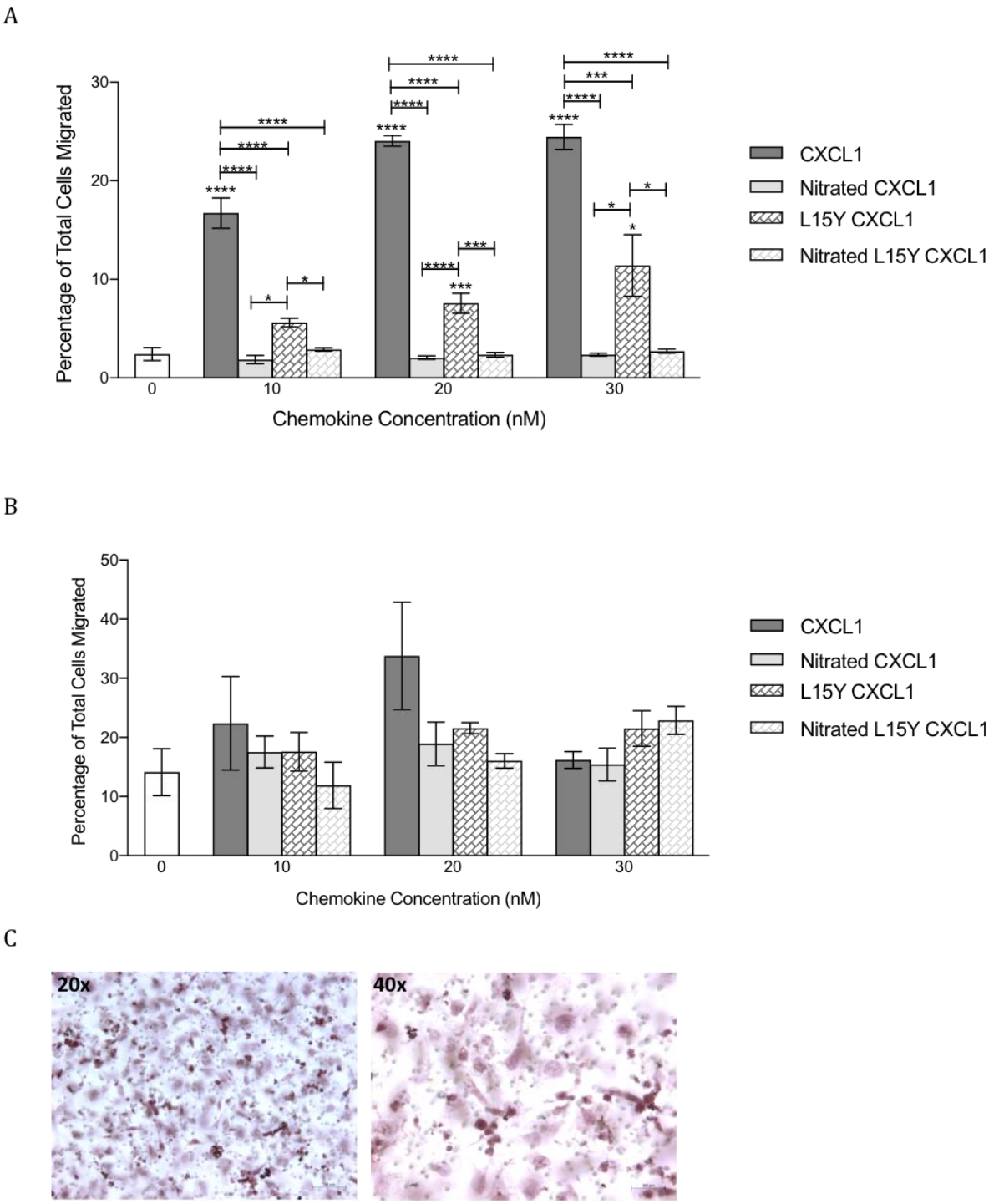

Figure 3-8. Ability of wild type CXCL11, nitrated CXCL1, L15Y CXCL1 and nitrated L15Y CXCL1 to induce neutrophil migration *in vitro*. A) Trans-filter chemotaxis assay, and B) Trans-endothelial chemotaxis assay, showing percentage of total neutrophils that migrated through a bare filter in response to 10nM, 20nM or 30nM of wild type CXCL1, nitrated CXCL1, L15Y mutant CXCL1, and nitrated L15Y mutant CXCL1. C) Images taken at 20x and 40x show the confluent layer of HMEC-1 cells stained with haematoxylin. Data shown in A) is combined from N=2, in B) is combined from N=3, and in C) is representative of N=3 experimental replicates (using neutrophils isolated from different blood donors), each with n=3 technical replicates. Statistical analysis was performed using a One Way ANOVA with Tukey's post-test for each concentration individually.

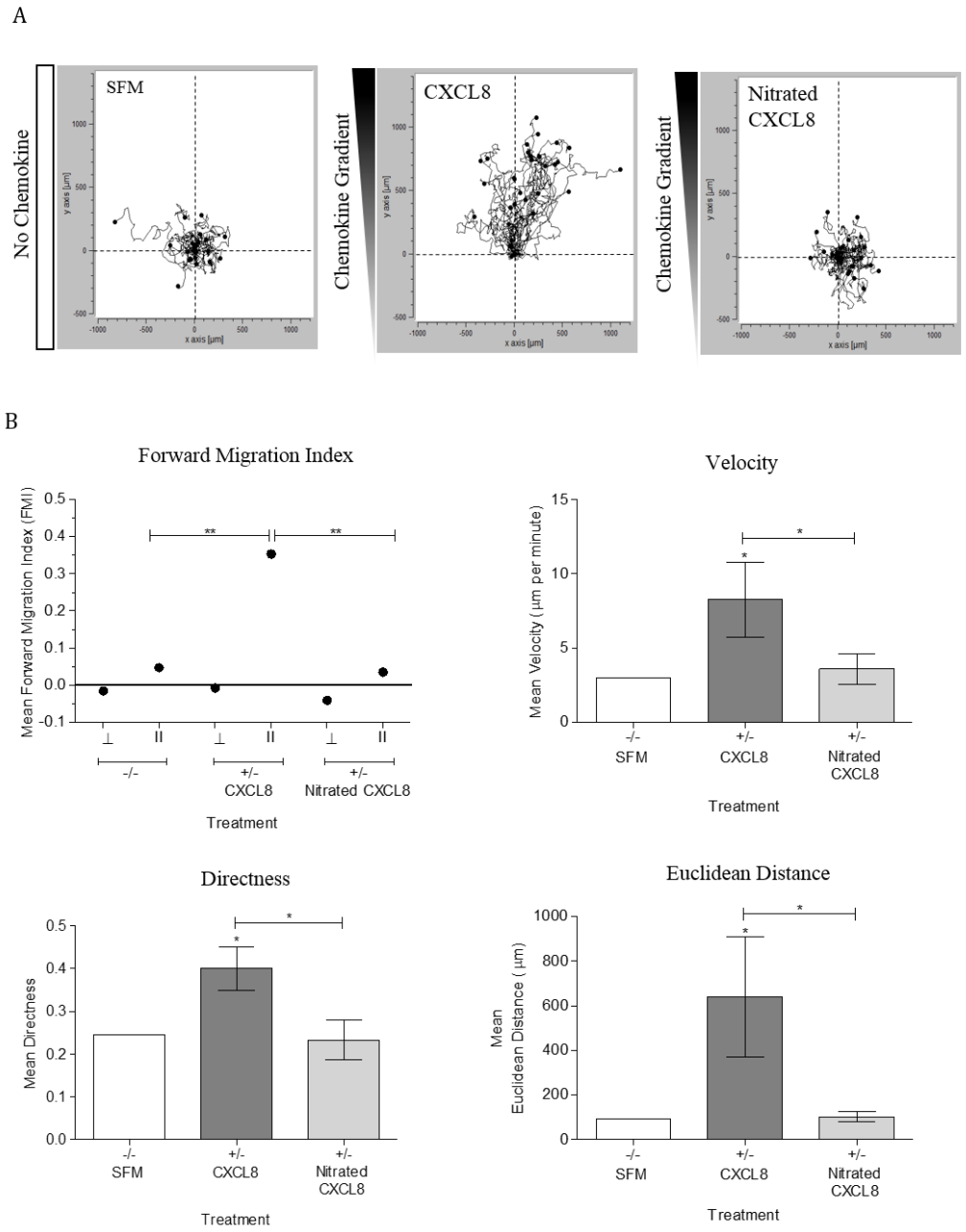

Figure 3-9. Ability of CXCL8 and Nitrated CXCL8 to induce neutrophil migration using Ibidi® µ-Slides and time-lapse microscopic analysis. The cells were seeded onto the slides and a chemotactic gradient was created using serum-free media (SFM) as a negative control and media containing either 30nM wild type or nitrated CXCL8. Cells were observed under a Nikon Multi-Modality inverted microscope, with one image taken every 2 minutes for 3 hours. Image analysis was performed using FIJI's manual tracking plugin, and the trajectories of 40 randomly chosen cells were plotted and analysed using the Chemotaxis and Migration Tool. A) Trajectory animations showing neutrophil chemotaxis in response to SFM, 30nM wild type CXCL8 or 30nM nitrated CXCL8. B) Trajectory analysis showing the mean forward migration index (perpendicular (⊥) and parallel (ll) to the direction of the chemokine gradient), velocity, Euclidean distance and directness of the cells analysed. Data shown in A) is representative of, and B) is combined from, N=3 experimental replicates (using neutrophils isolated from different blood donors), each with n=1 technical replicate. Statistical analysis was performed using a One Way ANOVA with Tukey's post-test.

3.3.2 Assessing the Ability of CXCL8 and Nitrated CXCL8 to Induce Neutrophil Chemotaxis *in vivo*

Having shown that nitration of CXCL8 impairs its ability to induce the migration of primary human neutrophils *in vitro*, I aimed to use the murine air pouch model to assess its functionality *in vivo*. Initial experiments were performed to optimise the concentration of CXCL8 needed to induce neutrophil recruitment, therefore PBS + 0.5% CMC ± 1μg or 3μg of CXCL8 was injected into the pouch. 4 hours later the pouch was lavaged and cells recovered, stained and analysed by flow cytometry. As shown in Figure 3-10A, as a general trend both 1μg and 3μg of CXCL8 appeared to induce the recruitment of neutrophils to the pouch at a higher level than the PBS only control, although this did not reach statistical significance. Monocyte/macrophage/dendritic cell recruitment appeared to stay at a constant basal level. In addition to analysis of cells within the pouch, $1cm^2$ sections of skin from the pouch was removed, embedded in paraffin and then stained with haematoxylin and eosin and for Ly6G to detect any neutrophils recruited to the skin of the pouch itself. This analysis found that 1μg CXCL8 induced the most inflammatory cell infiltrate (Figure 3-10B) and neutrophil infiltrate (Figure 3-10C) to the skin of the pouch. Thus, 1μg CXCL8 was used in all subsequent experiments. Experiments went on to compare cellular migration into the air pouch in response to 1μg CXCL8, 1μg nitrated CXCL8 or both together, however high neutrophil migration was found in response to all treatment groups, including the negative control group. No differences were observed between treatments in either intrapouch cell counts (Figure 3-11A) or immunohistochemical (Figure 3-11B and C) analysis.

I therefore used a different model - intraperitoneal recruitment - for subsequent experiments. Sterile clinical grade saline alone (negative control) or containing 1μg CXCL8 was injected into the peritoneum of the mice, and cells that had migrated into the peritoneum were assessed 6 hours later. These conditions were assessed alongside an additional control group of mice who received no treatment. In this model, some neutrophil recruitment was seen in response to the negative control group injected with saline in comparison to the "no treatment" group, and the CXCL8-treated group showed greater neutrophil recruitment than either control group (Figure 3-12A), although this was not statistically significant. Minimal recruitment of

monocytes/macrophages/dendritic cells was observed in all groups, and showed no difference between treatments. Immunohistochemical staining for Ly6G+ neutrophils in livers taken from these mice showed no significant changes in numbers of infiltrating neutrophils, demonstrating that the neutrophil response is specific and localised to the peritoneum (Figure 3-12B).

The same experimental design was then used to compare neutrophil recruitment in response to nitrated CXCL8, in comparison to wild type CXCL8 (Figure 3-13A). Again, injection of wild type CXCL8 induced a significant increase in neutrophil recruitment in comparison to both the control groups ($p=<0.05$) and nitrated CXCL8 group ($p=<0.05$). Injection of nitrated CXCL8 did not induce an increase in neutrophil recruitment in comparison to injection of saline alone. None ofthe treatments tested induced an increase in migration of monocytes/macrophages/dendritic cells. As before, no increase in neutrophil migration to the liver was observed in any treatment group (Figure 3-13B).

Nitrated CXCL8 is therefore unable to induce migration of primary human neutrophils *in vitro*, or murine neutrophils *in vivo*.

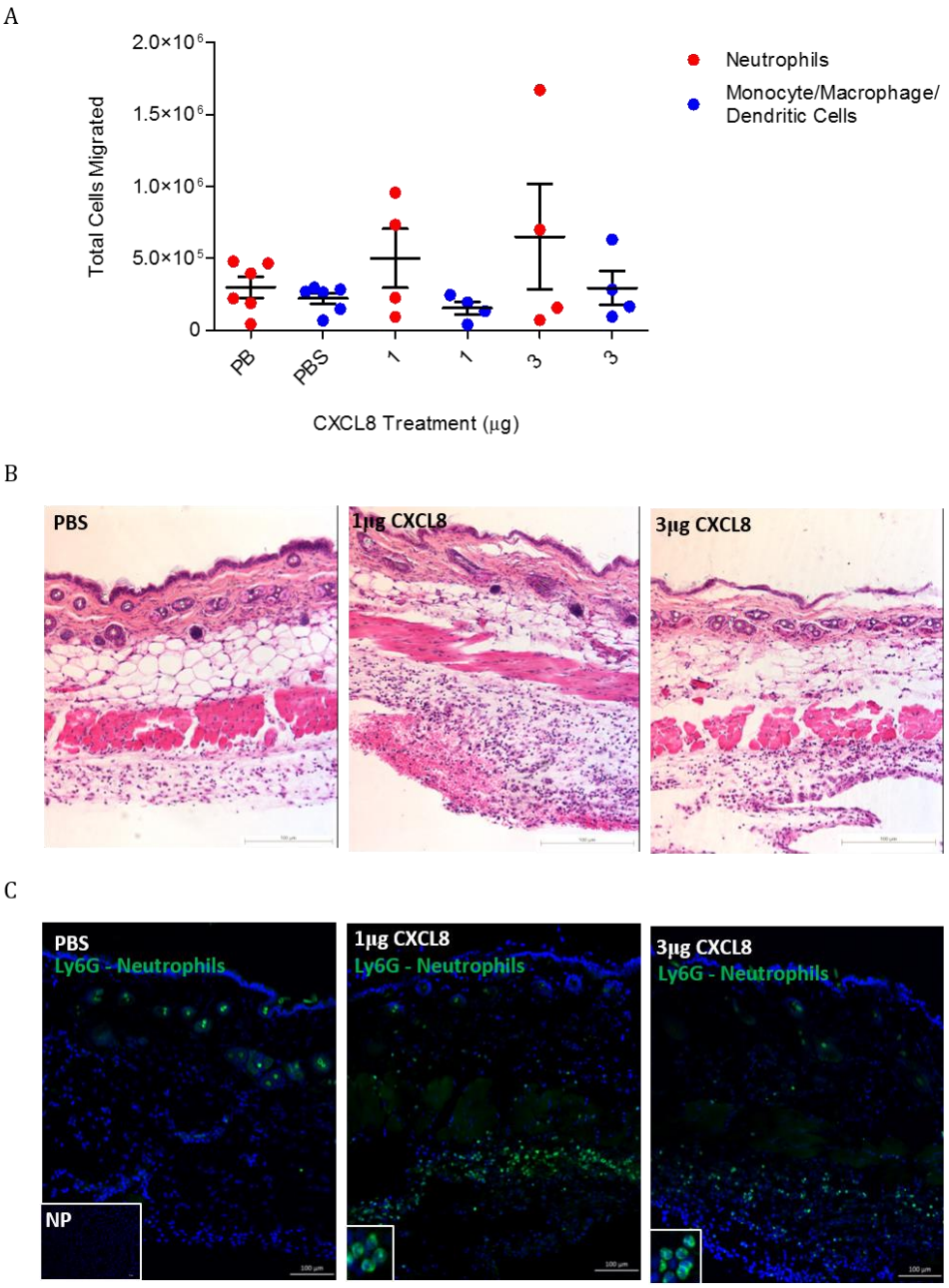

Figure 3-10. Optimising murine intra-pouch recruitment in response to CXCL8. A) Total neutrophil (red dots) and monocyte/macrophage/dendritic cell (blue dots) migration into air pouches 4 hours after intrapouch administration of PBS + 0.5% CMC, 1µg or 3 µg CXL8 (in PBS + 0.5% CMC) was determined. Cells were counted using a TALI automatic cell counter, then stained for CD45, CD14 and Ly6G. Amounts of each cell type (gated at CD45+ Ly6G+ or CD45+ CD14+) were recorded using a FACS Canto III flow cytometer and analysed using FlowJo V10 software. Each symbol represents an animal. 1cm skin sections were shaved and removed from the back of 2 animals per group and stained with B) Haematoxylin and Eosin, or C) anti-Ly6G primary antibody (127623, Biolegend) detected with a Dylight-488 conjugated secondary antibody (GtxMs-003-E488NHSX, Immunoreagents) to show neutrophil recruitment to the skin of the pouch. No primary antibody control is shown indented (NP), as are close-up images of individual Ly6G$^+$ cells. Images were taken at 10x magnification, and images shown are representative of 5 sections analysed per animal. Statistical analysis was performed using a One Way ANOVA with Tukey's post-test.

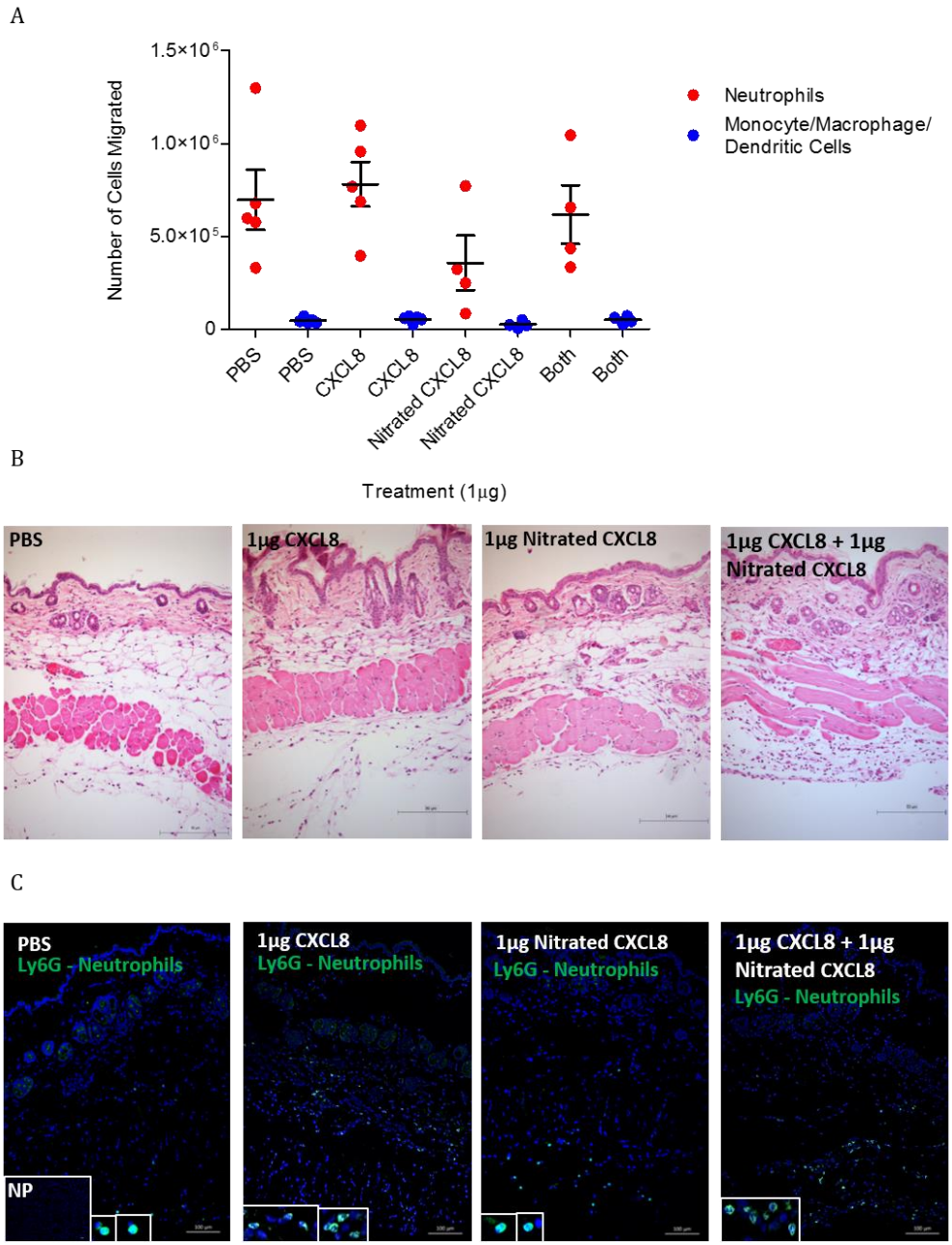

Figure 3-11. Murine intra-pouch recruitment in response to CXCL8 or nitrated CXCL8. A) Total neutrophil (red dots) and monocyte/macrophage/dendritic cell (blue dots) migration into air pouches 4 hours after intrapouch administration of PBS + 0.5% CMC, 1µg CXL8 (in PBS + 0.5% CMC), 1µg Nitrated CXL8 (in PBS + 0.5% CMC), or 1µg of each CXCL8 and Nitrated CXCL8 together, was determined. Cells were counted by using a TALI automatic cell counter, then stained for CD45, CD14 and Ly6G. Amounts of each cell type (gated at CD45+ Ly6G+ or CD45+ CD14+) were recorded using a FACS Canto III flow cytometer and analysed using FlowJo V10 software. Each symbol represents an animal. 1cm skin sections were shaved and removed from the back of 2 animals per group and stained with B) Haematoxylin and Eosin, or C) anti-Ly6G primary antibody (127623, Biolegend) detected with a Dylight-488 conjugated secondary antibody (GtxMs-003-E488NHSX, Immunoreagents) to show neutrophil recruitment to the skin of the pouch. No primary antibody control is shown indented (NP), as are close-up images of individual Ly6G$^+$ cells. Images were taken at 10x magnification, and images shown are representative of 5 sections analysed per animal. Statistical analysis was performed using a One Way ANOVA with Tukey's post-test.

A

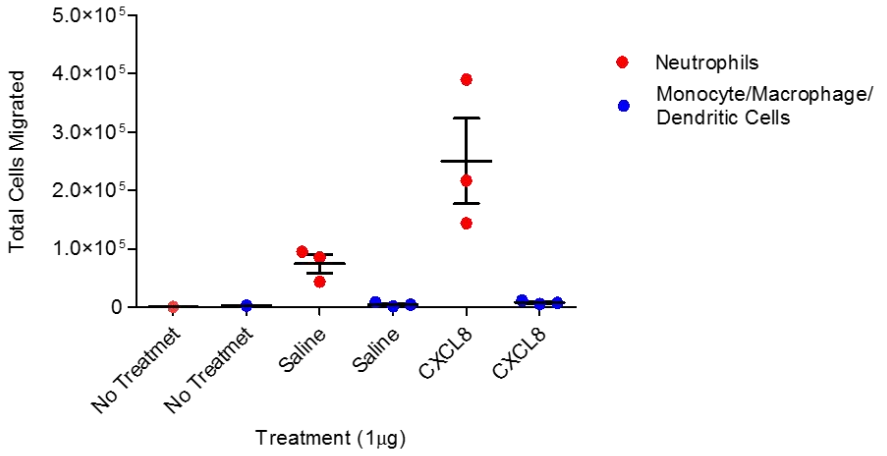

B

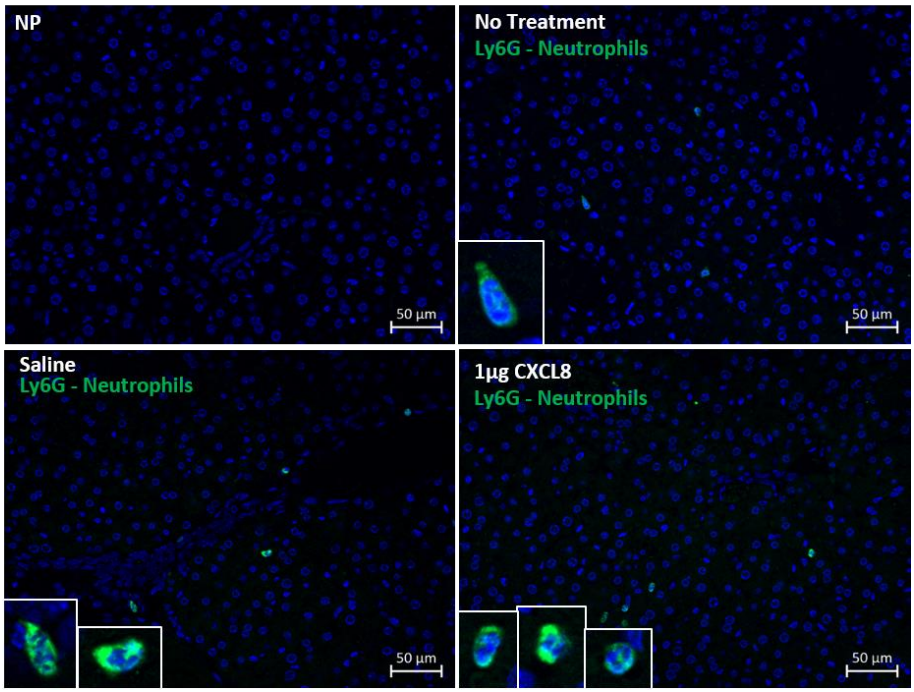

Figure 3-12. Murine intra-peritoneal recruitment in response to CXCL8. A) Total neutrophil (red dots) and monocyte (blue dots) migration into the mouse peritoneum 6 hours after intra-peritoneal administration of sterile clinical grade saline or 1µg wild type CXCL8. 500µl PBS ± 1µg of CXCL8 was injected in to the peritoneum of the mice, and was left for 6 hours to allow cells to migrate. Mice were then sacrificed, and the peritoneum lavaged with PBS + 3mM EDTA to collect cells. The lavage was then stained and the cells analysed and counted using a BD Accuri C6 flow cytometer. Shown are the total numbers of live neutrophils (Sytox Red$^-$ CD45$^+$ Ly6G$^+$, red dots) and live monocyte/macrophage/dendritic cells measured as a control (Sytox Red$^-$ CD45$^+$ CD14$^+$). Each dot represents an individual animal. B) Sections from the large lobe of the liver stained with anti-Ly6G primary antibody (127623, Biolegend) detected with a Dylight-488 conjugated secondary antibody (GtxMs-003-E488NHSX, Immunoreagents). No primary antibody control =NP. Close-up images of individual Ly6G$^+$ cells are indented. Images taken at 20x magnification, and images are representative of 5 sections stained from n=1 no treatment mouse, and n=2 mice from the other treatment groups. Statistical analysis was performed using a One Way ANOVA with Tukey's post-test.

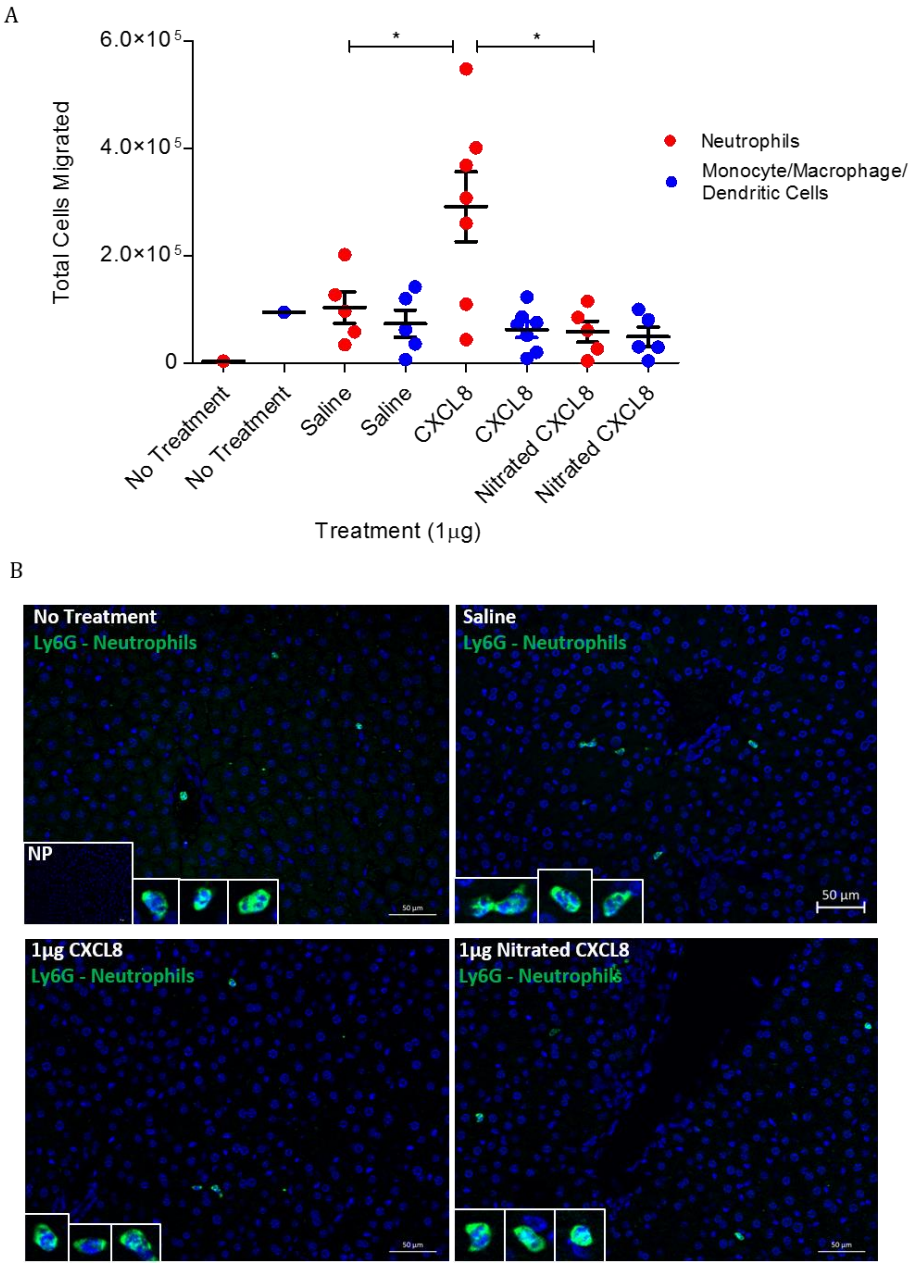

Figure 3-13. Murine intra-peritoneal recruitment in response to CXCL8 or nitrated CXCL8. A) Total neutrophil (red dots) and monocyte (blue dots) migration into the mouse peritoneum 6 hours after intra-peritoneal administration of sterile clinical grade saline, 1μg wild type CXCL8 or 1μg nitrated CXCL8. 500μl PBS ± 1μg of chemokine was injected in to the peritoneum the mice, and was left for 6 hours to allow cells to migrate. Mice were then sacrificed, and the peritoneum lavaged with PBS + 3mM EDTA to collect cells. The lavage was then stained and the cells analysed and counted using a BD Accuri C6 flow cytometer. Shown are the total numbers of live neutrophils (Sytox Red$^-$ CD45$^+$ Ly6G$^+$, red dots) and live monocyte/macrophage/dendritic cells measured as a control (Sytox Red$^-$ CD45$^+$ CD14$^+$). Each dot represents an individual animal. B) Sections from the large lobe of the liver stained with anti-Ly6G primary antibody (127623, Biolegend) detected with a Dylight-488 conjugated secondary antibody (GtxMs-003-E488NHSX, Immunoreagents). No primary antibody control is shown indented (NP), as are close-up images of individual Ly6G$^+$ cells. Images taken at 20x magnification, and images are representative of 5 sections stained from n=1 no treatment mouse, and n=2 mice from the other treatment groups. Statistical analysis was performed using a One Way ANOVA with Tukey's post-test.

3.3.3 Assessing the Receptor Signalling Capabilities of CXCL8 and CXCL8 Variants

In order to discover which aspects of chemokine biology (i.e. GAG binding or GPCR signalling) were affected by nitration and thus were the cause of the decrease in neutrophil recruitment seen after nitration, further experiments were performed.

Calcium flux assays were used to measure the ability of CXCL8, nitrated CXCL8, Y13F CXCL8 and nitrated Y13F CXCL8 to induce GPCR signalling and subsequent calcium mobilization in primary neutrophils labelled with Indo-1. Results in Figure 3-14A and B show that CXCL8 induced a calcium flux of ~350nM, a significant increase in comparison to neutrophils stimulated with PBS only ($p=<0.001$). Nitrated CXCL8 induced a 10-fold lower amount of calcium flux than wild type CXCL8 ($p=<0.01$), which was not statistically different from that of PBS-stimulated neutrophils which were used as a negative control. Y13F and nitrated Y13F CXCL8 also showed a significantly impaired ability to induce calcium flux, when compared to wild type CXCL8 ($p=<0.05$). Again, it appears that the loss of tyrosine 13 does inhibit chemokine function in the Y13F mutant chemokine, however a far more substantial inhibition occurs when tyrosine 13 is present and nitrated.

To verify these results, neutrophils were treated for 2, 5 or 10 minutes with 30nM of each of the chemokine variants, and Western blot analysis was performed on the lysates to detect phosphorylated-ERK as another downstream consequence of GPCR signalling. The results in Figure 3-15 show that CXCL8-treatment for 2 and 5, but not 10, minutes induces rapid ERK phosphorylation, with less phosphorylated ERK detected in neutrophils stimulated with Y13F or nitrated Y13F CXCL8. Stimulation with nitrated CXCL8 did not induce any detectable ERK phosphorylation.

As mentioned previously, both CXCR1 and CXCR2 are known to be involved in neutrophil chemotaxis in response to large and small concentrations of CXCL8 respectively. I aimed to confirm which of the two receptors was largely responsible for the signalling cascade resulting in calcium flux and ERK phosphorylation in response to wild type CXCL8. Thus trans-filter chemotaxis assays were performed, where neutrophils were incubated with 20μM neutralizing antibodies against CXCR1 and/or CXCR2 prior to migration in response to wild type CXCL8 only. The results in Figure 3-16 show that 30nM CXCL8 induces a significant increase in neutrophil migration in comparison to the negative control ($p=<0.05$), and only the CXCR1 neutralizing antibody

used at 20μM decreases this migration, although this decrease was not found to be statistically significant. Incubation with the anti-CXCR2 antibody showed no reduction in migration, and no additional reduction when used in combination with the anti-CXCR1 antibody.

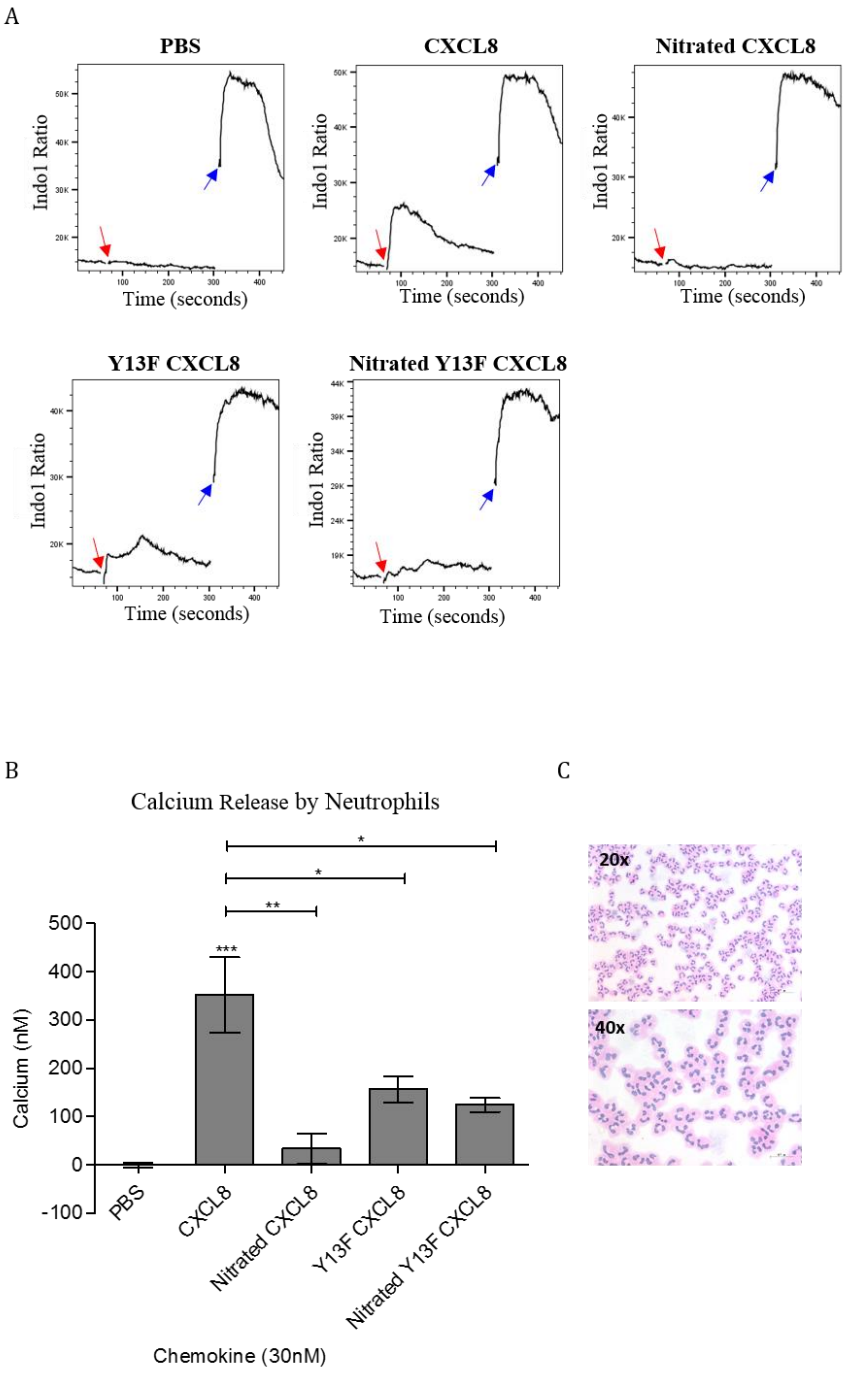

Figure 3-14. Ability of wild type CXCL8, nitrated CXCL8, Y13F CXCL8 and nitrated Y13F CXCL8 to induce calcium signalling in neutrophils. A) Calcium flux in response to PBS, 30nM of CXCL8, nitrated CXCL8, Y13F CXCL8 or nitrated Y13F CXCL8 added to the cells after 60 seconds (red arrow). 10µg/ml of Ionomycin was used as a positive control and added at 300 seconds (blue arrow). B) Calcium release (nM) in response to the above treatments calculated using the equation $[Ca^{2+}] = kd \times (R - Rmin) / (Rmax - R)$, where the kd = 844 nM/L [284,285]. C) Haematoxylin and Eosin staining of a cytospin collected from the cell population, showing a high percentage purity of neutrophils. Images were taken using light microscopy at 20x and 40x magnification. Data shown in A) and C) is representative of, and in B) is combined from, N=3 experimental replicates (using neutrophils isolated from different blood donors), each with n=1 technical replicate. Statistical analysis was performed using a One Way ANOVA with Tukey's post-test.

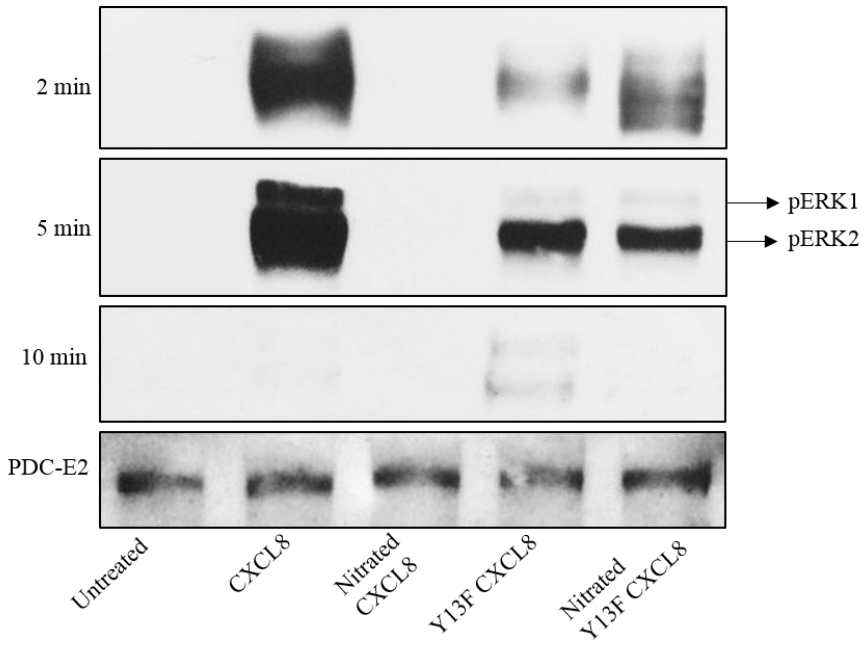

Figure 3-15. Ability of wild type CXCL8, nitrated CXCL8, Y13F CXCL8 and nitrated Y13F CXCL8 to induce ERK phosphorylation in neutrophils. Isolated neutrophils were treated for 2, 5 or 10 minutes with 30nM of the chemokine variants, with unstimulated cells used as a negative control. Lysates where then prepared and used in Western blotting experiments with an anti-phosphorylated ERK1/2 antibody (36-8800, ThermoFisher Scientific) followed by an anti-rabbit-HRP antibody (A6154, Sigma), as well as anti-pyruvate dehydrogenase complex (PDC-E2) antibody as loading control followed by anti-human-HRP antibody (AP112P, Sigma). Data shown is representative of N=3 experimental replicates (using neutrophils isolated from different blood donors), each with n=1 technical replicate.

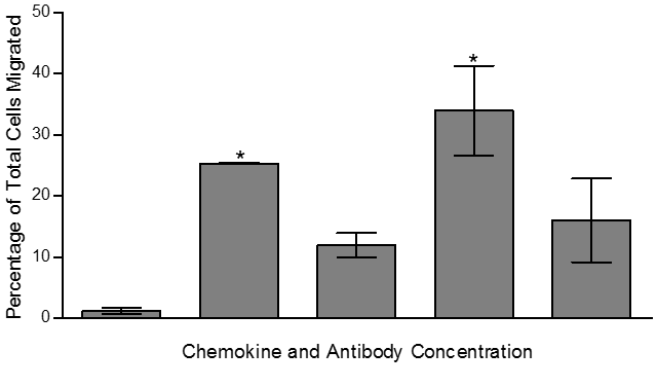

30nM CXCL8	-	+	+	+	+
20µM Anti-CXCR1	-	-	+	-	+
20µM Anti-CXCR2	-	-	-	+	+

Figure 3-16. Migration of neutrophils in response to CXCL8 following incubation with anti-CXCR1/CXCR2 antibodies. Trans-filter chemotaxis assays showing percentage of total neutrophils that migrated through a bare filter in response to 30nM CXCL8 after pre-treatment with 20µM anti-CXCR1 antibody (Ab89251, Abcam), anti-CXCR2 antibody (Ab10401, Abcam) or both antibodies together. Data shown is representative of N=3 experimental replicates (using neutrophils isolated from different blood donors), each with n=3 technical replicates. Statistical analysis was performed using a One Way ANOVA with Tukey's post-test.

3.3.4 Assessing the GAG Binding Capabilities of CXCL8 and CXCL8 Variants

In order to assess the ability of the CXCL8 variants to bind to GAGs, flow-based adhesion assays were performed using Cellix™ technology, whereby neutrophils were flown over an HMEC-1 endothelial cell monolayer untreated or pre-treated with TNF-α ± chemokine. This aimed to test the ability of the chemokine variants to bind to GAGs present on the endothelial cells, as measured by subsequent neutrophil adherence. Initial experiments involved optimising the detachment method used to remove HMEC-1 cells from tissue culture flasks before seeding onto Cellix™ VenaFlux Endothelial+ Biochips, and the concentration of TNF-α needed to stimulate the endothelial cells once coated onto the Biochip. This was done in order to induce an adequate increase in adhesion molecule expression, but without increasing the production of CXCL8 significantly.

Single immunofluorescence staining of chamber slides in Figure 3-17 below shows that detachment of cells with trypsin decreases expression of heparan sulphate for up to 6 hours, detachment with Accutase decreases expression for up to 2 hours, and detachment with PBS + 3mM EDTA does not affect heparan sulphate expression. Therefore, the latter was the detachment method used in all subsequent experiments to avoid the degradation/cleavage of GAGs as much as possible. To assess the optimum TNF-α concentration to use for stimulation and upregulation of adhesion molecule expression, HMEC-1 cells were treated for 2 hours or 16 hours with 1-10ng/ml of TNF-α, then stained for ICAM-1 and VCAM and analysed by flow cytometry. Cell supernatant was also collected and analysed for CXCL8 production by ELISA. All concentrations tested induced a significant upregulation of both VCAM and ICAM-1 when HMEC-1 cells were treated for both 2 hours and 16 hours, whereas CXCL8 production only increased significantly when cells were treated with 10ng/ml TNF-α for 2 hours or with 2.5, 5 and 10ng/ml for 16 hours (Figure 3-18A and B).

In order to achieve maximum upregulation of adhesion molecules, the 16 hour treatment was taken forward to be assessed in a flow-based adhesion assay, to measure the number of neutrophils adhering to channels coated with HMEC-1 monolayers previously treated with the varying concentrations of TNF-α. Time-lapse images were taken of each channel as neutrophils were flown across at 0.5 dyne/cm^2; a physiological flow rate mimicking that of the circulation. The number of adhering neutrophils were

then counted in each image, and calculated for each channel as shown in Figure 3-19A below. Figure 3-19B shows representative images from each channel, and an example image of a confluent HMEC-1 monolayer coating a channel. Only 5ng/ml and 10ng/ml TNF-α treatment inducing significant adhesion of neutrophils above the level of the negative control group ($p=<0.001$).

Various experiments were then performed to assess how pre-treatment of the HMEC-1 endothelial layer with CXCL8, nitrated CXCL8, Y13F CXCL8 and nitrated Y13F CXCL8 would affect neutrophil adhesion. This was attempted with HMEC-1 cells grown both statically and under flow conditions on the chip using a Kima pump, with 5ng/ml TNF-α treatment administered to the HMEC-1 cells statically at both 2 hours and 16 hours, and with varying concentration of the chemokine variants added to the HMEC-1 monolayers. Results proved inconsistent (data not shown), with no additional adhesion seen in response to CXCL8 treatment + TNF-α treatment above the level of TNF-α treatment alone.

As an alternative method to assess GAG binding, Surface Plasmon Resonance (SPR) was performed to assess the ability of CXCL8, nitrated CXCL8, Y13F CXCL8 and nitrated Y13F CXCL8 to bind to immobilized heparin as a model GAG under flow conditions. Results in Figure 3-20 show that nitration of both wild type and Y13F mutant CXCl8 almost completely abolishes binding to heparin. Nitration therefore affects CXCL8 function through inhibition of GAG binding as well as receptor signalling. Loss of Y13 without nitration shows a smaller decrease in binding in comparison to the wild type CXCL8 (Figure 3-20)., and also indicates altered binding properties for the Y13F mutant in comparison to the wild type chemokine. While neither curve reached saturation under the experimental conditions used, the binding curve observed for wild type CXCL8 shows two distinct binding modes indicated by the different trajectories within the curve – the fast off rate (at 200-250 seconds) and then binding which does not return to baseline (at 250-600 seconds). The former is indicative of chemokine monomers which quickly dissociate from the immobilised heparin, whereas the latter is indicative of chemokine oligomers forming on the surface of the chip as the multiple GAG-binding domains within oligomersers mean that the oligomer never fully detaches from the chip surface– when one binding domain dissociates another immediately re-associates. The binding curve observed for Y13F CXCL8 indicates only monomeric binding occurred in the case of the mutant chemokine.

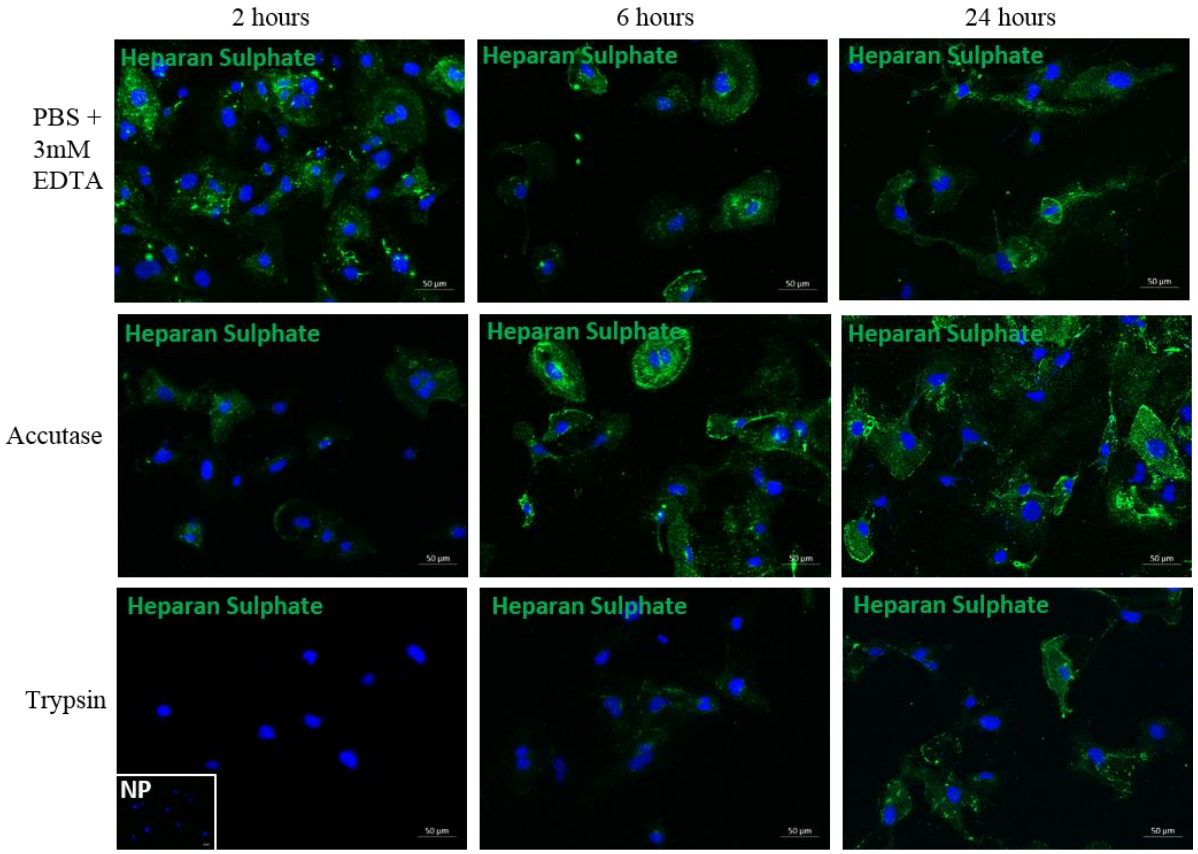

Figure 3-17. Single immunofluorescence staining to detect Heparan Sulphate expression by HMEC-1 cells 2, 6 or 24 hours after detachment from flasks using PBS + 3mM EDTA, Accutase or Trypsin. Staining was performed using an anti-human heparan sulphate antibody (10E4 clone) donated by a collaborator, and detected with a Goat anti-mouse-DyLight®488 conjugated secondary antibody (GtxMs-003-E488NHSX, Immunoreagents). No primary antibody control is shown indented (NP). Images were taken at 20x magnification, and images shown are representative of 5 fields of view imaged per chamber.

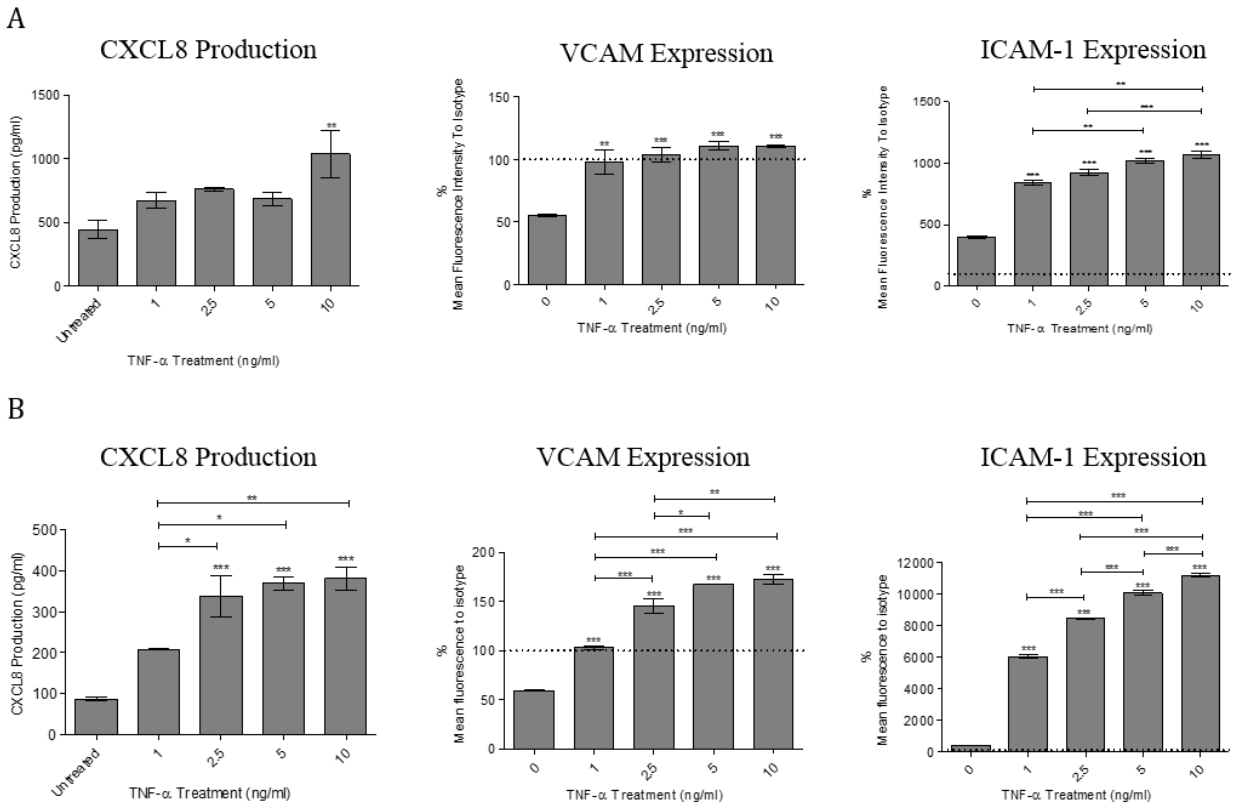

Figure 3-18. CXCL8 Production, and VCAM and ICAM-1 expression following TNF-α treatment. HMEC-1 cell expression of CXCL8 assessed using Peprotech's CXCL8 ELISA kit, and expression of VCAM (305805, Biolegend) and ICAM-1 (353105, Biolegend) assessed using flow cytometry as the percentage increase in mean fluorescence intensity as compared to the isotype control (12-4714-42, ThermoFisher Scientific), which is indicated at 100% by the dotted line, after A) 2 hours and B) 16 hours of treatment with 0-10ng/ml TNF-α. Data shown in A) is representative of N=3 experimental replicates, each with n=3 technical replicates, and in B) of N=2 experimental replicates, each with n=3 technical replicates. Statistical analysis was performed using a One Way ANOVA with Tukey's post-test.

A

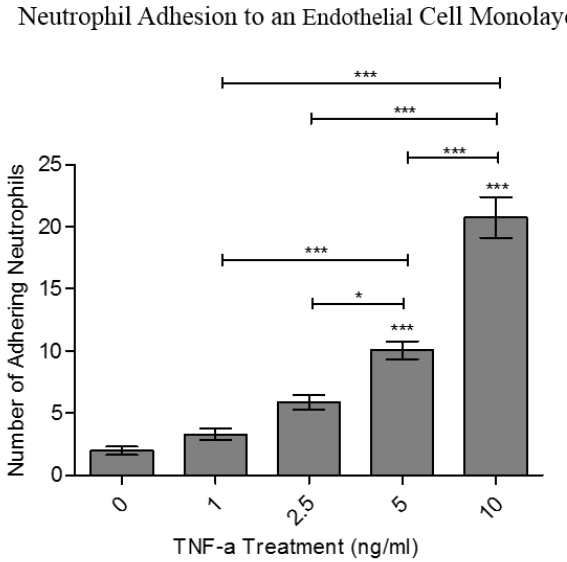

B

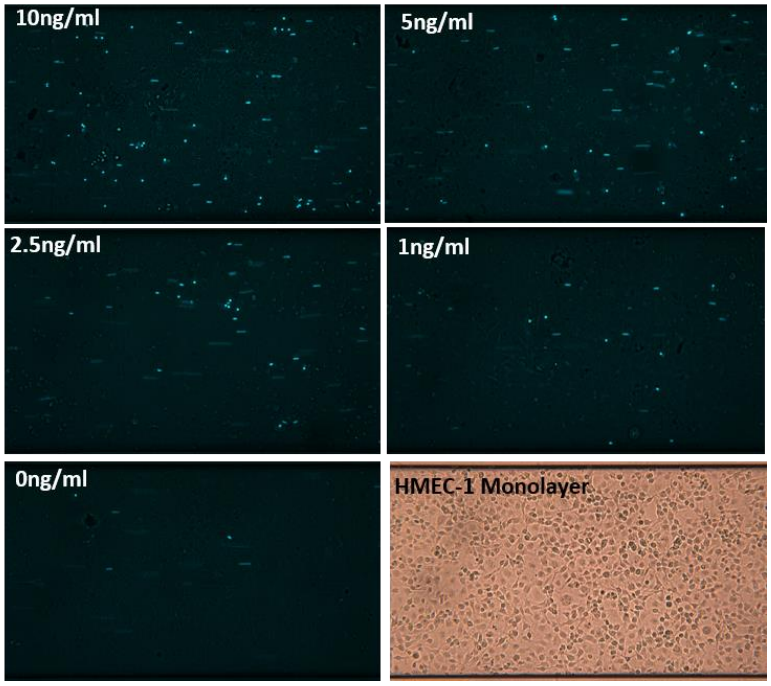

Figure 3-19. Neutrophil adhesion to an HMEC-1 monolayer treated for 16 hours with 0-10ng/ml TNF-α. Neutrophils were flown over HMEC-1 cell monolayers which has been pre-treated for 16 hours with a range of TNF-α concentrations (ng/ml) at 0.5 dyne/cm^2. Adhering neutrophils were counted using ImageJ, from 5 sequential images per position, 5 positions per channel. B) Fluorescent images of DiOCe(3) labelled neutrophils adhering to an HMEC-1 cell monolayer, and a brightfield image of the HMEC-1 monolayer. Both were taken using the Cellix™ imaging platform at 20x magnification. Data shown in A) and B) is representative of N=2 experimental replicates (using neutrophils isolated from different blood donors), each with n=2 technical replicates. Statistical analysis was performed using a One Way ANOVA with Tukey's post-test.

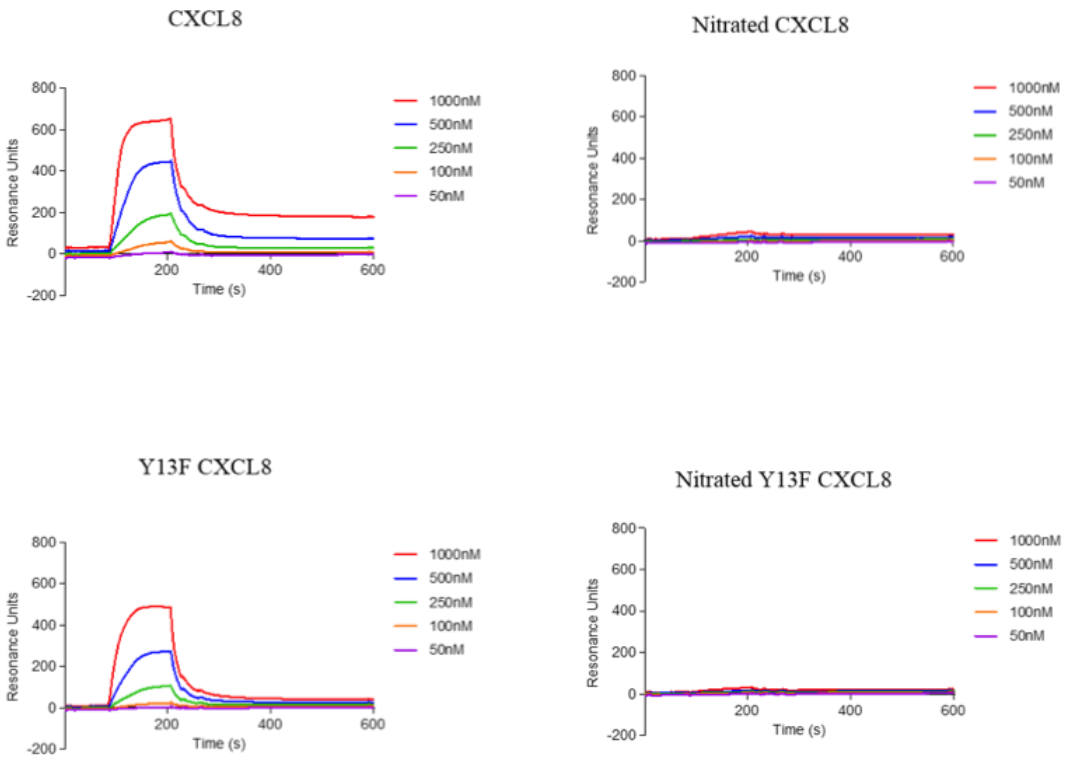

Figure 3-20. Altered heparin binding ability of CXCL8 when nitrated and/or mutated. Biacore was used to assess the ability of wild type CXCL8, nitrated CXCL8, Y13F mutant CXCL8 and nitrated Y13F CXCL8 to bind heparin. 50- 1000nM chemokine was flowed over immobilised heparin (159.6RU bound) and the alteration in resonance units (RU) as a result of binding is shown. Data shown is representative of N=3 experimental replicates, each with n=1 technical replicate.

3.3.5 Assessing the Ability of Nitrated CXCL8 to Inhibit the Function of CXCL8

Having found that nitration of CXCL8 impairs its ability to signal through its GPCRs and to bind to GAGs, I aimed to assess whether the nitrated chemokine was capable of inhibiting its wild type counterpart when neutrophils were treated with both chemokines in an equimolar ratio (30nM). In chemotaxis assays, Figure 3-21 shows that, as previously found, CXCL8 induces significant migration of neutrophils above the negative control in both trans-filter (A) ($p=<0.001$) and trans-endothelial (B) ($p=<0.01$) assays, and nitrated CXCL8 does not induce migration above the level of the negative control. Addition of both CXCL8 and nitrated CXCL8 together also shows significant migration in comparison to the negative control (A) ($p=<0.001$) (B) ($p=<0.05$), and this was found to be no different to treatment with CXCL8 alone.

The same pattern was observed in calcium flux assays shown in Figure 3-22A and B; addition of CXCL8 and nitrated CXCL8 together showed a significant increase in calcium release in comparison to the PBS control group ($p=<0.05$), but this was no different to calcium release after neutrophils were treated with CXCL8 alone.

Nitrated CXCL8 is therefore unable to inhibit the function of wild type CXCL8, when used at equimolar concentrations. Higher concentrations were not assessed in this study.

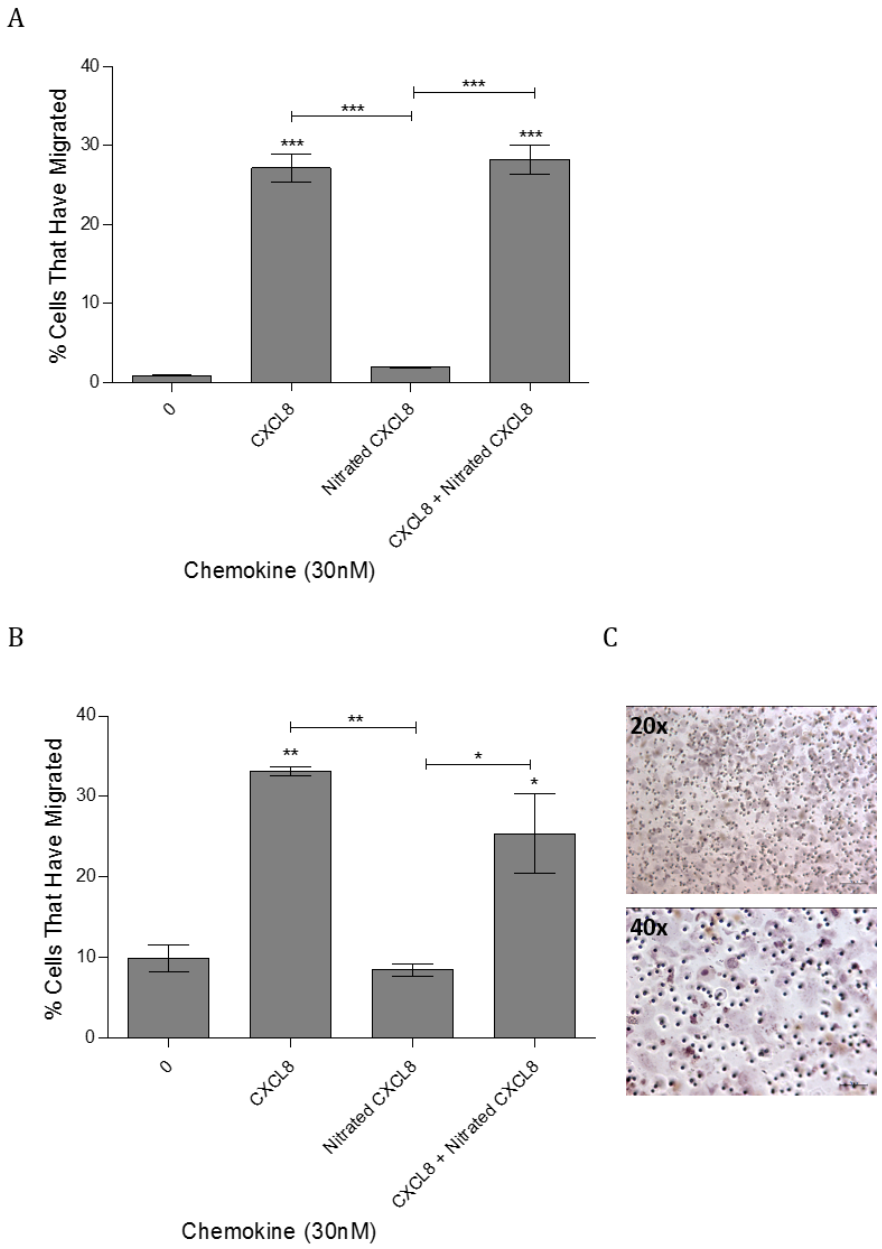

Figure 3-21. Ability of nitrated CXCL8 to inhibit neutrophil migration in response to wild type CXCL8 *in vitro*. A) Trans-filter chemotaxis assays and, B) Trans-endothelial chemotaxis assays, showing percentage of total neutrophils that migrated through a bare filter in response to 30nM wild type CXCL8, 30nM nitrated CXCL8, or 30nM of both together. C) Images taken at 20x and 40x show the confluent layer of HMEC-1 cells stained with haematoxylin. Data shown for A), B) and C) is representative of N=3 experimental replicates (using neutrophils isolated from different blood donors), each with n=3 technical replicates. Statistical analysis was performed using a One Way ANOVA with Tukey's post-test.

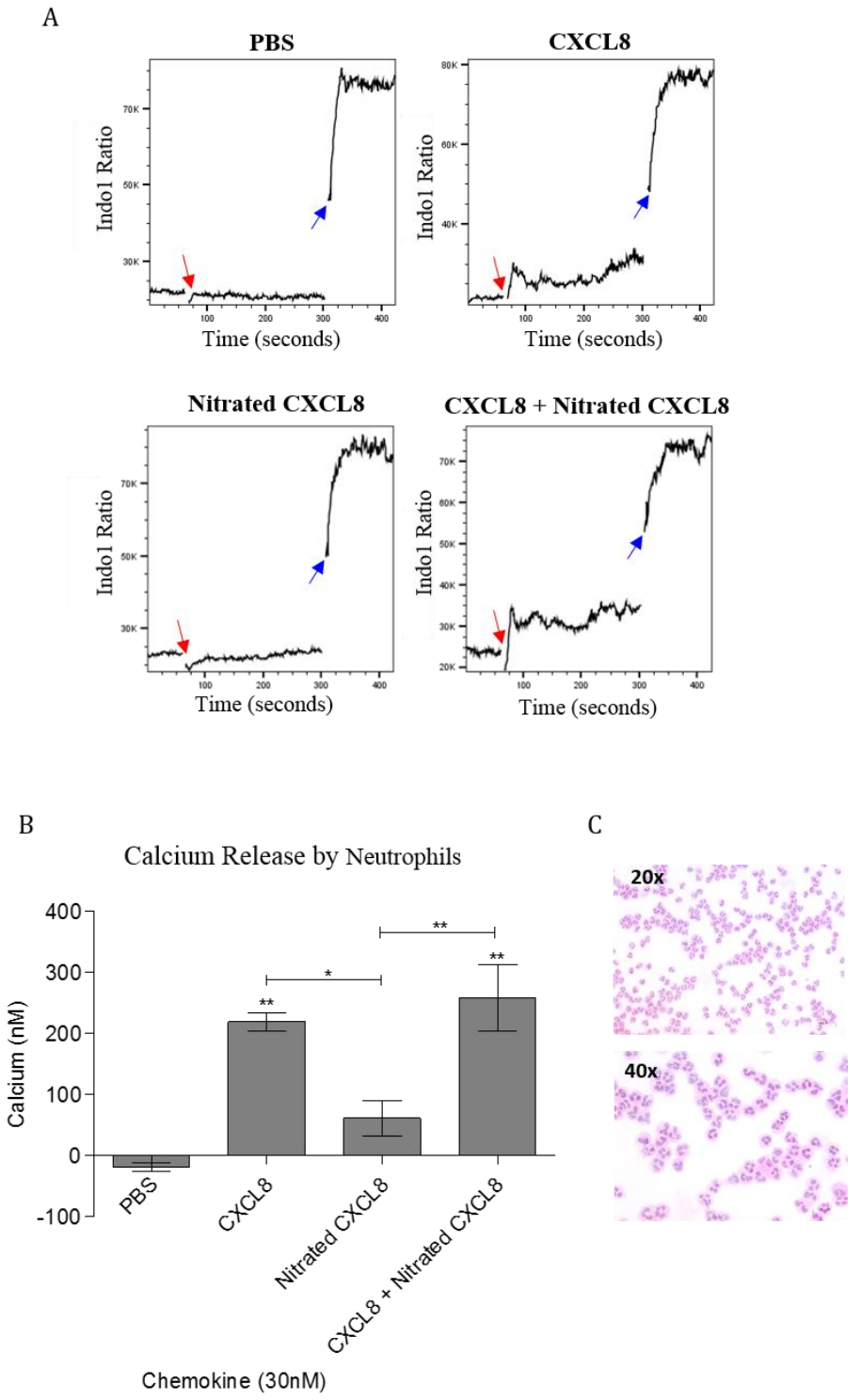

Figure 3-22. Ability of nitrated CXCL8 to inhibit the calcium signalling of wild type CXCL8 in neutrophils *in vitro*. A) Calcium flux in response to PBS, 30nM wild type CXCL8, 30nM nitrated CXCL8, or 30nM of each together added at 60 seconds (red arrows). 10µg/ml of Ionomycin was used as a positive control added at 300 seconds (blue arrows). B) Calcium release (nM) in response to the above treatments calculated using the equation $[Ca^{2+}]$ = kd x (R – Rmin) / (Rmax – R), where the kd = 844 nM/L [284,285]. C) Haematoxylin and Eosin staining of a cytospin collected from the cell population, showing a high percentage purity of neutrophils. Images were taken using light microscopy at 20x and 40x magnification. Data shown in A) and C) are representative of, and B) is combined from N=3 experimental replicates (using neutrophils isolated from different blood donors), each with n=1 technical replicate.

3.3.6 Determining Which Residues within CXCL8 Are Targets For Nitration by Peroxynitrite

In order to determine exactly which residues within CXCL8 were nitrated after incubation with peroxynitrite, I aimed to use ion trap mass spectrometry to fractionate the chemokine and assess the weights of the resulting fragments.

As described in section 3.2.7, nitrated CXCL8 was injected into the mass spectrometer and analysed by standard mass spectrometry. Then, through mass spectrometry/mass spectrometry (MS2) analysis, the most abundant peak (1205) was isolated, retained within the ion trap, then fractionated at the D-P bond to create an N-terminal fragment (1493.01), and a C-terminal fragment (820.14) as shown in Figure 3-23A. The charge state of each ion was determined by the number of peaks present within 1Da of each other, i.e. the 819.42 peak was determined to be triple charged, as between this peak and the peak at 820.42 there were three smaller peaks, each 0.33Da apart. Figure 3-23B demonstrates how these fragments were analysed, using the ion mass and the charge to calculate the molecular weight of each fragment. The amino acid sequence of each fragment is also shown in Figure 3-23C. The C-terminal fragments of both the wild type and nitrated chemokines had the same m/z and therefore same molecular mass, but the N-terminal fragment of the nitrated chemokine was found to have a molecular mass 45Da larger than that of the wild type chemokine. I can therefore conclude that incubation with peroxynitrite nitrates CXCL8 on one residue present within the N-terminal half of the chemokine. I attempted to perform MS3 analysis by isolating only the N-terminal ion (1493) and increasing the amplitude in order to fragment this ion into two daughter ions in order to further deduce which residue within the N-terminal fragment was nitrated, however this proved unsuccessful, resulting in either inadequate or excessive fragmentation.

ELISAs and dot blots were then performed to assess whether nitrated CXCL8 could be detect using an anti-3NT antibody. This proved successful in both experimental settings as shown in Figure 3-24, confirming that the addition of the single nitrate group on the N-terminal half of the chemokine observed during MS2 analysis is located on the sole tyrosine residue within CXCL8; Y13.

The same MS2 analysis principle was applied to nitrated Y13F CXCL8, which also showed no alteration to the C-terminal fragment of the chemokine, but a 45Da increase in mass of the N-terminal fragment in comparison to the calculated value for the N-terminal fragment of non-nitrated Y13F CXCL8 (Figure 3-25). This suggests that even with the substitution of Y13 for F, incubation with peroxynitrite nitrates this mutant CXCL8 on one residue present within the N-terminal half of the chemokine.

A

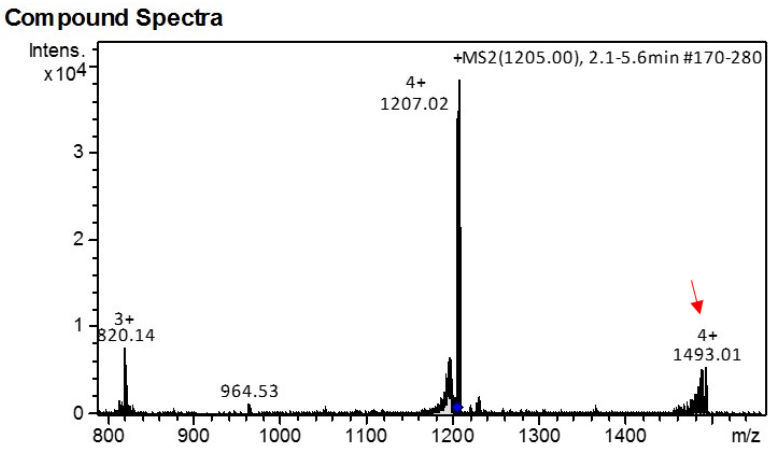

B

CXCL8			Nitrated CXCL8		
Protein	**Ion mass (charge)**	**Molecular Mass**	**Protein**	**Ion mass (charge)**	**Molecular Mass**
Full protein	1198.39 (+7)	(1198.39x7)-7 = 8381.73	Full protein + NO_2	1205 (+7)	(1205x7)-7 = 8428
C-terminal peptide	820.14 (+3)	(820.14x3)-3 = 2457.42	C-terminal peptide + NO_2	835.14 (+3)	(835.14x3)-3 = 2502.42
N-terminal peptide	1488 (+4)	(1488x4)-4 = 5948	N-terminal peptide + NO_2	1493.01 (+4)	(1493.01x4)-4 = 5968.04

C

Full length chemokine:
SAKELRCQCIKTYSKPFHPKFIKELRVIESGPHCANTEIIVKLSDGRELCLDPKENWVQRVVEKFLKRAENS

C-terminal peptide:
SAKELRCQCIKTYSKPFHPKFIKELRVIESGPHCANTEIIVKLSDGRELCLDPKENWVQRVVEKFLKRAENS

N-terminal peptide:
SAKELRCQCIKTYSKPFHPKFIKELRVIESGPHCANTEIIVKLSDGRELCLDPKENWVQRVVEKFLKRAENS

Figure 3-23. MS2 analysis of nitrated CXCL8. A) Shows the compound spectra for MS2 analysis of nitrated CXCL8. Nitrated CXCL8 was manually injected at and analysed by ion trap mass spectrometry. The most abundant ion was the 1205 peak, which corresponds to a +7 charged ion of the full length chemokine with one NO_2 group added (+45Da). This ion was selected and held within the ion trap, then fragmented to break the D-P bond, thus cleaving the chemokine into a C-terminal peptide and an N-terminal peptide. A triple charged ion of 820.14 corresponds to a peptide with no additional NO_2 groups, whereas the quadruple charged ion of 1493.01 (red arrow) is consistent with a peptide plus one NO_2 group – therefore, incubation of CXCL8 with peroxynitrite results in one NO_2 group being added to an amino acid within the N-terminal section of the chemokine. B) Shows the calculation method derived from the equation "peak readout = (m+z/z)" to determine the molecular mass of each ion. C) The CXCL8 amino acid sequence with the relative amino acids highlighted in red for each peak analysed. Data shown is from N=1 experiment, with n=1 technical replicate.

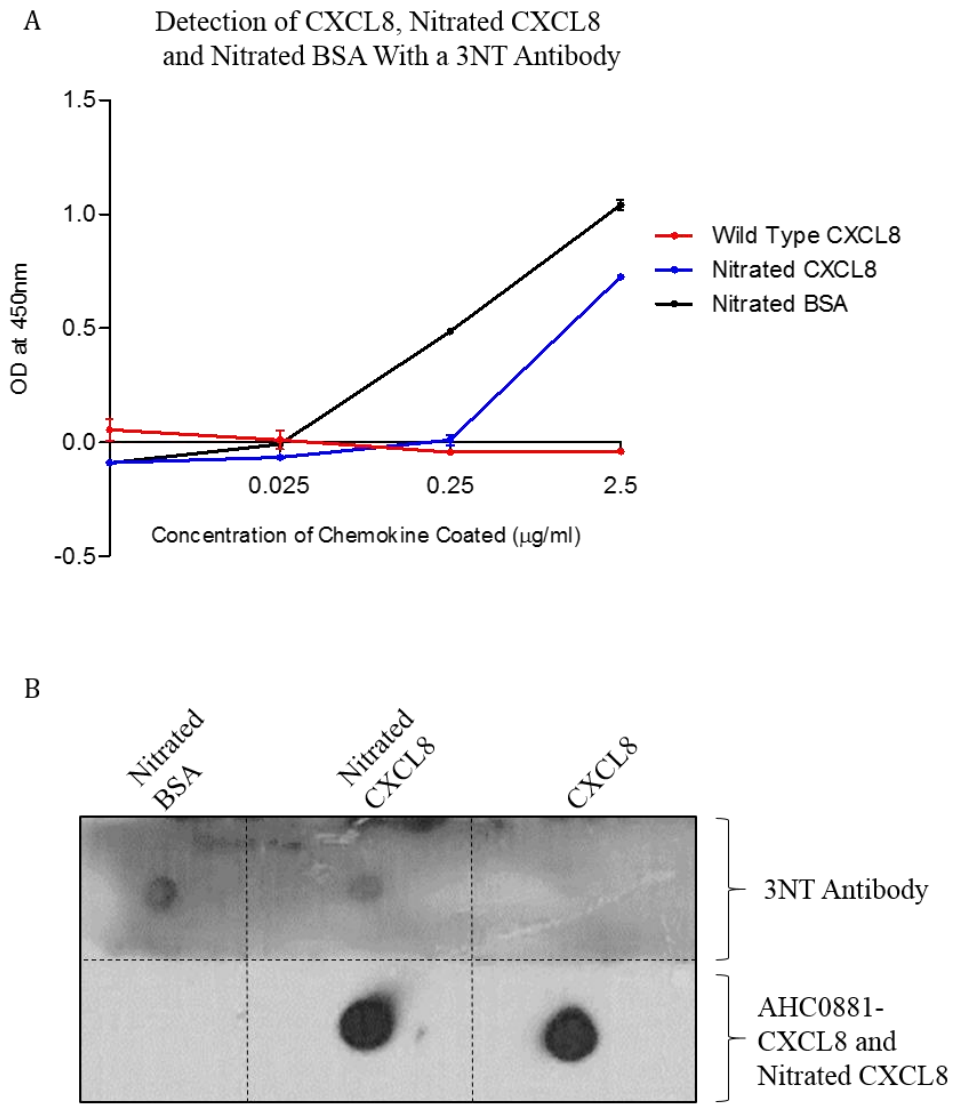

Figure 3-24. Assessing whether nitration of CXCL8 occurs on Y13. A) Direct ELISA using a 3NT polyclonal antibody (06-284, Millipore) at 1µg/ml followed by an anti-rabbit-HRP antibody (A6154, Sigma) to detect varying concentrations of wild type CXCL8, nitrated CXCL8 and nitrated BSA. Each concentration was tested in triplicate. B) Dot blot using the same 3NT polyclonal antibody, and a CXCL8 polyclonal antibody (AHC0881, Life Technologies) at 1µg/ml to detect 50ng of wild type CXCL8, nitrated CXCL8 and nitrated BSA. Data shown in A) is from N=1 experiment, each with n=3 technical replicates, and data shown in B) is representative of N=3 experimental replicates, each with n=1 technical replicate.

A

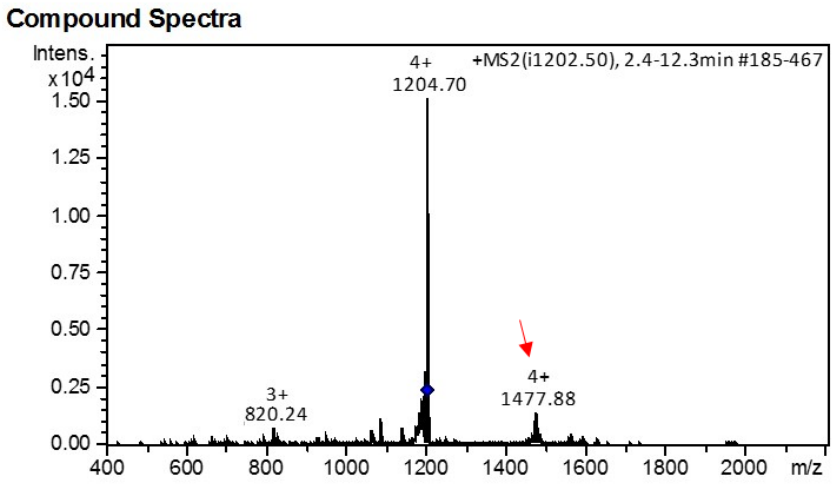

B

Y13F CXCL8			Nitrated Y13F CXCL8		
Protein	**Ion mass (charge)**	**Molecular Mass**	**Protein**	**Ion mass (charge)**	**Molecular Mass**
Full protein	1196.1 (+7)	(1196.1x7)-7 = 8365.7	Full protein + NO_2	1202.5 (+7)	(1202.5x7)-7 = 8410.5
C-terminal peptide	820.24 (+3)	(820.24x3)-3 = 2457.72	C-terminal peptide + NO_2	835.14 (+3)	(842.74x3)-3 = 2525.22
N-terminal peptide	1465.76 (+4)	(1465.76x4)-4 = 5859.04	N-terminal peptide + NO_2	1477.01 (+4)	(1477.01x4)-4 = 5904.04

C

Full length chemokine:

SAKELRCQCIKTFSKPFHPKFIKELRVIESGPHCANTEIIVKLSDGRELCLDPKENWVQRVVEKFLKRAENS

C-terminal peptide:

SAKELRCQCIKTFSKPFHPKFIKELRVIESGPHCANTEIIVKLSDGRELCLDPKENWVQRVVEKFLKRAENS

N-terminal peptide:

SAKELRCQCIKTFSKPFHPKFIKELRVIESGPHCANTEIIVKLSDGRELCLDPKENWVQRVVEKFLKRAENS

Figure 3-25. MS2 analysis of nitrated Y13F CXCL8. A) Shows the compound spectra for MS2 analysis of nitrated Y13F CXCL8. Nitrated Y13F CXCL8 was manually injected at and analysed by ion trap mass spectrometry. The most abundant ion was the 1202.5 peak, which corresponds to a +7 charged ion of the full length chemokine with one NO_2 group added (+45Da). This ion was selected and held within the ion trap, then fragmented to break the D-P bond, thus cleaving the chemokine into a C-terminal peptide and an N-terminal peptide. A triple charged ion of 820.24 corresponds to a peptide with no additional NO_2 groups, whereas the quadruple charged ion of 1477.88 (red arrow) is consistent with a peptide plus one NO_2 group – therefore, incubation of Y13F CXCL8 with peroxynitrite results in one NO_2 group being added to an amino acid within the N-terminal section of the chemokine. B) Shows the calculation method derived from the equation "peak readout = (m+z/z)" to determine the molecular mass of each ion. C) The Y13F CXCL8 amino acid sequence with the relative amino acids highlighted in red for each peak analysed. Data shown is from N=1 experiment, with n=1 technical replicate.

3.4 DISCUSSION

This chapter has highlighted the importance of studying post-translational nitration as an important mechanism of chemokine regulation, as it clearly has a profound impact on chemokine function both *in vitro* and *in vivo*.

3.4.1 CXCL8 Nitration and Chemotactic Function

Nitration of CXCL8 almost completely abolished primary human neutrophil chemotaxis in trans-filter chemotaxis assays, suggesting that nitration must affect the ability of CXCL8 to bind to CXCR1 and/or CXCR2 receptors, as no endothelial cells are present and therefore GAG binding is not applicable in this experimental setting. As observed in trans-filter assays, nitration of CXCL8 prevents it from inducing neutrophil migration through a monolayer of HMEC-1 endothelial cells in trans-endothelial chemotaxis assays. The nitrated chemokine also failed to recruit murine neutrophils to the mouse peritoneum *in vivo*.

Calcium flux assays and Western blots detecting ERK phosphorylation confirmed that this reduction in migration is at least partly due to the impaired ability of the nitrated chemokine to signal through its GPCRs present on primary human neutrophils. Visual inspection of the SPR data curves reveals gross differences in binding stability and crosslinking between wild type and nitrated CXCL8, which suggests that nitration also impairs the ability of CXCL8 to bind to immobilised heparin, suggesting that impaired GAG binding also contributes to the chemokine's lack of chemotactic capacity following incubation with peroxynitrite. Nitrated CXCL8 cannot inhibit the function of wild type CXCL8 when administered at equimolar ratios (30nM) in both chemotaxis assays and calcium flux assays. This is likely due to both GAG binding and receptor binding being impaired, although the latter is not confirmed. I have shown that nitration can inhibit GPCR signalling, but further experiments would need to be conducted to confirm if this is due to impaired binding.

These effects are unlikely to be attributed to the charge of the molecule as this is unaffected by nitration [95]. NMR analysis performed by Dr Rajarathnam (see Figure 3-26) shows the superimposed spectra for wild type CXCL8 (black) in comparison to nitrated CXCL8 (red). As the vast majority of the spectra align, this shows that nitration has very

little influence on chemokine tertiary structure, and so any changes in function must be due to nitration and cannot be attributed to global structural changes.

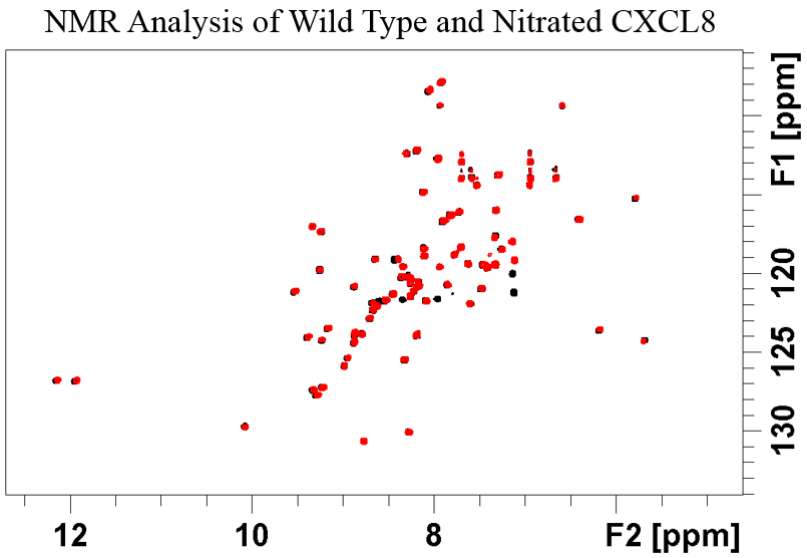

Figure 3-24. NMR data showing the superimposed spectra for wild type CXCL8 (black) and nitrated CXCL8 (red). The high degree of alignment indicated nitration does not affect the 3D folded structure of the chemokine. Unaligned peaks arise due to arginine side chains *(Professor Krishan Rajarathnam, unpublished data)*.

3.4.2 CXCL8 and Y13

The loss of Y13 achieved through generation of the Y13F mutant chemokine either did not affect, or slightly increased the chemotactic response of neutrophils, particularly at lower concentrations of 10nM (p=<0.001) or 20nM (p=<0.01). This indicates that Y13 is not essential for GPCR signalling or chemotactic function, as its loss does not prevent this response. A slight reduction in calcium flux was observed after neutrophils were treated with the Y13F mutant CXCL8 in comparison to wild type CXCL8 (p=<0.05), which could be attributed to partially impaired GPCR binding caused by the loss of Y13 which forms a hydrogen bond with D14 of CXCR1 [185], however this is not significant enough to impair migration. In trans-endothelial assays, fewer neutrophils migrated in response to the Y13F mutant than had migrated in response to this variant in trans-filter assays, however migration was not completely abolished, with percentages reducing from as high as 40% to as low as 10%. This suggests that Y13 could be involved in CXCL8's interaction with GAGs, although some effect on chemokine dimerization/oligomerisation is also possible, and could be indicated by the SPR experiments. This data confirmed that the Y13F mutant CXCL8 has a slightly reduced ability to bind to heparin than wild type CXCL8, and the patterns of the binding curves

generated also suggest different modes of binding. It appears that the wild type chemokine binds both as monomers (indicated by rapid dissociation) and as oligomers with increased avidity (indicated by a stable reading above baseline after dissociation caused when one GAG-binding domain within the oligomer immediately re-associates with the immobilised heparin as another dissociates). The rapid dissociation and return to baseline observed in the Y13F CXCL8 binding curve indicates that the mutant chemokine binds as a monomer only. This data could suggest that the substitution of tyrosine for phenylalanine in the Y13F mutant could affect the chemokine's ability to dimerise, although is not clear how this substitution would affect dimerization, as position 13 within CXCL8 is located at the periphery of the protein and not at the dimer interface as shown in Figure 1-7C, therefore further study would be required to determine if substituting tyrosine for phenylalanine does compromise dimerization. If proven to be true, however, this could explain the reduction in neutrophil trans-endothelial migration observed in response to the Y13F mutant CXCL8 in comparison to the wild type chemokine. Both tyrosine and phenylalanine have hydrophobic side chains [286], however substitution of tyrosine for phenylalanine will result in a change in the residue from polar to non-polar, and could affect the ability to form hydrogen bonds [287] – these alterations could possibly be responsible for the differences in chemotactic capacity observed between the wild type and mutant CXCL8.

As the nitrated Y13F mutant showed a reduction in the induction of chemotaxis when compared to the non-nitrated Y13F chemokine, there must be other residues within CXCL8 other than tyrosine, (or possibly the phenylalanine mutated in [288,289]), which is a target for peroxynitrite and is partly responsible for the induction of chemotaxis.

Ion trap MS2 analysis of nitrated CXCL8 and nitrated Y13F CXCL8 was performed in an attempt to determine which residues within the chemokines are modified by peroxynitrite, that cause the altered functionality observed in other experiments. These experiments confirmed that incubation of both wild type and Y13F CXCL8 with peroxynitrite result in the addition of one nitrate group to the N-terminal half of the chemokine. In the case of wild type CXCL8, this residue is confirmed to be Y13, as nitrated CXCL8 has shown to be detectable using an anti-3NT antibody, and the only tyrosine residue present within CXCL8 is Y13.

Initially the rationale behind generating the Y13F mutant CXCL8 was to mutate in a residue which could not be nitrated in order to confirm whether Y13 is the only target for nitration that will affect function, however evidence has since come to light that suggests that the phenylalanine actually is capable of being nitrated. This suggests that the nitration observed in MS2 analysis of nitrated Y13F CXCL8 is actually on F13 [288,289], and is supported by the fact that nitrated CXCL8 and nitrated Y13F CXCL8 showed statistically different functionality in trans-filter chemotaxis assays (30nM $p=<0.05$), which would not be the case if any residue other than the altered amino acid at position 13 was responsible for functionality and modified by peroxynitrite. This therefore implies that nitration at position 13 affects function regardless of the actual residue present, if that residue is a target for nitration.

3.4.3 CXCL1 Nitration and Chemotactic Function

To investigate the effect that nitration has on a chemokine with no naturally occurring tyrosine residues, and the subsequent effect of adding and then nitrating a tyrosine residue, CXCL1 was studied in addition to CXCL8.

Incubation of CXCL1 with peroxynitrite also inhibited its ability to induce neutrophil migration in trans-filter chemotaxis assays ($p=<0.001$), as it did in the case of CXCL8. This indicates that other amino acids (as CXCL1 contains no tyrosine, tryptophan or phenylalanine residues), which can be targets for peroxynitrite such as cysteine or histidine, must be required for CXCL1 function; the nitration or oxidation of which impairs its chemotactic ability. Nitration following introduction of a tyrosine residue artificially also induced no neutrophil migration. In trans-endothelial chemotaxis assays, although baseline migration in response to the negative control appears slightly higher in this experiment (which could be due to more activated donor neutrophils), migration in response to nitrated CXCL1 is reduced to this level in the trans-endothelial assay as it was in the trans-filter. Substitution of leucine at position 15 for tyrosine is shown to reduce chemotaxis by roughly half when compared to the wild type CXCL1. This indicates that L15 is in part, but not completely, responsible for the induction of neutrophil migration. This is not confirmed in the literature, however, L15 is within the N-loop of CXCL1 [290] which is a region of the chemokine known to be important in GPCR binding [2]. The addition of a tyrosine residue, which is then nitrated, produces the same effect as nitrating the wild type chemokine. Nitration therefore equally impairs the

function of CXCL1 regardless of the loss of leucine/introduction of tyrosine at position 15. Inconsistent results in trans-endothelial chemotaxis assays could be due to endogenous chemokine production by the HMEC-1 cells influencing neutrophil migration, or issues with neutrophil preparations. However, as the aim of these experiments was to explore the importance of tyrosine residues in nitration, and this question was largely answered by trans-filter chemotaxis assays, these experiments were not optimised further.

As with CXCL8, NMR analysis provided by Dr Rajarathnam (University of Texas Medical Branch) indicates that nitration of CXCL1 does not affect its tertiary structure, as the majority of the wild type spectra (black) aligns with that of the nitrated chemokine (red) (see Figure 3-27). The few superimposed peaks which do not align arise from arginine side chains. Both leucine and tyrosine contain hydrophobic side chains, meaning they are relegated to the centre of the folded protein. The L15Y substitution is therefore unlikely to change the 3D fold structure of CXCL1, and the reduction in migration seen in the mutant chemokine compared to the wild type is unlikely to be due to 3D structural changes [286,287]. However, leucine is non-polar, whereas tyrosine is polar, and interactions with leucine mainly occur through van der Waals forces, whereas tyrosine can also interact via hydrogen bond formation and aromatic stacking [287].The reduction in chemotaxis seen in response to the L15Y mutant could possibly be attributed to these potentially altered characteristics.

As CXCL1 does not contain any naturally occurring tyrosine residues, the reduction in function of wild type CXCL1 after incubation with peroxynitrite suggests that tyrosine cannot be the only residue that is a target for nitration and affects function. This means that we cannot predict how nitration will affect any given chemokine based on the location and number of tyrosine residues within its structure as initially hoped.

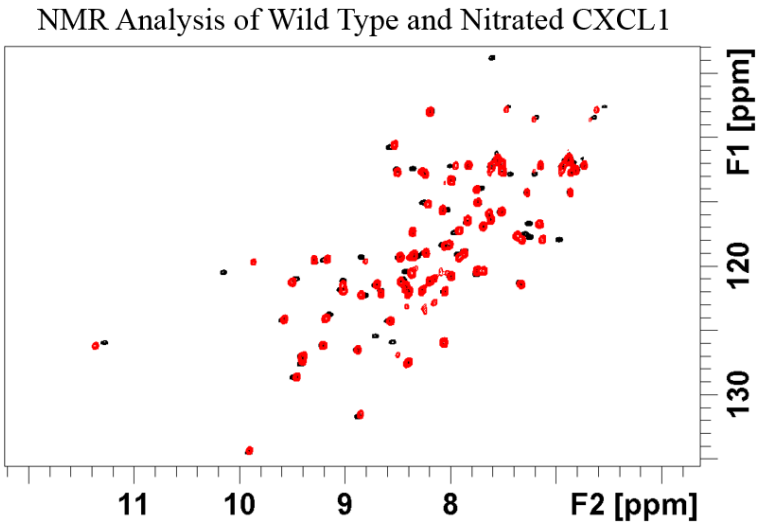

Figure 3-25. NMR data showing the superimposed spectra for wild type CXCL1 (black) and nitrated CXCL1 (red). The high degree of alignment indicated nitration does not affect the 3D folded structure of the chemokine. Unaligned peaks arise due to arginine side chains *(Professor Krishan Rajarathnam, unpublished data)*.

3.4.4 Future Studies

Further analysis could be performed to determine if nitration affects the ability of CXCL8 to form dimers, which are known to have a lower affinity for the chemokine's receptors, but a higher affinity for GAGs. The effect that dimerization would have on the function of the chemokine would likely depend on the ratio and positioning of wild type and nitrated monomers within the chemokine oligomer.

It would also be interesting to assess whether nitration affects the binding ability and affinity of CXCL8 for the atypical chemokine receptor ACKR1, as binding of the nitrated chemokine to this receptor would mean less is available for the wild type chemokine to bind to, which could potentially result in increased inflammation.

Chemotaxis assays and calcium flux assays to assess the function of nitrated CXCL8 and its ability to inhibit wild type CXCL8 could also be repeated using higher concentrations of chemokines. While the concentration range used (10-30nM) suggests that nitration abrogates CXCL8 function, testing a range of higher concentrations could show that nitration shifts the bell-shaped curve of the chemokine response to the right, meaning that the nitrated chemokine could still be functional, but at much higher concentrations than the wild type chemokine. This is shown diagrammatically in Figure 3-28 below, and could be the case as 30nM nitrated CXCL8 did appear to induce slight calcium flux, and 1000nM nitrated CXCL8 did give a small heparin binding signal above background in

SPR analysis. However, no significant difference between nitrated CXCL8 and negative controls has been observed in any experimental settings, suggesting the shift in functionality is quite substantial and therefore difficult to study as it is likely that very large concentrations of nitrated chemokine would be needed to achieve functionality comparable to that of wild type CXCL8.

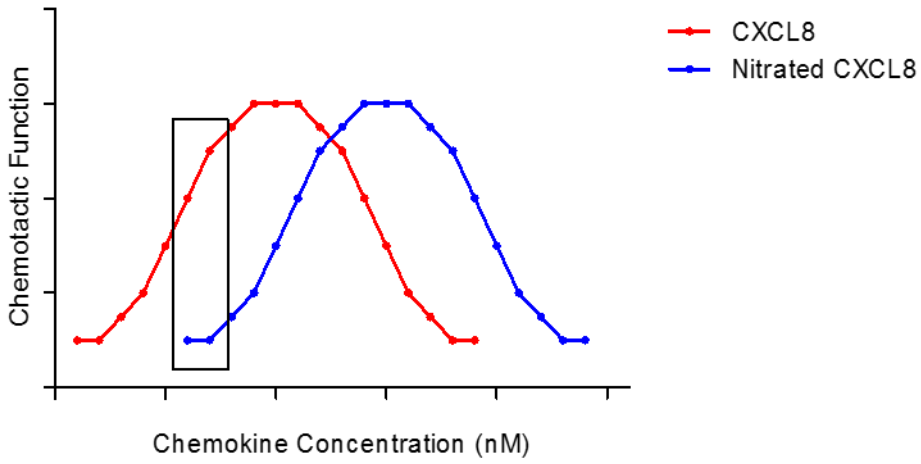

Figure 3-26. Hypothetical chemokine activity curves for CXCL8 and nitrated CXCL8. Diagram depicting the narrow window of CXCL8 and nitrated CXCL8 functionality observed by testing a limited range of concentrations.

Further point mutational analysis could be performed to synthesise a Y13 mutant variant of CXCL8 that is unable to be nitrated at this position, to fully determine the role of tyrosine in nitration and subsequent function alterations. MS2 analysis of CXCL1 could also help determine which amino acid is nitrated in the case of this chemokine.

This chapter has shown that nitration of CXCL8 reduces its ability to induce neutrophil migration *in vitro* and *in vivo*, that this is due to impaired receptor signalling and GAG binding, and that nitrated CXCL8 is unable to inhibit wild type CXCL8 at equimolar ratios. These studies have also shown that these effects are mediated by the addition of one nitrate group on the N-terminal half of CXCL8, which is confirmed to be on Y13.

4 DEVELOPING A METHOD TO DETECT NITRATED CXCL8 IN BIOLOGICAL SAMPLES

4.1 INTRODUCTION

Work described in the previous chapter showed that nitration of CXCL8 by peroxynitrite affects the chemokine's biological function and inhibits its ability to recruit neutrophils *in vitro* and *in vivo*. Nitration could therefore be said to render the inflammatory CXCL8 non-functional. These studies were conducted using CXCL8 which was nitrated by incubation with peroxynitrite in a laboratory setting, and while natural nitration of CXCL12 has been detected[122], there is a need to prove that this modification also occurs *in vivo* in the case of CXCL8.

The alteration in function caused by nitration means that it is essential to be able to differentiate between modified and unmodified chemokines, and measure both accurately in order to gain a complete understanding of the inflammatory situation. Previous work by Catriona Barker showed that nitrated CCL5 was detectable with currently available antibodies raised against the wild type chemokine, but nitrated CCL2 was not (Catriona Barker, PhD thesis). Measuring wild type chemokines only may not represent the true amount that has been produced and subsequently modified. In addition, unknowingly measuring both modified and unmodified chemokines together, but assuming this amount detected to be wild type chemokine only, is also misrepresentative. This could explain why the levels of many chemokines have been correlated with different disease states, but none have been developed further into clinical diagnostic assays. Increased levels of CXCL8 have been correlated with hepatocellular carcinoma[265], chronic obstructive pulmonary disease[246], acute respiratory distress[248], osteoarthritis[291] and Alzheimer's disease[255] to name a few. Measuring the ratio of wild type to nitrated CXCL8 could increase the significance of using this chemokine as a biomarker of disease severity or progression.

Detection of nitrated chemokines will improve our understanding of when they are produced and why, which could in turn improve understanding of the pathology of many diseases. Some disease/inflammatory states are more likely to facilitate nitration than others. For example, if peroxynitrite-mediated nitration occurs as a result of IRI and

oxidative stress as hypothesised, then the amount of nitrated CXCL8 or its ratio to wild type CXCL8 could be an important indicator of IRI severity. This could therefore be applicable in an organ transplant situation, where detecting nitrated chemokines like CXCL8 could be indicative of IRI in donor organs prior to transplant and in patient samples post-transplant.

The detection of other forms of chemokine modification, such as citrullination and truncation could also be further explored as any modification has the potential to alter epitopes and thus affect chemokine detectability, though this is beyond the scope of this project.

4.1.1 Specific Aims

- Assess whether commercially available antibodies can detect nitrated CXCL8
- Develop a novel antibody specific for nitrated CXCL8
- Develop the novel antibody into an ELISA to measure nitrated CXCL8 in patient samples

4.2 SPECIFIC MATERIALS AND METHODS

4.2.1 Sandwich ELISA

4.2.1.1 Assessing Commercially Available CXCL8 ELISA Kits

R&D's Human CXCL8 Duoset ELISA kit (DY208), and Peprotech's Human CXCL8 ELISA kit (900-T18) were used as per the manufacturer's instructions.

4.2.1.2 Developing a Sandwich ELISA to Detect Nitrated CXCL8

A basic sandwich ELISA protocol (as described in section 2.7.2) was followed, trialling different capture and detection antibody combinations. For biotinylation of AbD31649.1, a Lightning-Link® Kit (Innova Biosciences) was used as per the manufacturer's instructions.

4.2.2 High Performance Liquid Chromatography

4.2.2.1 Antibody Purification from C1 Hybridoma Cells

The antibody was purified from stored C1 ascites by high performance liquid chromatography (HPLC) using Hitrap protein G sepharose columns. 500ml batches of media were centrifuged to remove cells, filtered, and then run through columns at a flow rate of 0.3ml/minute overnight. The bound antibody was eluted using 0.1M glycine + 0.15M NaCl pH 2.6 and then concentrated.

4.2.2.2 Size Exclusion Serum Fractionation

This method used Superose 12 size exclusion chromatography columns (GE Healthcare), to fractionate normal human serum spiked with 10µg wild type CXCL8 or 6.6µg nitrated CXCL8. This would allow fractions containing high molecular weight/high abundance proteins to be diluted more than fractions containing the low molecular weight chemokine. The column was equilibrated with PBS at a flow rate of 0.5ml/minute. Serum was clarified by centrifugation at 18,000xg for 5 minutes and filtration through a 0.45µm filter, then diluted in PBS to 16mg/ml. CXCL8 or nitrated CXCL8 (10µg or 6.6µg respectively), was then added into 0.5ml of the diluted serum, which was loaded onto the column with PBS and run at 0.5ml/minute. 26x 1ml fractions were collected. To each fraction 5µl of Insulin at 10mg/ml was added as a protein

carrier to aid precipitation (as this is 3kDa it can be run off the bottom of any gel). To each fraction 0.5ml of 30% (w/v) trichloroacetic acid was added and fractions were left on ice for 30 minutes. Samples were then centrifuged at 18000xg (4°C) for 15 minutes. The supernatant was aspirated off and 400µl of ice-cold acetone added to each pellet, vortexed and re-centrifuged at 18,000xg (4°C) for 15 minutes. Supernatant was again aspirated and the pellet allowed to dry. 1x SDS-PAGE loading buffer was added (see below) to fractions and the pellet resuspended using a pipette tip.

Fraction 8: 50µl

Fractions 9 and 10: 100µl

Fractions 11, 12, 13 & 14: 300µl

Fractions 15-24: 50µl

0.5µl NaOH was added to re-neturalise the samples, which were then boiled for 5 minutes and extensively vortexed before spinning and loading onto an 18% SDS-PAGE gel (2µg). A Western blot was then performed as described in section 2.5 to detect CXCL8 and nitrated CXCL8.

4.3 RESULTS

4.3.1 Assessing the Ability of Commercially Available ELISA Kits to Detect Nitrated CXCL8

Data from a previous PhD student, Catriona Barker, showed that nitration of CCL2 prevents its detection by commercially available antibodies raised against the wild type molecule. Experiments were therefore conducted to assess whether commercially available ELISA kits and antibodies raised against wild type CXCL8 could detect nitrated CXCL8. Initial results in Figure 4-1 below show that two standard human CXCL8 ELISA Kits (from Peprotech and R&D Systems) were unable to detect nitrated CXCL8 to the same degree as the wild type chemokine, when used as per the manufacturer's instructions. R&D's kit showed an 8-fold lower OD reading, and Peprotech's kit a 7.7-fold lower OD reading, for the detection of 2000pg/ml of nitrated CXCL8 compared to the same concentration of wild type CXCL8. Further experiments were performed, which involved splitting the kits into their individual antibody components, to test the ability of each capture and detection antibody to bind nitrated CXCL8 individually, in direct ELISA assays. For these experiments, chemokine was coated directly onto the plate, and was detected using the biotinylated detection antibodies and streptavidin-HRP, or capture antibodies followed by HRP-conjugated relevant secondary antibodies. It was found that neither the capture nor detection antibodies from either kit were able to recognise the nitrated chemokine with the same affinity as the wild type chemokine. Both capture antibodies showed a ~6-fold lower OD reading, and both detection antibodies showed a ~13-fold lower OD reading, for the detection of nitrated CXCL8 than for wild type CXCL8, both at 100ng/ml.

A polyclonal rabbit anti-human CXCL8 antibody (AHC0881, Life Technologies), was then tested in the same manner using a direct ELISA method. Unlike the others tested, this antibody was found to have equal affinity for both wild type and nitrated CXCL8, as shown in Figure 4-2A. These results were confirmed by testing the antibody in a dot blot assay, where the same results were observed as shown in Figure 4-2B.

These initial experiments showed that current commercially available antibodies can either only detect wild type CXCL8, or in the case of one antibody, both wild type and

nitrated CXCL8, but currently there is no antibody available that can detect only the nitrated form of CXCL8 specifically.

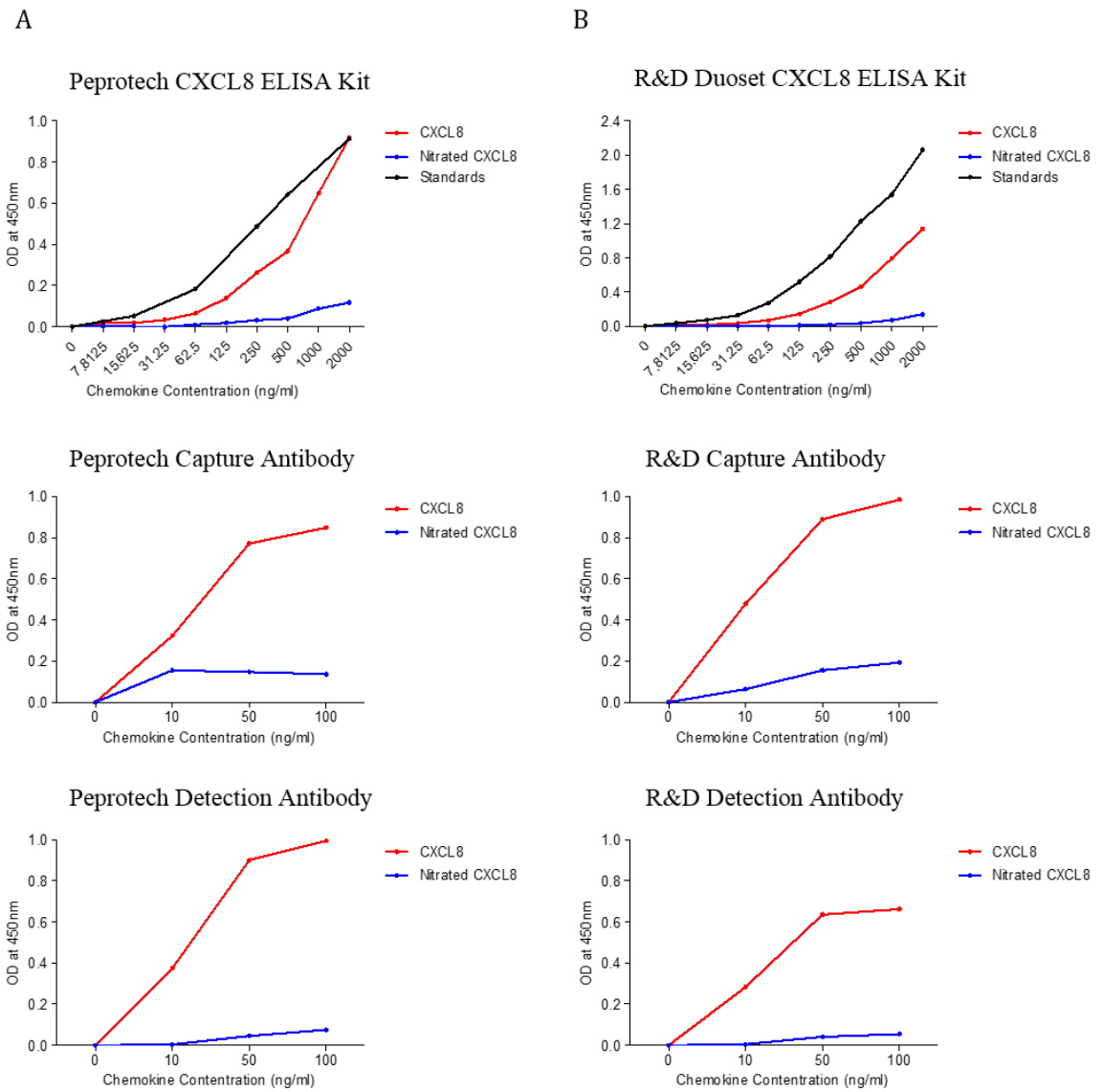

Figure 4-1. Nitration of CXCL8 alters its detectability by ELISA. Peprotech's CXCL8 ELISA kit A) and R&D's Human CXCL8 Duoset ELISA kit B) do not detect nitrated CXCL8 with the same affinity as wild type CXCL8. Varying concentrations of wild type CXCL8 or nitrated CXCL8 were detected using the sandwich ELISA kits intact as per the manufacturer's instructions. The capture and detection antibodies from each kit were also assessed individually in direct ELISA settings at their recommended working concentrations, to assess their ability to bind to wild type CXCL8 or nitrated CXCL8 coated directly onto ELISA plates at varying concentrations. Biotinylated secondary antibodies were detected using streptavidin-HRP, Peprotech's capture antibody was detected using an anti-rabbit-HRP antibody (A6154, Sigma), R&D's capture antibody was detected using an anti-mouse-HRP antibody (A3673, Sigma). Data shown is from N=1 experimental replicate, with n=3 technical replicates.

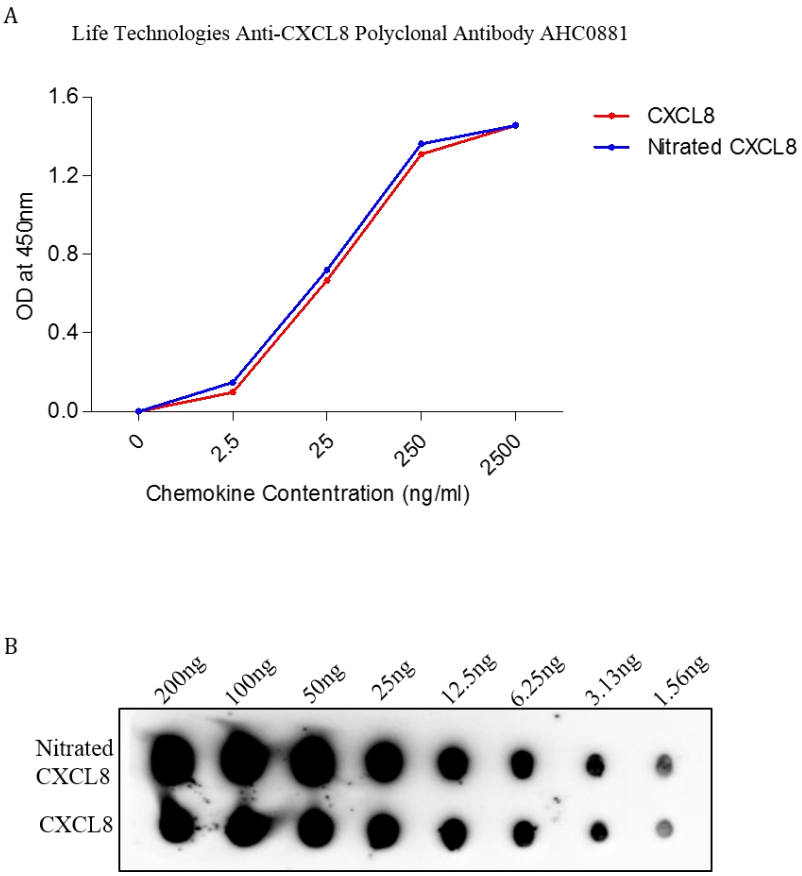

Figure 4-2. AHC0881 anti-CXCL8 polyclonal antibody has equal affinity for wild type and nitrated CXCL8. The ability of AHC0881 (Life Technologies) to detect varying concentrations of wild type and nitrated CXCL8 when used at 1µg/ml was tested in a direct ELISA A) and a dot blot B), both developed using an anti-rabbit-HRP secondary antibody (A6154, Sigma). Data shown in A) and B) is from N=1 experimental replicate, with n=1 technical replicate.

4.3.2 Assessing the Concentration of Wild Type CXCL8 in a Range of Samples

Before attempting to develop an anti-nitrated CXCL8 antibody, I assessed the concentration of wild type CXCL8, and the concentration of total protein, in a number of different respiratory samples as a reference point.

Respiratory samples were selected as the lung is known to be a positive control tissue for CXCL8, and CXCL8 is known to be expressed at high levels in many respiratory conditions [139,246,247]. These samples included bronchoalveolar lavage (BAL) samples from lung transplant patients, ventilator-associated pneumonia (VAP) patients, and one patient with inhaled chemical burns, along with perfusate samples taken at different time-points from lungs perfused *ex vivo* before transplantation, and secretions from primary nasal mucosa/polyp cells isolated and cultured *ex vivo*. Normal human serum samples were also tested to provide a systemic and non-diseased point of comparison. Results in Figure 4-3A show that normal human serum contains naturally low levels of CXCL8, ranging from 10pg/ml to 123pg/ml. BALs samples from VAP patients were found to contain varying concentrations of CXCL8 from 1.2ng/ml to 25ng/ml, with four samples showing no detectable CXCL8 present (Figure 4-3B). Nasal polyp cells secreted 13ng/ml CXCL8, whereas nasal mucosa cells secreted 113.5ng/ml (Figure 4-3C), and the BAL sample from the inhaled chemical burns patient contained 60pg/ml CXCL8 (Figure 4-3D). Of the perfusate samples analysed, only one lung sample showed no detectable CXCL8 at any of the time-points analysed (NCL15). All other samples showed a gradual increase in CXCL8 from the start to the end of perfusion at 1.5-2.5 hours, which is unsurprising as the *ex vivo* organ perfusion system is a closed circuit, so any CXCL8 secreted by the lung will continue to circulate and accumulate over time. However, what can be considered as the total wild type CXCL8 produced, (i.e. the amount present at the last time point of perfusion), varied greatly from ~50pg/ml to ~1ng/ml (Figure 4-4A). A similar degree of variation was observed in BALs samples from lung transplant patients, with 26 of the 42 samples analysed showing no detectable CXCL8, and 16 samples containing detectable CXCL8 ranging from 58pg/ml to 2ng/ml (Figure 4-4B).

Two samples from each of these groups were then assessed for total protein concentration by BCA assay, as shown in Figure 4-5A. The protein composition that made up this total was assessed by gel electrophoresis and silver staining as shown in Figure 4-5B, to separate the protein components by size. The BAL samples showed total

protein concentrations of 422µg/ml for the inhaled chemical burns patient, and 347µg/ml and 369µg/ml for the two lung transplant patients. One of the VAP patient BAL samples had 580µg/ml total protein, and the other had a higher concentration at 13,707µg/ml. All of the BAL samples had an abundance of one high molecular weight protein (97.4 - 116.3 kDa) and a low molecular weight protein (6-14.4 kDA), with some fainter protein bands detected in between these two. The primary nasal mucosa cell secretion had 1036µg/ml of protein, which was shown to be composed of many different bands of protein at many different molecular weights. The two perfusate samples analysed showed much higher protein concentrations than the other samples tested, at 46.6mg/ml and 47.3mg/ml, and this was shown to be largely due to an abundance of one particular protein with a molecular weight between 97.4 and 116.3 kDa.

These data together suggest that any anti-nitrated CXCL8 antibody developed would have to be able to detect concentrations of CXCL8 in the low pg/ml range, and would have to be able to detect this CXCL8 within a complex mix of many different proteins of different sizes and abundances.

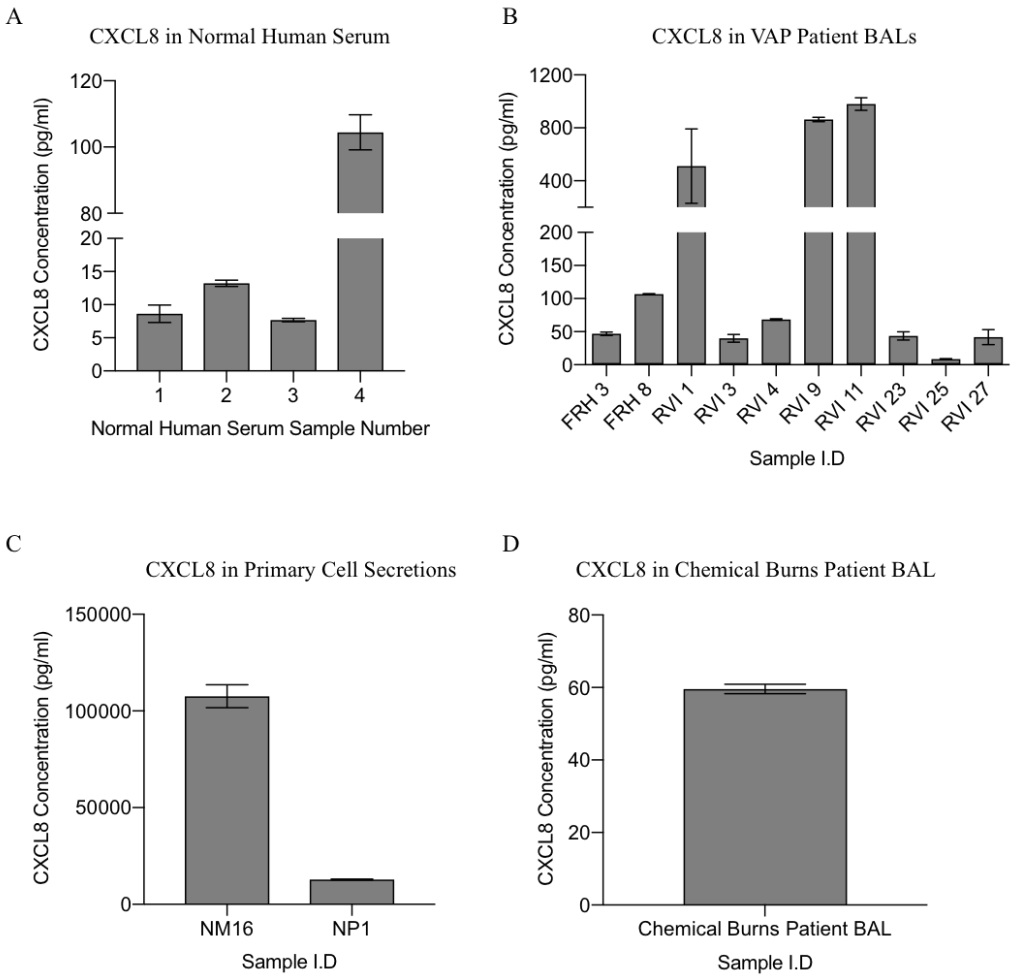

Figure 4-3. Amount of wild type CXCL8 present in a range of respiratory samples. A) 4 normal human serum samples, B) 10 bronchoalveolar lavage (BAL) samples from patients with ventilator-associated pneumonia (VAP) (coded "RVI"), C) 2 samples of cell secretions from cultured primary nasal mucosa cells (coded "NM") or polyp cells (coded "NP"), and D) a BAL sample from an inhaled chemical burns patient, were assessed using the Prof Paul Proost's CXCL8 sandwich ELISA assay developed in-house (Rega Institute, KU Leuven). Capture antibody used was a goat anti-human CXCL8 (#4576), followed by a mouse anti-human CXCL8 secondary antibody (MAB208, R&D), and an anti-mouse-HRP conjugated tertiary antibody (Jackson ImmunoReagents 115-035-146). Development was performed with TMB substrate, and the plate was read at 450nm (corrected). Data shown is from N=1 experimental replicate, with n=2 technical replicates.

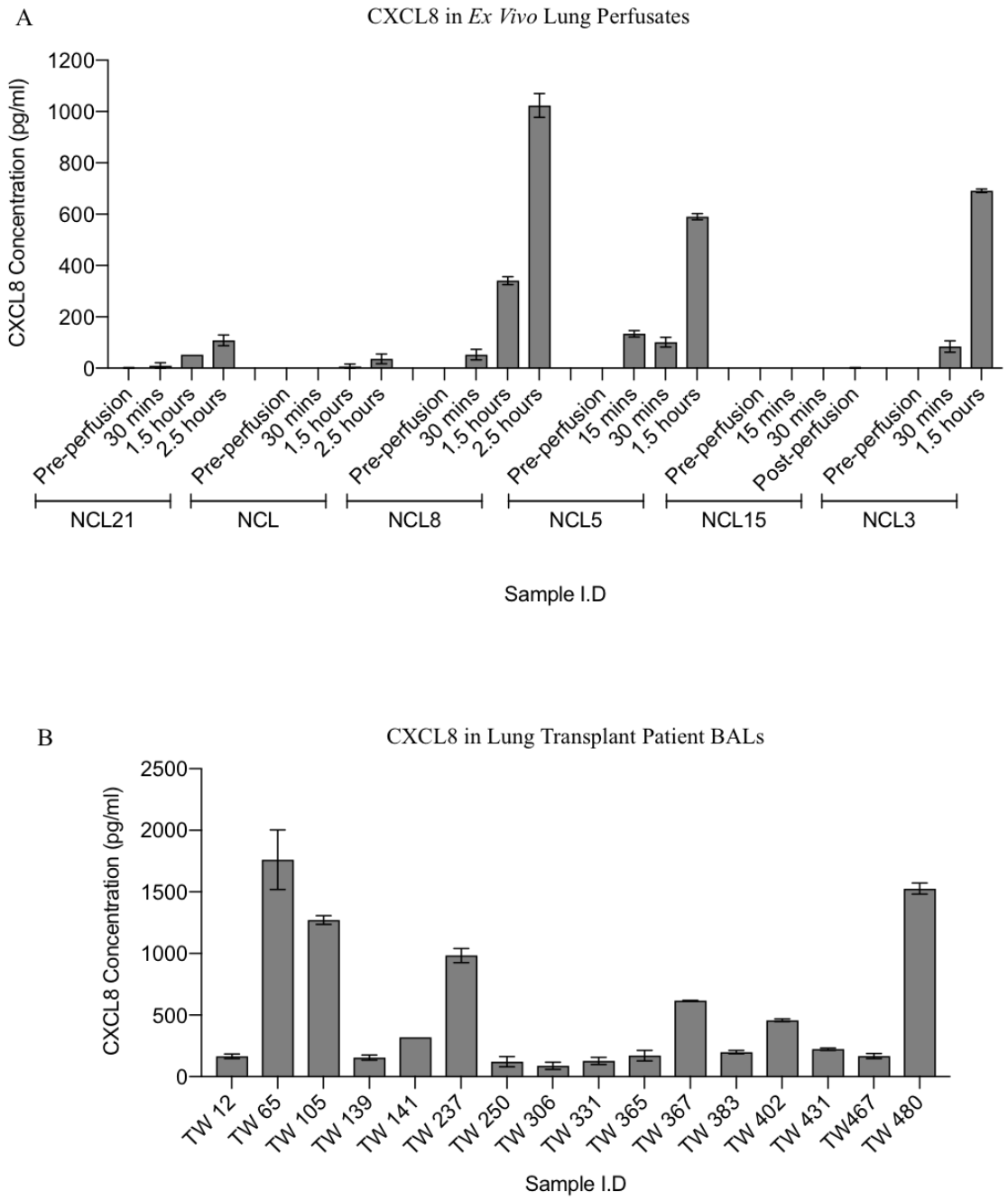

Figure 4-4. Amount of wild type CXCL8 present in a range of samples. A) perfusate samples taken at different timepoints for 6 *ex vivo* normothermic perfused lungs from the Develop UK study (coded "NCL"), and B) 42 bronchoalveolar lavage (BAL) samples from lung transplant patients (coded "TW"), was assessed using the Prof Paul Proost's CXCL8 sandwich ELISA assay developed in-house (Rega Institute, KU Leuven). Capture antibody used was a goat anti-human CXCL8 (#4576), followed by a mouse anti-human CXCL8 secondary antibody (MAB208, R&D), and an anti-mouse-HRP conjugated tertiary antibody (Jackson ImmunoReagents 115-035-146). Development was performed with TMB substrate, and the plate was read at 450nm (corrected). For B) the results from 16 of the samples are shown, as the other 26 samples were below the 31.25pg/ml detection limit of the assay. Data shown is from N=1 experimental replicate, with n=2 technical replicates.

A

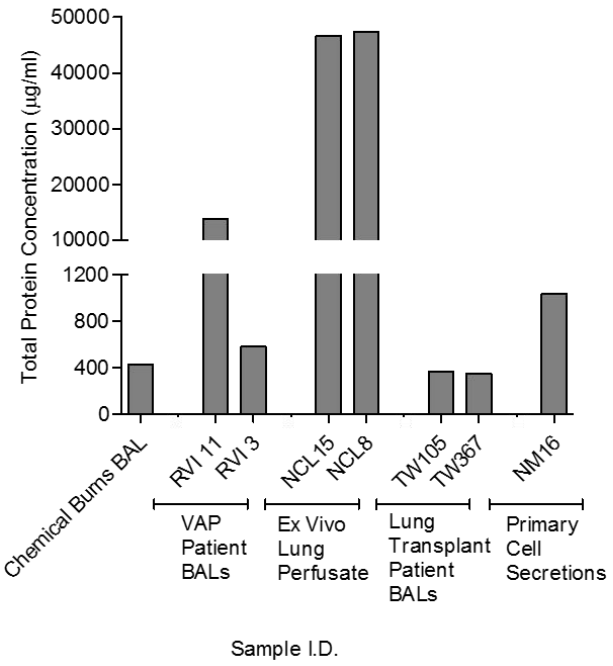

B

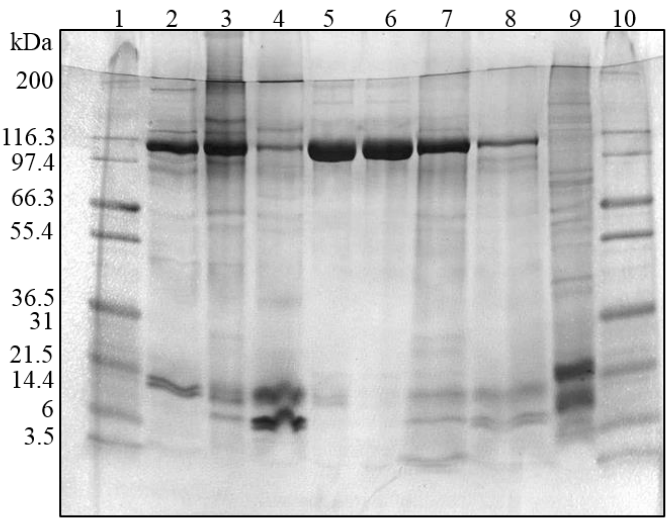

1. Size markers
2. Chemical Burns Patient BALs
3. VAP Patient BALs RVI 11
4. VAP Patient BALs RVI 3
5. *Ex Vivo* Lung Perfusate NCL15 > 4 hours
6. *Ex Vivo* Lung Perfusate NCL8 3 hours
7. Lung Transplant Patient TW105 BALs
8. Lung Transplant Patient TW367 BALs
9. Primary Nasal Mucosa NM16 Cell Secretions
10. Size markers

Figure 4-5. Total protein content and composition of samples. The protein content of two samples from each group was assessed by A) Bicinchoninic Acid assay and B) gel electrophoresis followed by silver staining. Data shown in A) is from N=1 experimental replicate, with n=2 technical replicates and B) is from N=1 experimental replicate, with n=1 technical replicate.

4.3.3 Abmart Antibody Candidate Validation

The results in section 4.3.2 highlight the need to develop an antibody that will specifically recognise nitrated, but not wild type, CXCL8 in highly complex samples. Efforts to this end were made in collaboration with Abmart.

Two colonies (C1 and C4) of hybridoma cell were generated by Abmart. These cells were generated to produce a monoclonal antibody raised against a short CXCL8 peptide containing a nitrated tyrosine residue, which would recognise nitrated CXCL8 specifically (and not the wild type chemokine), shown below.

Wild type peptide: Ac-QCIKTYSKP-NH_2

C1 peptide: Ac-QCIKTY(NO_2)SKP-NH_2

C4 peptide: Ac-IKTY(NO_2)SKPFHPC-N

4.3.3.1 Detection of Antibody Production by C1 Cells

All C4 cells received had tested positive for mycoplasma upon arrival, therefore they were not cultured further, but treatment for mycoplasma infection was attempted as described in section 2.3.8. A direct ELISA and Western blot using C1 cell media collected from various time-points confirmed that C1 cells were producing detectable amounts of antibody (see Figure 4-6). These experiments also confirmed that cryo-freezing cells in liquid nitrogen then resurrecting them did not affect the amount of antibody produced. Growing cells in media containing normal FBS, or charcoal-IgG-stripped FBS (which is necessary for ease of antibody purification) also did not affect antibody production. Cells were therefore grown and expanded in media containing charcoal-IgG-stripped FBS, and media containing the antibody was collected and stored upon cell passaging or freezing.

4.3.3.2 Purification of Antibody from Collected Media

Collected media was pooled, filtered and antibody was purified using HPLC with Hitrap protein G sepharose columns, eluted and concentrated to 8.6mg/ml.

A direct ELISA and Western blot (shown in Figure 4-7) using samples of each eluted fraction confirmed that fractions 4-10 contained eluted antibody.

4.3.3.3 C1 Antibody and C4 Ascites Isotype Testing

Abmart stated that both colonies should produce a monoclonal antibody, so in order to validate which isotype the purified antibody was, a direct ELISA and Western blot were performed using secondary antibodies against the heavy chains of specific IgG isotypes 1, 2a, 2b and 3 to detect the C1 antibody. The experiments were also performed on a sample of unpurified C4 ascites sent to us by the company.

As shown in Figure 4-8 below, the C1 antibody was not in fact monoclonal, but tested positive as a mix of IgG1 and IgG3, and the C4 ascites was positive for IgG1, IgG2a, IgG2b and IgG3.

4.3.3.4 C1 Antibody and C4 Ascites Specificity Validation

Although neither the C1 antibody nor C4 ascites was monoclonal, they would still be suitable for use in both the intended ELISA and tissue immunohistochemistry if they could successfully detect the presence of nitrated CXCL8 without detecting the wild type chemokine. To assess this, both dot blots and direct ELISAs were performed, using a 3NT antibody and nitrated BSA as controls, as well as the polyclonal rabbit anti-human CXCL8 antibody (AHC0881, Life Technologies), which was known to detect both wild type and nitrated CXCL8.

As shown in Figure 4-9A, the C1 antibody did not detect the wild type CXCL8, or the nitrated BSA in an ELISA, though neither did it detect the nitrated CXCL8 (lines in the red colour scheme). The controls were successful, as the CXCL8 polyclonal antibody detected both wild type and nitrated CXCL8 but not nitrated BSA (lines in the green colour scheme), and the 3NT antibody detected both the nitrated CXCL8 and nitrated BSA but not the wild type CXCL8 (lines in the blue colour scheme), as expected. Similar results were achieved using a dot blot technique (detecting chemokine directly spotted onto nitrocellulose membrane) as shown in Figure 4-9B. In this case, the C1 antibody could detect the short C1 peptide it was raised against, but could not detect the full length nitrated CXCL8 protein. Again, the controls were successful, as the 3NT antibody detected the C1 peptide, nitrated BSA and the nitrated CXCL8 – all of which contain nitrated tyrosine residues. The CXCL8 polyclonal antibody detected both wild type and nitrated CXCL8, without detecting the C1 peptide and nitrated BSA as expected.

The direct ELISA was repeated exactly as stated using the C4 ascites, with the same results shown below in Figure 4-10A; the C4 ascites could not detect nitrated CXCL8. The dot blot experiment was repeated, using only wild type and nitrated CXCL8, but samples were either in their native conformation or denatured. As shown in Figure 4-10B neither the C1 antibody nor C4 ascites detected either chemokine whether denatured or not, and the CXCL8 polyclonal antibody could detect chemokines whether denatured or not.

Work on the C1 and C4 hybridoma cells was not carried forward beyond this stage.

A

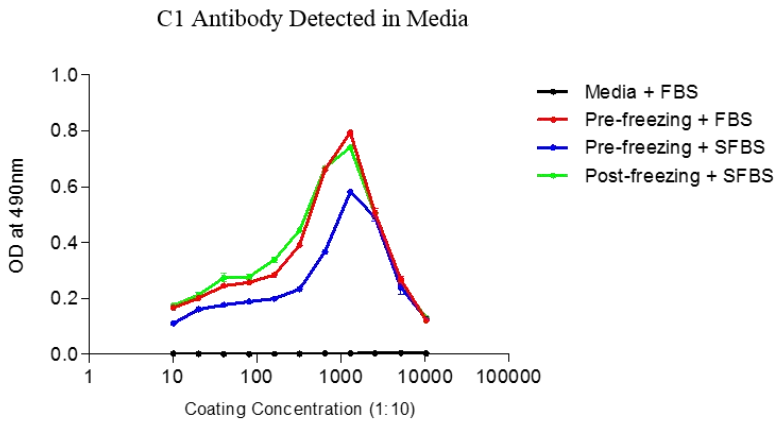

B

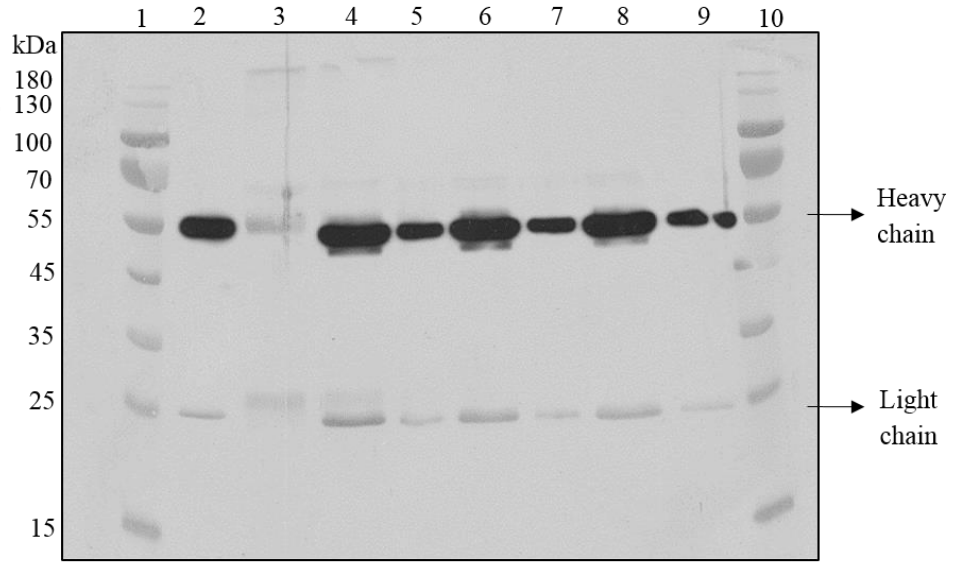

1. Size markers
2. DMEM + FBS only
3. Blank
4. Pre-freezing + FBS
5. Pre-freezing + FBS – 1/5 dilution
6. Pre-freezing + IgG-stripped FBS
7. Pre-freezing + IgG-stripped FBS – 1/5 dilution
8. Post-freezing + IgG-stripped FBS
9. Post-freezing + IgG-stripped FBS – 1/5 dilution
10. Size markers

Figure 4-6. Antibody production by C1 cells. Antibody production by C1 cells is unaffected by cryo-freezing followed by resurrection, or by the presence of normal vs. IgG-stripped FBS in culture media as determined by a direct ELISA A), and a Western blot B), both with detection using an anti-mouse IgG-HRP secondary antibody (A3673, Sigma). Data shown in A) is from N=1 experimental replicate, with n=3 technical replicates, and in B) is from N=1 experimental replicate, n=1 technical replicate.

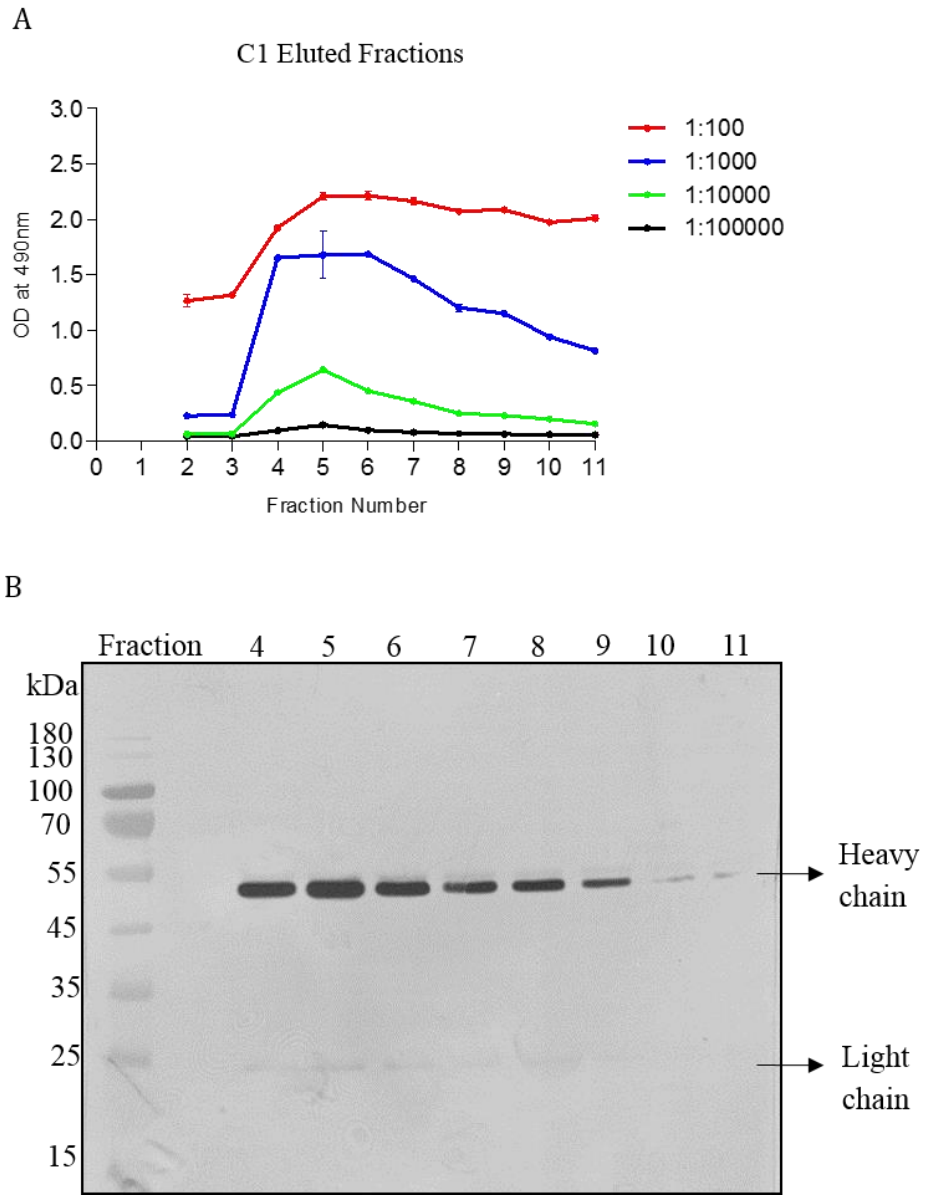

Figure 4-7. Isolating antibody from C1 media. HPLC antibody purification was successful, with fractions 4-10 containing eluted antibody, as determined by a direct ELISA A), and a Western blot B), both with using detection an anti-mouse IgG-HRP secondary antibody (A3673, Sigma). Data shown in A) is from N=1 experimental replicate, with n=3 technical replicates, and in B) is from N=1 experimental replicate, n=1 technical replicate.

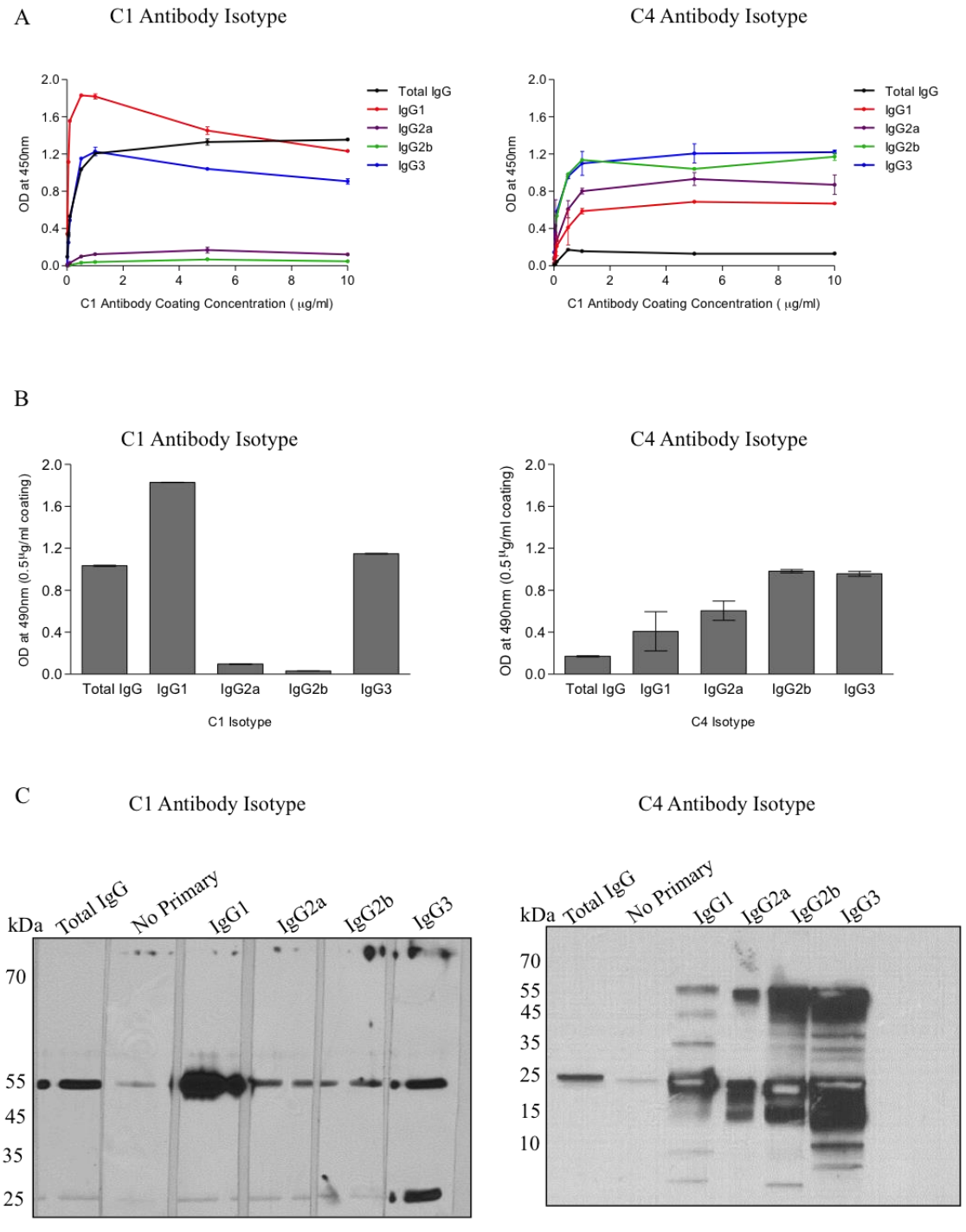

Figure 4-8. C1 antibody and C4 ascites isotyping. Isotypes were detected using antibodies against IgG1 (M-8144, Sigma), IgG2a (M-8269, Sigma), IgG2b (M-8394, Sigma) and IgG3 (M-9924, Sigma), developed with an anti-mouse-HRP secondary antibody (A3673, Sigma). The C1 antibody was confirmed as being polyclonal IgG1 and IgG3, and not monoclonal as stated. The C4 ascites was confirmed as positive for IgG1, IgG2a, IgG2b and IgG3. This was determined by a direct ELISA (A and B), and a Western blot (C). Data shown in A) and B) is from N=1, n=3 experiments, and data shown in C) is from N=1 experimental replicate, with n=1 technical replicate.

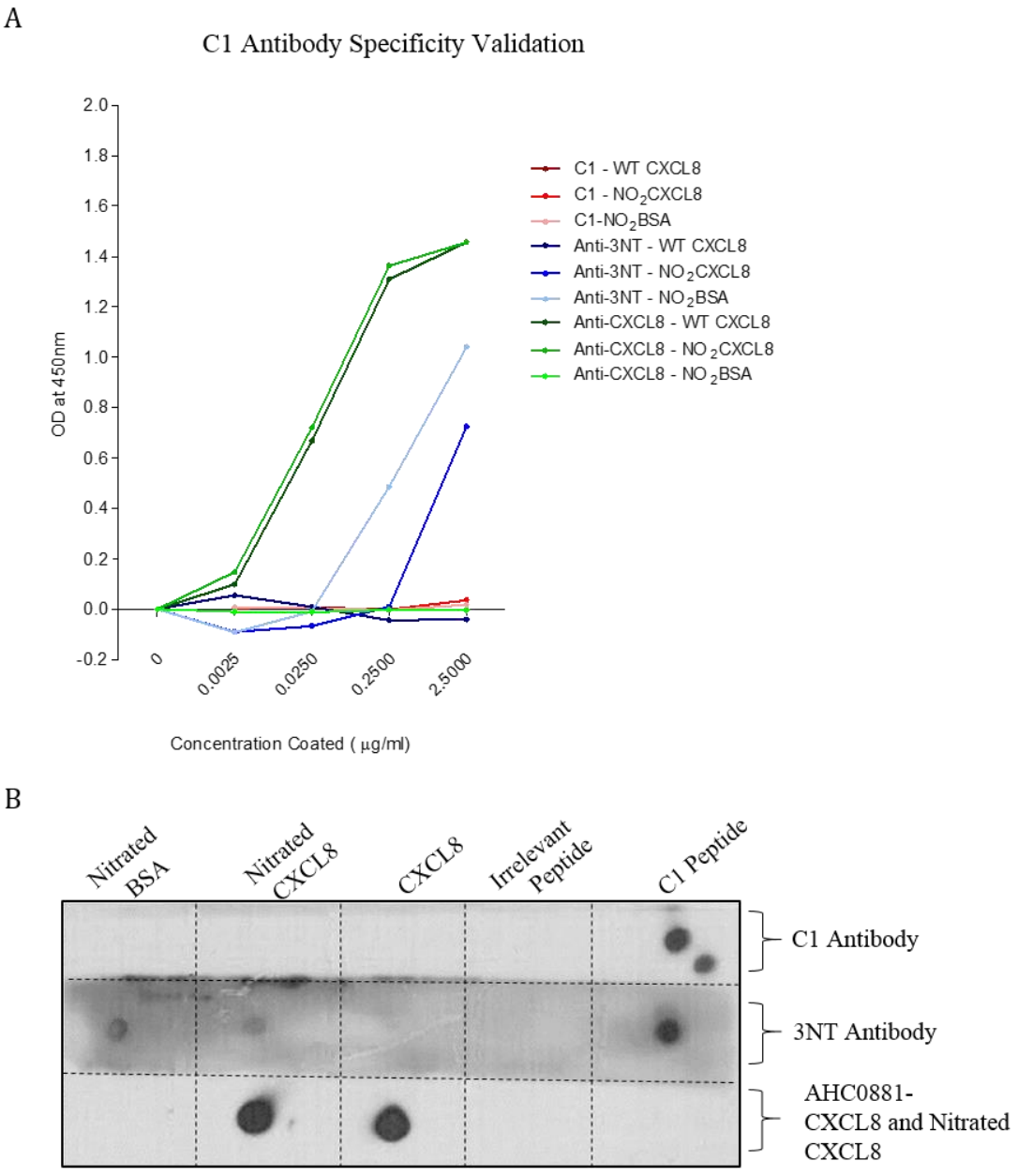

Figure 4-9. C1 antibody specificity. C1 antibody used at 20µg/ml cannot detect the full-length nitrated CXCL8 protein in either a direct ELISA at a range of concentrations A) or in a dot blot at 100ng B). The CXCL8 polyclonal antibody used at 5µg/ml (AHC0881, Life Technologies) could detect both wild type and nitrated CXCL8 in both experimental conditions, and the 3NT antibody used at 5µg/ml (06-284, Millipore) could detect the nitrated CXCL8 and nitrated BSA in the ELISA and the dot blot, as well as the C1 peptide in the dot blot. CXCL8 and 3NT primary antibodies were detected using an anti-rabbit-HRP secondary antibody (A6154, Sigma), and the C1 antibody was detected using an anti-mouse-HRP secondary antibody (A3673, Sigma). Data shown in A) is from N=1 experimental replicate, with n=3 technical replicates, and in B) is from N=3 experimental replicates, each with n=1 technical replicate.

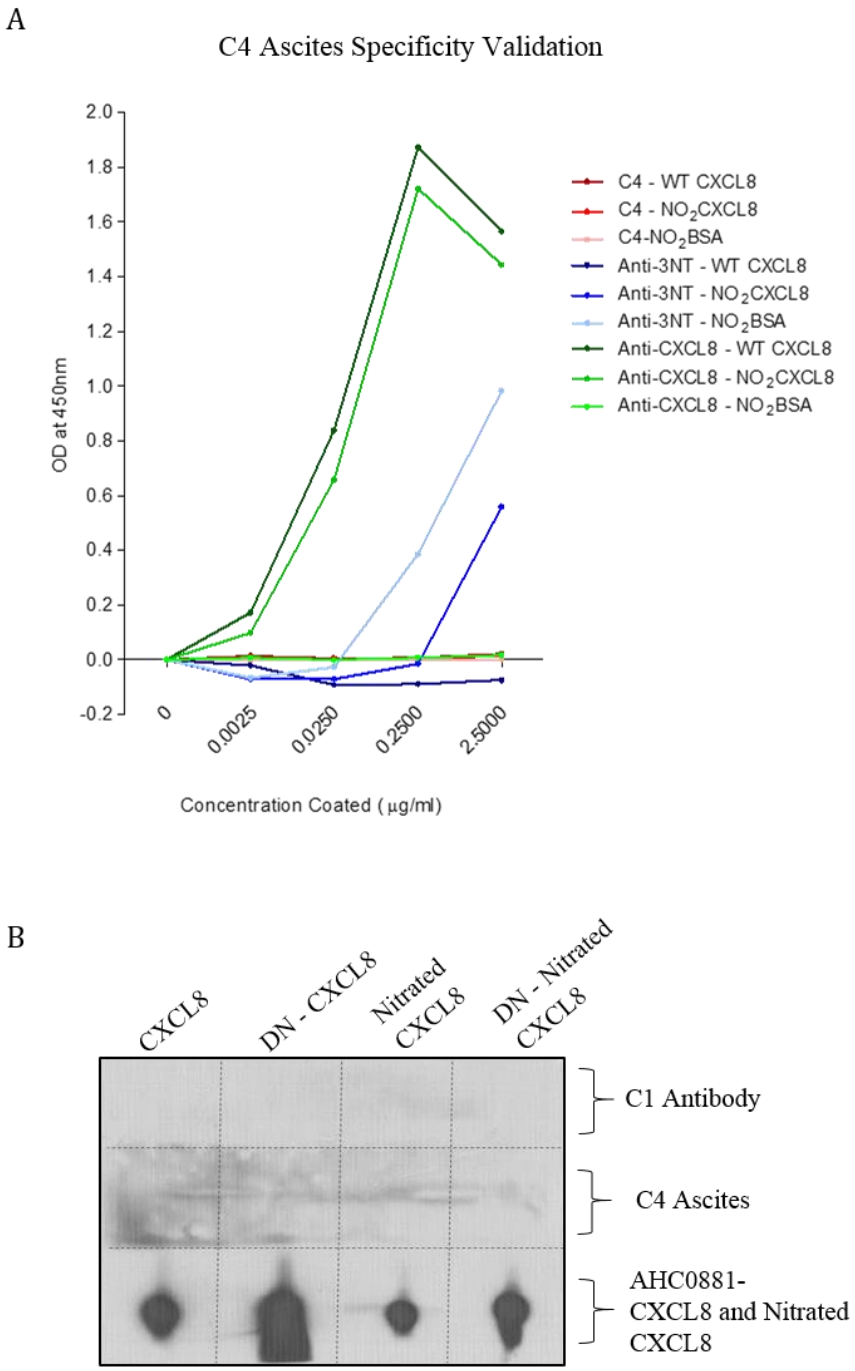

Figure 4-10. C4 ascites specificity. C4 ascites cannot detect the full-length nitrated CXCL8 protein in a direct ELISA at a range of concentrations A). The CXCL8 polyclonal antibody used (AHC0881, Life Technologies) could detect both wild type and nitrated CXCL8, and the 3NT antibody (06-284, Millipore) could detect the nitrated CXCL8 and nitrated BSA. Neither the C1 or C4 antibodies could detect 100ng of wild type or nitrated CXCL8 (denatured (DN) or undenatured) in a dot blot B), whereas the CXCL8 polyclonal antibody could detect both chemokines in both structural forms. CXCL8 and 3NT primary antibodies were detected using an anti-rabbit-HRP secondary antibody (A6154, Sigma), and the C1 antibody was detected using an anti-mouse-HRP secondary antibody (A3673, Sigma). Data shown in A) is from N=1 experimental replicate, with n=3 technical replicates, and in B) is from N=3 experimental replicates, each with n=1 technical replicate.

4.3.4 Bio-Rad Antibody Candidate Validation

Validation of Abmart antibodies was discontinued, and an alternative collaboration was sought with Bio-Rad.

Bio-Rad develop custom recombinant monoclonal HuCAL® antibodies using positive and negative screening of peptides or proteins against a phage display library of antibodies. This library consists of human antibody genes synthetically made to cover >95% of the structural immune repertoire, that are cloned in *E.Coli* expression vectors. Panning and screening was performed to find candidate antibodies that would recognise the full-length nitrated CXCL8 protein (which was verified as being nitrated using mass spectrometry after incubated with peroxynitrite), but not full-length wild type CXCL8 protein in Bio-Rad's optimised direct ELISA assays. Potential candidate antibodies that display >5-fold higher specificity for nitrated CXCL8 over wild type CXCL8 were produced as bivalent Fab-bacterial alkaline phosphatase fusion antibodies with FLAG® and Histidine6 tags (Figure 4-11), and sent to us for further validation. An example of Bio-Rad's initial validation data for the first batch of antibody candidates is shown in Figure 4-12.

Of the first batch of antibody candidates sent (AbD31663.1-AbD31682.1, shortened to 63-82), none showed higher affinity/selectivity for nitrated CXCL8 over wild type CXCL8 within the experimental set-up available in our laboratory, using a biotinylated anti-histidine6 secondary antibody followed by streptavidin-HRP and substrate shown in Figure 4-13. This was true in both a direct ELISA assay shown in Figure 4-14A, and in a dot blot assay shown in Figure 4-14B.

Following another round of screening using alternative conditions, five new candidate antibodies were sent (AbD31646.1- AbD31650.1, shortened to 46-50). I continued validation with four of these candidates, as one (candidate 48) showed minimal distinction between wild type and nitrated CXCL8 detectability in Bio-Rad's initial validation studies as shown in Figure 4-15. Initially validation experiments were performed as direct ELISA assays (using the same experimental set-up shown in Figure 4-13) detecting the candidates' ability to detect nitrated CXCL8 and wild type CXCL8, coated in 3 different concentration ranges. In each of these assessments nitrated BSA was also used at the highest concentration tested as a negative control, assessing the candidates' ability to bind to a non-specific nitrated protein. The highest range of

concentrations (1-100ng/ml) is shown as the first column of graphs in Figure 4-16 below, and at this range, only 46 (Figure 4-16A) and 49 (Figure 4-16C) showed reasonable degrees of specificity for nitrated CXCL8 over wild type CXCL8, but only for detection of the highest concentrations tested in each range. Candidates 46 and 49 retained their specificity for nitrated CXCl8 over wild type CXCL8 when a lower range of concentrations (0.1-10ng/ml) was tested as shown in the second column of graphs, although this specificity was lost when the concentrations were reduced further to 0.1-1ng/ml in the third column. Candidate 47 showed a higher affinity for wild type CXCL8 than nitrated CXCL8 at all concentrations tested (Figure 4-16B), and 50 showed similar affinities at all concentrations tested (Figure 4-16D).

For clarity, the detection of the highest concentration tested in each range is shown alone in Figure 4-17, with the OD readings for wild type CXCL8, nitrated CXCL8 and nitrated BSA grouped together for each antibody candidate. 46 showed an increased affinity for nitrated CXCL8 over wild type CXCL8 of ~5-fold when tested with 100ng/ml of either chemokine, ~11-fold at 10ng/ml and ~1-fold at 1ng/ml respectively. 49 showed corresponding values of ~2-fold, ~6-fold and ~1.3-fold. The candidates 46 and 49 therefore show specificity for nitrated CXCL8 at all concentrations tested, but with a detection sensitivity of between 1 and 10ng/ml. For all of the antibody candidates except 47, as the concentration ranges decreased the ability to distinguish between wild type and nitrated CXCL8 is reduced, as is the signal observed.

Work therefore progressed using candidates 46 and 49.

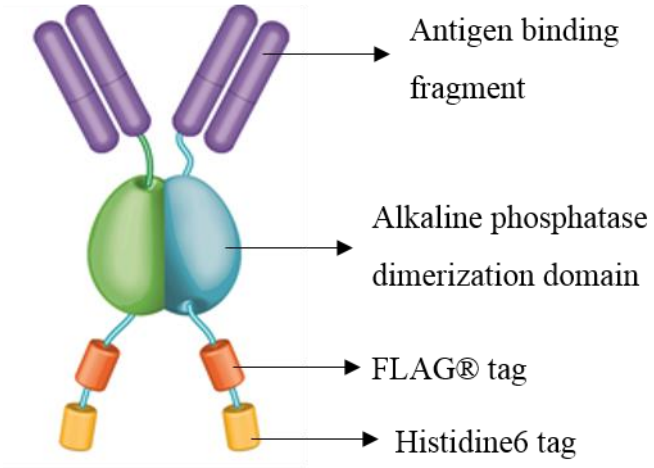

Figure 4-11. Structure of HuCAL® antibodies. Bivalent monoclonal antibody structure shown, with two antigen binding regions connected by an alkaline phosphatase dimerization domain with FLAG® and Histidine6 tags.

4.3.4.1 First Candidate Analysis

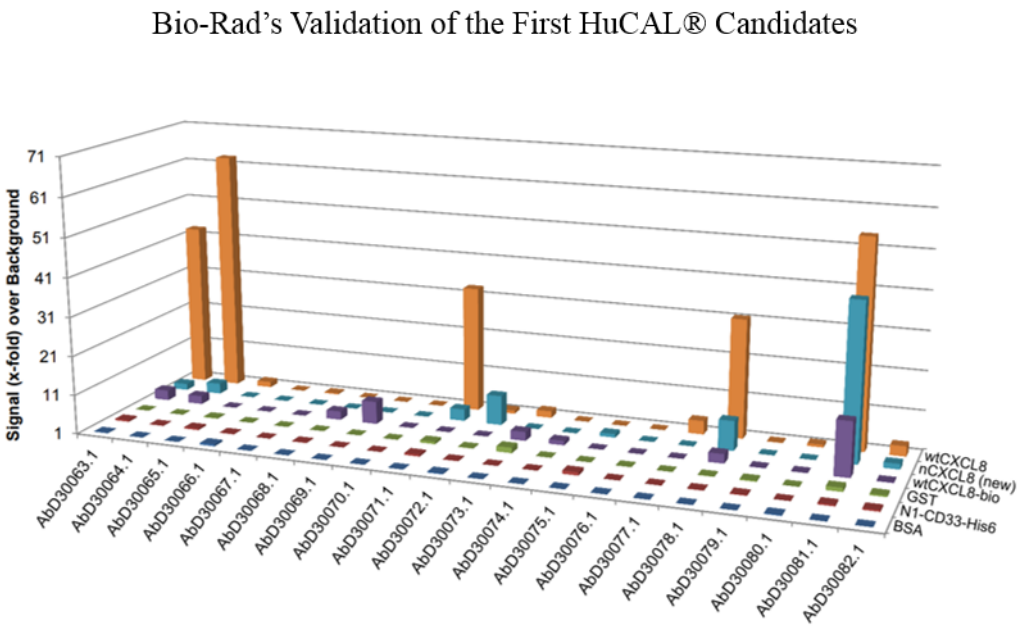

Figure 4-12. Bio-Rad's initial validation of the first batch of antibody candidates. Antibodies were tested by Bio-Rad in direct ELISA assays using their standard protocol.

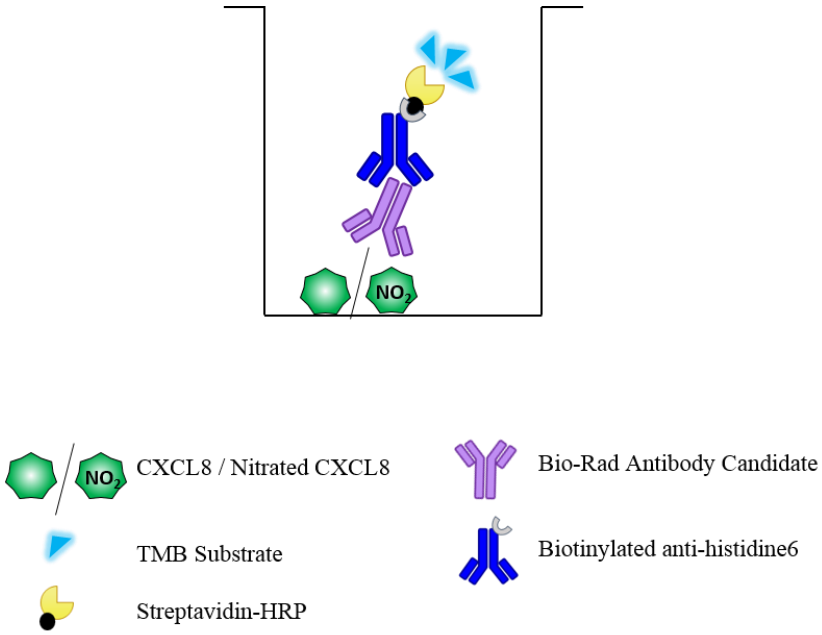

Figure 4-13. Direct ELISA experimental set-up using Bio-Rad antibody candidates as detection antibodies.

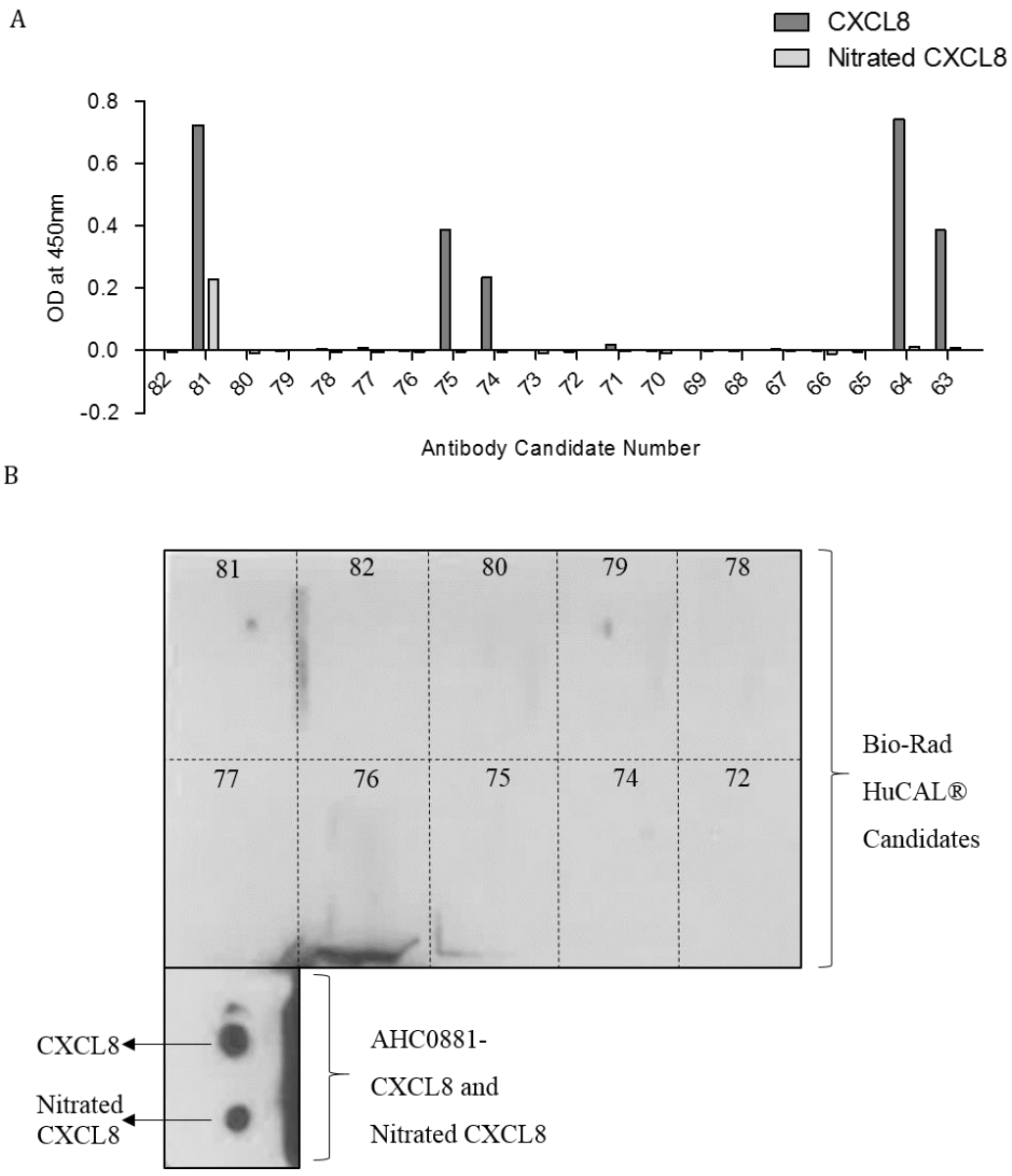

Figure 4-14. Validating the first batch of Bio-Rad antibody candidates. The ability of the antibodies to detect 250ng wild type or nitrated CXCL8 in a direct ELISA (detection was carried out using a biotinylated anti-histidine6 secondary antibody (MCA1396B, Bio-Rad), streptavidin-HRP and TMB substrate, and the plate was read at 450nm (corrected)) or B) 100ng wild type or nitrated CXCL8 in dot blot assays, when used at 2µg/ml. Data shown in A) is from N=1 experimental replicate, with n=3 technical replicates, and in B) is from N=3 experimental replicates, with n=1 technical replicate.

4.3.4.2 Second Candidate Analysis

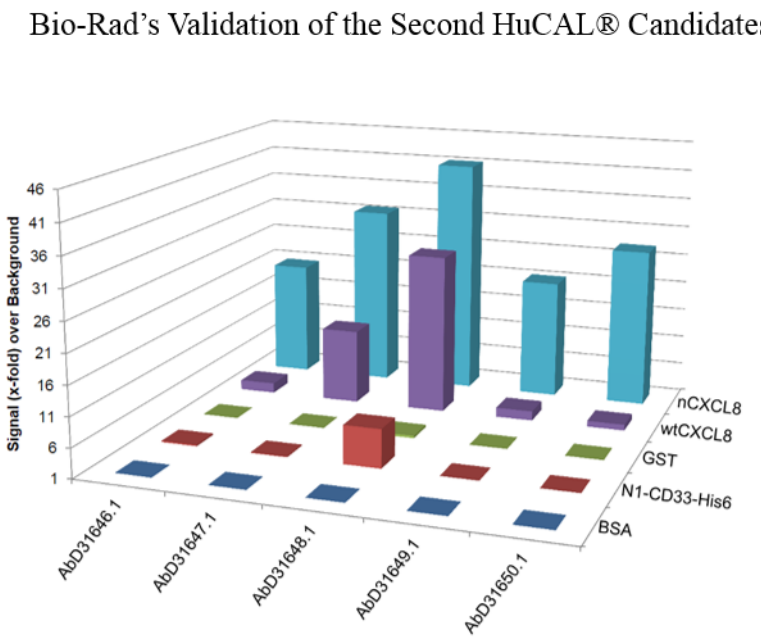

Figure 4-15. Bio-Rad's initial validation of the second batch of antibody candidates. Antibodies were tested by Bio-Rad in direct ELISA assays using their standard protocol.

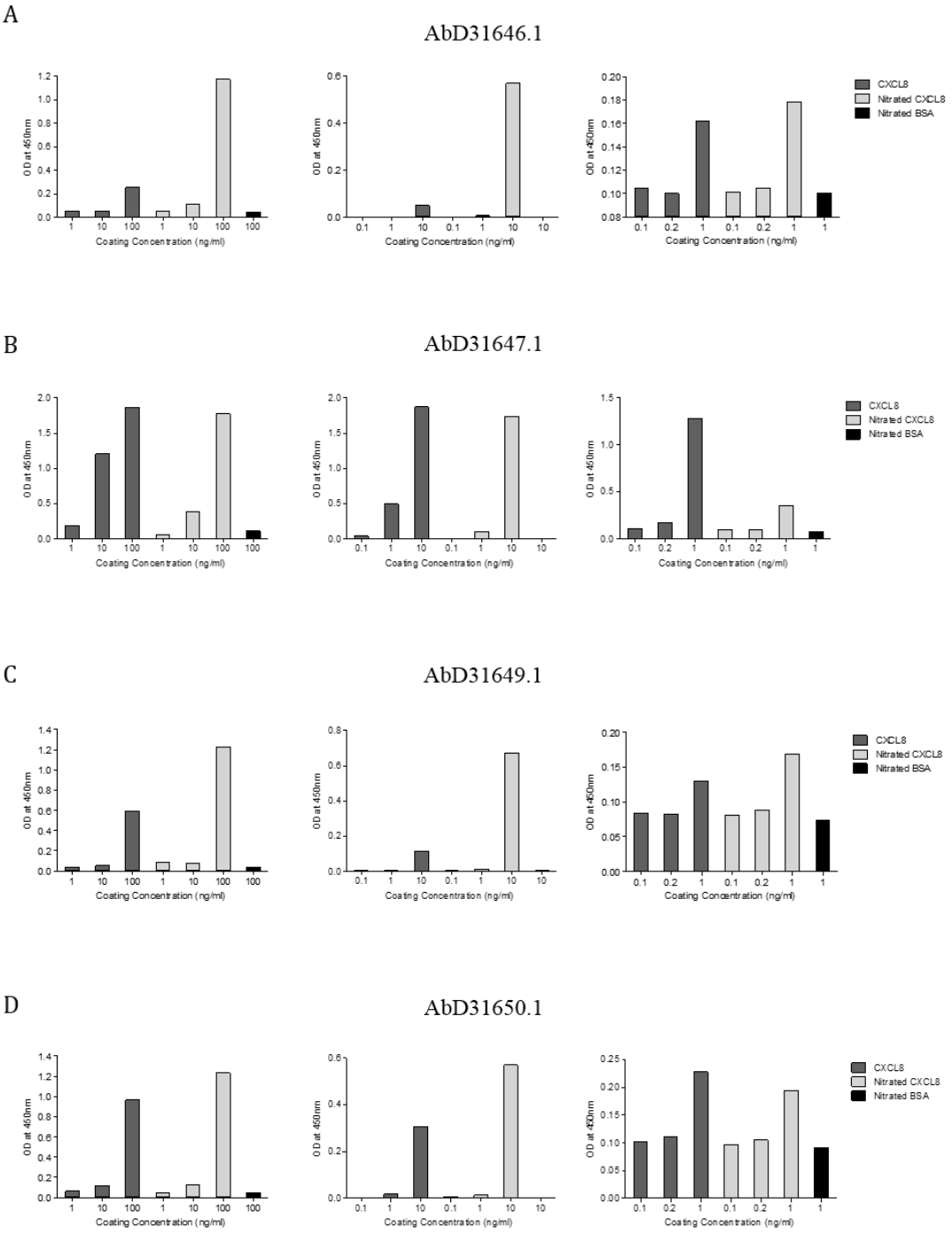

Figure 4-16. Validating the second batch of Bio-Rad antibody candidates using a direct ELISA. The ability of the antibodies A) AbD31646.1, B) AbD31647.1, C) AbD31649.1 and D) Abd31650.1 to detect 3 different concentration ranges of wild type or nitrated CXCL8 in a direct ELISA, when used at 2µg/ml. Concentration ranges tested were 1-100ng/ml (first column), 0.1-10ng/ml second column) and 0.1-1ng/ml (third column). Nitrated BSA was used as a control to test cross-reactivity with a non-specific nitrated protein at the highest concentration in each range. Detection was carried out using a biotinylated anti-histidine6 secondary antibody (MCA1396B, Bio-Rad), streptavidin-HRP and TMB substrate, and the plate was read at 450nm (corrected). Data shown is from N=1 experimental replicate, with n=3 technical replicates.

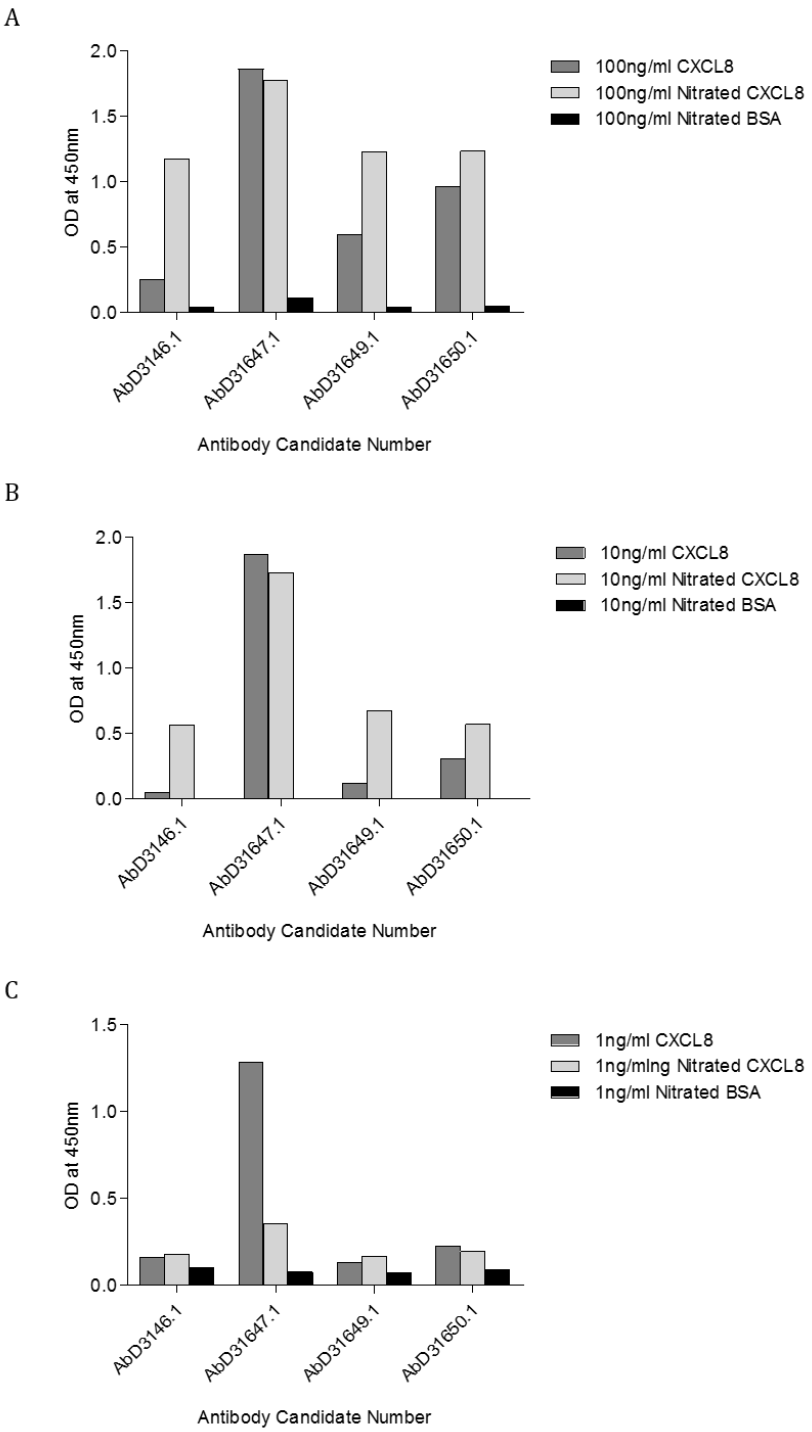

Figure 4-17. Validating the second batch of Bio-Rad antibody candidates using a direct ELISA. The highest concentrations in each of the three ranges tested are shown, with the OD readings for the detection of wild type CXCL8, nitrated CXCL8 and nitrated BSA grouped together for each antibody. A) shows the detection of 100ng/ml from the highest concentration range, B) shows the detection of 10ng/ml from the median concentration range, and C) shows the detection of 1ng/ml from the lowest concentration range. Detection was carried out using a biotinylated anti-histidine6 secondary antibody (MCA1396B, Bio-Rad), streptavidin-HRP and TMB substrate, and the plate was read at 450nm (corrected). Data shown is from N=1 experimental replicate, with n=3 technical replicates.

4.3.4.3 Validating Abd31646.1 and Abd31349.1 Specificity

Having found that candidates 46 and 49 showed the most differential specificity for nitrated CXCL8 over wild type CXCL8 (while showing no cross-reactivity with nitrated BSA) in direct ELISA assays, I aimed to assess the specificity of these two candidates in a dot blot assay. CXCL8, nitrated CXCL8, nitrated BSA and nitrated CXCL1 were all added to nitrocellulose membrane in 2µl dots at 6.2ng total (as the previous direct ELISA results indicated that the detection limit of 46 and 49 was between 1ng/ml and 10ng/ml). Figure 4-18A shows that detection with a rabbit polyclonal anti-CXCL8 antibody (AHC0881) showed clear positive signals for CXCL8 and nitrated CXCL8, with no signal for nitrated BSA or nitrated CXCL1 as expected. 46 showed no clear signal for the detection of any sample, whereas 49 did show a positive signal for nitrated CXCL8 only. Detection of the same samples with a 3NT antibody confirmed the presence of nitrated tyrosine residues in samples spiked with nitrated CXCL8, but not CXCL1 as this does not contain any tyrosine residues. No signal was observed for nitrated BSA, although the signal could be below the detection limit as low concentrations of the protein were added to the membrane.

As these initial experiments were conducted with each chemokine diluted in PBS, I then aimed to assess if these two candidates were able to show the same selectivity when detecting nitrated CXCL8 in a complex mix of proteins. This was tested by spiking PBS or normal human serum with nitrated CXCL8 or wild type CXCL8, and assessing antibody detection as previously described. Higher sample concentrations were used in this assay to increase signal. Figure 4-18B shows the detection of 100ng of wild type CXCL8 or nitrated CXCL8 in 2µl of PBS or normal human serum. Basal PBS and serum without the addition of any chemokine were included as negative controls. Detection with AHC0881 showed a clear signal for both wild type and nitrated CXCL8 in both PBS and serum as expected, with no signal detected for the basal PBS control and some signal for the serum control, indicating the natural presence of CXCL8 within this sample. Both 46 and 49 also showed no signal for the basal PBS, and a clear increase in signal was observed when either PBS or serum was spiked with nitrated CXCL8. 46 does also appear to show a faint signal for wild type CXCL8 at these higher concentrations used. Both antibodies did, however, also give a positive signal for basal serum.

The same signal for basal serum was observed when samples were tested in direct ELISA assays detected with 49 alone as shown in Figure 4-19; a signal which did not increase despite the addition of varying concentrations of nitrated CXCL8 and was greater than the signal for equivalent concentrations of nitrated CXCL8 diluted in PBS. These data together suggested that either the antibodies were binding to other non-specific proteins present in serum, or there exists a very high concentration of nitrated CXCL8 naturally present in serum.

In order to test these theories, I spiked normal human serum with 10µg wild type CXCL8 or 6.6µg nitrated CXCL8 and performed fractionation by size exclusion chromatography. Figure 4-20 shows the HPLC trace, indicating that the majority of the protein was eluted in fractions 6-23, with maximum elution occurring in fraction 12.

The fractions could then be diluted differentially to prevent the dilution of the chemokine but allowing high abundance proteins to be diluted enough to be run on an 18% SDS gel. Firstly, the serum samples were run on such a gel and stained with Coomassie® Blue to visualise the molecular weights of the proteins present in each fraction. The results are shown in Figure 4-21. In Figure 4-21A (showing the staining of fraction from serum spiked with wild type CXCL8), fractions 7-13 are shown to contain a high abundance of high molecular weight proteins. Figure 4-21B shows the same results in fractions 6-11 for serum spiked with nitrated CXCL8. In both cases, fractions 15-18 show protein bands around the molecular weight of chemokines such as CXCL8 at 8-10kDa.

Fractions were then run on triplicate18% SDS-PAGE followed by Western blot analysis with detection using a rabbit polyclonal anti-CXCL8 antibody (AHC0881) know to detect both wild type and nitrated CXCL8 spiked into the samples. Detection was also performed using antibodies 46 and 49, to assess their specificity for nitrated CXCL8. The results in Figure 4-22A show that the CXCL8 polyclonal antibody detects both wild type and nitrated CXCL8 with bands at the correct molecular weights for CXCL8 monomers, and nitrated CXCL8 monomers and dimers. Detection with 46 (Figure 4-22B) shows that this antibody does recognise other non-specific proteins present in serum, with clear defined bands visible at 25 and 55 kDa in fractions 11-16 from serum samples spiked with both wild type and nitrated CXCL8, as well as non-specific background staining present on the membrane. Detection with 49 showed a slightly cleaner membrane with

less non-specific background staining (Figure 4-22C). This antibody also detected clear defined bands at 25 and 55 kDa, but these were only present in the fraction from serum samples spiked with nitrated CXCL8 and not wild type CXCL8. When exposed for a longer time (as indicated by the black arrow) bands at the correct molecular weight for nitrated CXCL8 were also visible. Both 46 and 49 therefore recognise other non-specific proteins present in serum, in addition to nitrated CXCL8.

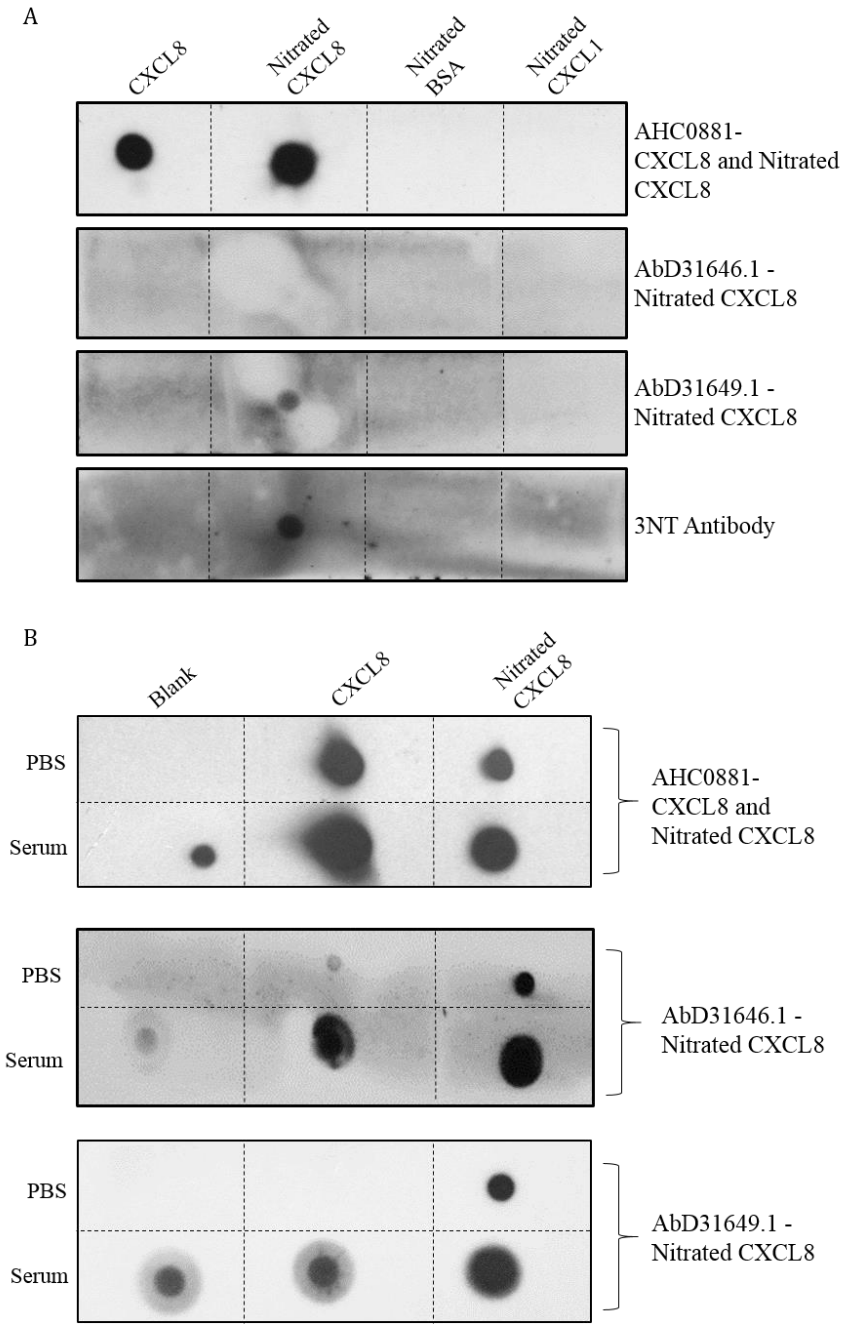

Figure 4-18. Validating the specificity of AbD31646.1 and AbD31649.1 using a dot blot. A) 6.2ng of CXCL8, nitrated CXCL8, nitrated BSA or nitrated CXCL1 were added in 2µl dots to nitrocellulose membrane in replicate strips. B) 100ng of CXCL8 or nitrated CXCL8 was spiked in to PBS or serum and added as a 2µl dots to nitrocellulose membrane in replicate strips. For both A) and B) Each strip was incubated with a different primary antibody for detection; a rabbit polyclonal anti-CXCL8 antibody (AHC0881) at 1µg/ml, a 3NT antibody (ab61392, Abcam) at 1µg/ml, AbD31646.1 at 2µg/ml or AbD31649.1 at 2µg/ml. AHC0881 was detected using an anti-rabbit-HRP secondary antibody (A6154, Sigma), ab61392 with an anti-mouse-HRP secondary antibody (A3673, Sigma), and AbD31646.1/AbD31649.1 using a biotinylated anti-histidine6 secondary antibody (MCA1396B, Bio-Rad), streptavidin-HRP and ECL substrate. Data shown is from N=3 experimental replicates, each with n=1 technical replicates.

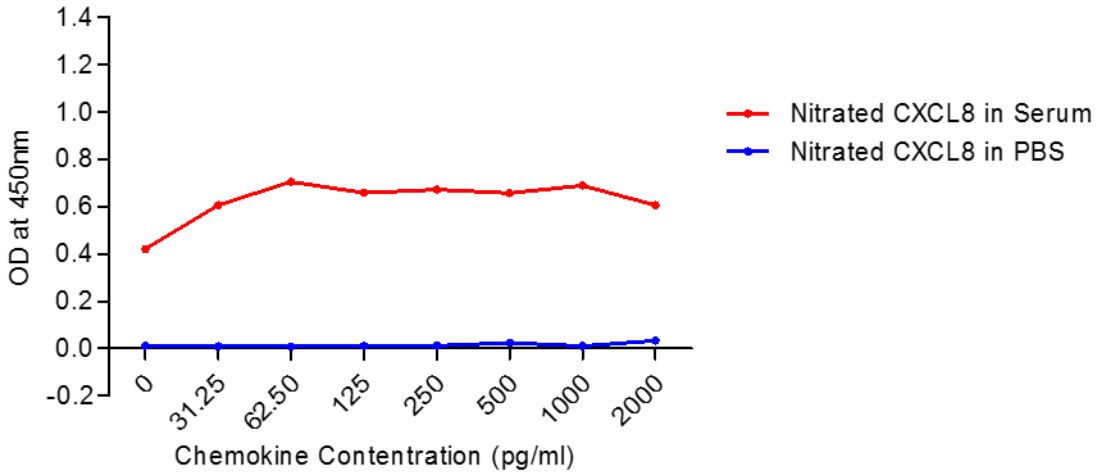

Figure 4-19. Validating the specificity of Abd31649.1 using a direct ELISA. Nitrated CXCL8 was coated onto an Immulon HB4X ELISA plate at a range of concentrations (pg/ml) in either PBS or normal human serum. Detection was performed using AbD31649.1 at 2µg/ml, followed by a biotinylated anti-histidine6 secondary antibody (MCA1396B, Bio-Rad), streptavidin-HRP and ECL substrate. Data shown is from N=1 experimental replicates, each with n=2 technical replicates.

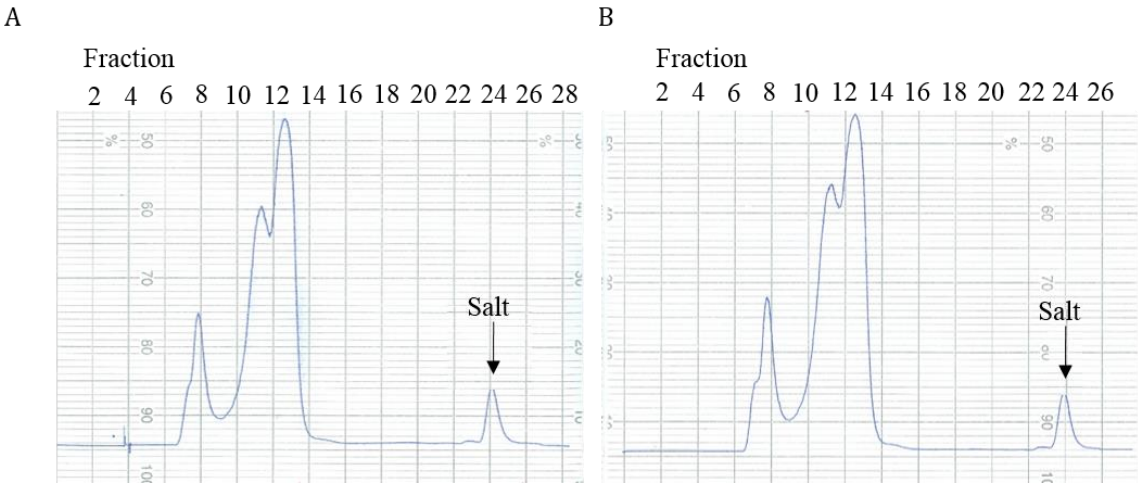

Figure 4-20. Spiked serum fractionating by size exclusion high performance liquid chromatography (HPLC). UV trace of the HPLC performed showing the elution of protein, as 8mg /0.5ml of serum spiked with A) 10µg of wild type CXCL8 or B) 6.6µg of nitrated CXCL8 was flown through a Superose 12 column at 0.5ml/minute. The trace shows peaks corresponding to the elution of the protein and salt. Data shown is from N=1 experimental replicate, with n=1 technical replicate.

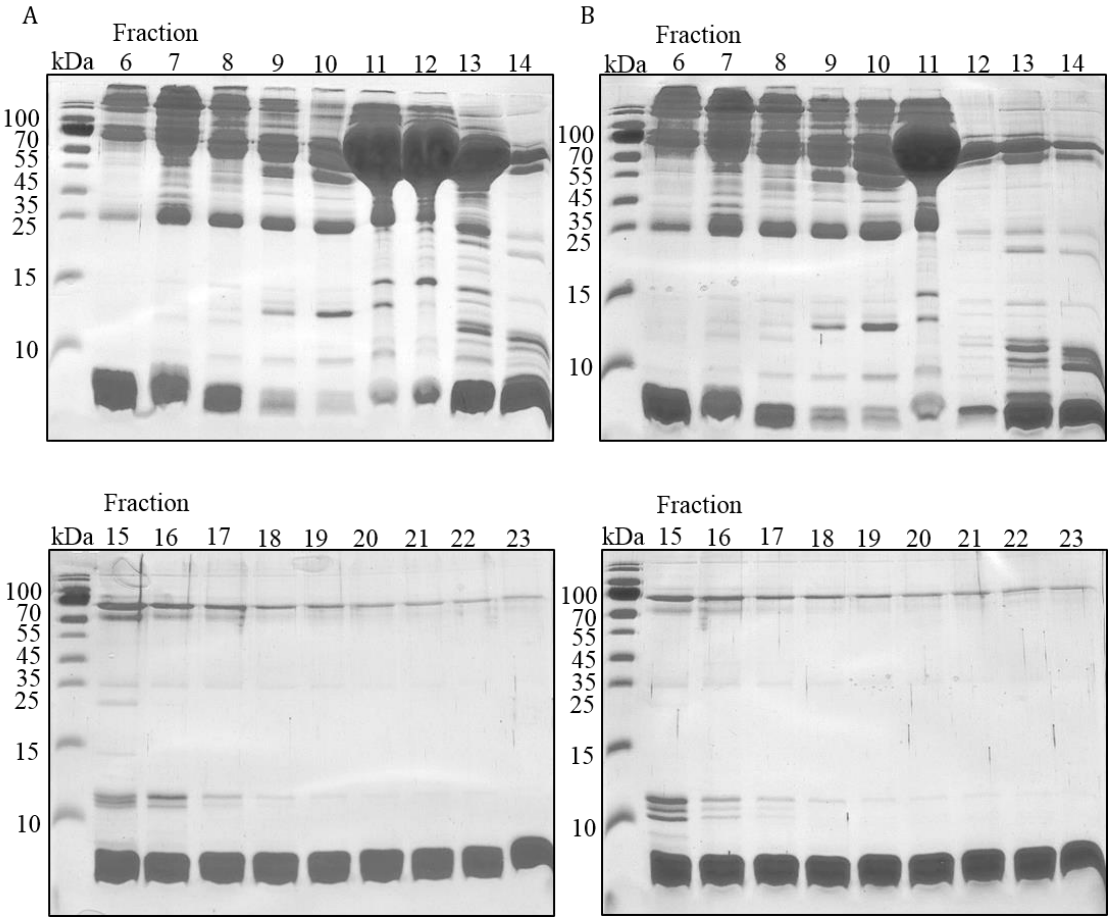

Figure 4-21. Coomassie® Blue analysis to determine protein content of spiked serum fractions. Fractions from size exclusion high performance liquid chromatography (HPLC) performed on serum samples spiked with A) 10µg of wild type CXCL8 or B) 6.6µg of nitrated CXCL8 run on 18% SDS-PAGE and stained with Coomassie® Blue. Data shown is from N=1 experimental replicate, with n=1 technical replicate.

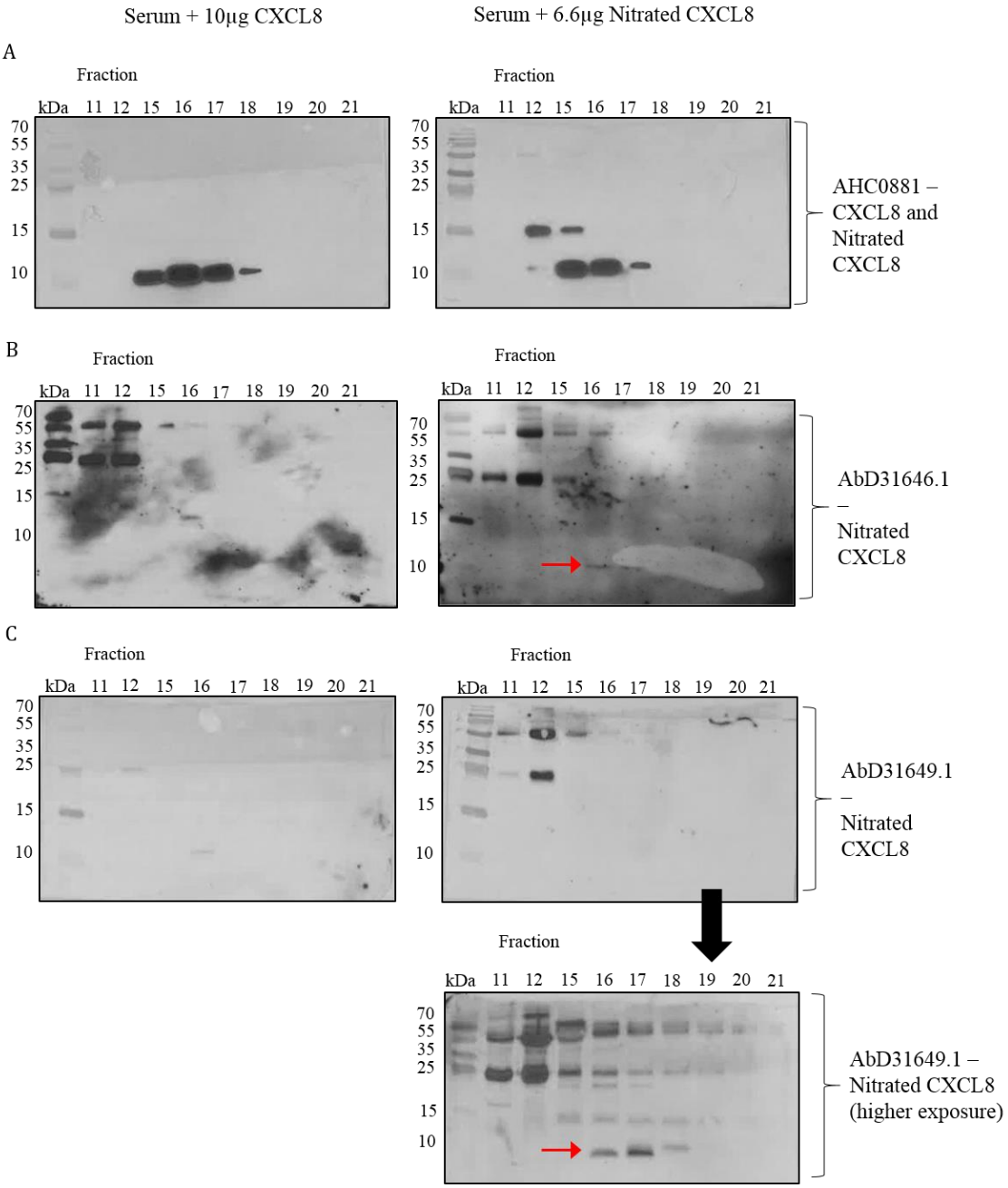

Figure 4-22. Validating the specificity of AbD31646.1 and AbD31649.1 using a Western blot. SDS-PAGE and Western blot analysis of spiked serum samples fractionated by size exclusion high performance liquid chromatography (HPLC). Gels were run in triplicate and the resulting membranes after protein transfer were stained with A) a rabbit polyclonal anti-CXCL8 antibody (AHC0881) at 1µg/ml, B) AbD31646.1 at 2µg/ml and C) AbD31649.1 at 2µg/ml. Detection for A) was carried out using an anti-rabbit-HRP secondary antibody (A6154, Sigma), and for B) and C) using a biotinylated anti-histidine6 secondary antibody (MCA1396B, Bio-Rad), streptavidin-HRP and ECL substrate. Red arrows indicate possible correct detection of nitrated CXCL8 monomers. Data shown is from N=2 experimental replicates, each with n=1 technical replicate.

4.3.4.4 Developing a Sandwich ELISA using AbD31649.1

Both antibody candidates 46 and 49 were shown to have specificity for nitrated CXCL8 over wild type CXCL8. Both were also shown to cross-react with non-specific proteins present in human serum. Thus neither antibody is suitable for use in a direct ELISA. As 49 gave a cleaner Western blot with less non-specific background staining, this antibody was carried forward for development into a sandwich ELISA assay.

Initial experiments involved using 48 as a capture antibody at a range of concentrations, as this antibody was shown by Bio-Rad to have affinity for both wild type and nitrated CXCL8 (Figure 4-15). It was therefore used in attempts to capture both wild type CXCL8 and nitrated CXCL8 diluted to 10ng/ml in PBS. This concentration was known to be within detection limits for wild type CXCL8 when using the detection antibody from R&D's Human CXCL8 Duoset ELISA kit, and for nitrated CXCL8 when using 49 as the detection antibody. As the 48 and 49 antibodies were of the same format, to avoid cross-reactivity that would result from using the biotinylated anti-histidine6 antibody as a tertiary step, 49 was directly biotinylated using Lightning-Link® Rapid Biotin Kit (Expedeon). This experimental set-up is shown in Figure 4-23. Results shown in Figure 4-24A for the detection of nitrated CXCL8 indicate cross-reactivity between the detection antibody (49) and the capture antibody (48), due to almost identical signals being observed when nitrated CXCL8 was added in comparison to PBS only. Figure 4-24B shows the detection of wild type CXCL8 using R&D's IL8 Duoset detection antibody after capture with 48, with no signal observed at any concentration of capture antibody used. These results indicate that 48 and 49, and 48 and AHC0881 are both incompatible as capture-detection antibody pairs.

Further sandwich ELISA development trials were carried out at the Rega Institute, KU Leuven. These involved testing a polyclonal goat anti-CXCL8 antibody (Rega #4576) that the group have developed in house, and regularly use in CXCL8 ELISA assays, for use as a potential capture antibody. This experimental set-up is shown in Figure 4-25. The capture antibody was coated at a dilution of 1/100 (triple the concentration than the group regularly use the antibody at). Wild type CXCL8 (at a range of concentrations) was detected using a mouse anti-CXCL8 monoclonal secondary antibody, followed by a biotinylated anti-mouse tertiary antibody. Nitrated CXCL8 (at a range of concentrations) was detected using biotinylated 49. While a clear S-shaped curve of detection was

observed for wild type CXCL8 in this assay, no signal was observed for any of the concentrations of nitrated CXCL8 used (the highest of which were again within the known detection limit of the detection antibody 49) (Figure 4-26). Rega #4576 was also therefore deemed unsuitable as a capture antibody for use in this sandwich ELISA.

The next potential capture antibody trialled was the polyclonal rabbit anti-human CXCL8 antibody (AHC0881, Life Technologies). The protocol was followed exactly as described above, using this capture antibody instead of Rega #4576 as shown in Figure 4-27. Again, a clear S-shaped curve of detection was observed for wild type CXCL8. A signal above background was observed for 10ng/ml nitrated CXCL8 (OD at 450nm of 0.313) (Figure 4-28), although not for any lower concentrations of nitrated CXCL8 tested. This capture-detection antibody pair was therefore taken forward for further development to improve assay sensitivity.

A checkerboard-style sandwich ELISA assay was performed to determine the optimal concentrations of AHC0881 and 49 to be used in combination. Results in Figure 4-29 show that, at the range of concentrations trialled, 5µg/ml was the optimal concentration for both antibodies to be used at together. Further development work is required if this anitbody pair is to be suitable for the selective detection of low levels of nitrated CXCL8 in biological samples.

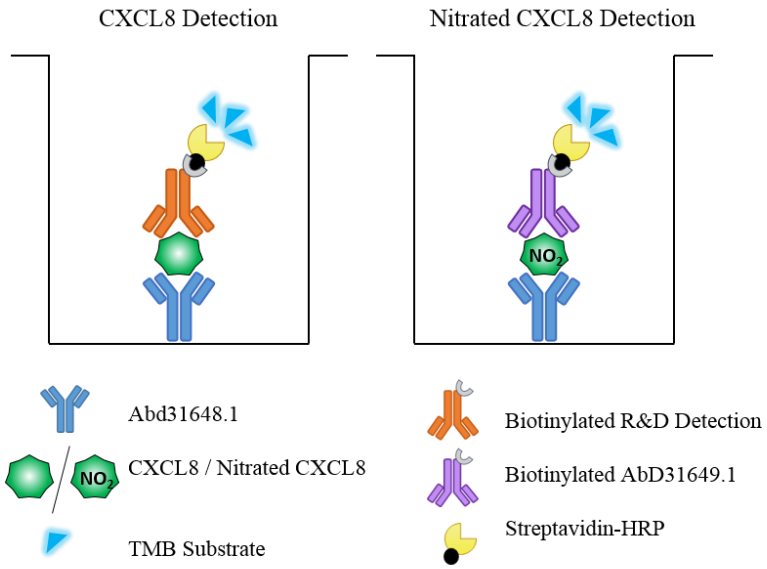

Figure 4-23. Sandwich ELISA experimental set-up using AbD31648.1 as a capture antibody.

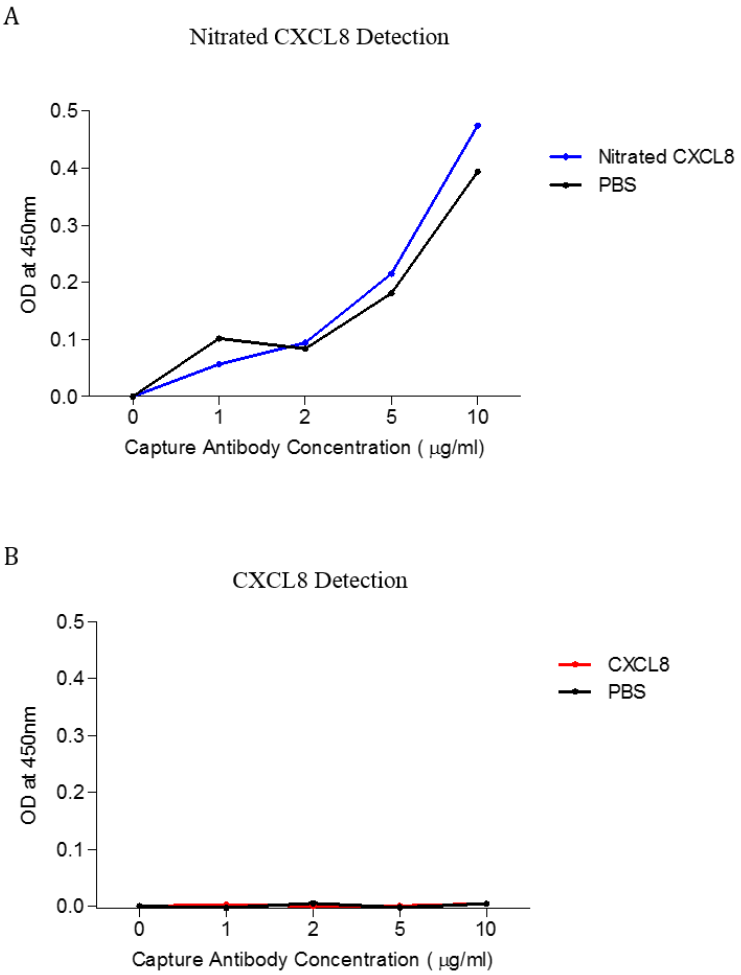

Figure 4-24. Sandwich ELISA trial using AbD31648.1 as a capture antibody. AbD31648.1 was coated onto an Immulon HB4X ELISA plate at a range of concentrations (µg/ml) in coating buffer. Chemokine was then added at 10ng/ml, followed by A) nitrated CXCL8 detection using biotinylated-AbD31649.1 at 2µg/ml then streptavidin-HRP followed by TMB substrate.or B) wild type CXCL8 detection using R&D's Human CXCL8 Duoset ELISA kit detection antibody (HRP conjugated) The plate was read at 450nm (corrected). Data shown is from N=1 experimental replicate, with n=3 technical replicates.

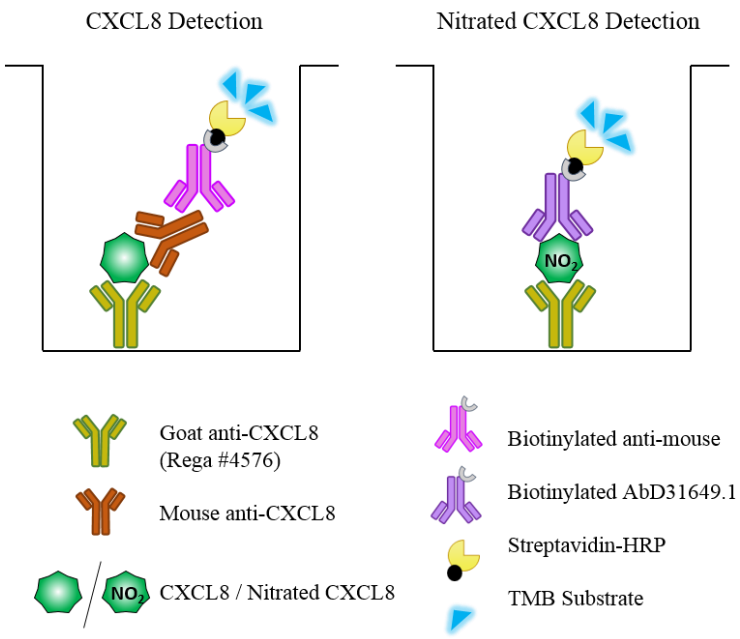

Figure 4-25. Sandwich ELISA experimental set-up using Rega #4576 polyclonal goat anti-CXCL8 as a capture antibody.

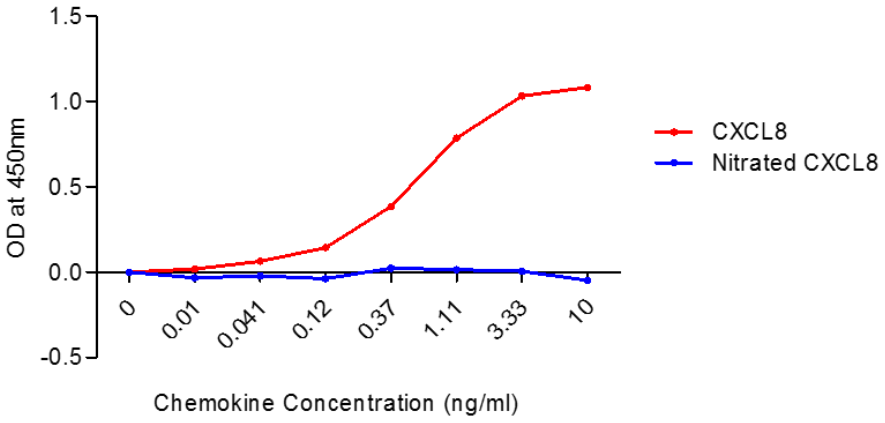

Figure 4-26. Sandwich ELISA trial using Rega #4576 polyclonal goat anti-CXCL8 as a capture antibody. Rega #4576 was coated onto an Immulon 4HBX ELISA plate at 1/100 in coating buffer. Chemokine was then added at a range of concentrations (ng/ml). Wild type CXCL8 was detected using a mouse-anti-CXCL8 secondary antibody then biotinylated anti-mouse tertiary antibody. Nitrated CXCL8 detection using biotinylated-AbD31649.1 at 2µg/ml. For both streptavidin-HRP was added followed by TMB substrate. The plate was read at 450nm (corrected). Data shown is from N=1 experimental replicate, with n=3 technical replicates.

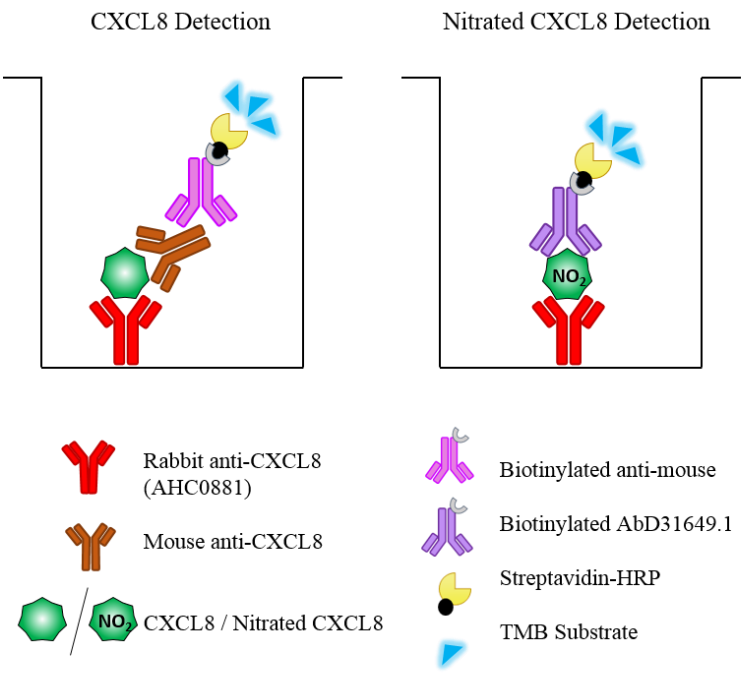

Figure 4-27. Sandwich ELISA experimental set-up using polyclonal rabbit anti-human CXCL8 (AHC0881, Life Technologies) as a capture antibody.

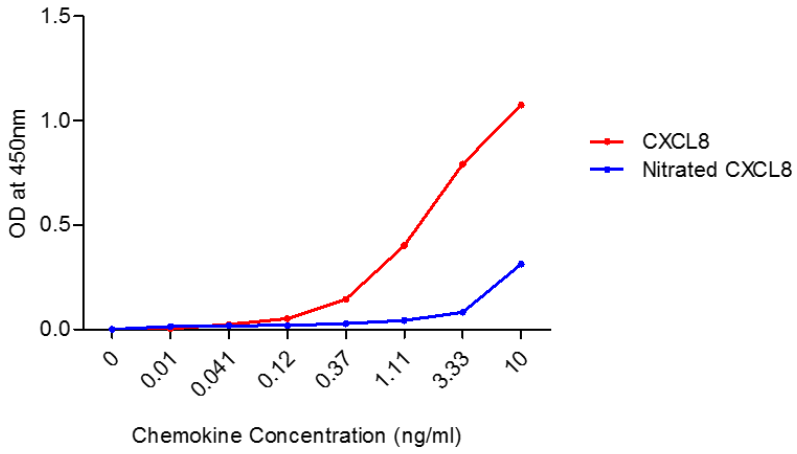

Figure 4-28. Sandwich ELISA trial using polyclonal rabbit anti-human CXCL8 (AHC0881, Life Technologies) as a capture antibody. AHC0881 was coated onto an Immulon 4HBX ELISA plate at 1µg/ml in coating buffer. Chemokine was then added at a range of concentrations (ng/ml). Wild type CXCL8 was detected using a mouse-anti-CXCL8 secondary antibody then biotinylated anti-mouse tertiary antibody. Nitrated CXCL8 detection using biotinylated-AbD31649.1 at 2µg/ml. For both streptavidin-HRP was added followed by TMB substrate. The plate was read at 450nm (corrected). Data shown is from N=1 experimental replicate, with n=3 technical replicates.

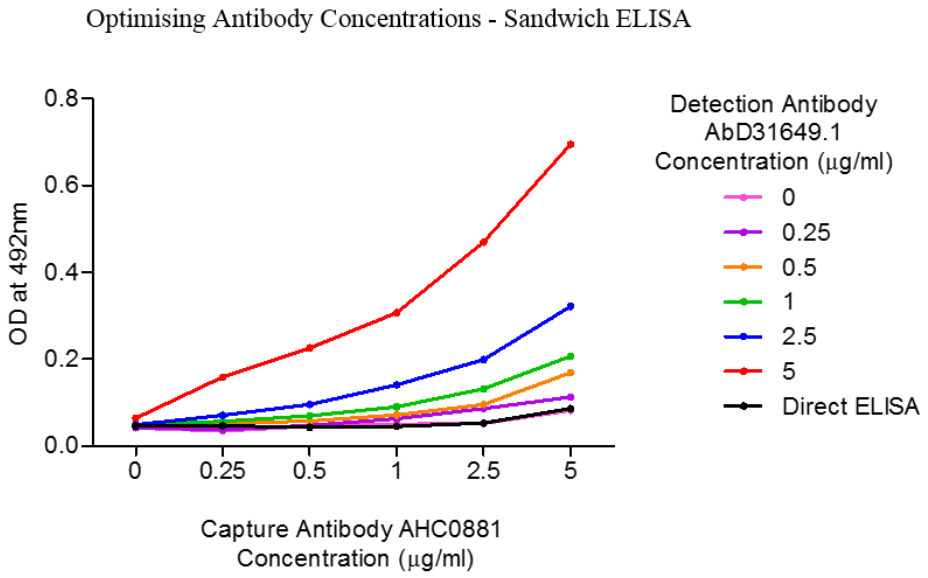

AHC0881 Concentration (µg/ml) →

AbD31649.1 Concentration (µg/ml) ↓

	0	0.25	0.5	1	2.5	5	Direct ELISA
0	0.042	0.043	0.046	0.05	0.049	0.064	0.046
0.25	0.035	0.038	0.052	0.057	0.071	0.159	0.047
0.5	0.046	0.048	0.058	0.07	0.096	0.226	0.043
1	0.05	0.063	0.072	0.09	0.141	0.307	0.045
2.5	0.052	0.086	0.096	0.132	0.199	0.47	0.053
5	0.082	0.113	0.169	0.207	0.322	0.695	0.086

Figure 4-29. Checkerboard sandwich ELISA to optimise the concentration of capture and detection antibodies. AHC0881 was coated onto an Immulon 4HBX ELISA plate at a range of concentrations (µg/ml) in coating buffer. Nitrated CXCL8 was then added at a constant concentration of 10ng/ml, and detected with a range of concentrations (µg/ml) of AbD31649.1 followed by biotinylated anti-histidine6 secondary antibody (MCA1396B, Bio-Rad), streptavidin-HRP and OPD substrate. The plate was read at 492nm (corrected). The same assay was also performed as a direct ELISA assay (black line) to determine if sensitivity was improved by the addition of a capture antibody. Data shown is from N=1 experimental replicate, with n=3 technical replicates.

4.3.4.5 Validating AbD31649.1 for Use in Immunofluorescence

With the aim of using the novel Bio-Rad antibody Abd31649.1 to detect the presence of nitrated CXCL8 in patient tissue biopsy samples (the amount of which could be correlated with disease severity), attempts were made to validate the use of this antibody in immunofluorescence staining. In all experiments, double immunofluorescence staining was also performed to detect CXCL8 (polyclonal rabbit anti-CXCL8, AHC0881, Life Technologies) and 3NT (ab61392, Abcam) as a likely

indicator of the potential presence of nitrated CXCL8. In order for staining to be considered specific, any signal visualised with AbD31649.1 should only occur in the areas where CXCL8 and 3NT appear to co-localise.

Initial experiments were trialled using unfixed frozen chamber slides in order to bypass the need for any optimisation of antigen retrieval methods. Chambers were seeded with HMEC-1 cells (cultured as described in section 2.3.3), and treated with different stressing agents in order to increase the expression of CXCL8 and its possible nitration. These included a bacterial-derived stressing agent (1µg/ml LPS for 6 hours) and an oxidative stressing agent (200µM H_2O_2 for 2 hours followed by 4 hour recovery). A previous PhD student, Catriona Barker, had optimised these treatments. Staining was then performed to detect CXCL8 (detected using a Dylight-550 conjugated secondary antibody (red)), and 3NT (detected using a Dylight-488 conjugated secondary antibody (green)), or nitrated CXCL8 using AbD31649.1 at 25µg/ml (a 1/50 dilution) (detected using a biotinylated anti-histidine6 secondary antibody and streptavidin-Alexa594 (red)). Results in Figure 4-30 show that both LPS and H_2O_2 treatment induce an upregulation of CXCL8 expression, with H_2O_2 also inducing an upregulation of 3NT expression that co-localises with the CXCL8 staining, indicating the potential presence of nitrated CXCL8. No positive staining was seen in chambers treated the same way but stained using AbD31649.1.

Experiments were repeated as shown in Figure 4-31, with the H_2O_2 treatment changed to a 6 hour treatment with 600µM peroxynitrite (also previously optimised by Catriona Barker), in an attempt to increase protein nitration. In this case, results indicated that treatment with LPS but not peroxynitrite increased the upregulation of both CXCL8 and 3NT, and only the LPS-treated cells showed any positive staining with AbD31649.1. This staining appears to be granular and is only present in the nucleus and does not appear in the cytoplasmic regions of the cells where CXCL8 and 3NT co-localise, indicating that this could be non-specific staining.

The same staining protocol was tested in paraffin-embedded lung sections, as lung is a known positive control tissue for CXCL8, which expresses high levels of 3NT. Results are shown in Figure 4-32. Antigen retrieval was performed using Citrate buffer for CXCL8 and 3NT (as was previously optimised for these antibodies), and Citrate buffer, Tris EDTA buffer, or trypsin enzymatic digestion for AbD31649.1. Staining for CXCL8 and

3NT showed intense expression of both markers across the lung tissue, with much of the staining co-localising. Only antigen retrieval using Tris EDTA gave any positive staining when AbD31649.1 was used, and this resembled the granular nuclear staining observed in treated chamber slides, not the strong cytoplasmic staining observed for CXCL8 and 3NT in both tissue and cells.

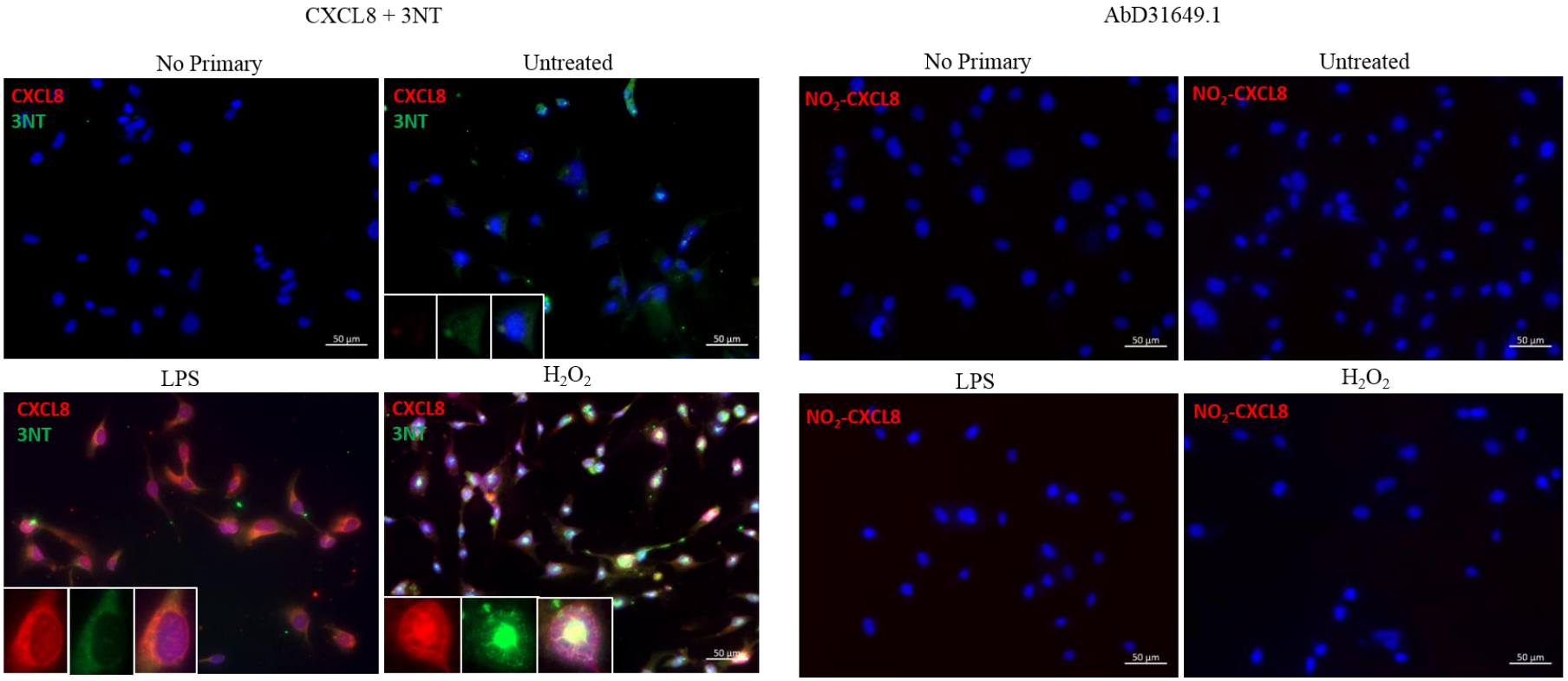

Figure 4-30. Using AbD31649.1 in immunofluorescence staining. HMEC-1 cells were treated in chamber slides for 6 hours with 1µg/ml LPS, and for 2 hours with 200µM H_2O_2 followed by 4 hours of recovery in normal media. Slides were fixed in ice-cold methanol, and stained for both CXCL8 (AHC0881, Life Technologies) detected using an anti-rabbit-DyLight550 conjugated secondary antibody (red) (GtxRb-003-D550NHSX, Immunoreagents) and 3NT (ab61392, Abcam) detected using an anti-mouse-DyLight488 conjugated secondary antibody (green) (GtxMs-003-E488NHSX, Immunoreagents), or AbD31649.1 (detected using a biotinylated anti-histidine6 secondary antibody and streptavidin-Alexa594 (red)) to detect the potential presence of nitrated CXCL8 (NO_2-CXCL8). Close-up images of individual $CXCL8^+$ $3NT^+$ cells are shown indented. Images were taken at 20x magnification, and images shown are representative of 5 fields of view imaged per chamber.

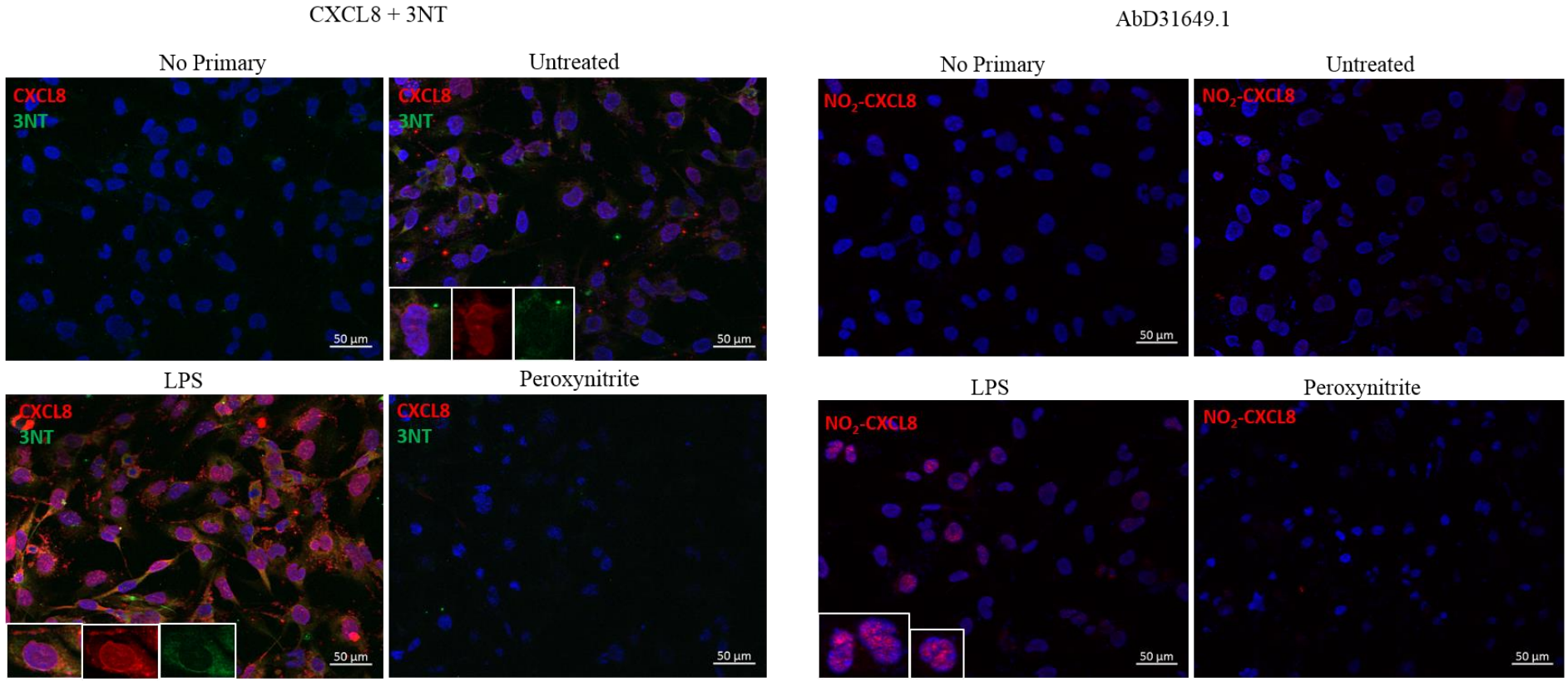

Figure 4-31. Using AbD31649.1 in immunofluorescence staining. HMEC-1 cells were treated in chamber slides for 6 hours with 1µg/ml LPS, and for 2 hours with 600µM peroxynitrite. Slides were fixed in ice-cold methanol, and stained for both CXCL8 (AHC0881, Life Technologies) detected using an anti-rabbit-DyLight550 conjugated secondary antibody (red) (GtxRb-003-D550NHSX, Immunoreagents) and 3NT (ab61392, Abcam) detected using an anti-mouse-DyLight488 conjugated secondary antibody (green) (GtxMs-003-E488NHSX, Immunoreagents), or AbD31649.1 (detected using a biotinylated anti-histidine6 secondary antibody and streptavidin-Alexa594 (red)) to detect the potential presence of nitrated CXCL8 (NO_2-CXCL8). Close-up images of individual $CXCL8^+$ $3NT^+$ cells are shown indented. Images were taken at 20x magnification, and images shown are representative of 5 fields of view imaged per chamber.

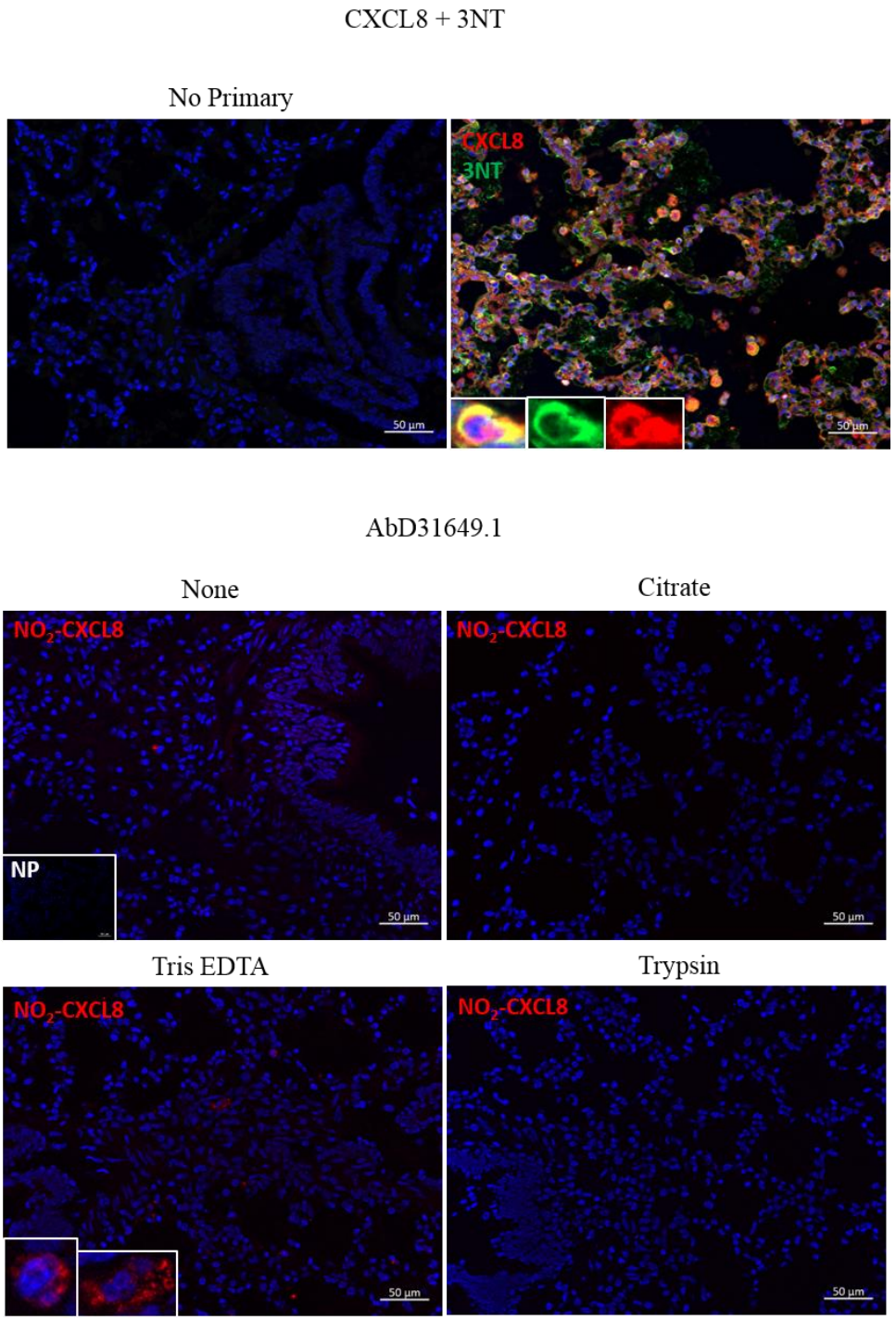

Figure 4-32.Using AbD31649.1 in immunofluorescence staining. Paraffin-embedded lung sections were processed and stained for both CXCL8 (AHC0881, Life Technologies) detected using an anti-rabbit-DyLight550 conjugated secondary antibody (red) (GtxRb-003-D550NHSX, Immunoreagents)and 3NT (ab61392, Abcam) detected using an anti-mouse-DyLight488 conjugated secondary antibody (green) (GtxMs-003-E488NHSX, Immunoreagents), or AbD31649.1 (detected using a biotinylated anti-histidine6 secondary antibody and streptavidin-Alexa594 (red)) to detect the potential presence of nitrated CXCL8 (NO_2-CXCL8). Different antigen retrieval methods were trialled for AbD31649.1 staining. No primary antibody control is shown indented (NP), as are close-up images of individual NO_2-CXCL8$^+$ cells. Images were taken at 20x magnification, and shown are representative of 5 fields of view imaged per chamber. Insert - no primary antibody control.

4.3.5 Detection of Nitrated CXCL8 in a Bronchoalveolar Lavage Sample from a Patient with Ventilator-Associated Pneumonia

Due to the sandwich ELISA for nitrated CXCL8 still being under development, I attempted to detect naturally occurring nitrated CXCL8 using a Western blot method. The samples selected for analysis were some of the bronchoalveolar lavage (BAL) samples from ventilator-associated pneumonia (VAP) patients, as these samples contained relatively high levels of wild type CXCL8 as assessed by ELISA (Figure 4-3), which was therefore also likely to be detectable by Western blot, and relatively low levels of total protein (Figure 4-5), which meant these samples could likely be run undiluted on an 18% SDS-PAGE gel. BAL samples from healthy control patients were also included, and the secretions from primary nasal mucosa cells (NM16) was also included as a positive control for the detection of wild type CXCL8, due to its high CXCL8 content. Samples were run on triplicate g, and detection was performed using a rabbit polyclonal anti-CXCL8 antibody (AHC0881) know to detect both wild type and nitrated CXCL8, Bio-Rad candidate 49 and a 3-NT antibody – positive staining of the same band with all three antibodies would indicate the presence of nitrated CXCL8.

Figure 4-33A shows that all 5 VAP patient BAL samples (RVI 1, 4, 9, 11 and 23) contain detectable levels of wild type CXCL8, which is supported by previous ELISA data in Figure 4-3. Sample RVI 1 also shows that this band is also visible when detected with 49 (Figure 4-33B) and 3-NT antibodies (Figure 4-33C), indicated by the red arrows. These results suggest that this sample contains naturally occurring nitrated CXCL8. Control patient BAL samples were negative for CXCL8 (Figure 4-33A), nitrated CXCL8 (Figure 4-33B) and 3-NT (Figure 4-33C), and NM16 was positive for CXCL8 (Figure 4-33A) but negative for nitrated CXCL8 (Figure 4-33B) and 3-NT (Figure 4-33C).

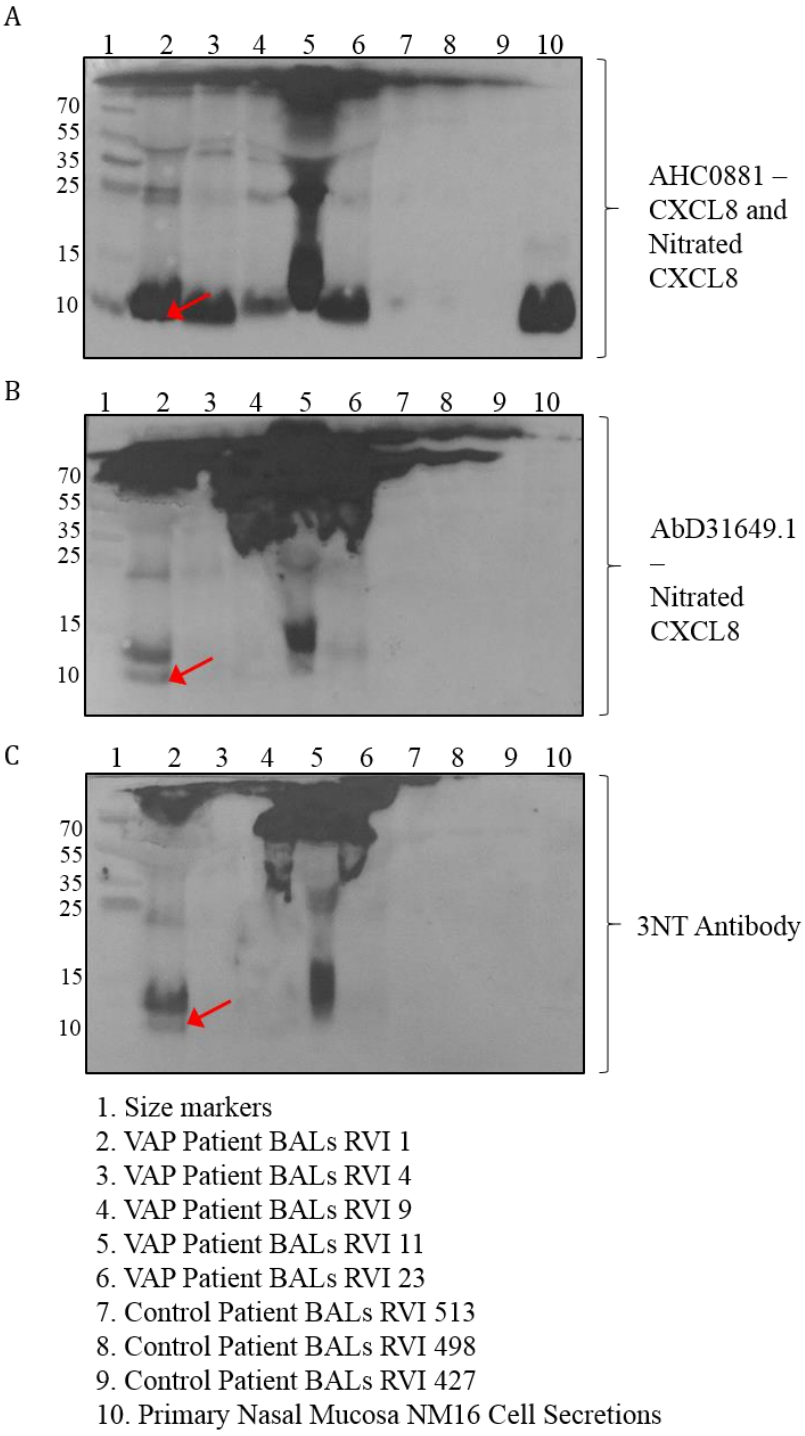

Figure 4-33. Detection of naturally occurring nitrated CXCL8. SDS-PAGE and Western blot analysis of 5 bronchoalveolar lavage (BAL) samples from patients with ventilator-associated pneumonia (VAP) (coded "RVI"), 3 BAL samples from healthy controls, and 1 sample of cell secretions from cultured primary nasal mucosa cells (coded "NM"). Gels were run in triplicate and the resulting membranes after protein transfer were stained with A) a rabbit polyclonal anti-CXCL8 antibody (AHC0881) at 1µg/ml, B) AbD31649.1 at 2µg/ml and C) 3NT (ab61392, Abcam) at 1µg/ml. Detection for A) was carried out using an anti-rabbit-HRP secondary antibody (A6154, Sigma), for B) using a biotinylated anti-histidine6 secondary antibody (MCA1396B, Bio-Rad) followed by streptavidin-HRP, and for C) using an anti-mouse-HRP secondary antibody (A3673, Sigma), all followed by ECL substrate. Red arrows indicate possible correct detection of nitrated CXCL8 monomers. Data shown is from N=1 experimental replicate, with n=1 technical replicate.

4.4 DISCUSSION

Currently available anti-CXCL8 antibodies are either specific for wild type CXCL8 only, or are capable of recognising both wild type and nitrated CXCL8. None, however, exist that are specific for nitrated CXCL8 only.

Analysis of wild type CXCL8 concentration and total protein concentration in a range of respiratory samples showed that CXCL8 can be present at a wide range of concentrations, from as low as 10pg/ml in normal human serum, to as high as 25ng/ml in VAP patients BAL samples and 113.5ng/ml in primary nasal mucosal cell secretions. These values detected are in agreement with the general trend reported in the literature, where CXCL8 is present at low concentrations during health, and increases up to low ng/ml ranges during disease [245,292,293], however such high CXCL8 concentrations as found in the primary cell secretions have only been reported previously in monocytes infected with *M. Tuberculosis* [294-297]. In addition to varying concentrations of CXCL8, these samples also showed a large degree of variation in their total protein concentrations and compositions. For example, the BAL sample from the inhaled chemical burns patient showed a total protein concentration of 422µg/ml, which was made up of a large number of proteins present at low abundance, whereas perfusate samples had a protein concentration over 10-fold higher (~47mg/ml), which were largely comprised of one high molecular weight protein present in abundance. Therefore any novel antibody developed would need to be able to detect a large range of concentrations of the nitrated CXCL8, from within a highly complex mixture of proteins, where the chemokine is likely present as a very small minority.

Attempts at developing such an antibody in collaboration with Abmart were disappointing. The cells provided were continually mycoplasma infected, the antibodies produced by the cells were not monoclonal, and while they were capable of recognising the linear peptides they were raised against, neither the C1 purified antibody nor the C4 ascites could recognise the full nitrated chemokine in its native form, in a direct ELISA or dot blot assay.

Bio-Rad have had previous success in generating antibodies against post-translationally modified proteins, such as AbyD03055, which recognises a modified version of the DJ-1

protein with one oxidised cysteine residue at position 106 [298]. It was hopeful, therefore, that their phage display library and screening methods would yield more positive results than the previous attempts. The second set of antibody candidate proved to be most successful, as both 46 and 49 could specifically detect nitrated CXCL8, but not wild type CXCL8, to a sensitivity of between 1ng/ml and 10ng/ml. However, Western blot analysis of fractionated serum spiked with CXCL8/nitrated CXCL8 confirmed that both antibodies bound to other proteins present in serum, due to the presence of clear defined bands particularly at 25kDa and 55kDa. These are higher molecular weights than the 8381/8426 Da signal expected for CXCL8/nitrated CXCL8 respectively. For 46 these bands were visible in fractions from both wild type and nitrated CXCL8-spiked serum, but 49 only detected bands at these weights in fractions from serum spiked with nitrated CXCL8. These are unlikely to be due to nitrated CXCL8 being bound to higher molecular weight carrier proteins such as albumin, as the weights do not correspond and the samples had been denatured, meaning any interacting proteins should have dissociated. The band seen at 55kDa could be due to the antibodies cross-reacting with Activated Protein C (a zymogen present in human plasma) [299,300], or Transthyretin (TTR) (a transport protein in the serum and cerebrospinal fluid)[301]. The 25kDa band could be due to cross-reaction with serum amyloid P[302]. These proteins should be present in both serum samples whether they were spiked with wild type CXCL8 or nitrated CXCL8, and so does not explain why 49 detected these bands only in the serum sample spiked with nitrated CXCL8. The possibility exists that the non-specific positive signals observed when staining with the Bio-Rad candidates could be due to the secondary antibodies or streptavidin-conjugated HRP (and not the Bio-Rad candidate primary antibodies) binding to other proteins, as "no primary antibody" controls were not assessed. This is potentially unlikely as the secondary antibodies used were raised against the histidine6 tag and so should not cross-react with serum proteins, but it is something that should be validated for both the secondary antibody and tertiary HRP detection reagents. These results meant that the antibodies would need to be incorporated into a sandwich ELISA assay, where a capture and detection system would solve the issue of cross-reactivity.

Several capture and detection antibody combinations were trialled, and the results are summarised below in Table 4-1. Bio-Rad's 48 was unsuccessful as a capture antibody, as 49 appears to cross-react with this when used to detect nitrated CXCL8 (due to identical

signal observed between wells incubated with nitrated CXCL8 or PBS as a negative control). The curved pattern of binding observed is likely due to the different concentrations of 48 coated, as the chemokine and detection antibody 49 were used at constant concentrations (10ng/ml and 2µg/ml respectively). Candidate 48 was also unsuccessful when used as a capture antibody to detect wild type CXCL8, as no signal was observed. This suggests that either this antibody is inefficient at binding wild type CXCL8 (unlikely as Bio-Rad's initial validation data showed that it bound both wild type and nitrated CXCL8), or that this antibody and the detection antibody from R&D's Human CXCL8 ELISA Duoset kit bind to the same epitope on CXCL8, making them incompatible as a sandwich ELISA antibody pair.

It is likely that this is also the reason that using the 3NT antibody (capture) and 49 (detection) was unsuccessful (data not shown), as for 49 to differentiate between wild type and nitrated CXCL8, where the only difference is one nitrated tyrosine residue, its binding will likely involve this residue, which in this experimental set-up would be already bound to the 3NT capture antibody and therefore be unavailable to the detection antibody.

The Rega #4576 antibody was also unsuccessful as a capture antibody, as its use with 49 as a detection antibody showed no signal for nitrated CXCL8, suggesting that this antibody, like the commercially available antibodies tested, cannot bind to nitrated CXCL8.

The rabbit polyclonal anti-CXCL8 antibody (AHC0881) showed some promise as a capture antibody, as its use with 49 as a detection antibody gave a positive signal for the detection of 10ng/ml nitrated CXCL8 diluted in PBS. A checkerboard ELISA suggests that using both antibodies at 5µg/ml would produce a maximum detection signal, but further studies are needed to determine if this antibody pair would also detect wild type CXCL8 diluted in PBS, and both wild type and nitrated CXCL8 in a more complex mix such as serum when used at these concentrations. While AHC0881 showed equal affinity for wild type and nitrated CXCL8 in initial studies, it was apparent that this affinity was within the range of low ng/ml, which is considerably lower affinity than antibodies used in commercial CXCL8 ELISA kits, whose affinity is low pg/ml. This antibody pairing needs to be optimised further in order to try to improve the sensitivity and lower limit

of detection if this sandwich ELISA antibody pair is to be used to detect nitrated CXCL8 in any patient samples.

Use of 49 in immunofluorescence yielded uncertain results, with some granular staining observed. Due to time and resource constraints more experimental replicates would need to be performed in order to confirm this staining pattern. It is worth noting, however, that if results in Chapter 3 are correct and nitration of CXCL8 prevents its binding to GAGs, then it is likely that very little nitrated chemokine would actually be immobilised on the cell surface and thus be detectable using immunofluorescence. This again highlights the importance of developing an ELISA assay to detect unbound nitrated CXCL8 in cell media or patient biological fluids.

In summary this chapter has shown that it is possible to generate an antibody, which shows specificity for nitrated CXCL8 over wild type CXCL8 which, with further development, could potentially be used to detect nitrated CXCL8 in patient samples. In the longer term, the creation of a panel-type assay to detect and measure all forms of modification (nitration, citrullination, truncation, glycosylation etc.) of a chemokine would give the most complete and accurate information about chemokine expression and natural regulation. I have shown that, even with antibody candidate 49 in its current un-optimised state, it is possible to detect naturally occurring nitrated CXCL8, as was found in one BAL sample from a VAP patient. While preliminary, this result could be the first recorded detection of naturally occurring nitrated CXCL8, and should be corroborated by the testing of greater numbers of patient samples from a range of diseases. If nitration could be confirmed as being a direct result of IRI (through its detection in organ transplant patient samples for example, then a panel–type assay detecting wild type and nitrated forms of a range of pro and anti-inflammatory chemokines could prove to be an even more accurate indicator of IRI severity still.

Capture Antibody	Sample	Detection Antibody	Detection Method	Result
AbD31648.1 at 10-1µg/ml in coating buffer	10ng/ml CXCL8/nitrated CXCL8 in PBS	Biotinylated AbD31649.1 at 2µg/ml	Streptavidin-HRP - TMB	**FAIL.** No difference in signal observed between incubation with nitrated CXCL8 and PBS. Likely that the capture antibody cross-reacted with the detection antibody.
Rabbit anti-3NT (ab61392) at 5µg/ml in coating buffer	5-200pg/ml nitrated CXCL8 in serum	AbD31649.1 at 2µg/ml	Biotinylated anti-histidine6 (MCA1396B)– streptavidin-HRP - TMB	**FAIL.** No development (data not shown). Likely that the capture and detection antibodies bind the same epitope on nitrated CXCL8 and so are incompatible.
Rega #4576 at 1/100 in coating buffer	0.1-10ng/ml CXCL8/nitrated CXCL8 in PBS	Biotinylated AbD31649.1 at 2µg/ml	Streptavidin-HRP - TMB	**FAIL.** No detectable signal for nitrated CXCL8. Likely that the capture antibody cannot bind nitrated CXCL8.
Rabbit polyclonal anti-CXCL8 (AHC0881) at 1/100 in coating buffer	0.1-10ng/ml CXCL8/nitrated CXCL8 in PBS	Biotinylated AbD31649.1 at 2µg/ml	Streptavidin-HRP - TMB	**SUCCESS.** Weak detection signal for 10ng/ml nitrated CXCL8.

Table 4-1.Summary of trialled sandwich ELISA assay set-ups.

5 DETERMINING HOW STRESS AFFECTS CXCL8 PRODUCTION AND NITRATION

Some of the work described in this chapter was carried out with the assistance of Charlotte Skipsey (Undergraduate Student) and Emily Astles (Masters Student), whom I supervised throughout their dissertation projects.

5.1 INTRODUCTION

The immune system has evolved over time to combat assaults and insults from a range of sources such as pathogens, irritants or inflammatory cellular components. In order to efficiently deal with each challenge, the immune system must be able to elicit targeted responses from specialised immune cell types in response to specific stimuli.

Chemokine signalling is an important aspect of this response. Homeostatic chemokines like CXCL12/13/14 or CCL18/19/21 are constitutively expressed under normal physiological conditions, whereas the expression of inflammatory chemokines like CXCL1/2/3/5/6/7/8 or CCL2/3/5/7 is upregulated during times of stress [303], usually in response to pro-inflammatory cytokines such as TNF-α [304], IL-1β [305] or IFN-γ [306]. It is worth noting that many chemokines such as CXCL9/10/11, or CCL1/17/20/22, cannot be clearly classified as solely homeostatic or solely inflammatory, and these are known as dual-function [303]. The expression of select chemokines not only ensures that only certain leukocytes are recruited at the correct time-points during inflammation, but the effects these chemokines have on leukocytes can also influence how these cells behave within the inflammatory environment once they have migrated and infiltrated into the tissue [307]. The signalling pathways initiated by chemokine-GPCR binding depend upon the cell type (this can be both leukocytes and tissue cells of the affected organ) and transcription factors involved, and it is the cross talk between multiple signalling pathways that fine-tunes the end response to one that is appropriate for the stimulus.

CXCL8 production is a key pathogenic aspect of a huge range of diseases, from infections to autoimmune disorders and cancers, and understanding how nitrated CXCL8 functions and under what conditions it is produced, could help improve our knowledge of the biological processes underlying many diseases.

I aimed to assess CXCL8 production and nitration in response to stress using two different disease models. A breast cancer model and a cardiac model were chosen as in both environments CXCL8 is known to be expressed and implicated in disease pathophysiology, and both environments are susceptible to oxidative stress during disease, that could facilitate nitration.

5.1.1 CXCL8 in Breast Cancers

Breast cancer cells commonly express the CXCL8 GPCRs CXCR1 and CXCR2, making CXCL8 an important factor in breast cancer initiation, development and metastasis [308] . Serum levels of CXCL8 are elevated in breast cancer patients in comparison to control samples [309], and high expression is mostly correlated with oestrogen receptor negative (ER-), progesterone receptor negative (PR-) and human epidermal growth factor receptor-2 negative (HER2-) cancers [308,310]. CXCL8 was found to be expressed in invasive ductal grade I and III tumours, and was mainly produced by the epithelial cells. It was found to be higher in grade III than I, and be upregulated in distant metastasis [311].

Many solid tumours including breast cancer tumours often possess a group of stem cells that are capable of self-renewal, contribute to metastasis and resistance to chemotherapy. These cells also express CXCR1 – and blocking the interactions between CXCR1 and CXCL8 using a CXCR1-specific neutralizing antibody or Repertaxin (a CXCR1/CXCR2 inhibitor) prevents CXCL8-mediated cancer stem cell recruitment and survival [312].

There is also potential for CXCL8 to be post-translationally nitrated in breast cancer, as CXCL8 is produced by triple negative breast cancers, primary tumour-derived cells, and the MDA-MB-231 immortalised breast cancer cell line in response to hypoxia, which causes an increase in production of reactive oxygen and nitrogen species [313] . These reactive species and CXCL8 are therefore produced in the same environment and potentially by the same cells. Expression of both CXCL8 and iNOS (therefore NO) were upregulated in MDA-MB-231 cells in response to hypoxia, IFN-γ, serum starvation and exogenous NO in a feed-forward loop [314]. Production of CXCL8 within a hypoxic environment and in the presence of NO (needed to form peroxynitrite), means that nitration of CXCL8 is likely to occur.

5.1.2 CXCL8 in the Heart

CXCL8 expression in the heart is known to be upregulated in certain conditions. CXCL8 has been shown to increase in the infarct zone post-myocardial infarction [315], and is thought to contribute to neovessel formation and angiogenesis in the healing heart [316]. CXCL8 expression has been shown to increase systemically as well as locally, with elevated CXCL8 observed in patient serum within the first 22 hours of acute myocardial infarction [317] and in the plasma of patients with a previous history of myocardial infarction where it has been correlated with cardiovascular risk factors [318,319], but not in myocardial reperfusion in patients undergoing reconstructive mitral valve surgery [320]. Blockade of CXCL8 using intravenous administration of a monoclonal antibody reduced IRI in a rabbit model of myocardial infarction [321]. Clearly the expression of CXCL8 within the cardiac environment is tightly regulated and only occurs in response to specific stimuli.

The cellular sources of CXCL8 also vary. Isolated human cardiac fibroblasts have been shown to secrete CXCL8 and upregulate expression of neutrophil-adhesion markers in response to pro-inflammatory stimuli such as treatment with IL-1[322]. Cardiac endothelial cells have also been shown to secrete CXCL8 (thought to promote angiogenesis) in response to stimuli from degranulating mast cells during myocardial infarction [323]. CXCL8 is also known to be produced by macrophages from atheromatous plaques [324]. These data suggest that cardiac fibroblasts, as well as cardiac endothelial cells and leukocytes can mediate neutrophil recruitment to the injured heart through CXCL8 production.

As many of the circumstances described above (where CXCL8 has been reported to be upregulated) involve ischaemia and reperfusion, the CXCL8 is likely expressed in an environment where oxidative stress is occurring and reactive species are present. CXCL8 therefore has the potential to be nitrated within these circumstances.

In both of the diseases described, it must be noted that the CXCL8 detected is likely to only be the wild type molecule, and the total amount of both unmodified and modified chemokine is still likely unknown. It is important to understand what the source of this CXCL8 is in these different diseases (i.e. which cells are the main producers of CXCL8 under which circumstances), and to understand how the potential for the CXCL8

produced to become nitrated varies in relation to its cellular source and the causative stress.

5.1.3 Specific Aims

I aimed to determine how different types of stress (bacterial-derived stress induced by LPS, nitrative stress induced by peroxynitrite, and oxidative stress induced by hydrogen peroxide) would affect the production of CXCL8 in a breast cancer model (using MCF-7 and MDA-MB-231 cells) and cardiac environment model (using HMEC-1 and AC10 cells). I also aimed to assess whether the CXCL8 produced can be nitrated during these different inflammatory situations.

- Determine how different types of stress affect CXCL8 gene and protein expression in a breast cancer model
- Determine how different types of stress affect CXCL8 gene and protein expression in a cardiac model
- Assess the potential for the CXCL8 produced in both of these experimental settings to be nitrated in the presence of different types of stressors

5.2 SPECIFIC MATERIALS AND METHODS

5.2.1 Cell Culture and Treatments

MCF-7 cells, MDA-MB-231 cells, HMEC-1 cells and AC10 cells were cultured as described in section 2.3.

Cells were seeded onto 6 well plates at a density of 20,000-30,000 cells per well and were allowed to grow until 80% confluency.

Cells were then treated with 1µg/ml LPS (Sigma), 600µM peroxynitrite (Cambridge Bioscience) (the concentration of which was assessed daily before use using a NanoDrop), 200µM hydrogen peroxide (Sigma), or media alone (as an untreated negative control) for 2 hours, 6 hours or 16 hours. These concentrations had been optimised for a 6 hour treatment by a previous student, Catriona Barker, and the additional 2 and 16 hour time-points were added to mimic acute and chronic stress. Each treatment was repeated in duplicate. For the LPS and peroxynitrite treatments, the cells were left in media containing the stressing agent for the times stated. For the hydrogen peroxide treatments, the 6 hour treatment consisted of 2 hours in treated media then 4 hours recovery in plain media, and the 16 hour treatment consisted of 2 hours in treated media then 14 hours recovery in plain media due to its cytotoxic nature.

Following treatment, the media from each well was removed, centrifuged for 5 minutes at 10,000xg and stored at -20°C, then cells were detached for use in RNA isolation or functional assessments, or were fixed in ice cold methanol for immunofluorescence staining.

5.2.2 Viability Assays

This method was used to ensure the treatments concentrations and durations would not be cytotoxic to the cells. Following treatments, the media from the wells (containing any floating dead cells) was collected. The cells remaining in the plate were then trypsinised to detach them, and combined with the media that had been removed (thus combining cells that had detached during treatment and cells that remained attached to the plate). The cell suspension was then centrifuged at 500xg for 5 minutes, and resuspended in plain media. A sample of the cell suspension was stained with an equal volume of 0.4% Trypan Blue (Sigma), pipetted onto a haemocytometer, and imaged under the Cellix™

microscope. Images were taken of 4x 1mm^2 squares per treatment, with each treatment tested in duplicate. The number of live/dead cells was counted manually for each image, and the percentage viability was calculated.

5.2.3 RNA Isolation and cDNA Synthesis

These methods were carried out using an RNeasy Pro Kit (Qiagen) and Tetro cDNA Synthesis Kit (Bioline), as described in 2.8 and as per the manufacturer's instructions, using lysed cells collected from plates after the treatments described above.

As shown in Figure 5-1 the RNA, when run on a 2% agarose gel and visualised using a transilluminator under UV light, shows the two clear bands of the intact ribosomal RNA 28S and 18S subunits. The concentration and purity (assessed by 260/280 and 260/230 ratios) of the RNA were measured using a Nanodrop Spectrophotometer.

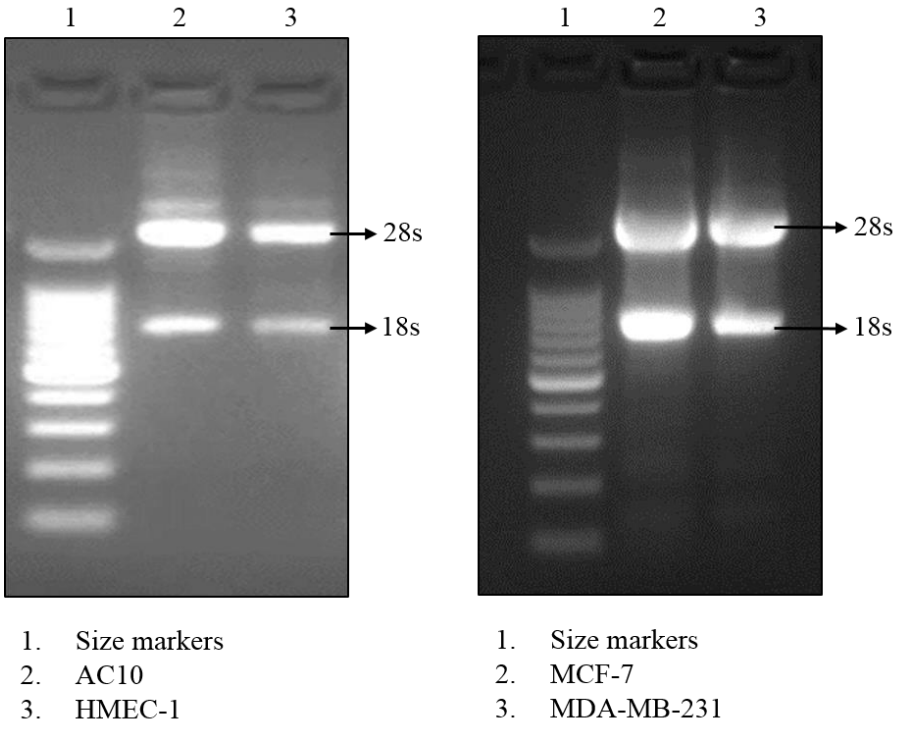

Figure 5-1. Assessment of RNA integrity. Following RNA isolation as per Qiagen's RNeasy Pro Kit, the RNA was run on a 1% agarose gel and visualised using an AlphaImager. This clearly shows in the intact 28S and 18S ribosomal RNA subunits in A) AC10 and HMEC-1 RNA, and B) MCF-7 and MDA-MB-231 RNA. Data shown is from N=1 experimental replicate, with n=1 technical replicate.

5.2.4 Proliferation Assay

Due to breast cancer cell lines being inherently proliferative and self-perpetuating, this method was used to assess how acute, moderate, and chronic treatment with each of the stressing agents affected proliferation of the MCF-7 and MDA-MB-231 cells.

Following treatment in 96-well tissue culture plates, cells were incubated with 2% PMS (an electron-coupling agent) in 30µg/ml of tetrazolium salt (XTT) labelling reagent (The Cell Proliferation Kit II, Roche) at 0, 24, 48 and 72 hours post-treatment. Proliferating cells (i.e. those that are metabolically active) cleaved the XTT into a soluble formazan dye, which is orange in colour. The concentration of this dye can be read using a Synergy™HT spectrophotometer and the Gen5™ software (BioTek), at 450nm (corrected). The optical density is a direct correlation to cellular proliferation.

Initial experiments were performed to determine the optimal time to allow the plate to develop for after the addition of the XTT before being read (Figure 5-2), using the 6 hour intermediate treatment in both cell lines. This was done to ensure sufficient development had occurred to allow for differences between groups to be observed, but also to ensure that over-development did not occur, which may obscure differences between groups due to XTT depletion, for example, 4 hours of development was deemed optimal, and used in all subsequent experiments.

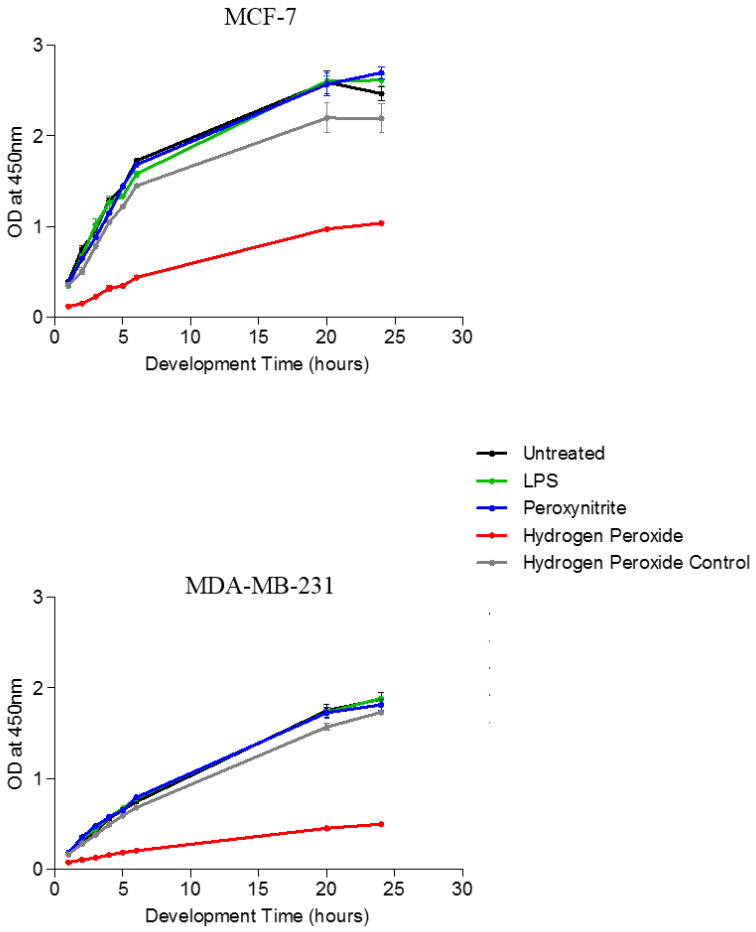

Figure 5-2. Optimising the development time for XTT proliferation assays. MCF-7 and MDA-MB-231 cells were treated with 1µg/ml lipopolysaccharide (LPS) or 600µM peroxynitrite for 6 hours, or 200µM hydrogen peroxide 2 hours + 4 hours recovery. Untreated cells and cells in recovery periods received complete media. Media containing 30µg/ml XTT was added at immediately after treatment (time zero), the cells were then left to metabolise the XTT. The optical density of the formazan dye metabolite was read at 1, 2, 3, 4, 5, 6, 20 and 24 hours at 450nm (corrected), as a direct correlation to cell proliferation. Data shown is combined from N=1 experimental replicate, each with n=2 technical replicates.

5.2.5 Wound-Healing Assay

In order to test how acute, moderate, and chronic treatment with each of the stressing agents would affect the ability of the MCF-7 and MDA-MB-231 cells to migrate and metastasise, wound healing assays were performed as shown below in Figure 5-3A.

Cells were seeded into 12-well tissue culture plates at $1x10^5$ cells/ml and treated as described previously. Cells were then trypsinised, and seeded into 2-well silicone inserts (Ibidi®) placed in 24-well tissue culture plates at $5\text{-}10x10^3$ cells/70µl per chamber, and cultured for 24 hours until >90% confluent. Left-hand chambers contained untreated cells, and right-hand chambers contained cells treated with LPS/peroxynitrite/hydrogen peroxide. Inserts were then removed, and the two resulting separate cultures were washed in PBS to remove cellular debris before being covered with complete media. Plates were placed in a Nikon BioStation Incubator with robotic arm and microscope, and each well was imaged once every hour for 20 hours to visualise the two separate cell cultures migrating to close the gap between them.

Analysis is performed using Nikon NIS software by adding a line at the average cell front at time zero (T0), then moving to the next image taken 1 hour later (T1) and adding another line at the point that the average cell front has migrated to. A horizontal distance calculating bar can be added between these two lines to assess the distance the cells have migrated within this hour. This can then be repeated for the distance migrated between T1 and T2, T2 and T3, T3 and T4 etc. which were then averaged, and this was performed separately for the two separate populations of cells within the insert. Figure 5-3B shows the total distance migrated by untreated and hydrogen peroxide treated MD-MB-231 cells over 10 hours, to highlight the differential migration that can be observed.

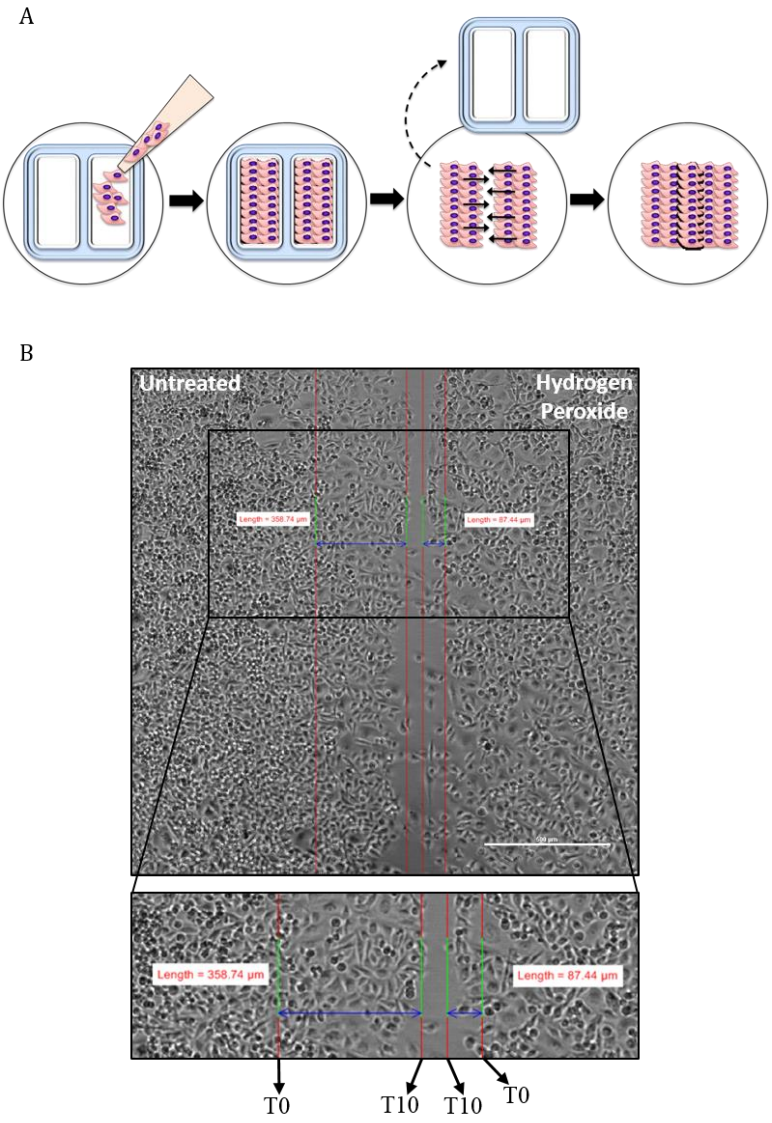

Figure 5-3. Diagrammatic representation of a wound-healing assay. A) Cells are seeded into both chambers of a 2-well insert (Ibidi®) placed in each well of a 24 well tissue culture plate, and grown for 24 hours to confluency. The insert is removed leaving a clear gap between the two cultures of cells, and the plate placed in a Nikon BioStation incubator and microscope set up. Each well of the plate is imaged once every hour for 20 hours as the cells migrate and close the gap. Images are taken at 10x and 4x magnification. The time taken for cells to migrate and close the gap is analysed using Nikon NIS software. B) Analysis is performed by measuring the distance from the average cell front at time zero (T0) and the subsequent image taken 1 hour later (T1). This was repeated for T1 to T2, T2 to T3 and T3 to T4 etc., which were then averaged. Shown is the image comparing the total migration of untreated (left) vs. hydrogen peroxide treated (right) MDA-MB-231 cells after 10 hours (T10), to highlight the differences in migration that can be observed.

5.2.6 Immunohistochemistry and Immunofluorescence

5.2.6.1 Sirius Red Staining

This method was used to histologically assess the extent of the infarct region within mouse hearts 1, 3 and 5 days after ligation of the left anterior descending coronary artery to induce a myocardial infarction (MI) (Figure 5-4) (surgery performed by Dr Rachel Redgrave).

Following the same de-paraffinisation and rehydration protocol described in section 2.6.2, slides were incubated in Fast Green for 5 minutes, and then washed in two changes of acidified water. Slides were then incubated in PicroSirius Red for 1 hour at room temperature then washed in two changes of acidified water. Slides were rapidly dehydrated in three changes of 100% ethanol, cleared in xylene and mounted in DPX.

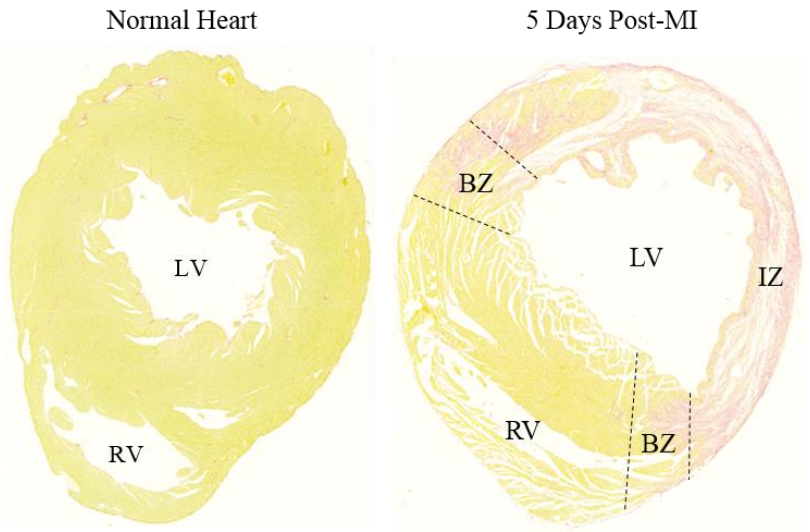

Figure 5-4. Assessment of murine myocardial infarction (MI). PicoSirius Red and Fast Green staining of 4µm paraffin embedded sections from a mouse model of myocardial infarction generated through permanent ligation of the left anterior descending coronary artery. Collagen/fibrosis appears red, healthy myocardium appears green. Labels indicate the left ventricle (LV), right ventricle (RV), border zone (BZ) and infarct zone (IZ). Tiled images were taken at 10x magnification.

5.3 RESULTS

5.3.1 Cell Viability after Stress

Initial viability assays were performed to ensure that the acute, intermediate and chronic treatments with different stressors administered would not cause such extensive cell death as would impair further studies. Cells were therefore treated and mixed with an equal volume of 0.4% Trypan Blue (Sigma), then live/dead cells were counted using a haemocytometer and light microscope.

In the breast cancer model, results show that hydrogen peroxide treatment significantly reduced MCF-7 cell viability in comparison to that of untreated cells. Acute hydrogen peroxide treatment reduced viability from 92% to 75% ($p=<0.001$), intermediate treatment from 87% to 64% ($p=<0.001$), and chronic treatment from 91% to 72% ($p=<0.05$) (Figure 5-5A). For MDA-MB-231 cells, only intermediate and chronic hydrogen peroxide treatment significantly reduced viability to values of 75% ($p=<0.001$) and 64% ($p=<0.001$) respectively (Figure 5-5B), in comparison to the 96% and 97% observed for matched untreated cells. In in all cases, however, viability was still above 60% and so was deemed acceptable. LPS and peroxynitrite treatment did not affect viability in either cell line.

In the cardiac model, untreated AC10 viability ranged from 95-98.3%. Intermediate treatments with both LPS and hydrogen peroxide treatment significantly reduced AC10 cell viability to 85% ($p=<0.01$) and 71% ($p=<0.001$) respectively (Figure 5-6A), however as viability was still acceptable in both cases, no adjustments to treatment protocols were made. Figure 5-6B shows that none of the treatments significantly reduced HMEC-1 cell viability from the 94% average observed for untreated cells. Peroxynitrite treatment did not affect viability in either cell line.

All treatments were deemed suitable and carried forward for further experiments.

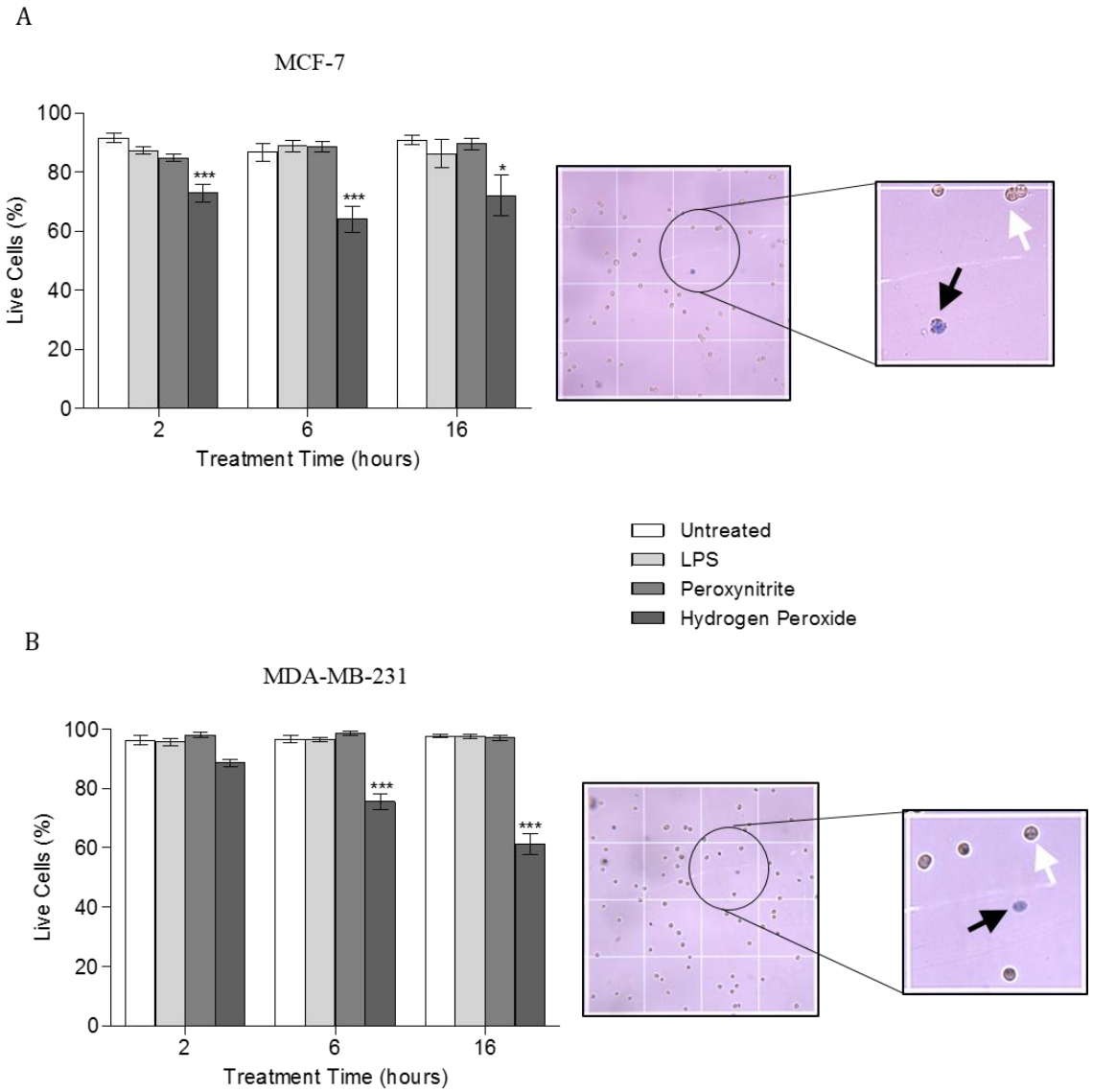

Figure 5-5. Viability of MCF-7 and MDA-MB-231 cells after treatment. A) MCF-7 cells and B) MDA-MB-231 cells were treated with 1µg/ml lipopolysaccharide (LPS) or 600µM peroxynitrite for 2, 6 or 16 hours, or 200µM hydrogen peroxide for 2 hours, 2 hours + 4 hours recovery, or 2 hours + 14 hours recovery. Untreated cells and cells in recovery periods received complete media. Following treatment cells were mixed with an equal volume of 0.4% Trypan Blue, and added to a haemocytometer where the number of live (white arrows) and dead (black arrows) cells were counted in 4x 1mm^2 squares (images shown are representative of one 1mm^2 square). The percentage of live cells was calculated and averaged. Statistical analysis was performed using a One Way ANOVA with Tukey's post-test. Data shown is combined from N=1 experimental replicate, with n=2 technical replicates.

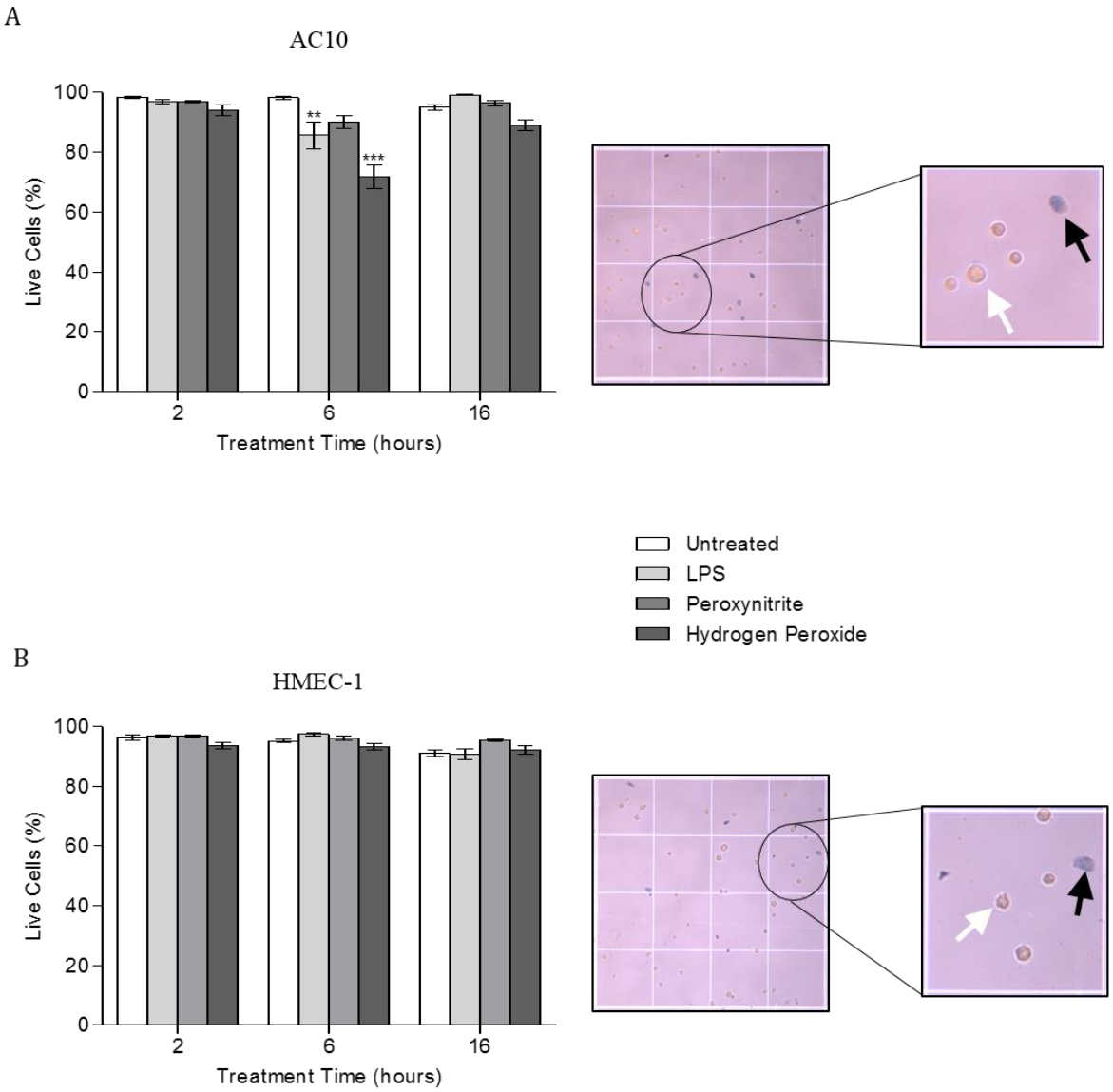

Figure 5-6. Viability of AC10 and HMEC-1 cells after treatment. A) AC10 cells and B) HMEC-1 cells were treated with 1μg/ml lipopolysaccharide (LPS) or 600μM peroxynitrite for 2, 6 or 16 hours, or 200μM hydrogen peroxide for 2 hours, 2 hours + 4 hours recovery, or 2 hours + 14 hours recovery. Untreated cells and cells in recovery periods received complete media. Following treatment cells were mixed with an equal volume of 0.4% Trypan Blue, and added to a haemocytometer where the number of live (white arrows) and dead (black arrows) cells were counted in 4x 1mm^2 squares (images shown are representative of one 1mm^2 square). The percentage of live cells was calculated and averaged. Statistical analysis was performed using a One Way ANOVA with Tukey's post-test. Data shown is combined from N=1 experimental replicate, with n=2 technical replicates.

5.3.2 Determining How Stress Affects CXCL8 Production in a Breast Cancer Model

I aimed to assess how different stressors would affect CXCL8 production in both non-metastatic (MCF-7) and metastatic (MDA-MB-231) breast cancer cell lines. MCF-7 cells and MDA-MB-231 cells were treated, then media was removed, centrifuged, and the amount of CXCL8 protein secreted by the cells was measured using R&D's Human CXCL8 Duoset ELISA kit. CXCL8 gene expression was measured as fold change relative to HPRT-1 (an endogenous control gene), using RT-qPCR performed on cDNA from cells that were lysed following the removal of their media for protein analysis. This meant that CXCL8 gene and protein expression could be assessed in the same cells.

Results in Figure 5-7E show that in MCF-7 cells, intermediate hydrogen peroxide treatment increased CXCL8 gene expression by 38-fold ($p=<0.05$), and chronic hydrogen peroxide treatment increased CXCL8 gene expression by 93-fold ($p=<0.001$), in comparison to matched untreated cells. Acute hydrogen peroxide treatment also increased CXCL8 gene expression by 6-fold, however this result was not found to be statistically significant. This pattern is mirrored in the CXCL8 protein secretion measured (Figure 5-7F), with intermediate hydrogen peroxide treatment inducing the secretion of ~40pg/ml CXCL8 in comparison to undetectable levels of CXCL8 in matched untreated cells from the same time-point ($p=<0.001$). Chronic hydrogen peroxide induced the secretion of ~126pg/ml CXCL8; a 12.6-fold increase from the ~10pg/ml CXCL8 secreted by matched untreated cells from the same time-point ($p=<0.001$). LPS and peroxynitrite treatment induced no increase in CXCL8 gene expression or protein secretion, with values for these treatments equivalent to those of matched untreated cells (Figure 5-7A-D).

In MDA-MB-231 cells, acute, intermediate and chronic LPS treatment all increased CXCL8 gene expression in comparison to matched untreated cells (Figure 5-8A), however as the fold changes for these treatments were 1.9, 1.7 and 2.1 respectively, while statistically significant they are unlikely to relate to an actual increase in CXCL8 gene expression of any consequence. This is confirmed by the results in Figure 5-8B, which show that LPS treatments does not induce an increase in CXCL8 secretion above the level secreted by matched untreated cells. Both acute and intermediate (but not chronic) hydrogen peroxide treatments, however, caused significant increases in CXCL8 gene expression 3-fold ($p=<0.01$) and 11-fold ($p=<0.001$) respectively (Figure 5-8E).

Increases in CXCL8 protein expression were also observed in response to intermediate and chronic hydrogen peroxide treatment, with the treatments resulting in 1.4ng/ml and 2ng/ml CXCL8 secretion respectively, both of which are ~2-fold higher than the amount secreted by their respective matched untreated cells (Figure X5-8F). Peroxynitrite treatment did not result in any changes in CXCL8 gene or protein expression (Figure 5-8C and D).

It was also observed that MDA-MB-231 cells naturally secrete more CXCL8 than MCF-7 cells in culture. MDA-MB-231 cells secreted ~280pg/ml CXCL8 after 2 hours in culture, which accumulated to ~1ng/ml after 16 hours in culture, in comparison to the 30-50pg/ml secreted by MCF-7 cells after 2 hour in culture which did not increase with time (Figure 5-7 and 5-8).

Oxidative stress, but not bacterial or nitrative stress, induces a significant upregulation in CXCL8 gene and protein expression in MCF-7 and MDA-MB-231 cells, which, as a general trend, increased in relation to the duration of treatment increased from acute to intermediate, and intermediate to chronic.

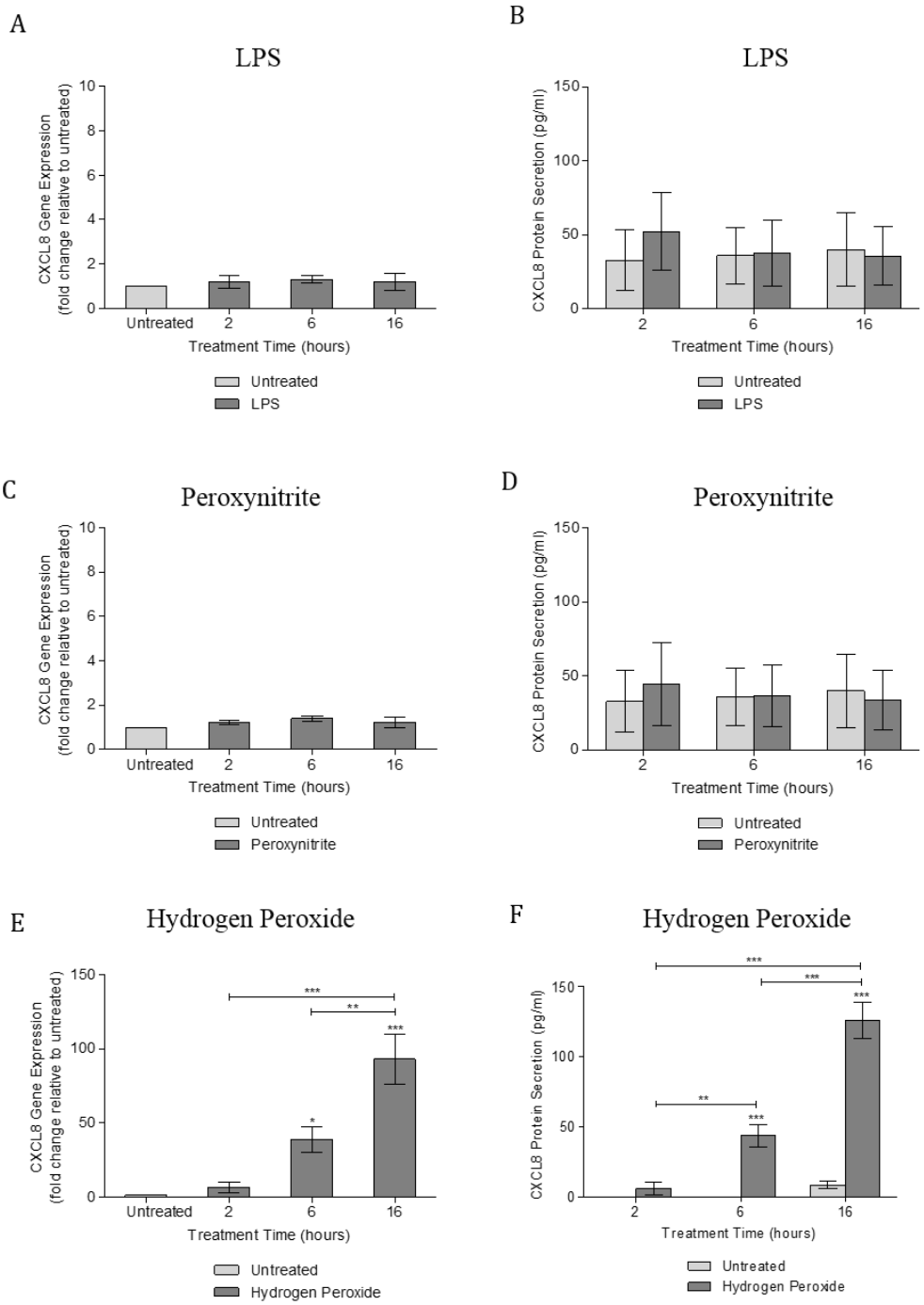

Figure 5-7. CXCL8 gene and protein expression in MCF-7 cells following stress. MCF-7 cells were treated with 1µg/ml lipopolysaccharide (LPS) or 600µM peroxynitrite for 2, 6 or 16 hours, or 200µM hydrogen peroxide for 2 hours, 2 hours + 4 hours recovery, or 2 hours + 14 hours recovery. Untreated cells and cells in recovery periods received complete media. Following treatment, A, C, E) CXCL8 gene expression (as fold change normalised to HPRT1) was assessed using RT-qPCR and B, D, F) CXCL8 protein expression in the supernatant was assessed using R&D's Human CXCL8 Duoset ELISA kit. Statistical analysis was performed using a One Way ANOVA with Tukey's post-test. Data shown in A) and B) is combined from N=3 experimental replicates, each with n=2 technical replicates.

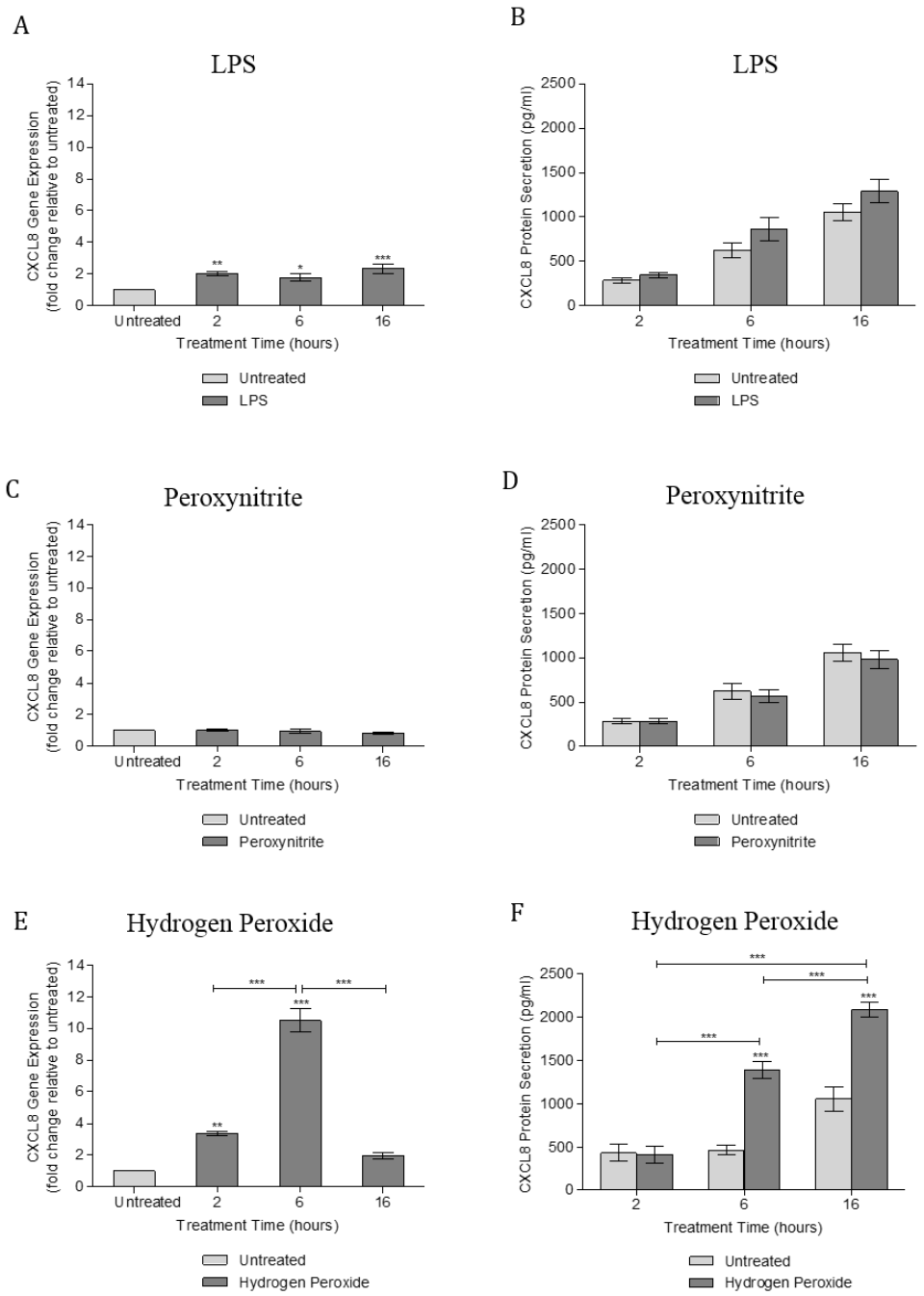

Figure 5-8. CXCL8 gene and protein expression in MDA-MB-231 cells following stress. MDA-MB-231 cells were treated with 1µg/ml lipopolysaccharide (LPS) or 600µM peroxynitrite for 2, 6 or 16 hours, or 200µM hydrogen peroxide for 2 hours, 2 hours + 4 hours recovery, or 2 hours + 14 hours recovery. Untreated cells and cells in recovery periods received complete media. Following treatment, A, C, E) CXCL8 gene expression (as fold change normalised to HPRT1) was assessed using RT-qPCR and B, D, F) CXCL8 protein expression in the supernatant was assessed using R&D's Human CXCL8 Duoset ELISA kit. Statistical analysis was performed using a One Way ANOVA with Tukey's post-test. Data shown in A) and B) is combined from N=3 experimental replicates, each with n=2 technical replicates.

5.3.3 Determining How Stress Affects the Ability of Breast Cancer Cells to Proliferate and Migrate

Having shown that different stressors can differentially upregulate CXCL8 expression, I aimed to assess how these different stressors might affect breast cancer cell functionality in terms of their ability to proliferate (to reflect the aggressiveness of a tumour) and migrate (to reflect metastasis in the body).

Following treatment in 96 well plates, cells were allowed to recover for 0, 24, 48 or 72 hours, after which XTT substrate was added. This was left for 4 hours to allow any proliferating cells to metabolise the XTT and produce formazan dye as a product, the optical density of which was then read on a spectrophotometer. The OD value measured is therefore directly correlated to cell proliferation.

Results show that acute, intermediate and chronic hydrogen peroxide treatments all significantly reduce proliferation immediately after treatment in both MCF-7 ($p=<0.05$-0.001) (Figure 5-9) and MDA-MB-231 cells ($p=<0.05$-0.001) (Figure 5-10) in comparison to matched untreated cells. For MCF-7 cells, proliferation was on average 1.4-fold lower following acute treatment, 1.3-fold lower following intermediate treatment, and 1.7-fold lower following chronic treatment. For MDA-MB-231 cells, proliferation was 1-fold lower on average following acute and intermediate treatments, and 1.2-fold lower following chronic treatment. Proliferation then remains statically reduced in both cell lines from 0-72 hours after treatment, time-points beyond 72 hours were not assessed. Treatment for any duration with LPS or peroxynitrite did not significantly alter proliferation in either MCF-7 or MDA-MB-231 cells.

The ability of cells to migrate following treatment was then assessed using wound healing assays, whereby untreated cells (left) and treated cells (right) were grown in 2-well inserts (Ibidi®), which when removed leave a cell-free "wound" between the two populations. Cells are then imaged every hour for 20 hours as they migrate to close the "wound", and the average hourly migration of the two cell fronts were calculated separately.

Similarly to the proliferation assays, Figure 5-11 shows that MCF-7 cells that received acute, intermediate or chronic hydrogen peroxide treatment migrated at an average of 3.3μm/hour; significantly less (3-4-fold on average) than matched untreated cells which

migrated at an average of 13µm/hour (p=<0.001). The same pattern was observed in MDA-MB-231 cells, with all hydrogen peroxide treatments reducing migration from 13.5µm/hour in untreated cells to 4.4µm/hour - a 2-3-fold reduction (p=<0.01) (Figure 5-12).

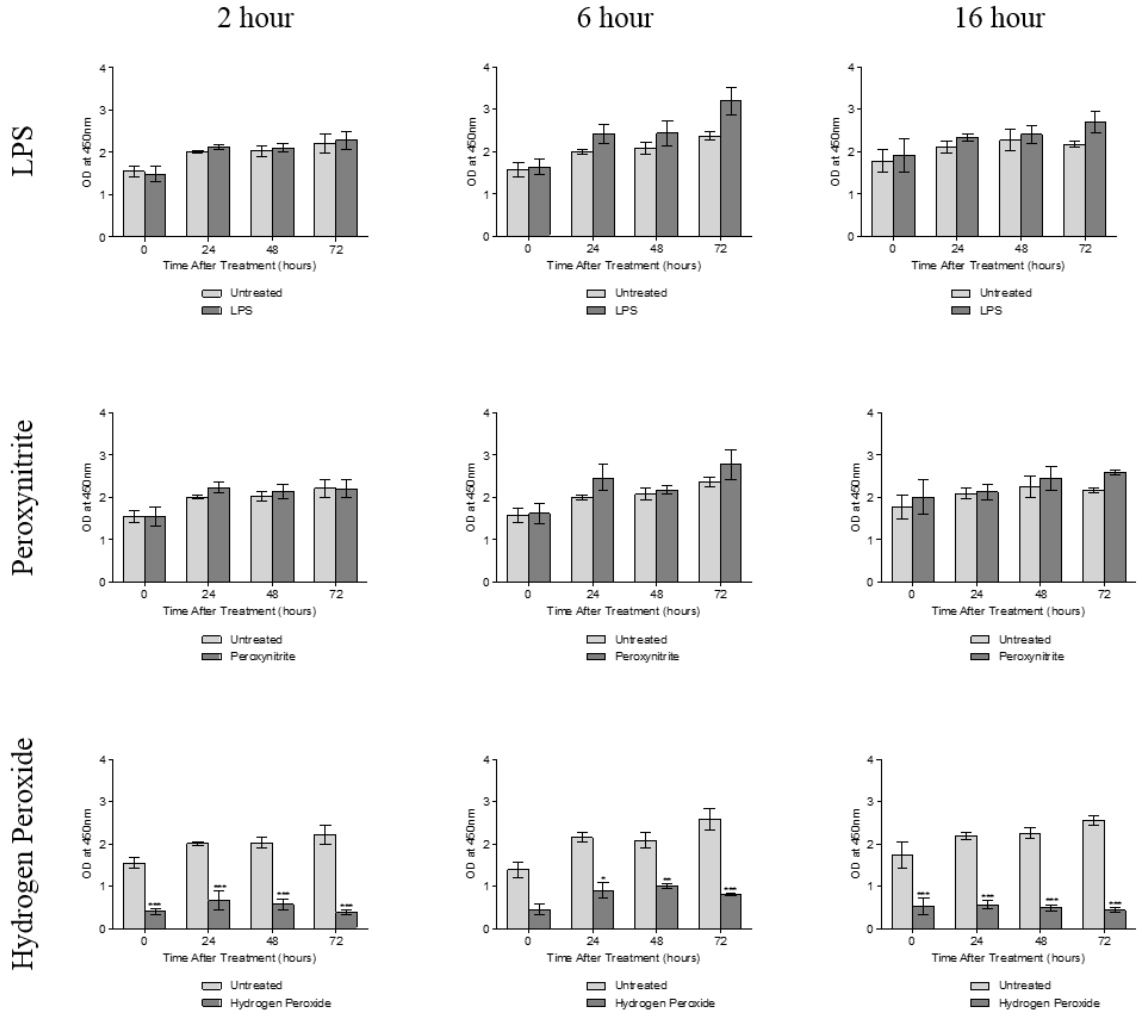

Figure 5-9. Metabolic activity of MCF-7 cells following stress. MCF-7 cells were treated with 1µg/ml lipopolysaccharide (LPS) or 600µM peroxynitrite for 2, 6 or 16 hours, or 200µM hydrogen peroxide for 2 hours, 2 hours + 4 hours recovery, or 2 hours + 14 hours recovery. Untreated cells and cells in recovery periods received complete media. Media containing 30µg/ml XTT was added at 0, 24, 48 and 72 hours post-treatment, the cells were then left to metabolise the XTT for 4 hours, and the optical density of the formazan dye metabolite was read at 450nm (corrected), as a direct correlation to cell proliferation. Statistical analysis was performed using a One Way ANOVA with Tukey's post-test. Data shown is combined from N=3 experimental replicates, each with n=2 technical replicates.

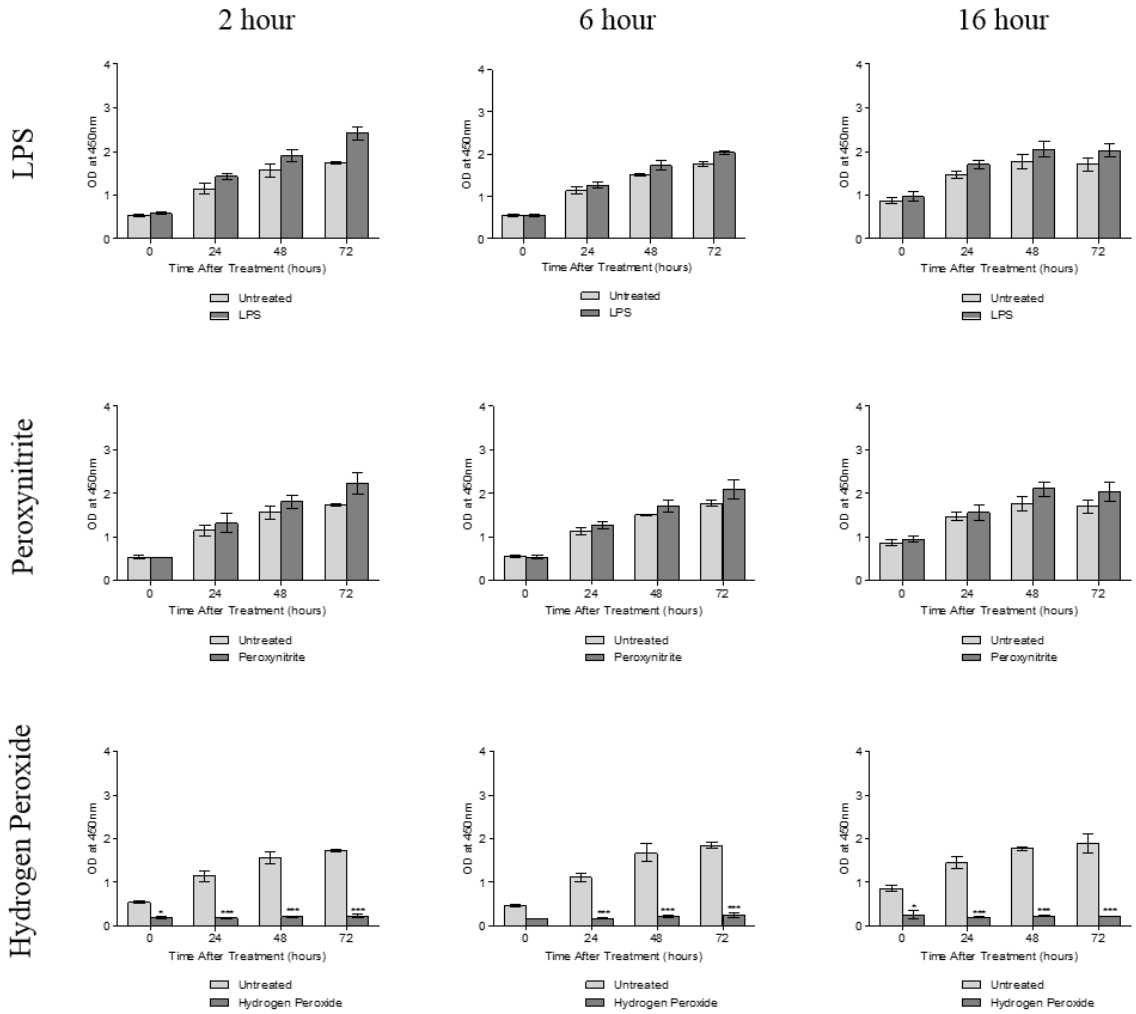

Figure 5-10. Metabolic activity of MDA-MB-231 cells following stress. MDA-MB-231 cells were treated with 1µg/ml lipopolysaccharide (LPS) or 600µM peroxynitrite for 2, 6 or 16 hours, or 200µM hydrogen peroxide for 2 hours, 2 hours + 4 hours recovery, or 2 hours + 14 hours recovery. Untreated cells and cells in recovery periods received complete media. Media containing 30µg/ml XTT was added at 0, 24, 48 and 72 hours post-treatment, the cells were then left to metabolise the XTT for 4 hours, and the optical density of the formazan dye metabolite was read at 450nm (corrected), as a direct correlation to cell proliferation. Statistical analysis was performed using a One Way ANOVA with Tukey's post-test. Data shown is combined from N=3 experimental replicates, each with n=2 technical replicates.

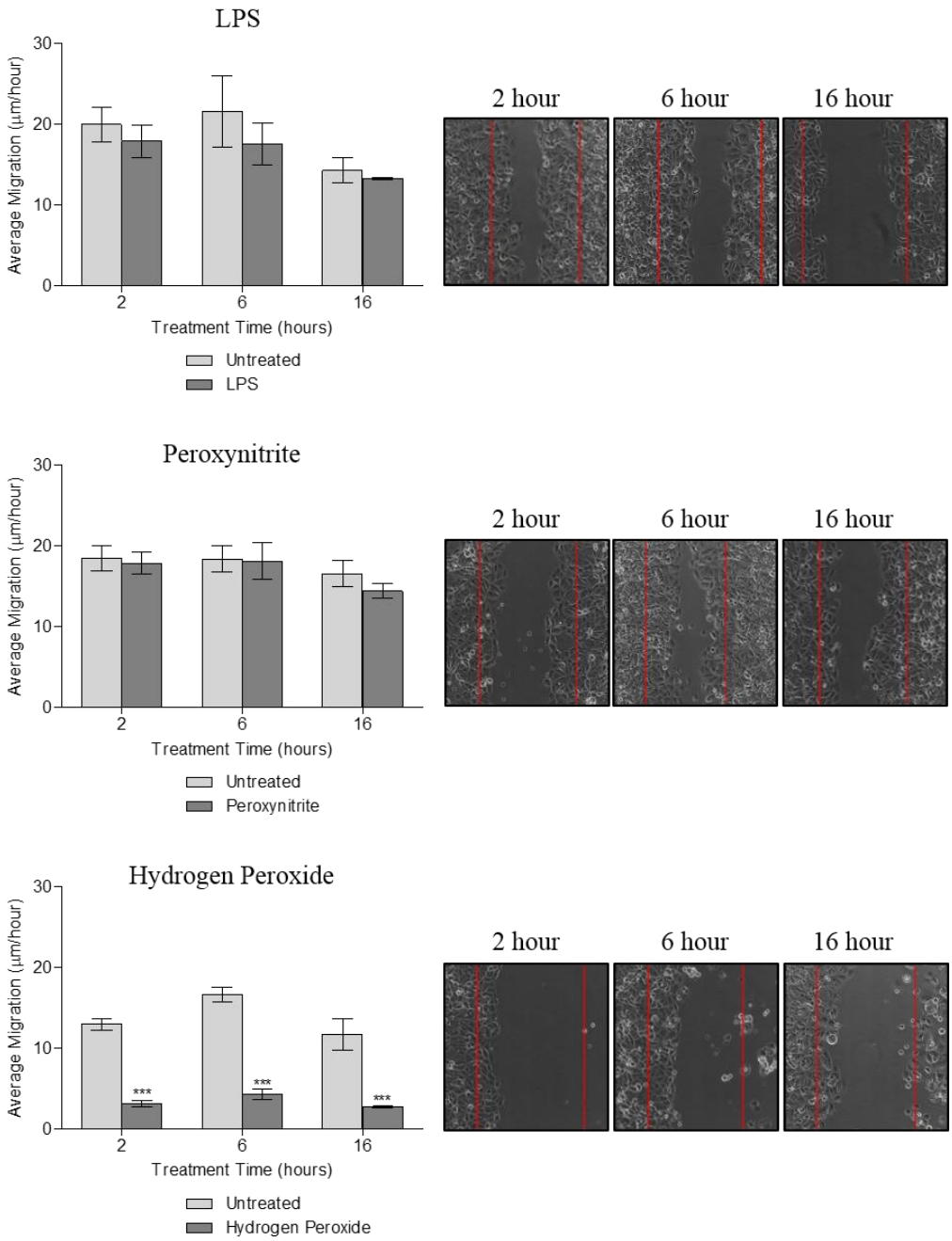

Figure 5-11. Migration of MCF-7 cells following stress. MCF-7 cells were treated with 1µg/ml lipopolysaccharide (LPS) or 600µM peroxynitrite for 2, 6 or 16 hours, or 200µM hydrogen peroxide for 2 hours, 2 hours + 4 hours recovery, or 2 hours + 14 hours recovery. Untreated cells and cells in recovery periods received complete media. Following treatment cells were seeded into 2-well inserts (Ibidi®) in 24 well plates, with untreated cells on the left and treated cells on the right and grown for 24 hours before the insert was removed leaving a "wound" between the two cell fronts. Plates were imaged at 10x magnification once an hour for 20 hours in the Nikon BioStation. Migration distance per hour was calculated using Nikon NIS software and the average plotted. Example images shown were taken at T10 (10 hours), with red lines indicating the position of the cell front at T0 (start of imaging). Statistical analysis was performed using a One Way ANOVA with Tukey's post-test. Data shown is combined from N=3 experimental replicates, each with n=1 technical replicate.

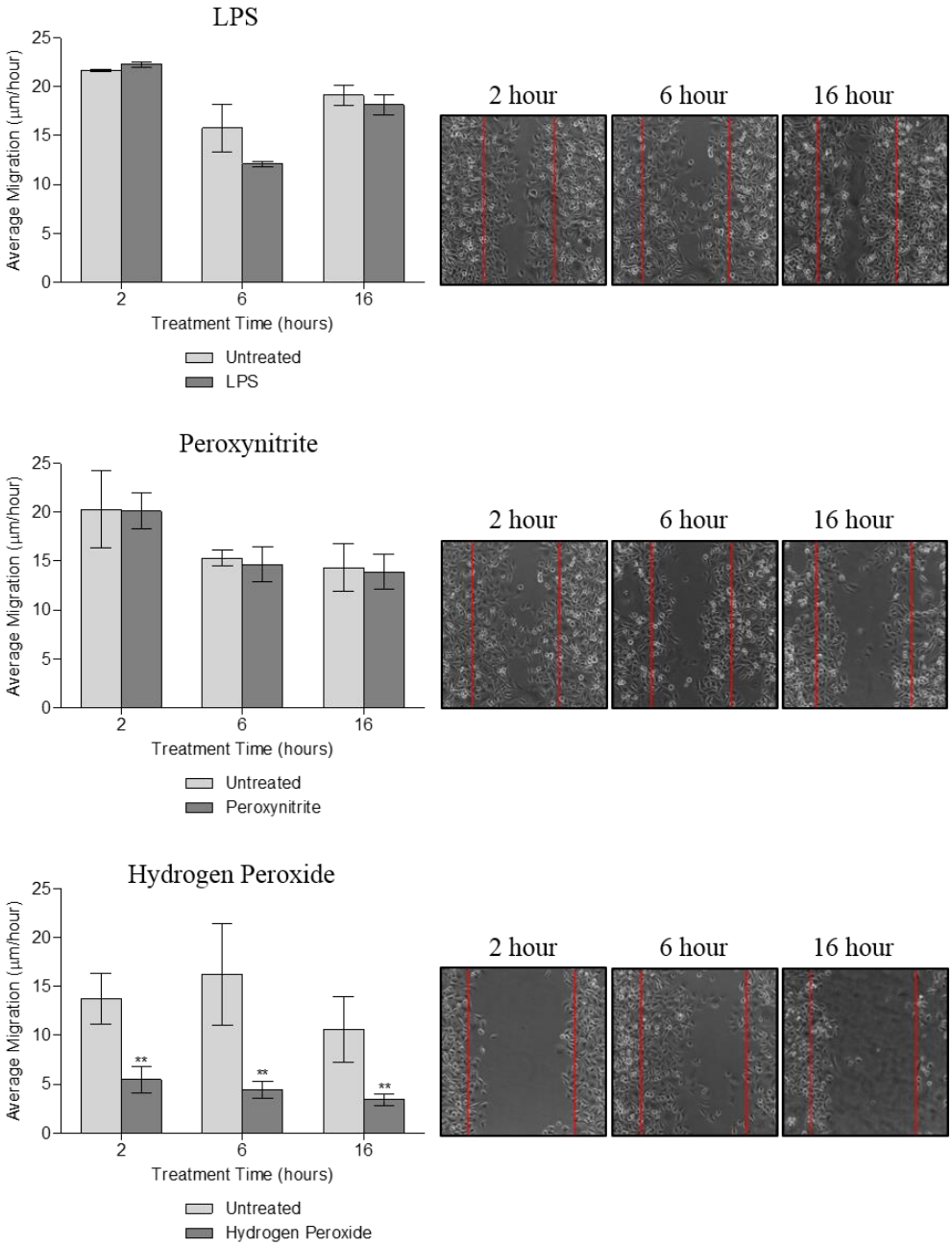

Figure 5-12. Migration of MDA-MB-231 cells following stress. MDA-MB-231 cells were treated with 1µg/ml lipopolysaccharide (LPS) or 600µM peroxynitrite for 2, 6 or 16 hours, or 200µM hydrogen peroxide for 2 hours, 2 hours + 4 hours recovery, or 2 hours + 14 hours recovery. Untreated cells and cells in recovery periods received complete media. Following treatment cells were seeded into 2-well inserts (Ibidi®) in 24 well plates, with untreated cells on the left and treated cells on the right and grown for 24 hours before the insert was removed leaving a "wound" between the two cell fronts. Plates were imaged at 10x magnification once an hour for 20 hours in the Nikon BioStation. Migration distance per hour was calculated using Nikon NIS software and the average plotted. Example images shown were taken at T10 (10 hours), with red lines indicating the position of the cell front at T0 (start of imaging). Statistical analysis was performed using a One Way ANOVA with Tukey's post-test. Data shown is combined from N=3 experimental replicates, each with n=1 technical replicate.

5.3.4 Assessing the Potential for CXCL8 Nitration in a Breast Cancer Model

Having established that wild type CXCL8 protein secretion by both MCF-7 and MDA-MB-231 cells increases following oxidative stress but not bacterial or nitrative stress, I aimed to assess whether the CXCL8 produced was likely to be nitrated in any of these circumstances. Due to the development of an anti-nitrated CXCL8 antibody still being a work in progress, this was tested using double immunofluorescence to detect CXCL8 and 3NT (co-localisation of which indicated nitrated CXCL8) in cells treated in chamber slides.

Staining for these two markers in MCF-7 cells (Figure 5-13) suggests a low level expression of CXCL8 in untreated cells, which generally does not increase and remains consistent in response to LPS and peroxynitrite treatments. The intensity of CXCL8 staining increases in response to hydrogen peroxide treatment, and remains constant over the acute, intermediate and chronic treatments. Little 3NT staining is detected, and this does not appear to increase in response to any of the treatments. While 3NT and CXCL8 staining can clearly be observed in the same cells, reliably identifying areas of co-localisation between the two markers is difficult due to their different intensities of staining. The same pattern can be seen for MDA-MB-231 cells in Figure 5-14, however CXCL8 staining in these cells appears more intense than in MCF-7 cells, and an increase in CXCL8 staining can also be observed following 2 hours of peroxynitrite treatment in these cells.

Untreated MCF-7 cells show a higher intensity of CXCL8 staining than untreated MDA-MB-231 cells, and several different staining patterns of cells were observed in both cell lines both treated and untreated, and have been highlighted in the indented images within the figures. These show nuclear, perinuclear and cytoplasmic CXCL8 expression. These results suggest the potential presence of nitrated CXCL8 in both cell lines in response to oxidative stress, but this is not conclusive.

In order to compare expression of CXCL8 and 3NT between clinical breast cancer samples and breast cancer cell lines, the staining was repeated using sections of biopsies from non-cancerous and cancerous regions within the breast tissue of a patient with confirmed invasive ductal carcinoma of non-specific type, as well as metastatic and non-metastatic lymph nodes from the same patient (Figure 5-15). Non-metastatic lymph nodes showed uniform low expression of both CXCL8 and 3NT, which largely co-

localised throughout the tissue indicating the potential presence of nitrated CXCL8. In the metastatic lymph node, a number of highly $CXCL8^+$ cells with round morphology can be observed. These $CXCL8^+$ cells show little co-localisation with 3NT (suggesting the CXCL8 detected is most likely wild type), and there is generally less 3NT staining throughout the whole tissue in this case.

A similar staining pattern is observed in the breast tissue, with non-cancerous tissue showing higher levels of 3NT, and low levels of CXCL8 staining, and the cancerous tissue again showing less 3NT expression but a high number of $CXCL8^+$ cells.

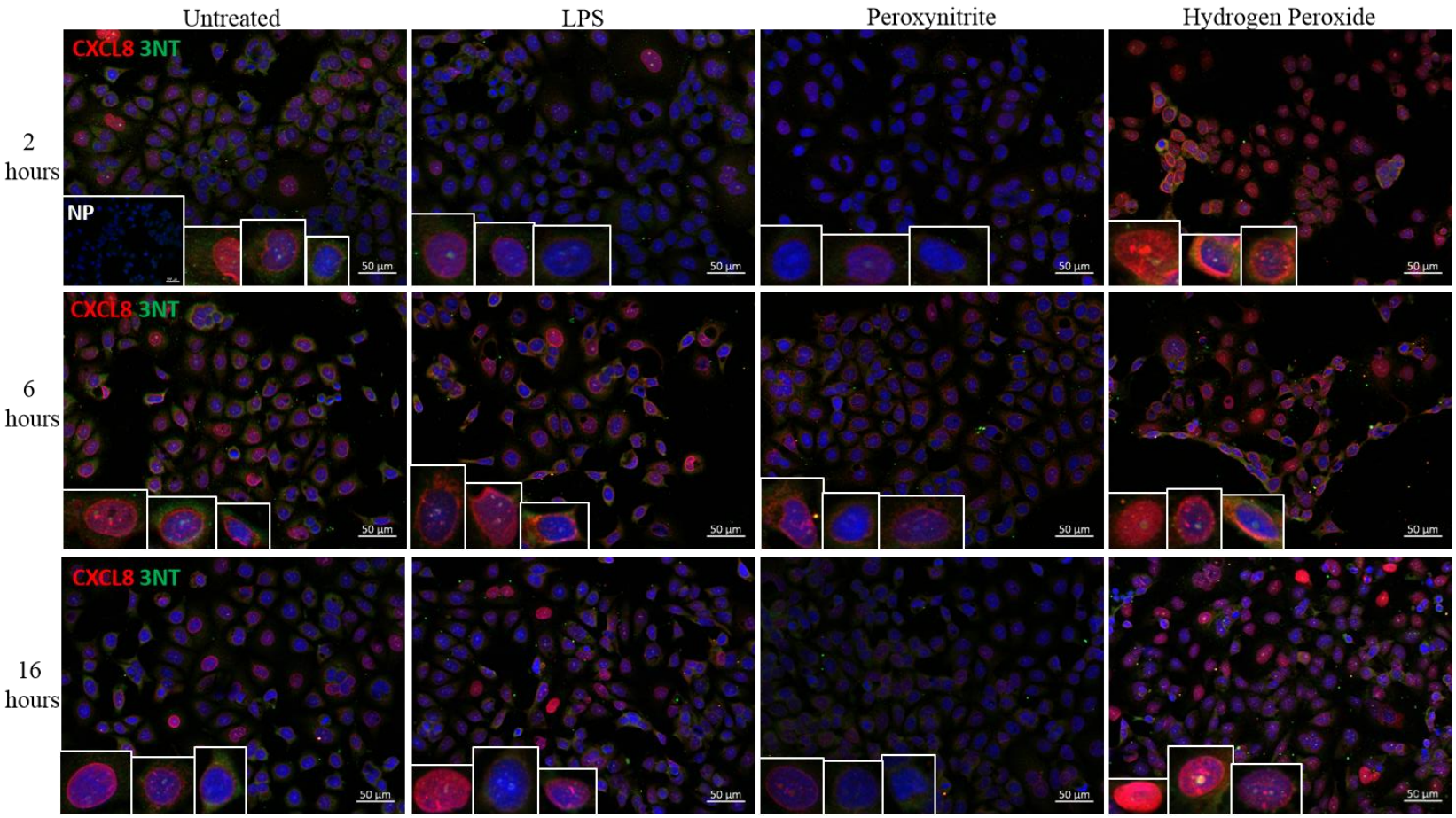

Figure 5-13. CXCL8 and 3-nitrotyrosine (3NT) protein expression in MCF-7 cells following stress. MCF-7 cells were treated with 1µg/ml lipopolysaccharide (LPS) or 600µM peroxynitrite for 2, 6 or 16 hours, or 200µM hydrogen peroxide for 2 hours, 2 hours + 4 hours recovery, or 2 hours + 14 hours recovery. Untreated cells and cells in recovery periods received complete media. Following treatment, slides were fixed in ice-cold methanol, and stained for both CXCL8 (AHC0881, Life Technologies) detected using an anti-rabbit-DyLight550 conjugated secondary antibody (red) (GtxRb-003-D550NHSX, Immunoreagents) and 3NT (ab61392, Abcam) detected using an anti-mouse-DyLight488 conjugated secondary antibody (green) (GtxMs-003-E488NHSX, Immunoreagents) to detect the potential presence of nitrated CXCL8 (NO_2-CXCL8). No primary antibody control is shown indented (NP), as are close-up images of individual cells with different staining patterns. Images were taken at 20x magnification, and images shown are representative of 5 fields of view imaged per chamber.

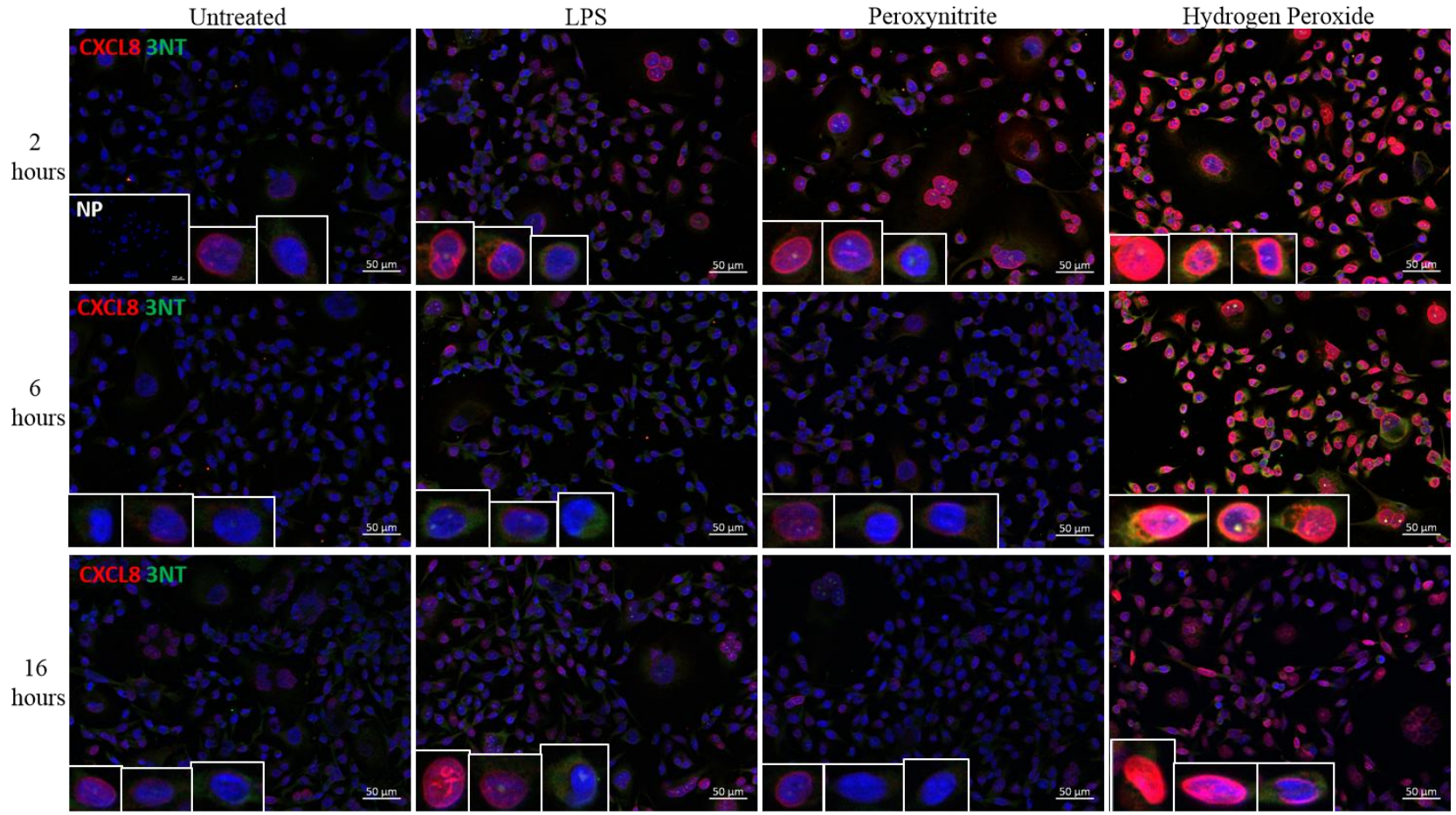

Figure 5-14. CXCL8 and 3-nitrotyrosine (3NT) protein expression in MDA-MB-231 cells following stress. MDA-MB-231 cells were treated with 1µg/ml lipopolysaccharide (LPS) or 600µM peroxynitrite for 2, 6 or 16 hours, or 200µM hydrogen peroxide for 2 hours, 2 hours + 4 hours recovery, or 2 hours + 14 hours recovery. Untreated cells and cells in recovery periods received complete media. Following treatment, slides were fixed in ice-cold methanol, and stained for both CXCL8 (AHC0881, Life Technologies) detected using an anti-rabbit-DyLight550 conjugated secondary antibody (red) (GtxRb-003-D550NHSX, Immunoreagents) and 3NT (ab61392, Abcam) detected using an anti-mouse-DyLight488 conjugated secondary antibody (green) (GtxMs-003-E488NHSX, Immunoreagents) to detect the potential presence of nitrated CXCL8 (NO_2-CXCL8). No primary antibody control is shown indented (NP), as are close-up images of individual cells with different staining patterns. Images were taken at 20x magnification, and images shown are representative of 5 fields of view imaged per chamber.

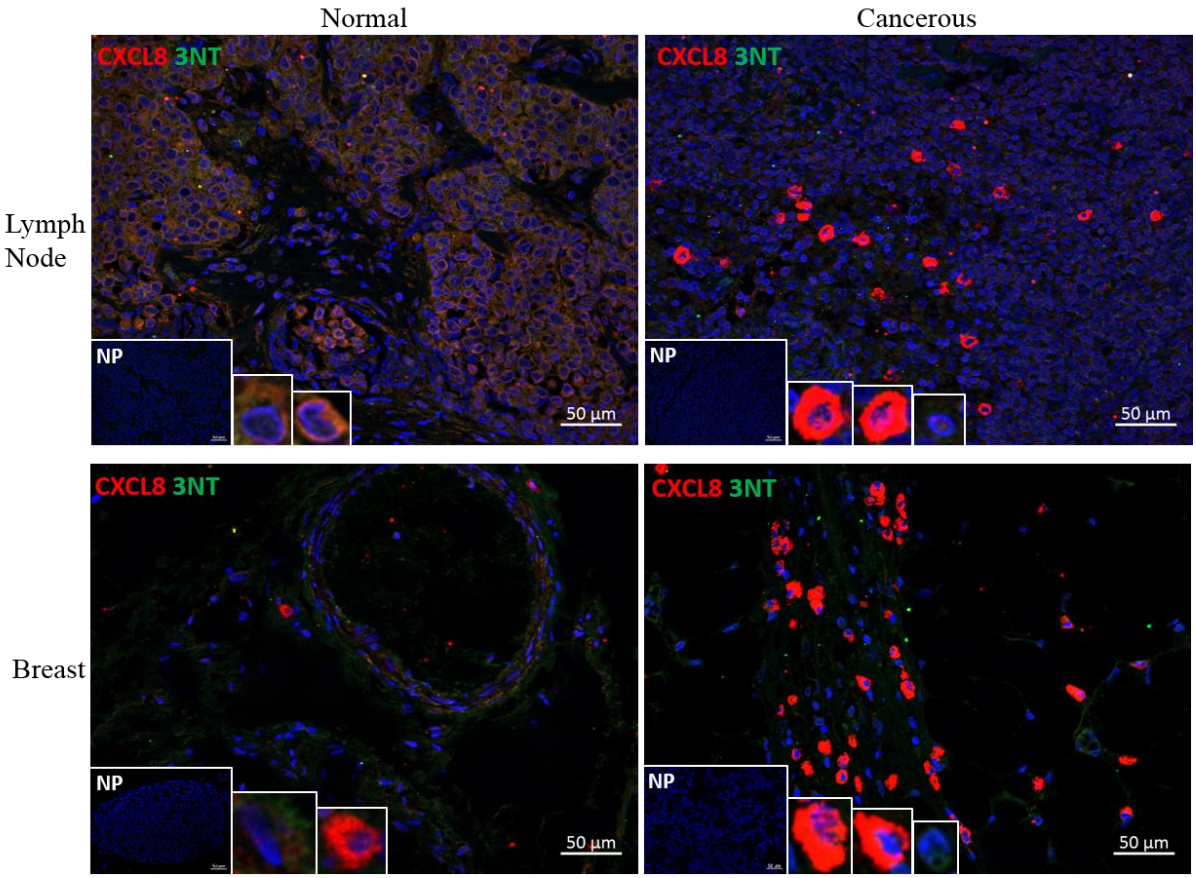

Figure 5-15. CXCL8 and 3-nitrotyrosine (3NT) protein expression in breast and lymph node. Sections of breast (n=2) and lymph node (n=2) tissue were stained for both CXCL8 (AHC0881, Life Technologies) detected using an anti-rabbit-DyLight550 conjugated secondary antibody (red) (GtxRb-003-D550NHSX, Immunoreagents) and 3NT (ab61392, Abcam) detected using an anti-mouse-DyLight488 conjugated secondary antibody (green) (GtxMs-003-E488NHSX, Immunoreagents) to detect the potential presence of nitrated CXCL8 (NO_2-CXCL8). No primary antibody controls are shown indented (NP), as are close-up images of individual $CXCL8^+$ or $CXCL8^+$ $3NT^+$ cells. Images were taken at 20x magnification, and images shown are representative of 5 fields of view imaged per section.

5.3.5 Determining How Stress Affects CXCL8 Production in a Cardiac Model

The same treatments used to induce oxidative, bacterial and nitrative stress where then applied to AC10 cardiomyocyte cells and HMEC-1 endothelial cells to assess how stress affects these cells as different components of the cardiac environment.

In AC10 cells, only chronic hydrogen peroxide treatment induced a significant increase in CXCL8 gene expression of ~7-fold (p=<0.001) (Figure 5-16E). This was mirrored in the protein secretion analysis by ELISA, whereby the general trend suggests an increase in CXCL8 secretion following chronic hydrogen peroxide treatment above the level secreted by matched untreated cells, however this did not reach statistical significance (Figure 5-16F). Neither LPS nor peroxynitrite treatment induced any significant change in CXCL8 gene or protein expression in these cells (Figure 5-16A-D).

HMEC-1 cells showed a different response to stress, with bacterial stress induced by LPS treatment causing a significant upregulation in CXCL8 gene expression (Figure 5-17A). Acute LPS treatment induced a ~9-fold increase (P=<0.05), intermediate treatment induced a 10.3~fold increase (p=<0.01), and chronic treatment induced a ~7-fold increase which was not found to be statistically significant. All durations of LPS treatment did, however, result in a significant increase in CXCL8 protein secretion (p=<0.001) (Figure 5-17B). Acute treatment resulted in an average secretion of 181pg/ml CXCL8, intermediate treatment 1.7ng/ml, and chronic treatment 2.4ng/ml in comparison to the 80pg/ml, 217pg/ml and 716pg/ml secreted by matched untreated cells. In this cell line neither hydrogen peroxide nor peroxynitrite treatment (for any duration) significantly affected CXCL8 gene or protein expression (Figure 5-17C-F).

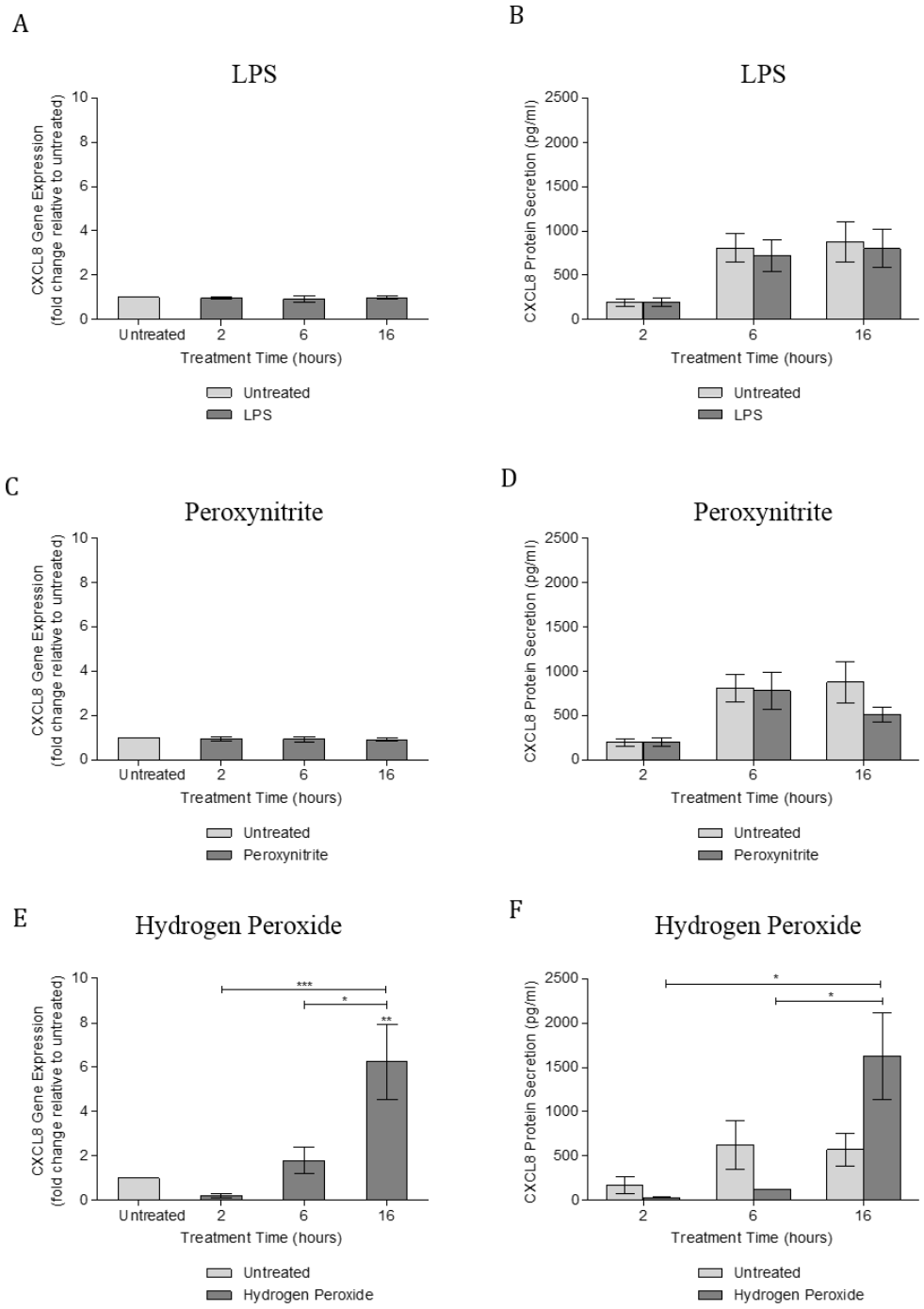

Figure 5-16. CXCL8 gene and protein expression in AC10 cells following stress. AC10 cells were treated with 1µg/ml lipopolysaccharide (LPS) or 600µM peroxynitrite for 2, 6 or 16 hours, or 200µM hydrogen peroxide for 2 hours, 2 hours + 4 hours recovery, or 2 hours + 14 hours recovery. Untreated cells and cells in recovery periods received complete media. Following treatment, A, C, E) CXCL8 gene expression (as fold change normalised to HPRT1) was assessed using RT-qPCR and B, D, F) CXCL8 protein expression in the supernatant was assessed using R&D's Human CXCL8 Duoset ELISA kit. Statistical analysis was performed using a One Way ANOVA with Tukey's post-test. Data shown in A) and B) is combined from N=3 experimental replicates, each with n=2 technical replicates.

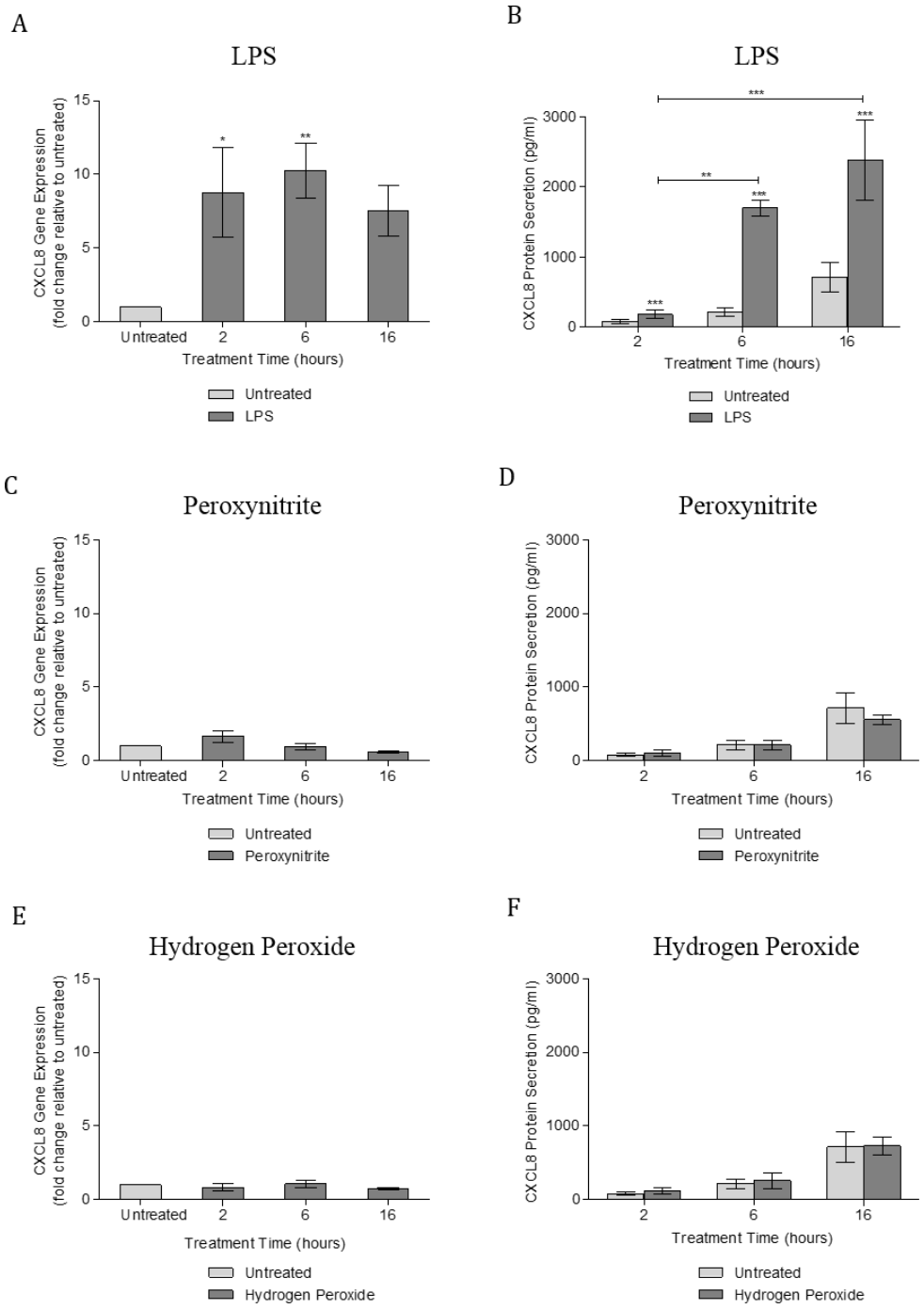

Figure 5-17. CXCL8 gene and protein expression in HMEC-1 cells following stress. HMEC-1 cells were treated with 1μg/ml lipopolysaccharide (LPS) or 600μM peroxynitrite for 2, 6 or 16 hours, or 200μM hydrogen peroxide for 2 hours, 2 hours + 4 hours recovery, or 2 hours + 14 hours recovery. Untreated cells and cells in recovery periods received complete media. Following treatment, A, C, E) CXCL8 gene expression (as fold change normalised to HPRT1) was assessed using RT-qPCR and B, D, F) CXCL8 protein expression in the supernatant was assessed using R&D's Human CXCL8 Duoset ELISA kit. Statistical analysis was performed using a One Way ANOVA with Tukey's post-test. Data shown in A) and B) is combined from N=3 experimental replicates, each with n=2 technical replicates.

5.3.6 Assessing the Potential for CXCL8 Nitration in a Cardiac Model

As with breast cancer cell lines, immunofluorescence staining was also performed to detect CXCL8 surface expression and possible nitration. Results in Figure 5-18 show that untreated AC10 cells appear to express little to no CXCL8 and have almost no detectable 3NT. Staining suggests there is a slight increase in CXCL8 expression in LPS treated cells, and in 3NT expression in peroxynitrite treated cells which both appear to be highest during acute treatment and decrease over intermediate and chronic treatment. As the intensity of these staining patterns are low, this likely corresponds to the lack of change in CXCL8 expression observed in ELISA assays. Hydrogen peroxide treatment appears to increase CXCL8 expression at all durations of treatment, which likely links to the trend towards an increase in CXCL8 protein secretion observed by ELISA assay, although the latter was only observed during chronic treatment whereas surface expression appears to increase during all treatment durations.

HMEC-1 cells, when untreated, also showed almost no detectable CXCL8 or 3NT expression, and this was found to be unaltered by peroxynitrite treatment of any duration (Figure 5-19). LPS treatment, however, did appear to cause an increase in CXCL8 surface expression in these cells, which increases in intensity as the duration of treatment increases. This staining pattern is in agreement with the pattern of CXCL8 protein secretion observed in ELISA assays. Hydrogen peroxide treatment also appears to cause some CXCL8 surface expression increase which is highest in intensity during acute treatment, but decreases as recovery time increases in through the intermediate and chronic treatments. This pattern is different than that observed in ELISA assays, which suggests that hydrogen peroxide does not increase CXCL8 gene expression or protein secretion, but could indicate that these cells are able to cope with and recover from this treatment.

In this instance, I also had access to mouse heart tissue from an MI model generated by permanent ligation of the left anterior descending coronary artery (Dr Rachel Redgrave, Professor Helen Arthur). As mice do not express CXCL8, staining in hearts from 1, 3 and 5 days post-MI single staining was performed to detect 3NT only, as a measure of general protein nitration in relation to ischaemic injury. This was compared to normal mouse heart tissue.

Figure 5-20 shows that 3NT staining of cardiomyocytes in the right ventricle (RV) (i.e. a site distant to the infarct zone) is low level, only clearly detectable 1 day after MI, and reduces gradually over 3 and 5 days post-MI. Closer to the injured region of the heart, low level 3NT staining can be seen in both the infarct zone (IZ) and border zone (BZ) post-MI, with a few highly $3NT^+$ cells present in the BZ. By day 3 post-MI (the peak inflammatory phase), staining has increased in both the IZ and BZ, as has the number of highly $3NT^+$ infiltrating cells. By 5 days post-MI, as healing moves towards the more pro-fibrotic and anti-inflammatory phase, 3NT expression on cardiomyocytes has reduced to a similar level observed in the RV, with some $3NT^+$ infiltrating cells remaining within the IZ but not BZ.

This suggests that during cardiac ischaemic injury, reactive species like peroxynitrite are rapidly produced following injury, leading to the nitration of proteins within the vicinity on both cardiomyocytes and infiltrating cells during the initial inflammatory phase post-MI, as evidenced by 3NT staining.

Staining for both CXCL8 and 3NT was also performed in clinical samples from patients who were undergoing ventricular assist device (VAD) implantation (as a non-transplant cardiac procedure for comparison), and in biopsy sections taken 1 month post –heart transplant in both in healthy patients and those with confirmed allograft rejection (Figure 5-21). CXCL8 and 3NT expression was shown to vary between samples, with VAD patient and non-rejecting transplant patient biopsies showing generally similar low level CXCL8 and 3NT staining mainly on cardiomyocytes. The greatest variability in staining pattern was observed between biopsy samples from transplant patients experiencing allograft rejection, although most showed small patches of increased CXCL8 expression. One biopsy section from this group showed higher levels of staining for both CXCL8 and 3NT than any other, and also showed a high degree of co-localisation between these markers, indicating the possible presence of nitrated CXCL8.

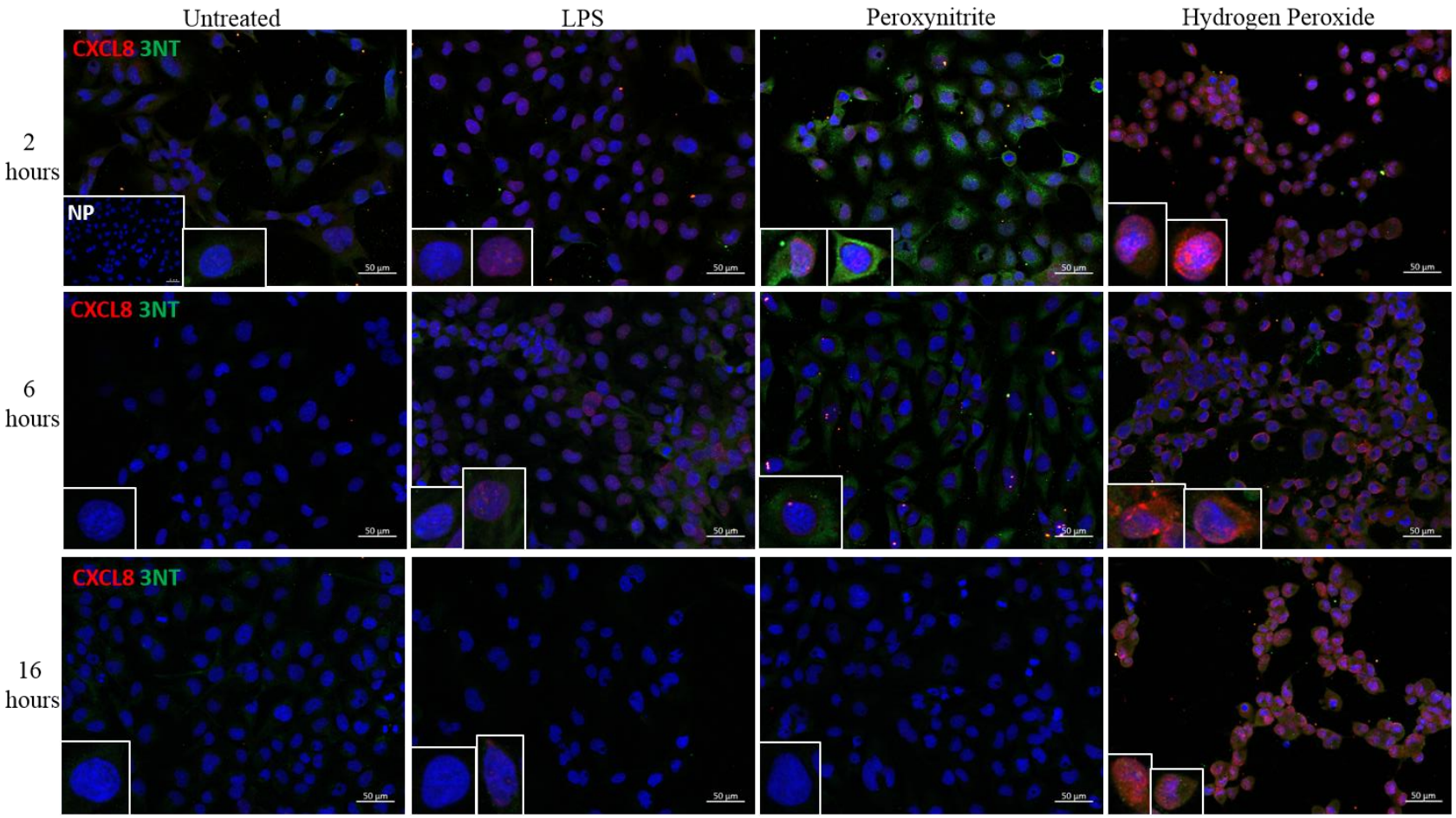

Figure 5-18. CXCL8 and 3-nitrotyrosine (3NT) protein expression in AC10 cells following stress. AC10 cells were treated with 1µg/ml lipopolysaccharide (LPS) or 600µM peroxynitrite for 2, 6 or 16 hours, or 200µM hydrogen peroxide for 2 hours, 2 hours + 4 hours recovery, or 2 hours + 14 hours recovery. Untreated cells and cells in recovery periods received complete media. Following treatment, slides were fixed in ice-cold methanol, and stained for both CXCL8 (AHC0881, Life Technologies) detected using an anti-rabbit-DyLight550 conjugated secondary antibody (red) (GtxRb-003-D550NHSX, Immunoreagents) and 3NT (ab61392, Abcam) detected using an anti-mouse-DyLight488 conjugated secondary antibody (green) (GtxMs-003-E488NHSX, Immunoreagents) to detect the potential presence of nitrated CXCL8 (NO_2-CXCL8). No primary antibody control is shown indented (NP), as are close-up images of individual cells with different staining patterns. Images were taken at 20x magnification, and images shown are representative of 5 fields of view imaged per chamber.

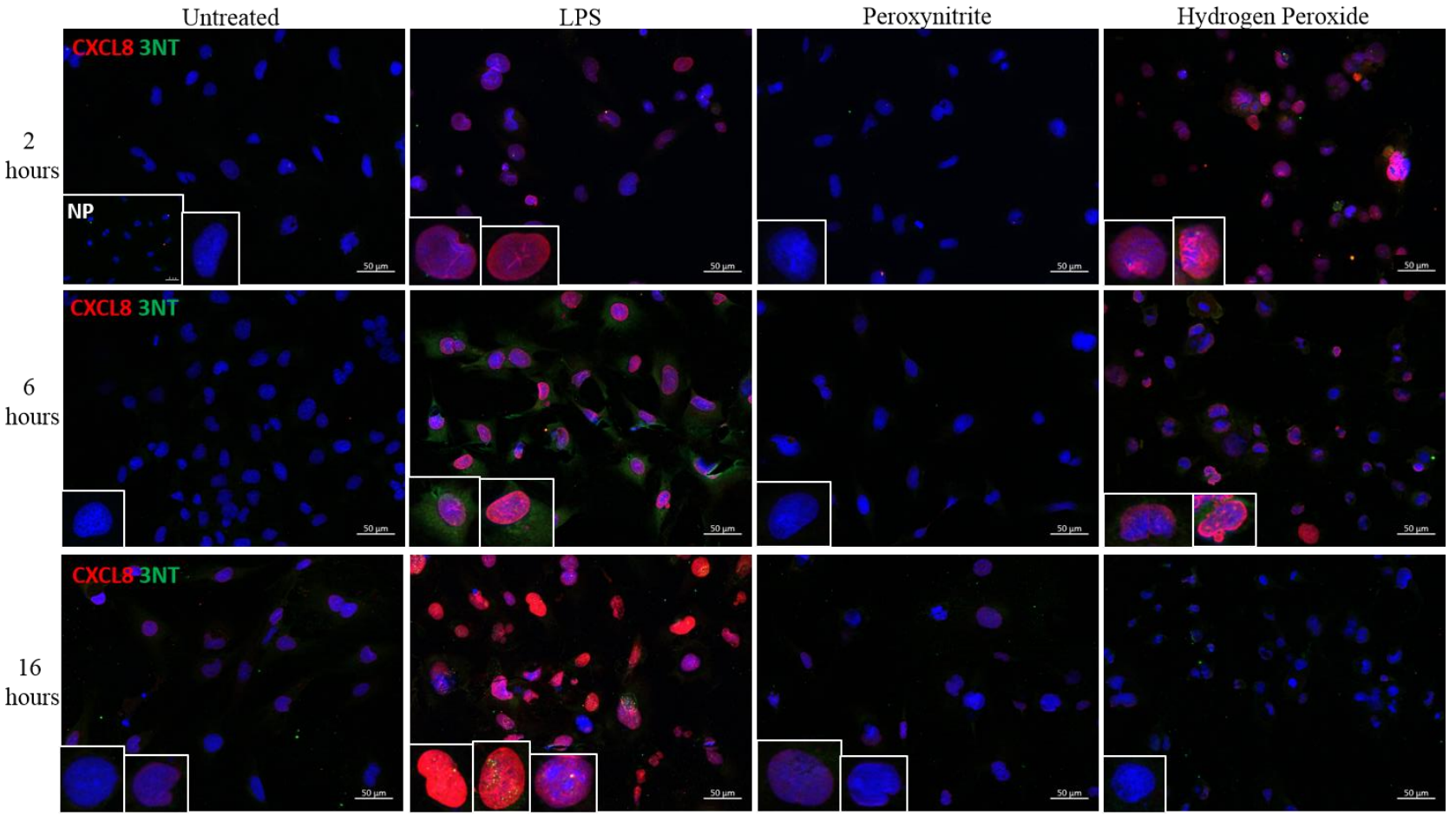

Figure 5-19. CXCL8 and 3-nitrotyrosine (3NT) protein expression in HMEC-1 cells following stress. HMEC-1 cells were treated with 1µg/ml lipopolysaccharide (LPS) or 600µM peroxynitrite for 2, 6 or 16 hours, or 200µM hydrogen peroxide for 2 hours, 2 hours + 4 hours recovery, or 2 hours + 14 hours recovery. Untreated cells and cells in recovery periods received complete media. Following treatment, slides were fixed in ice-cold methanol, and stained for both CXCL8 (AHC0881, Life Technologies) detected using an anti-rabbit-DyLight550 conjugated secondary antibody (red) (GtxRb-003-D550NHSX, Immunoreagents) and 3NT (ab61392, Abcam) detected using an anti-mouse-DyLight488 conjugated secondary antibody (green) (GtxMs-003-E488NHSX, Immunoreagents) to detect the potential presence of nitrated CXCL8 (NO_2-CXCL8). No primary antibody control is shown indented (NP), as are close-up images of individual cells with different staining patterns. Images were taken at 20x magnification, and images shown are representative of 5 fields of view imaged per chamber.

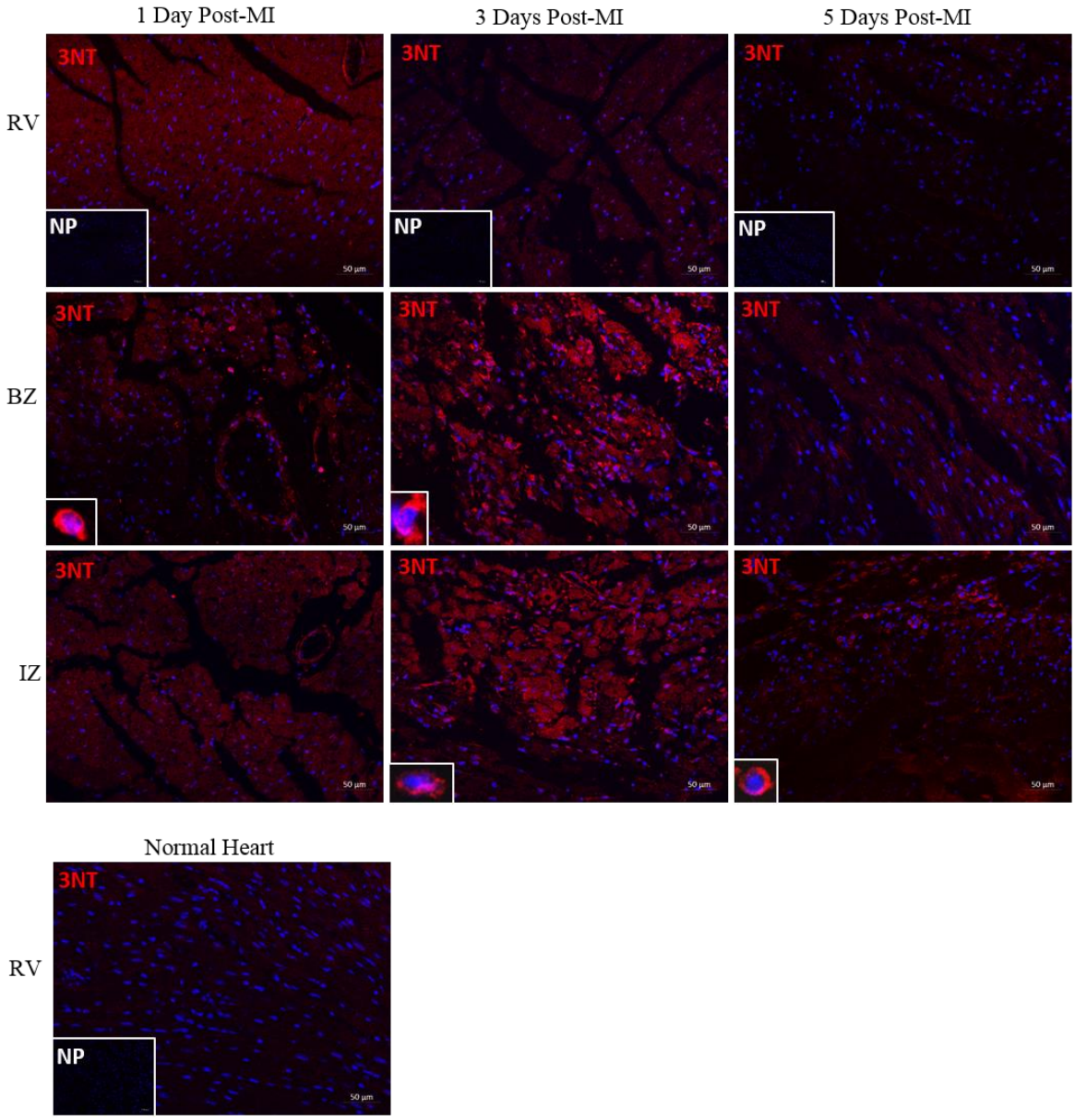

Figure 5-20. Protein nitration within the heart following myocardial infarction (MI). Single immunofluorescent staining showing the expression of 3NT (06-284, Millipore) detected using an anti-rabbit-DyLight550 conjugated secondary antibody (red) (GtxRb-003-D550NHSX, Immunoreagents) in the right ventricle (RV), border zone (BZ) and infarct zone (IZ) of mouse hearts harvested at days 1, 3 and 5 post-myocardial infarction, and a normal mouse heart (n=2 for each time-point). Myocardial infarction (MI) was generated by permanent ligation of the left anterior descending coronary artery. No primary antibody control is shown indented (NP), as are close-up images of individual $3NT^+$ cells. Images were taken at 20x magnification, and shown are representative of 5 fields of view imaged per chamber.

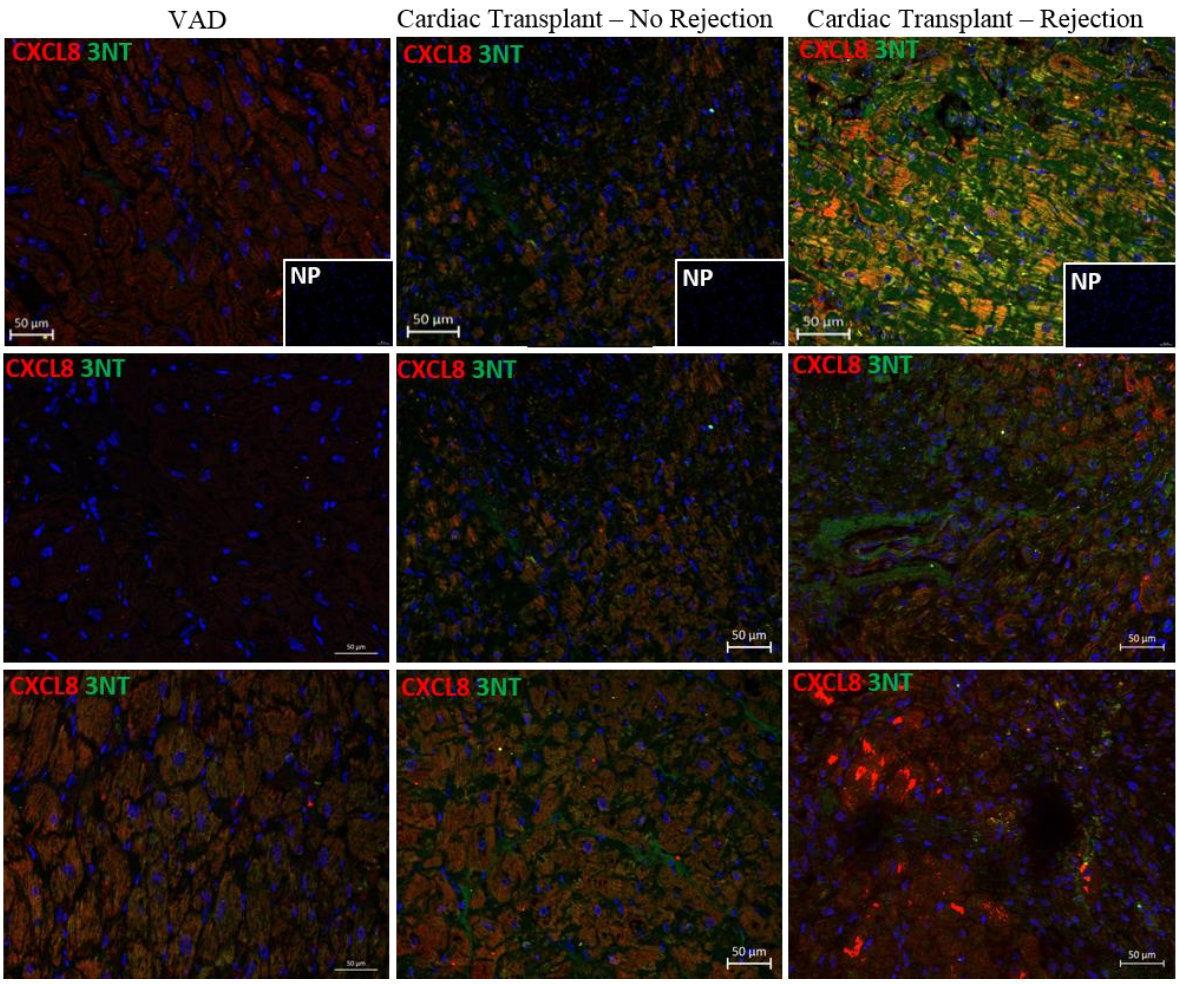

Figure 5-21. CXCL8 and 3-nitrotyrosine (3NT) protein expression in the heart. Sections of heart tissue from in patient biopsies taken at the time of VAD implantation (n=5), or one month post-heart transplant with (n=5)/without (n=4) rejection, were stained for both CXCL8 (AHC0881, Life Technologies) detected using an anti-rabbit-DyLight550 conjugated secondary antibody (red) (GtxRb-003-D550NHSX, Immunoreagents) and 3NT (ab61392, Abcam) detected using an anti-mouse-DyLight488 conjugated secondary antibody (green) (GtxMs-003-E488NHSX, Immunoreagents) to detect the potential presence of nitrated CXCL8 (NO_2-CXCL8). No primary antibody control is shown indented (NP). Images were taken at 20x magnification, and images shown are representative of 5 fields of view imaged per section from 3 representative samples from each group.

5.3.7 CXCL8 and 3NT Expression in a Range of Tissues

As varying staining patterns were observed for CXCL8 and 3NT in all the samples assessed by immunofluorescence, additional staining was performed on a range of tissue types shown in Figure 5-22. Large bowel, small intestine and tonsil expressed high levels of 3NT with little CXCL8 detected. Kidney showed a high intensity of CXCL8 staining within the tubules, and placenta shows global low level CXCL8 expression. Tissue from lung and hepatocellular carcinoma showed the highest degree of co-localisation of CXCL8 and 3NT, although in different staining patterns. Lung tissue shows

more global expression of 3NT with CXCL8 staining more localised to certain epithelial cells, whereas in hepatocellular carcinoma CXCL8 is more globally expressed with small areas of high intensity 3NT staining. Some highly CXCL8^{+} cells were visible in the large bowel and liver, similar to the cells previously observed in the cancerous breast tissue and lymph node in Figure 5-15. These images depict the naturally varying levels of expression of both CXCL8 and 3NT within tissues, and highlight the need for a specific anti-nitrated CXCL8 antibody if the expression of nitrated CXCL8 is to be documented and confirmed.

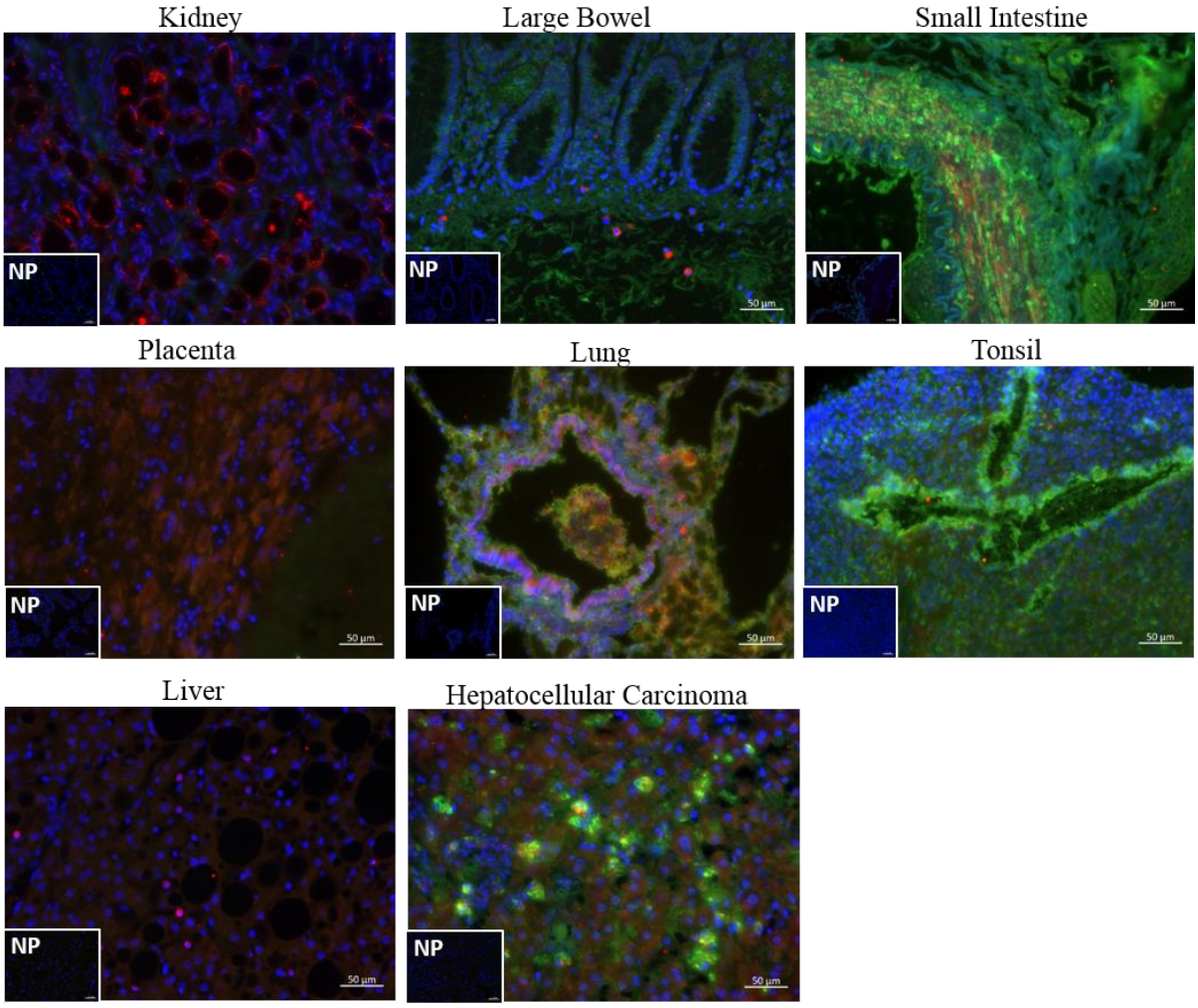

Figure 5-22.CXCL8 and 3-nitrotyrosine (3NT) protein expression in different tissues. Sections of heart tissue were stained for both CXCL8 (AHC0881, Life Technologies) detected using an anti-rabbit-DyLight550 conjugated secondary antibody (red) (GtxRb-003-D550NHSX, Immunoreagents) and 3NT (ab61392, Abcam) detected using an anti-mouse-DyLight488 conjugated secondary antibody (green) (GtxMs-003-E488NHSX, Immunoreagents) to detect the potential presence of nitrated CXCL8 (NO_2-CXCL8). No primary antibody controls are shown indented (NP). Images were taken at 20x magnification, and images shown are representative of 5 fields of view imaged per section from 1 sample per tissue type.

5.4 DISCUSSION

5.4.1 CXCL8 Production and Nitration in a Breast Cancer Model

In both MCF-7 and MDA-MB-231 cells, only oxidative stress but not bacterial or nitrative stress induced an increase in CXCL8 gene and protein expression, as well as a reduction in proliferation and migratory capacity in both cell lines.

The difference in baseline CXCL8 protein secretion between the two cell lines could be reflective of their different phenotypes, and has been previously documented [325]. The higher CXCL8 secretion observed by MDA-MB-231 cells could be due to their more aggressive and metastatic nature which is well documented [271,272], in comparison to the less aggressive and non-metastatic MCF-7s. This is supported by documentation of higher CXCL8 expression being linked to metastasis and worse prognosis in clinical patient samples [308-311]. Regardless of whether breast cancer cells produce naturally high (MDA-MB-231) or low (MCF-7) levels of CXCL8, oxidative stress mediated by hydrogen peroxide causes significant increases in both gene and protein expression above this level. This is supported by literature where hydrogen peroxide treatment has been reported to increase CXCL8 expression in squamous carcinoma cells [326]. The reduction in proliferation and migration observed following acute, intermediate and chronic hydrogen peroxide could be due to the oxidative stress causing cells to become senescent [327,328], although further analysis would be needed to confirm this.

The increase in CXCL8 expression without an increase in 3NT expression observed by immunofluorescence in treated cells correlates with the increase in wild type CXCL8 observed in ELISA assays, suggesting surface expression of CXCL8 mirrors CXCL8 secretion. While untreated MCF-7 cells showed higher CXCL8 expression as detected by immunofluorescence than untreated MDA-MB-231 cells, a greater increase in CXCL8 staining in MDA-MB-231 cells than in MCF-7 cells observed in response to hydrogen peroxide treatment also reflects the higher amounts of CXCL8 secreted by these cells. Cancerous tissue appears to be associated with the presence of highly $CXCL8^{+}$ cells, which are largely undetected in non-cancerous equivalent tissue. Lower 3NT expression in cancerous tissue compared to non-cancerous tissue suggests that the increased CXCL8 staining detected is likely to be wild type. These could be infiltrating leukocytes or breast cancer cells, although this is unconfirmed as no further characterisation was

performed, and no other patient samples were tested. Staining experiments would need to be repeated with greater sample numbers to confirm these trends.

5.4.2 CXCL8 Production and Nitration in a Cardiac Model

Analysis of CXCL8 gene and protein expression following stress in this model suggests that AC10 cardiomyocytes are most susceptible to oxidative stress, as only hydrogen peroxide treatment resulted in a significant upregulation in CXCL8 gene expression, and a trend towards an upregulation in protein expression, although this was not statistically significant.

HMEC-1 cells were the only cell line to show little response to hydrogen peroxide – as acute, intermediate and chronic treatment with this stressor induced no changes in CXCL8 gene expression or protein secretion, although some surface expression of CXCL8 was detected using immunofluorescence. This observation is supported by Lakshminarayanan, *et al*, who found that 800μM hydrogen peroxide treatment did not upregulate CXCL8 protein expression in HMEC-1 cells [329]. These cells instead appeared to be more senstitive to bacterial-dervied stress, as all durations of treatment significantly upregulated CXCL8 gene expression and protein expression, with the latter increasing in conjunction with the length of treatment. HMEC-1 cells have been previously shown to respond to LPS treatment when administered at 100μg/ml, although this study suggests that these cells are sensitive to LPS even at concentrations of 1μg/ml [330,331].

Strong 3NT staining in the initial inflammatory phase post-MI in mice, and in the AC10 cells subjected to acute peroxynitrite treatment, suggests that production of radicals and subsequent protein nitration is likely to occur rapidly after ischaemic injury rather than during the fibrotic phase of wound healing. Staining for 3NT alone in mouse heart tissue and CXCL8 with 3NT in human heart tissue shows that both cardiomyocytes and infiltrating cells can be targets of protein nitration, and both cardiomyocytes[98-101] and neutrophils/macrophages[105,219,225,228-230,332] could be potential sources of the peroxynitrite mediating the nitration within this environment, although this is not confirmed. The production of CXCL8 and 3NT within the same vicinity (leading to their co-localisation), was observed in one case of cardiac allograft rejection, normal lung tissue, and in liver tisse from a hepatocellular carcionoma biopsy and indicates that nitrated CXCL8 is likely to be present in a range of tissues and disease states. Repeats of

these staining experiments, and those performed on the breast cancer model cell lines and tissue would need to be performed in order to confirm these observed patterns.

5.4.3 Future Studies

Due to time and resource constraints, functional assessments such as proliferation could not be completed for cells in the cardiac model as they were for the breast cancer model. Ideally, future work could involve testing the effects of the different stressors in primary cells for both models (e.g. isolated primary breast cancer cells or isolated primary cardiomyocytes, for example). Co-culture models could also be performed to mimic the complexity of the tumour microenvironment [333], and allow multiple components from the cardiac environment, such as endothelial cells and fibroblasts as well as cardiomyocytes [334], to be cultured in close proximity to enable cross-talk. These studies would be likely to yield results that are more reflective of how these cell types would behave *in vivo*.

Future experiments could also involve assessing how the different cells used in this chapter respond to direct treatment with CXCL8 or nitrated CXCL8, as HMEC-1s [335], MCF-7s [336], MDA-MB-231s [336] are all documented to express CXCR1 and CXCR2. No data is available regarding AC10 expression of CXCR1/CXCR2, however primary cardiomyocytes are known to express CXCR2 [337].

One limitation of the studies conducted in both models is the concentrations of reagents used. While these had been optimized by a previous student, they may not have been optimal for the cell lines used in this study. As both MCF-7 and MDA-MB-231 cells both express TLR4, they should respond to LPS treatment, and a study by Yang *et al* (2014) found that treatment with 10μg/ml LPS increased invasiveness in MDA-MB-231 cells and increased migration in MCF-7 cells [338]. The lack of response to LPS observed in this study could therefore be due to an inadequate treatment concentration. Peroxynitrite treatment showed no real effect on any of the parameters assessed in either model other than a slight increase in 3NT surface expression by AC10 cells following treatment, and this could be due to this unstable molecule reacting almost instantly when diluted into treatment media (peroxynitrite has a half-life of 10ms) [79], meaning that very little/none may have actually reached the cells. In future studies, a peroxynitrite donor molecule such as 3-morpholinosydnonimine (SIN-1) [339,340] could be used to ensure treatment reliability. The concentration of 200μM used for hydrogen peroxide treatments could

also be further optimized. Stone *et al* state that at applied concentrations of 0.1-10μM hydrogen peroxide acts as a signalling molecule and induces epithelial-to-mesenchymal transition, increased migration and proliferation, however between 10μM and 100μM it can induce oxidative stress and growth arrest [341]. It is therefore likely that the 200μM used in these studies induced cellular senescence, and future studies could involve testing a range of hydrogen peroxide concentrations to fully span its range of possible effects.

The development of a novel specific anti-nitrated CXCL8 antibody (possibly candidate 49) would ideally be a key component in the future work for both disease models in this chapter. A specific and sensitive antibody would allow for the detection of nitrated CXCL8 in the supernatant from treated cells to complement the wild type CXCL8 measurements collected as part of this project. The antibody could also possibly be used to detect nitrated CXCL8 on cell surfaces by immunofluorescence to confirm/build upon the staining performed using CXCL8 and 3NT together, however results in Chapter 3 suggest that the nitrated chemokine has impaired GAG-binding ability, potentially meaning that nitrated CXCL8 is more likely to be present unbound in the supernatant rather than immobilized on cell surfaces. Work could also be expanded to detect wild type and nitrated CXCL8 in patient tissue and serum samples from, for example, different stages and gradings of breast cancer, pre and post-heart transplant, or post-myocardial infarction. Ethical approval was attained for the collection of serum and tumour tissue samples from breast cancer patients as part of this project (study number NAHPB-136) but unfortunately none could be collected for testing during the time of this study, although such samples would be useful to continue this research. This testing could also be rolled out to other patient samples from different diseases with ischaemic components, and where CXCL8 plays a role, in order to fully characterize ratio of wild type to nitrated CXCL8 in relation to ischaemia-reperfusion injury/oxidative stress.

6 FINAL DISCUSSION

6.1 SUMMARY OF AIMS AND OUTCOME

6.1.1 Characterise the biological activity of chemokines and variants *in vitro* and *in vivo*

Work in Chapter 3 has established that nitration of CXCL8 by peroxynitrite renders the chemokine almost completely non-functional, reducing its ability to recruit human neutrophils *in vitro* and murine neutrophils *in vivo*. This reduction in function is likely due to impaired receptor signalling as confirmed by calcium flux assays and detection of phosphorylated ERK in primary human neutrophils, and impaired GAG binding as confirmed by surface plasmon resonance assays and by an *in vivo* murine intraperitoneal recruitment model (although the latter encompasses both GPCR signalling and GAG binding as neutrophils cross the endothelium and extravasate into the peritoneum). The GPCR and ACKR binding capabilities of nitrated CXCL8 should also be assessed, using a method such as radio-ligand binding assays, for example.

Mass spectrometry analysis confirmed that incubation with peroxynitrite results in the addition of one nitrate group to CXCL8, and that this occurs in the N-terminal half of the chemokine. As nitrated CXCL8 was detectable using an anti-3-NT antibody, this confirms that the nitrate group is added to tyrosine13 within CXCL8. Despite this finding, tyrosine cannot be the only amino acid that has the potential to be nitrated and affect chemokine function. A nitrated Y13F mutant variant of CXCL8 (which contains phenylalanine instead of tyrosine at position 13) and nitrated CXCL1 (which contains no tyrosine residues) also both showed impaired abilities to induce neutrophil migration *in vitro*. This means that the effect that nitration has on a chemokine cannot be predicted by the location and number of tyrosine residues, but that the effect that nitration has on each chemokine must be studied individually in a case-by-case manner.

Studies also showed that nitrated CXCL8 cannot inhibit the function of wild type CXCL8 when administered in equimolar concentrations as tested in calcium flux assays and chemotaxis assays *in vitro*, although the function of nitrated CXCL8 and its ability to inhibit wild type CXCL8 should be also explored using a greater range of concentrations than was used in these studies.

6.1.2 Develop a method to detect nitrated CXCL8

Chapter 4 has highlighted the difficulties that surround antibody development, from using peptides versus full proteins to raise antibodies, to issues with cross-reactivity, specificity and sensitivity. My work involved the initial stages of antibody discovery and development, and resulted in the production of a novel antibody, candidate 49, which shows specificity for nitrated CXCL8 over wild type CXCL8, and has an approximate limit of detection between 1ng/ml and 10ng/ml in direct assays. This antibody does, however, also show cross-reactivity with other proteins present in serum, meaning that it would need to be used as part of a sandwich ELISA assay for the testing of any patient biological fluids. It is suitable however, for use in Western blot analysis, which although an unsuitable method for any clinical assay development, allowed me to analyse a small number of VAP patient BAL samples, and to detect the presence of naturally occurring nitrated CXCL8 in one of these samples. Sample RVI 1 contained a band around the correct weight for nitrated CXCL8, which was detectable with a CXCL8 polyclonal antibody (known to detect wild type and nitrated CXCL8), candidate 49, and a 3-NT antibody. This result is still preliminary due to detection only occurring in one sample, but could represent the first detection of naturally occurring nitrated CXCL8. Western blot analysis of greater numbers of patient samples from a range of diseases could be performed to corroborate this result, alongside the development of a sandwich ELISA assay, which would be more suitable for testing large numbers of patient samples simultaneously and in a more time-efficient manner.

The incorporation of a suitable antibody such as candidate 49 into a novel ELISA assay will require further validation involving assessment of the limit of blank (highest "apparent" amount of analyte measured when testing blank samples containing no analyte), limit of detection (lowest analyte concentration that can be reliably distinguished from the limit of blank value), limit of quantitation (lowest analyte concentration that can be reliably distinguished from the limit of blank value, that also meets targets for bias and imprecision), and reproducibility measurements [342]. Perhaps the optimum antibody pair for use in a sandwich assay to detect nitrated CXCL8 would be a capture antibody raised against the C-terminal end of the chemokine, which would therefore orientate the chemokine in the correct position for detection of the nitrated N-terminal end by a detection antibody specific for nitrated CXCL8 (such as antibody candidate 49 that was assessed in this project). This antibody requires further

development work in order for it to be incorporated into a fully validated assay that could be used to detect nitrated CXCL8 reliably in large numbers of patient samples. Another method of detection that could be used to measure nitrated CXCL8 is mass spectrometry, as shown in Chapter 3. The experiments in this study were performed on pure samples of chemokine, and would not be suitable for analysis of a complex sample containing a mix of proteins such as serum. A pre-purification step would be necessary to isolate the chemokine from the sample in order for it to be analysed. This would most likely involve an antibody-based pull-down/purification technique, which would again require a high affinity antibody that would bind to both wild type and nitrated CXCL8, or specific antibodies for each of these chemokine variants individually.

6.1.3 Determine how stress effects CXCL8 production and nitration

Testing the effects of bacterial, nitrative and oxidative stress in metastatic MDA-MB-231 and non-metastatic MCF-7 breast cancer cell lines in Chapter 5 suggests that only oxidative stress significantly increases upregulation of CXCL8 gene expression, protein expression, and protein secretion in both cell lines. Testing the same stressors in a cardiac model revealed that AC10 cardiomyocytes are most likely to upregulate CXCL8 following oxidative stress, but that HMEC-1 endothelial cells are more responsive to bacterial-derived stress. In this study, the anti-nitrated CXCL8 antibody was not developed to a sufficient standard to allow the measurement of nitrated CXCL8 in these experimental models to be correlated with wild type CXCL8 concentrations. This data would be key to understanding when CXCL8 nitration is likely to occur, although assessing this in primary cell lines or co-culture models would likely be more representative of the inflammatory scenarios occurring *in vivo*. Using a wider range of concentrations of the stressing agents, as well as a more reliable nitrative stress-inducer such as SIN-1 would also likely improve upon the accuracy of results gathered.

6.2 CONCLUSIONS AND IMPLICATIONS

This project has emphasised the complexities of the chemokine system, which have perhaps been previously underestimated. Results presented show that post-translational modifications can alter the functionality of chemokines, making their further study of great importance. As most studies to date, including this present one, have found that nitration decreases chemokine function [119,121-124,173], nitration of

chemokines could be a novel natural mechanism to dampen and resolve inflammation, preventing excessive leukocyte recruitment. This theory is shown diagrammatically in Figure 6-1, where injured cells produce wild type CXCL8 which is present at its highest concentration close to the site of injury in the form of a dynamic "cloud", existing in an equilibrium of GAG and GPCR bound and unbound monomers and dimers. This CXCL8 recruits neutrophils to the inflamed region where degranulation may occur. Within this inflammatory situation, the damaged endothelial cells, tissue cells and degranulating neutrophils upregulate production of enzymes such as iNOS, NADPH and XOD, which produce NO and O_2^- that will react together and form peroxynitrite. As well as its damaging effects previously discussed, peroxynitrite is also likely to nitrate any localised CXCL8, which will render it non-functional, preventing it from binding to GAGs and GPCRs. This will inhibit its ability to contribute to the CXCL8 gradient formation, as well as preventing it from recruiting further neutrophils, thus likely contributing to the resolution of inflammation. This could be supported by the increased inflammation observed in patients with chronic granulomatous disease, where a defect in the NADPH enzyme that inhibits phagocytosis and leads to recurrent infections is also likely to impair protein nitration (due to reduced superoxide anion production) [343]. This could also be supported by studies conducted on IL-10, where incubation with peroxynitrite has been shown to increase the cytokine's anti-inflammatory activity [344,345], but the study of a wider range of both pro and anti-inflammatory chemokines/cytokines would be required to confirm this.

The data presented in the second results chapter show that, at least in the case of CXCL8, most antibodies raised against the wild type chemokine cannot detect the nitrated chemokine, meaning that all current measurements of CXCL8 are only likely to be reflective of the amount of wild type chemokine present. This may provide an inaccurate picture of the overall inflammatory situation, and the ratio of wild type to nitrated chemokine may be a more complete and informative indicator of the type and severity of inflammation occurring. While the expression of wild type CXCL8 is well known to increase during inflammation, and nitration of CXCL8 is likely to occur during increased inflammation, this is not yet confirmed due to a lack of reliable detection methods. It is also unknown, therefore, whether the ratio of wild type to nitrated CXCL8 remains constant or also changes in relation to the severity of inflammation.

The results in the third results chapter highlight that different forms of stress (nitrative, oxidative and bacterial) can elicit a different response in terms of CXCL8 production in different cell lines. While nitration of CXCL8 was not reliably detected in these experiments, they show that as CXCL8 production may vary depending upon the type of insult/injury, so may nitration. This further reinforces the need for a reliable anti-nitrated CXCL8 antibody in order to determine if nitration is directly related to IRI and oxidative stress as hypothesised, possibly by measuring the amount of wild type and nitrated CXCL8 in donor organs perfused *ex vivo* before transplantation, or in serum samples from organ transplant patients post-surgery, where IRI is known to occur. If this theory is proven, then this could inform which disease types/patient samples are likely to contain nitrated CXCL8 and how its expression relates to disease severity. The ratio of wild type to nitrated CXCL8 could be indicative of the severity of IRI sustained during transplantation, for example, and could help stratify those patients at risk of graft dysfunction.

In order to better understand the quantity and patterns in expression of nitrated and wild type chemokines and their relationships with disease states, there is a need to develop novel antibodies to enable the detection of nitrated chemokines separately from their wild type counterparts, which could be extrapolated out to other forms of modified chemokines, such as truncated and citrullinated variants. Teasing apart and quantifying the relative amounts of all chemokine forms, if the functionality and circumstances of production of each is understood, would allow for the most complete and accurate assessment of how post-translational modifications regulate chemokine function during inflammation. This knowledge could also help to improve the development of therapeutics targeting the chemokine system, and their use as clinical biomarkers which has been disappointing to date, through better understanding of natural chemokine regulation.

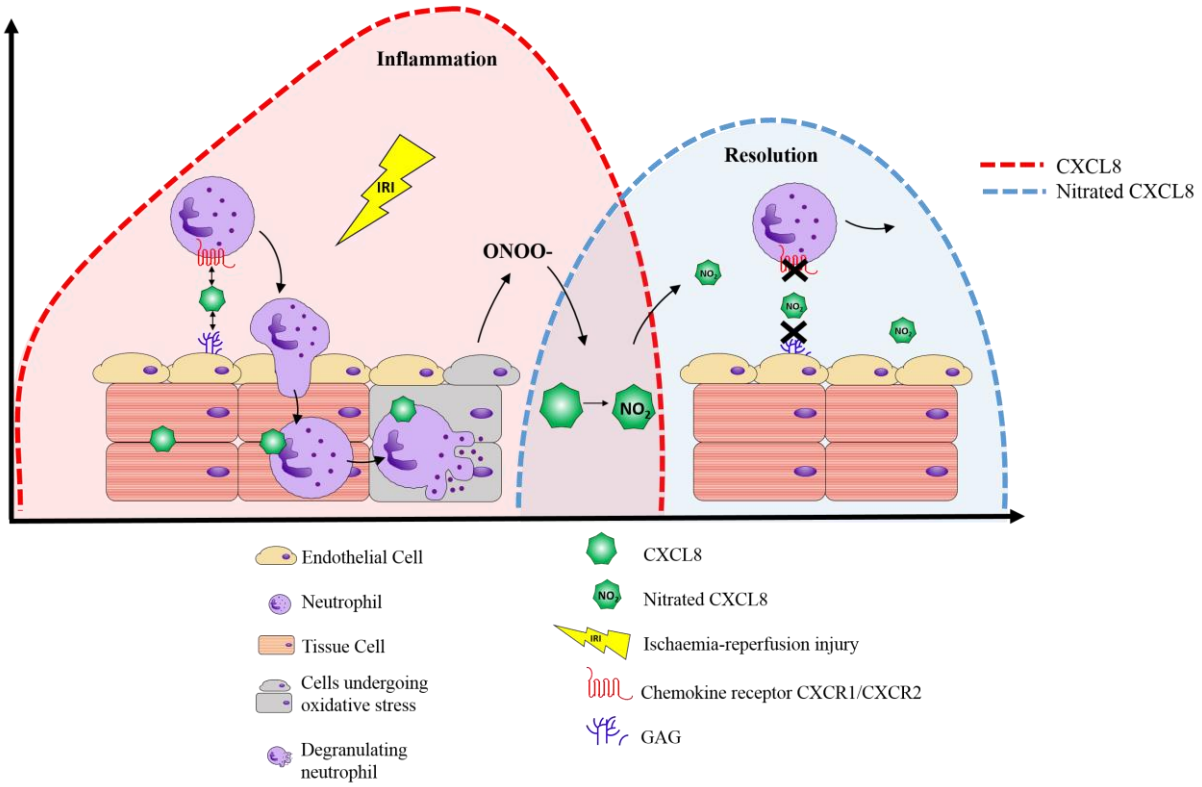

Figure 6-1.Proposed role for CXCL8 nitration in the resolution of inflammation during ischaemia-reperfusion injury (IRI). A CXCL8 gradient localised to the site of injury exists as an "equilibrated cloud" of bound and unbound chemokine monomers/dimers, likely transiently binding to glycosaminoglycans (GAGs) and G-protein-coupled receptors (GPCRs) (CXCR1/CXCR2) present on neutrophils. Neutrophils then adhere to the endothelium and extravasate into the tissue. At peak inflammation, degranulating neutrophils and tissue/endothelial cells damaged by IRI (grey) contribute to the production of peroxynitrite ($ONOO^-$), which nitrates CXCL8. Nitration renders CXCL8 almost completely non-functional, inhibiting its ability to bind to GPCRs and GAGs, therefore preventing further neutrophil recruitment. CXCL8 nitration could therefore pose as a natural mechanism involved in the resolution of inflammation.

REFERENCES

1 Martins-Green, M., Petreaca, M. & Wang, L. Chemokines and their receptors are key players in the orchestra that regulates wound healing. *Advances in wound care* **2**, 327-347 (2013).

2 Rajagopalan, L. & Rajarathnam, K. Structural basis of chemokine receptor function—a model for binding affinity and ligand selectivity. *Bioscience Reports* **26**, 325-339 (2006).

3 Kufareva, I., Salanga, C. L. & Handel, T. M. Chemokine and chemokine receptor structure and interactions: implications for therapeutic strategies. *Immunology and Cell Biology* **93**, 372-383 (2015).

4 Kleist, A. B. *et al.* New paradigms in chemokine receptor signal transduction: Moving beyond the two-site model. *Biochemical Pharmacology* **114**, 53-68 (2016).

5 Moser, B. & Willimann, K. Chemokines: role in inflammation and immune surveillance. *Annals of the rheumatic diseases* **63**, ii84-ii89 (2004).

6 Le, Y., Zhou, Y., Iribarren, P. & Wang, J. Chemokines and chemokine receptors: their manifold roles in homeostasis and disease. *Cell Mol Immunol* **1**, 95-104 (2004).

7 Tachibana, K. *et al.* The chemokine receptor CXCR4 is essential for vascularization of the gastrointestinal tract. *Nature* **393**, 591 (1998).

8 Zou, Y.-R., Kottmann, A. H., Kuroda, M., Taniuchi, I. & Littman, D. R. Function of the chemokine receptor CXCR4 in haematopoiesis and in cerebellar development. *Nature* **393**, 595 (1998).

9 Gombert, M. *et al.* CCL1-CCR8 interactions: an axis mediating the recruitment of T cells and Langerhans-type dendritic cells to sites of atopic skin inflammation. *The Journal of Immunology* **174**, 5082-5091 (2005).

10 Choi, W.-T. & An, J. Biology and clinical relevance of chemokines and chemokine receptors CXCR4 and CCR5 in human diseases. *Experimental Biology and Medicine* **236**, 637-647 (2011).

11 Van Raemdonck, K., Van den Steen, P. E., Liekens, S., Van Damme, J. & Struyf, S. CXCR3 ligands in disease and therapy. *Cytokine & growth factor reviews* **26**, 311-327 (2015).

12 Hernandez, P. A. *et al.* Mutations in the chemokine receptor gene CXCR4 are associated with WHIM syndrome, a combined immunodeficiency disease. *Nature genetics* **34**, 70 (2003).

13 Bursill, C. A., Channon, K. M. & Greaves, D. R. The role of chemokines in atherosclerosis: recent evidence from experimental models and population genetics. *Current opinion in lipidology* **15**, 145-149 (2004).

14 Bachelerie, F. *et al.* International Union of Pharmacology. LXXXIX. Update on the extended family of chemokine receptors and introducing a new nomenclature for atypical chemokine receptors. *Pharmacological reviews* **66**, 1 (2014).

15 Nibbs, R. J. B. & Graham, G. J. Immune regulation by atypical chemokine receptors. *Nature Reviews Immunology* **13**, 815 (2013).

16 Bachelerie, F. *et al.* New nomenclature for atypical chemokine receptors. *Nature Immunology* **15**, 207-208 (2014).

17 Bonecchi, R. & Graham, G. J. Atypical chemokine receptors and their roles in the resolution of the inflammatory response. *Frontiers in immunology* **7**, 224 (2016).

18 Fukuma, N. *et al.* A role of the Duffy antigen for the maintenance of plasma chemokine concentrations. *Biochemical and biophysical research communications* **303**, 137-139 (2003).

19 Levoye, A., Balabanian, K., Baleux, F., Bachelerie, F. & Lagane, B. CXCR7 heterodimerizes with CXCR4 and regulates CXCL12-mediated G protein signaling. *Blood* **113**, 6085-6093 (2009).

20 Zarbock, A. *et al.* Chemokine homeostasis vs. chemokine presentation during severe acute lung injury: the other side of the Duffy antigen receptor for chemokines. *American Journal of Physiology-Lung Cellular and Molecular Physiology* **298**, L462-L471 (2010).

21 Allison, A. C. Genetic control of resistance to human malaria. *Current opinion in immunology* **21**, 499-505 (2009).

22 Wu, F.-Y. *et al.* Chemokine decoy receptor d6 plays a negative role in human breast cancer. *Molecular Cancer Research* **6**, 1276-1288 (2008).

23 Griffith, J. W., Sokol, C. L. & Luster, A. D. Chemokines and chemokine receptors: positioning cells for host defense and immunity. *Annual review of immunology* **32**, 659-702 (2014).

24 Lazennec, G. & Richmond, A. Chemokines and chemokine receptors: new insights into cancer-related inflammation. *Trends in molecular medicine* **16**, 133-144 (2010).

25 Cameron, M. J. & Kelvin, D. J. in *Madame Curie Bioscience Database [Internet]* (Landes Bioscience, 2013).

26 Abcam. *Chemokines and their receptors* <https://www.abcam.com/pathways/chemokines-and-their-receptors> (

27 Proudfoot, A., Johnson, Z., Bonvin, P. & Handel, T. Glycosaminoglycan interactions with chemokines add complexity to a complex system. *Pharmaceuticals* **10**, 70 (2017).

28 Yang, S. *et al.* Simultaneous analyses of N-linked and O-linked glycans of ovarian cancer cells using solid-phase chemoenzymatic method. *Clinical proteomics* **14**, 3 (2017).

29 Rek, A., Krenn, E. & Kungl, A. Therapeutically targeting protein–glycan interactions. *British journal of pharmacology* **157**, 686-694 (2009).

30 Thompson, S. *et al.* Regulation of Chemokine Function: The Roles of GAG-Binding and Post-Translational Nitration. *International journal of molecular sciences* **18**, 1692 (2017).

31 Sarrazin, S., Lamanna, W. C. & Esko, J. D. Heparan sulfate proteoglycans. *Cold Spring Harbor perspectives in biology* **3**, a004952 (2011).

32 Proudfoot, A. E. I. *et al.* Glycosaminoglycan binding and oligomerization are essential for the in vivo activity of certain chemokines. *Proceedings of the National Academy of Sciences* **100**, 1885-1890 (2003).

33 Rajarathnam, K., Sepuru, K. M., Joseph, P. R. B., Sawant, K. V. & Brown, A. J. Glycosaminoglycan Interactions Fine-Tune Chemokine-Mediated Neutrophil Trafficking: Structural Insights and Molecular Mechanisms. *Journal of Histochemistry & Cytochemistry* **66**, 229-239 (2018).

34 Joseph, P. R. B., Sawant, K. V. & Rajarathnam, K. Heparin-bound chemokine CXCL8 monomer and dimer are impaired for CXCR1 and CXCR2 activation: implications for gradients and neutrophil trafficking. *Open biology* **7**, 170168 (2017).

35 Bedke, J. *et al.* A novel CXCL8 protein-based antagonist in acute experimental renal allograft damage. *Molecular Immunology* **47**, 1047-1057 (2010).

36 Taylor, K. R. & Gallo, R. L. Glycosaminoglycans and their proteoglycans: host-associated molecular patterns for initiation and modulation of inflammation. *The FASEB Journal* **20**, 9-22 (2006).

37 Rot, A. Neutrophil attractant/activation protein-1 (interleukin-8) induces in vitro neutrophil migration by haptotactic mechanism. *European Journal of Immunology* **23**, 303-306 (1993).

38 Lortat-Jacob, H., Grosdidier, A. & Imberty, A. Structural diversity of heparan sulfate binding domains in chemokines. *Proceedings of the National Academy of Sciences* **99**, 1229-1234 (2002).

39 Sadir, R., Imberty, A., Baleux, F. & Lortat-Jacob, H. Heparan sulfate/heparin oligosaccharides protect stromal cell-derived factor-1 (SDF-1)/CXCL12 against proteolysis induced by CD26/dipeptidyl peptidase IV. *Journal of Biological Chemistry* **279**, 43854-43860 (2004).

40 Ellyard, J. I. *et al.* Eotaxin Selectively Binds Heparin AN INTERACTION THAT PROTECTS EOTAXIN FROM PROTEOLYSIS AND POTENTIATES CHEMOTACTIC ACTIVITY IN VIVO. *Journal of Biological Chemistry* **282**, 15238-15247 (2007).

41 Metzemaekers, M., Van Damme, J., Mortier, A. & Proost, P. Regulation of chemokine activity–a focus on the role of dipeptidyl peptidase IV/CD26. *Frontiers in immunology* **7**, 483 (2016).

42 Handel, T. M. *et al.* Regulation of protein function by glycosaminoglycans-as exemplified by chemokines. *Annual Review of Biochemistry* **74**, 385-410 (2005).

43 Monneau, Y., Arenzana-Seisdedos, F. & Lortat-Jacob, H. The sweet spot: how GAGs help chemokines guide migrating cells. *Journal of leukocyte biology* **99**, 935-953 (2016).

44 Dyer, D. P., Salanga, C. L., Volkman, B. F., Kawamura, T. & Handel, T. M. The dependence of chemokine–glycosaminoglycan interactions on chemokine oligomerization. *Glycobiology* **26**, 312-326 (2015).

45 Papakonstantinou, E. & Karakiulakis, G. The 'sweet'and 'bitter'involvement of glycosaminoglycans in lung diseases: pharmacotherapeutic relevance. *British journal of pharmacology* **157**, 1111-1127 (2009).

46 Das, S. T. *et al.* Monomeric and dimeric CXCL8 are both essential for in vivo neutrophil recruitment. *PLoS One* **5** (2010).

47 Rajarathnam, K., Prado, G. N., Fernando, H., Clark-Lewis, I. & Navarro, J. Probing receptor binding activity of interleukin-8 dimer using a disulfide trap. *Biochemistry* **45**, 7882-7888 (2006).

48 Paavola, C. D. *et al.* Monomeric monocyte chemoattractant protein-1 (MCP-1) binds and activates the MCP-1 receptor CCR2B. *Journal of Biological Chemistry* **273**, 33157-33165 (1998).

49 Laurence, J. S., Blanpain, C., Burgner, J. W., Parmentier, M. & LiWang, P. J. CC chemokine MIP-1β can function as a monomer and depends on Phe13 for receptor binding. *Biochemistry* **39**, 3401-3409 (2000).

50 Czaplewski, L. G. *et al.* Identification of amino acid residues critical for aggregation of human CC chemokines macrophage inflammatory protein (MIP)-1α, MIP-1β, and RANTES characterization of active disaggregated chemokine variants. *Journal of Biological Chemistry* **274**, 16077-16084 (1999).

51 Rajarathnam, K. *et al.* Neutrophil-activating peptide-2 and melanoma growth-stimulatory activity are functional as monomers for neutrophil activation. *Journal of Biological Chemistry* **272**, 1725-1729 (1997).

52 Rajarathnam, K. *et al.* Neutrophil activation by monomeric interleukin-8. *Science* **264**, 90-92 (1994).

53 Booth, V., Keizer, D. W., Kamphuis, M. B., Clark-Lewis, I. & Sykes, B. D. The CXCR3 binding chemokine IP-10/CXCL10: structure and receptor interactions. *Biochemistry* **41**, 10418-10425 (2002).

54 Jin, H., Shen, X., Baggett, B. R., Kong, X. & LiWang, P. J. The human CC chemokine MIP-1β dimer is not competent to bind to the CCR5 receptor. *Journal of Biological Chemistry* **282**, 27976-27983 (2007).

55 Gangavarapu, P. *et al.* The monomer-dimer equilibrium and glycosaminoglycan interactions of chemokine CXCL8 regulate tissue-specific neutrophil recruitment. *Journal of Leukocyte Biology* **91**, 259-265 (2012).

56 Miller, M. & Mayo, K. Chemokines from a structural perspective. *International journal of molecular sciences* **18**, 2088 (2017).

57 Salanga, C. L. *et al.* Multiple glycosaminoglycan-binding epitopes of monocyte chemoattractant protein-3/CCL7 enable it to function as a non-oligomerizing chemokine. *Journal of Biological Chemistry* **289**, 14896-14912 (2014).

58 Guan, E., Wang, J. & Norcross, M. A. Identification of human macrophage inflammatory proteins 1α and 1β as a native secreted heterodimer. *Journal of Biological Chemistry* **276**, 12404-12409 (2001).

59 Nesmelova, I. V. *et al.* Platelet factor 4 and interleukin-8 CXC chemokine heterodimer formation modulates function at the quaternary structural level. *Journal of Biological Chemistry* **280**, 4948-4958 (2005).

60 Koenen, R. R. *et al.* Disrupting functional interactions between platelet chemokines inhibits atherosclerosis in hyperlipidemic mice. *Nature medicine* **15**, 97 (2009).

61 Von Hundelshausen, P. *et al.* Chemokine interactome mapping enables tailored intervention in acute and chronic inflammation. *Science translational medicine* **9**, eaah6650 (2017).

62 Jansma, A., Handel, T. M. & Hamel, D. J. Homo-and Hetero-Oligomerization of Chemokines. *Methods in enzymology* **461**, 31-50 (2009).

63 Crown, S. E., Yu, Y., Sweeney, M. D., Leary, J. A. & Handel, T. M. Heterodimerization of CCR2 chemokines and regulation by glycosaminoglycan binding. *Journal of Biological Chemistry* **281**, 25438-25446 (2006).

64 Salanga, C. L., O'Hayre, M. & Handel, T. Modulation of chemokine receptor activity through dimerization and crosstalk. *Cellular and molecular life sciences* **66**, 1370-1386 (2009).

65 Hauser, M. A. *et al.* Inflammation-induced CCR7 oligomers form scaffolds to integrate distinct signaling pathways for efficient cell migration. *Immunity* **44**, 59-72 (2016).

66 Metzemaekers, M., Vanheule, V., Janssens, R., Struyf, S. & Proost, P. Overview of the mechanisms that may contribute to the non-redundant activities of interferon-inducible CXC chemokine receptor 3 ligands. *Frontiers in immunology* **8**, 1970 (2018).

67 Paoletti, S. *et al.* A rich chemokine environment strongly enhances leukocyte migration and activities. *Blood* **105**, 3405-3412 (2005).

68 Wang, X., Sharp, J. S., Handel, T. M. & Prestegard, J. H. in *Progress in molecular biology and translational science* Vol. 117 531-578 (Elsevier, 2013).

69 Amin, M. *et al.* Regulation and involvement of matrix metalloproteinases in vascular diseases. *Frontiers in bioscience (Landmark edition)* **21**, 89 (2016).

70 Tester, A. M. *et al.* LPS responsiveness and neutrophil chemotaxis in vivo require PMN MMP-8 activity. *PloS one* **2**, e312 (2007).

71 Wolf, M., Albrecht, S. & Märki, C. Proteolytic processing of chemokines: implications in physiological and pathological conditions. *The international journal of biochemistry & cell biology* **40**, 1185-1198 (2008).

72 Van den Steen, P. E. *et al.* Gelatinase B/MMP-9 and neutrophil collagenase/MMP-8 process the chemokines human GCP-2/CXCL6, ENA-78/CXCL5 and mouse GCP-2/LIX and modulate their physiological activities. *The FEBS Journal* **270**, 3739-3749 (2003).

73 Dean, R. A. *et al.* Macrophage-specific metalloelastase (MMP-12) truncates and inactivates ELR+ CXC chemokines and generates CCL2,-7,-8, and-13 antagonists: potential role of the macrophage in terminating polymorphonuclear leukocyte influx. *Blood* **112**, 3455-3464 (2008).

74 Van den Steen, P. E., Husson, S. J., Proost, P., Van Damme, J. & Opdenakker, G. Carboxyterminal cleavage of the chemokines MIG and IP-10 by gelatinase B and neutrophil collagenase. *Biochemical and biophysical research communications* **310**, 889-896 (2003).

75 Kurupati, P. *et al.* Chemokine-cleaving Streptococcus pyogenes protease SpyCEP is necessary and sufficient for bacterial dissemination within soft tissues and the respiratory tract. *Molecular microbiology* **76**, 1387-1397 (2010).

76 Proost, P. *et al.* Citrullination of CXCL8 by peptidylarginine deiminase alters receptor usage, prevents proteolysis, and dampens tissue inflammation. *The Journal of Experimental Medicine* **205**, 2085-2097 (2008).

77 Loos, T. *et al.* Citrullination of CXCL10 and CXCL11 by peptidylarginine deiminase: a naturally occurring posttranslational modification of chemokines and new dimension of immunoregulation. *Blood* **112**, 2648-2656 (2008).

78 Struyf, S. *et al.* Citrullination of CXCL12 differentially reduces CXCR4 and CXCR7 binding with loss of inflammatory and anti-HIV-1 activity via CXCR4. *The Journal of Immunology* **182**, 666-674 (2009).

79 Szabó, C., Ischiropoulos, H. & Radi, R. Peroxynitrite: biochemistry, pathophysiology and development of therapeutics. *Nature Reviews Drug Discovery* **6**, 662-680 (2007).

80 Vogt, W. Oxidation of methionyl residues in proteins: tools, targets, and reversal. *Free Radical Biology and Medicine* **18**, 93-105 (1995).

81 Pacher, P., Beckman, J. S. & Liaudet, L. Nitric oxide and peroxynitrite in health and disease. *Physiological Reviews* **87**, 315-424 (2007).

82 Nuriel, T., Hansler, A. & Gross, S. S. Protein nitrotryptophan: formation, significance and identification. *Journal of proteomics* **74**, 2300-2312 (2011).

83 Alvarez, B. *et al.* Inactivation of human Cu, Zn superoxide dismutase by peroxynitrite and formation of histidinyl radical. *Free Radical Biology and Medicine* **37**, 813-822 (2004).

84 Verrastro, I., Pasha, S., Jensen, K. T., Pitt, A. R. & Spickett, C. M. Mass spectrometry-based methods for identifying oxidized proteins in disease: advances and challenges. *Biomolecules* **5**, 378-411 (2015).

85 Bartesaghi, S. & Radi, R. Fundamentals on the biochemistry of peroxynitrite and protein tyrosine nitration. *Redox biology* **14**, 618-625 (2017).

86 Salvadori, M., Rosso, G. & Bertoni, E. Update on ischemia-reperfusion injury in kidney transplantation: Pathogenesis and treatment. *World journal of transplantation* **5**, 52 (2015).

87 Saidi, R. F. & Kenari, S. K. H. Liver ischemia/reperfusion injury: an overview. *Journal of Investigative Surgery* **27**, 366-379 (2014).

88 Okada, M. *et al.* SPRED2 deficiency may lead to lung ischemia–reperfusion injury via ERK1/2 signaling pathway activation. *Surgery today*, 1-7 (2018).

89 Korkmaz-Icöz, S. *et al.* Impairment of the Akt pathway in transplanted Type 1 diabetic hearts is associated with post-transplant graft injury. *Interactive cardiovascular and thoracic surgery* (2018).

90 Turer, A. T. & Hill, J. A. Pathogenesis of myocardial ischemia-reperfusion injury and rationale for therapy. *The American journal of cardiology* **106**, 360-368 (2010).

91 Eltzschig, H. K. & Eckle, T. Ischemia and reperfusion [mdash] from mechanism to translation. *Nature medicine* **17**, 1391-1401 (2011).

92 Mancini, A. *et al.* Thyroid Hormones, Oxidative Stress, and Inflammation. *Mediators of Inflammation* **2016** (2016).

93 Siti, H. N., Kamisah, Y. & Kamsiah, J. The role of oxidative stress, antioxidants and vascular inflammation in cardiovascular disease (a review). *Vascular Pharmacology* **71**, 40-56 (2015).

94 Finkel, T. Signal transduction by reactive oxygen species. *The Journal of cell biology* **194**, 7-15 (2011).

95 Barker, C. E., Ali, S., O'Boyle, G. & Kirby, J. A. Transplantation and inflammation: implications for the modification of chemokine function. *Immunology* **143**, 138-145 (2014).

96 Thompson-Gorman, S. L. & Zweier, J. L. Evaluation of the role of xanthine oxidase in myocardial reperfusion injury. *Journal of Biological Chemistry* **265**, 6656-6663 (1990).

97 Gondouin, B. *et al.* Plasma xanthine oxidase activity is predictive of cardiovascular disease in patients with chronic kidney disease, independently of uric acid levels. *Nephron* **131**, 167-174 (2015).

98 Turko, I. V. & Murad, F. Protein nitration in cardiovascular diseases. *Pharmacological Reviews* **54**, 619-634 (2002).

99 Dedon, P. C. & Tannenbaum, S. R. Reactive nitrogen species in the chemical biology of inflammation. *Archives of biochemistry and biophysics* **423**, 12-22 (2004).

100 Pacher, P., Schulz, R., Liaudet, L. & Szabó, C. Nitrosative stress and pharmacological modulation of heart failure. *Trends in pharmacological sciences* **26**, 302-310 (2005).

101 Buchwalow, I. B. *et al.* Inducible nitric oxide synthase in the myocard. *Molecular and cellular biochemistry* **217**, 73-82 (2001).

102 Szabó, G. *et al.* Catalytic peroxynitrite decomposition improves reperfusion injury after heart transplantation. *The Journal of thoracic and cardiovascular surgery* **143**, 1443-1449 (2012).

103 Chung, H. Y. *et al.* Xanthine dehydrogenase/xanthine oxidase and oxidative stress. *Age* **20**, 127-140 (1997).

104 Wink, D. A. *et al.* DNA deaminating ability and genotoxicity of nitric oxide and its progenitors. *Science* **254**, 1001-1003 (1991).

105 Korthuis, R. J. & Granger, D. N. Reactive oxygen metabolites, neutrophils, and the pathogenesis of ischemic-tissue/reperfusion. *Clinical cardiology* **16**, 19-26 (1993).

106 Lim, C. H., Dedon, P. C. & Deen, W. M. Kinetic analysis of intracellular concentrations of reactive nitrogen species. *Chemical Research in Toxicology* **21**, 2134-2147 (2008).

107 Lowenstein, C. J. & Snyder, S. H. Nitric oxide, a novel biologic messenger. *Cell* **70**, 705-707 (1992).

108 Wang, W., Sawicki, G. & Schulz, R. Peroxynitrite-induced myocardial injury is mediated through matrix metalloproteinase-2. *Cardiovascular research* **53**, 165-174 (2002).

109 Szabo, C. *et al.* in *FASEB JOURNAL.* A1166-A1166 (FEDERATION AMER SOC EXP BIOL 9650 ROCKVILLE PIKE, BETHESDA, MD 20814-3998 USA).

110 Jagtap, P. & Szabó, C. Poly (ADP-ribose) polymerase and the therapeutic effects of its inhibitors. *Nature reviews Drug discovery* **4**, 421-440 (2005).

111 Szabo, C. Multiple pathways of peroxynitrite cytotoxicity. *Toxicology letters* **140**, 105-112 (2003).

112 Batthyány, C. *et al.* Tyrosine-Nitrated Proteins: Proteomic and Bioanalytical Aspects. *Antioxidants & Redox Signaling* **26**, 313-328 (2016).

113 Lee, W. H., Gounarides, J. S., Roos, E. S. & Wolin, M. S. Influence of peroxynitrite on energy metabolism and cardiac function in a rat ischemia-reperfusion model. *American Journal of Physiology-Heart and Circulatory Physiology* **285**, 1385-1395 (2003).

114 Sakurai, M. *et al.* Quantitative Analysis of Cardiac 3-L-Nitrotyrosine During Acute Allograft Rejection In An Experimental Heart Transplantation. *Transplantation* **68**, 1818-1822 (1999).

115 Thuraisingham, R. C., Nott, C. A., Dodd, S. M. & Yaqoob, M. M. Increased nitrotyrosine staining in kidneys from patients with diabetic nephropathy. *Kidney International* **57**, 1968-1972 (2000).

116 Ahmed, U., Anwar, A., Savage, R. S., Thornalley, P. J. & Rabbani, N. Protein oxidation, nitration and glycation biomarkers for early-stage diagnosis of osteoarthritis of the knee and typing and progression of arthritic disease. *Arthritis Research & Therapy* **18** (2016).

117 Pennathur, S. *et al.* Oxidative modifications of protein tyrosyl residues are increased in plasma of human subjects with interstitial lung disease. *American Journal of Respiratory and Critical Care Medicine* **193**, 861-868 (2016).

118 Aydın, A. *et al.* Oxidative stress and nitric oxide related parameters in type II diabetes mellitus: effects of glycemic control. *Clinical Biochemistry* **34**, 65-70 (2001).

119 Sato, E., Simpson, K. L., Grisham, M. B., Koyama, S. & Robbins, R. A. Effects of Reactive Oxygen and Nitrogen Metabolites on RANTES and IL-5-Induced Eosinophil Chemotactic Activity in vitro. *The American Journal of Pathology* **155**, 591-598 (1999).

120 Molon, B. *et al.* Chemokine nitration prevents intratumoral infiltration of antigen-specific T cells. *The Journal of Experimental Medicine* **208**, 1949-1962 (2011).

121 Barker, C. E. *et al.* CCL2 nitration is a negative regulator of chemokine-mediated inflammation. *Scientific Reports* **7** (2017).

122 Janssens, R. *et al.* Natural nitration of CXCL12 reduces its signaling capacity and chemotactic activity in vitro and abrogates intra-articular lymphocyte recruitment in vivo. *Oncotarget* **7**, 62439 (2016).

123 Sato, E., Simpson, K. L., Grisham, M. B., Koyama, S. & Robbins, R. A. Inhibition of MIP-1α-induced human neutrophil and monocyte chemotactic activity by reactive oxygen and nitrogen metabolites. *Journal of Laboratory and Clinical Medicine* **135**, 161-169 (2000).

124 Sato, E., Simpson, K. L., Grisham, M. B., Koyama, S. & Robbins, R. A. Effects of reactive oxygen and nitrogen metabolites on eotaxin-induced eosinophil chemotactic activity in vitro. *American journal of respiratory cell and molecular biology* **22**, 61-67 (2000).

125 Sengupta, S. & Bhattacharjee, A. Dynamics of Protein Tyrosine Nitration and Denitration: A Review. *J Proteo Genomics* **1**, 105 (2016).

126 Larosche, I. *et al.* Hepatic mitochondrial DNA depletion after an alcohol binge in mice: probable role of peroxynitrite and modulation by manganese superoxide dismutase. *Journal of Pharmacology and Experimental Therapeutics* **332**, 886-897 (2010).

127 Moon, K. H. *et al.* Inactivation of oxidized and S-nitrosylated mitochondrial proteins in alcoholic fatty liver of rats. *Hepatology* **44**, 1218-1230 (2006).

128 Abdelmegeed, M. A. & Song, B.-J. Functional roles of protein nitration in acute and chronic liver diseases. *Oxidative medicine and cellular longevity* **2014** (2014).

129 Ahsan, H. 3-Nitrotyrosine: a biomarker of nitrogen free radical species modified proteins in systemic autoimmunogenic conditions. *Human immunology* **74**, 1392-1399 (2013).

130 Thomson, L. *et al.* Identification of immunoglobulins that recognize 3-nitrotyrosine in patients with acute lung injury after major trauma. *American journal of respiratory cell and molecular biology* **36**, 152-157 (2007).

131 Kuo, W.-N., Kanadia, R. N., Shanbhag, V. P. & Toro, R. Denitration of peroxynitrite-treated proteins by 'protein nitratases' from rat brain and heart. *Molecular and cellular biochemistry* **201**, 11-16 (1999).

132 Sabetkar, M., Low, S. Y., Naseem, K. M. & Bruckdorfer, K. R. The nitration of proteins in platelets: significance in platelet function1, 2. *Free Radical Biology and Medicine* **33**, 728-736 (2002).

133 Koeck, T. *et al.* Rapid and selective oxygen-regulated protein tyrosine denitration and nitration in mitochondria. *Journal of Biological Chemistry* **279**, 27257-27262 (2004).

134 Smallwood, H. S. *et al.* Identification of a denitrase activity against calmodulin in activated macrophages using high-field liquid chromatography− FTICR mass spectrometry. *Biochemistry* **46**, 10498-10505 (2007).

135 Léger, C. L., Torres-Rasgado, E., Fouret, G. & Carbonneau, M. A. First evidence for an LDL-and HDL-associated nitratase activity that denitrates albumin-bound nitrotyrosine—Physiological consequences. *IUBMB life* **60**, 73-78 (2008).

136 Matsushima, K. *et al.* Molecular cloning of a human monocyte-derived neutrophil chemotactic factor (MDNCF) and the induction of MDNCF mRNA by interleukin 1 and tumor necrosis factor. *Journal of Experimental Medicine* **167**, 1883-1893 (1988).

137 Kendrick, A. A. *et al.* The dynamics of interleukin-8 and its interaction with human CXC receptor I peptide. *Protein Science* **23**, 464-480 (2014).

138 Mehrad, B., Keane, M. P. & Strieter, R. M. Chemokines as mediators of angiogenesis. *Thrombosis and Haemostasis* **97**, 755-762 (2007).

139 Mukaida, N. Pathophysiological roles of interleukin-8/CXCL8 in pulmonary diseases. *American Journal of Physiology-Lung Cellular and Molecular Physiology* **284**, L566-L577 (2003).

140 Tanino, Y. *et al.* Kinetics of chemokine–glycosaminoglycan interactions control neutrophil migration into the airspaces of the lungs. *The Journal of Immunology* **184**, 2677-2685 (2010).

141 Sarmiento, J. *et al.* Diverging mechanisms of activation of chemokine receptors revealed by novel chemokine agonists. *PloS one* **6**, e27967 (2011).

142 Lowman, H. B. *et al.* Exchanging interleukin-8 and melanoma growth-stimulating activity receptor binding specificities. *Journal of Biological Chemistry* **271**, 14344-14352 (1996).

143 Hebert, C. A., Vitangcol, R. V. & Baker, J. B. Scanning mutagenesis of interleukin-8 identifies a cluster of residues required for receptor binding. *Journal of Biological Chemistry* **266**, 18989-18994 (1991).

144 Moser, B. *et al.* Interleukin-8 antagonists generated by N-terminal modification. *Journal of Biological Chemistry* **268**, 7125-7128 (1993).

145 Clark-Lewis, I., Dewald, B., Geiser, T., Moser, B. & Baggiolini, M. Platelet factor 4 binds to interleukin 8 receptors and activates neutrophils when its N terminus is modified with Glu-Leu-Arg. *Proceedings of the National Academy of Sciences* **90**, 3574-3577 (1993).

146 Schraufstätter, I. U., Ma, M., Oades, Z. G., Barritt, D. S. & Cochrane, C. G. The Role of Tyr and Lys of Interleukin-8 in the High Affinity Interaction with the Interleukin-8 Receptor Type A. *Journal of Biological Chemistry* **270**, 10428-10431 (1995).

147 Clark-Lewis, I., Dewald, B., Loetscher, M., Moser, B. & Baggiolini, M. Structural requirements for interleukin-8 function identified by design of analogs and CXC chemokine hybrids. *Journal of Biological Chemistry* **269**, 16075-16081 (1994).

148 Hammond, M. E. W. *et al.* Receptor recognition and specificity of interleukin-8 is determined by residues that cluster near a surface-accessible hydrophobic pocket. *Journal of Biological Chemistry* **271**, 8228-8235 (1996).

149 Samanta, A. K., Oppenheim, J. J. & Matsushima, K. Interleukin 8 (monocyte-derived neutrophil chemotactic factor) dynamically regulates its own receptor expression on human neutrophils. *Journal of Biological Chemistry* **265**, 183-189 (1990).

150 Campbell, L. M., Maxwell, P. J. & Waugh, D. J. J. Rationale and means to target pro-inflammatory interleukin-8 (CXCL8) signaling in cancer. *Pharmaceuticals* **6**, 929-959 (2013).

151 Dyer, D. P. *et al.* TSG-6 inhibits neutrophil migration via direct interaction with the chemokine CXCL8. *The Journal of Immunology* **192**, 2177-2185 (2014).

152 Feniger-Barish, R., Ran, M., Zaslaver, A. & Ben-Baruch, A. Differential modes of regulation of cxc chemokine-induced internalization and recycling of human CXCR1 and CXCR2. *Cytokine* **11**, 996-1009 (1999).

153 Stillie, R., Farooq, S. M., Gordon, J. R. & Stadnyk, A. W. The functional significance behind expressing two IL-8 receptor types on PMN. *Journal of leukocyte biology* **86**, 529-543 (2009).

154 Hammond, M. E. *et al.* IL-8 induces neutrophil chemotaxis predominantly via type I IL-8 receptors. *The Journal of Immunology* **155**, 1428-1433 (1995).

155 Quan, J. M. *et al.* Antibodies against the N-terminus of IL-8 receptor A inhibit neutrophil chemotaxis. *Biochemical and biophysical research communications* **219**, 405-411 (1996).

156 Chuntharapai, A. & Kim, K. J. Regulation of the expression of IL-8 receptor A/B by IL-8: possible functions of each receptor. *The Journal of Immunology* **155**, 2587-2594 (1995).

157 Ludwig, A. *et al.* The CXC-chemokine neutrophil-activating peptide-2 induces two distinct optima of neutrophil chemotaxis by differential interaction with interleukin-8 receptors CXCR-1 and CXCR-2. *Blood* **90**, 4588-4597 (1997).

158 Joseph, P. R. B., Mosier, P. D., Desai, U. R. & Rajarathnam, K. Solution NMR characterization of chemokine CXCL8/IL-8 monomer and dimer binding to glycosaminoglycans: structural plasticity mediates differential binding interactions. *Biochemical Journal* **472**, 121-133 (2015).

159 Kuschert, G. S. V. *et al.* Identification of a glycosaminoglycan binding surface on human interleukin-8. *Biochemistry* **37**, 11193-11201 (1998).

160 Nasser, M. W. *et al.* Differential activation and regulation of CXCR1 and CXCR2 by CXCL8 monomer and dimer. *The Journal of Immunology* **183**, 3425-3432 (2009).

161 Baldwin, E. T. *et al.* Crystal structure of interleukin 8: symbiosis of NMR and crystallography. *Proceedings of the National Academy of Sciences* **88**, 502-506 (1991).

162 Burrows, S. D. *et al.* Determination of the monomer-dimer equilibrium of interleukin-8 reveals it is a monomer at physiological concentrations. *Biochemistry* **33**, 12741-12745 (1994).

163 Joseph, P. R. B. & Rajarathnam, K. Solution NMR characterization of WT CXCL 8 monomer and dimer binding to CXCR 1 N-terminal domain. *Protein Science* **24**, 81-92 (2015).

164 Leong, S. R. *et al.* IL-8 single-chain homodimers and heterodimers: Interactions with the chemokine receptors CXCR1, CXCR2, and DARC. *Protein Science* **6**, 609-617 (1997).

165 Joseph, P. R. B. *et al.* Proline substitution of dimer interface β-strand residues as a strategy for the design of functional monomeric proteins. *Biophysical journal* **105**, 1491-1501 (2013).

166 Williams, G. *et al.* Mutagenesis Studies of Interleukin-8 IDENTIFICATION OF A SECOND EPITOPE INVOLVED IN RECEPTOR BINDING. *Journal of Biological Chemistry* **271**, 9579-9586 (1996).

167 Fernando, H., Chin, C., Rösgen, J. & Rajarathnam, K. Dimer dissociation is essential for interleukin-8 (IL-8) binding to CXCR1 receptor. *Journal of Biological Chemistry* **279**, 36175-36178 (2004).

168 Rajagopalan, L., Rösgen, J., Bolen, D. W. & Rajarathnam, K. Novel Use of an Osmolyte To Dissect Multiple Thermodynamic Linkages in a Chemokine Ligand–Receptor System. *Biochemistry* **44**, 12932-12939 (2005).

169 Clore, G. M., Appella, E., Yamada, M., Matsushima, K. & Gronenborn, A. M. Three-dimensional structure of interleukin 8 in solution. *Biochemistry* **29**, 1689-1696 (1990).

170 Rajarathnam, K., Clark-Lewis, I. & Sykes, B. D. 1H NMR solution structure of an active monomeric interleukin-8. *Biochemistry* **34**, 12983-12990 (1995).

171 Matsushima, K. *et al.* Molecular cloning of a human monocyte-derived neutrophil chemotactic factor (MDNCF) and the induction of MDNCF mRNA by interleukin 1 and tumor necrosis factor. *The Journal of experimental medicine* **167**, 1883-1893 (1988).

172 Loos, T., Opdenakker, G., Van Damme, J. & Proost, P. Citrullination of CXCL8 increases this chemokine's ability to mobilize neutrophils into the blood circulation. *Haematologica* **94**, 1346-1353 (2009).

173 Sato, E., Simpson, K. L., Grisham, M. B., Koyama, S. & Robbins, R. A. Reactive nitrogen and oxygen species attenuate interleukin-8-induced neutrophil chemotactic activity in vitro. *Journal of Biological Chemistry* **275**, 10826-10830 (2000).

174 Vitiello, D., Neagoe, P.-E., Sirois, M. G. & White, M. Effect of everolimus on the immunomodulation of the human neutrophil inflammatory response and activation. *Cellular & molecular immunology* **12**, 40-52 (2015).

175 Boyle, E. M. *et al.* Inhibition of interleukin-8 blocks myocardial ischemia-reperfusion injury. *The Journal of Thoracic and Cardiovascular Surgery* **116**, 114-121 (1998).

176 Tsuruma, T., Yagihashi, A., Tarumi, K. & Hirata, K. in *Transplantation proceedings.* 2644-2645 (Elsevier).

177 Ezerzer, C., Dolgin, M., Skovorodnikova, J. & Harris, N. Chemokine receptor-derived peptides as multi-target drug leads for the treatment of inflammatory diseases. *Peptides* **30**, 1296-1305 (2009).

178 Hayashi, S. *et al.* Synthetic hexa-and heptapeptides that inhibit IL-8 from binding to and activating human blood neutrophils. *The Journal of Immunology* **154**, 814-824 (1995).

179 Cacalano, G. *et al.* Neutrophil and B cell expansion in mice that lack the murine IL-8 receptor homolog. *Science* **265**, 682-684 (1994).

180 Frendéus, B. *et al.* Interleukin 8 receptor deficiency confers susceptibility to acute experimental pyelonephritis and may have a human counterpart. *Journal of Experimental Medicine* **192**, 881-890 (2000).

181 El-Sawy, T., Belperio, J. A., Strieter, R. M., Remick, D. G. & Fairchild, R. L. Inhibition of polymorphonuclear leukocyte–mediated graft damage synergizes with short-

term costimulatory blockade to prevent cardiac allograft rejection. *Circulation* **112**, 320-331 (2005).

182 Tarzami, S. T. *et al.* Opposing effects mediated by the chemokine receptor CXCR2 on myocardial ischemia-reperfusion injury: recruitment of potentially damaging neutrophils and direct myocardial protection. *Circulation* **108**, 2387-2392 (2003).

183 Moriconi, A. *et al.* Design of noncompetitive interleukin-8 inhibitors acting on CXCR1 and CXCR2. *Journal of medicinal chemistry* **50**, 3984-4002 (2007).

184 Busch-Petersen, J. *et al.* Danirixin: a reversible and selective antagonist of the cxc chemokine receptor 2. *Journal of Pharmacology and Experimental Therapeutics* **362**, 338-346 (2017).

185 Jiang, S.-J. *et al.* Peptides derived from CXCL8 based on in silico analysis inhibit CXCL8 interactions with its receptor CXCR1. *Scientific reports* **5**, 18638 (2015).

186 Citro, A. *et al.* CXCR1/2 inhibition enhances pancreatic islet survival after transplantation. *The Journal of clinical investigation* **122**, 3647-3651 (2012).

187 Souza, D. G. *et al.* Repertaxin, a novel inhibitor of rat CXCR2 function, inhibits inflammatory responses that follow intestinal ischaemia and reperfusion injury. *British journal of pharmacology* **143**, 132-142 (2004).

188 Garau, A. *et al.* Neuroprotection with the CXCL8 inhibitor repertaxin in transient brain ischemia. *Cytokine* **30**, 125-131 (2005).

189 Bertini, R. *et al.* Noncompetitive allosteric inhibitors of the inflammatory chemokine receptors CXCR1 and CXCR2: prevention of reperfusion injury. *Proceedings of the National Academy of Sciences of the United States of America* **101**, 11791-11796 (2004).

190 Cugini, D. *et al.* Inhibition of the chemokine receptor CXCR2 prevents kidney graft function deterioration due to ischemia/reperfusion. *Kidney international* **67**, 1753-1761 (2005).

191 Battaglia, M., Allegretti, M. & PiemontijL, L. CXCR1/2 Inhibition Blocks and Reverses Type 1 Diabetes in Mice. *Diabetes* **64**, 329 (2015).

192 Sousa, L. F. d. C. *et al.* Blockade of CXCR1/2 chemokine receptors protects against brain damage in ischemic stroke in mice. *Clinics* **68**, 391-394 (2013).

193 Coelho, F. M. *et al.* The chemokine receptors CXCR1/CXCR2 modulate antigen-induced arthritis by regulating adhesion of neutrophils to the synovial microvasculature. *Arthritis & Rheumatism* **58**, 2329-2337 (2008).

194 Barsante, M. M. *et al.* Blockade of the chemokine receptor CXCR2 ameliorates adjuvant-induced arthritis in rats. *British journal of pharmacology* **153**, 992-1002 (2008).

195 Bizzarri, C. *et al.* ELR+ CXC chemokines and their receptors (CXC chemokine receptor 1 and CXC chemokine receptor 2) as new therapeutic targets. *Pharmacology & therapeutics* **112**, 139-149 (2006).

196 Vanheule, V. *et al.* CXCL9-derived peptides differentially inhibit neutrophil migration in vivo through interference with glycosaminoglycan interactions. *Frontiers in Immunology* **8** (2017).

197 Al Faruque, H. *et al.* Stepwise inhibition of T cell recruitment at post-capillary venules by orally active desulfated heparins in inflammatory arthritis. *PloS One* **12** (2017).

198 Nagata, K. *et al.* Unfractionated heparin after TBI reduces in vivo cerebrovascular inflammation, brain edema and accelerates cognitive recovery. *Journal of Trauma and Acute Care Surgery* **81**, 1088-1094 (2016).

199 Riffo-Vasquez, Y. *et al.* A Non-Anticoagulant Fraction of Heparin Inhibits Leukocyte Diapedesis into the Lung by an Effect on Platelets. *American Journal of Respiratory Cell and Molecular Biology* **55**, 554-563 (2016).

200 Arimateia, D. S., da Silva Brito, A., de Azevedo, F. M., de Andrade, G. P. V. & Chavante, S. F. Heparin fails to inhibit the leukocyte recruitment for an extended time following inflammatory stimulus. *Pharmaceutical Biology* **53**, 72-77 (2015).

201 O'Boyle, G., Mellor, P., Kirby, J. A. & Ali, S. Anti-inflammatory therapy by intravenous delivery of non-heparan sulfate-binding CXCL12. *The FASEB Journal* **23**, 3906-3916 (2009).

202 Johnson, Z. *et al.* Interference with heparin binding and oligomerization creates a novel anti-inflammatory strategy targeting the chemokine system. *The Journal of Immunology* **173**, 5776-5785 (2004).

203 Severin, I. C. *et al.* Characterization of the chemokine CXCL11-heparin interaction suggests two different affinities for glycosaminoglycans. *Journal of Biological Chemistry* **285**, 17713-17724 (2010).

204 Lacy, P. Mechanisms of degranulation in neutrophils. *Allergy, Asthma & Clinical Immunology* **2**, 98 (2006).

205 Kolaczkowska, E. & Kubes, P. Neutrophil recruitment and function in health and inflammation. *Nature Reviews Immunology* **13**, 159-175 (2013).

206 Rot, A. & Von Andrian, U. H. Chemokines in innate and adaptive host defense: basic chemokinese grammar for immune cells. *Annu. Rev. Immunol.* **22**, 891-928 (2004).

207 McCracken, J. M. & Allen, L.-A. H. Regulation of human neutrophil apoptosis and lifespan in health and disease. *Journal of cell death* **7**, 15-23 (2014).

208 Harvath, L. in *Cell Motility Factors* 35-52 (Springer, 1991).

209 Sadik, C. D., Kim, N. D. & Luster, A. D. Neutrophils cascading their way to inflammation. *Trends in immunology* **32**, 452-460 (2011).

210 Ley, K., Laudanna, C., Cybulsky, M. I. & Nourshargh, S. Getting to the site of inflammation: the leukocyte adhesion cascade updated. *Nature Reviews Immunology* **7**, 678 (2007).

211 Nourshargh, S. & Alon, R. Leukocyte migration into inflamed tissues. *Immunity* **41**, 694-707 (2014).

212 Borregaard, N. & Cowland, J. B. Granules of the human neutrophilic polymorphonuclear leukocyte. *Blood* **89**, 3503-3521 (1997).

213 Kjeldsen, L., Sengelov, H., Lollike, K., Nielsen, M. & Borregaard, N. Isolation and characterization of gelatinase granules from human neutrophils. *Blood* **83**, 1640-1649 (1994).

214 Číž, M. & Lojek, A. Modulation of neutrophil oxidative burst via histamine receptors. *British journal of pharmacology* **170**, 17-22 (2013).

215 Chen, Y. & Junger, W. G. Measurement of oxidative burst in neutrophils. *Leucocytes*, 115-124 (2012).

216 Klebanoff, S. J., Kettle, A. J., Rosen, H., Winterbourn, C. C. & Nauseef, W. M. Myeloperoxidase: a front-line defender against phagocytosed microorganisms. *Journal of leukocyte biology* **93**, 185-198 (2013).

217 Nosal, R. *et al.* On the pharmacology of oxidative burst of human neutrophils. *Physiological research* **64**, S445 (2015).

218 Slauch, J. M. How does the oxidative burst of macrophages kill bacteria? Still an open question. *Molecular microbiology* **80**, 580-583 (2011).

219 Epstein, F. H. & Weiss, S. J. Tissue destruction by neutrophils. *New England Journal of Medicine* **320**, 365-376 (1989).

220 Inauen, W., Suzuki, M. & Granger, D. N. Mechanisms of cellular injury: potential sources of oxygen free radicals in ischemia/reperfusion. *Microcirculation, Endothelium, and Lymphatics* **5**, 143-155 (1988).

221 Barletta, K. E., Ley, K. & Mehrad, B. Regulation of neutrophil function by adenosine. *Arteriosclerosis, thrombosis, and vascular biology* **32**, 856-864 (2012).

222 Frangogiannis, N. G. Targeting the inflammatory response in healing myocardial infarcts. *Current medicinal chemistry* **13**, 1877-1893 (2006).

223 Cai, S. *et al.* Prolonged Mouse Cardiac Graft Cold Storage via Attenuating Ischemia-Reperfusion Injury Using a New Antioxidant-Based Preservation Solution. *Transplantation* (2016).

224 Shandelya, S. M., Kuppusamy, P., Weisfeldt, M. L. & Zweier, J. L. Evaluation of the role of polymorphonuclear leukocytes on contractile function in myocardial reperfusion injury. Evidence for plasma-mediated leukocyte activation. *Circulation* **87**, 536-546 (1993).

225 Granger, D. N. Role of xanthine oxidase and granulocytes in ischemia-reperfusion injury. *American Journal of Physiology-Heart and Circulatory Physiology* **255**, H1269-H1275 (1988).

226 Carden, D. L. & Korthuis, R. J. Mechanisms of postischemic vascular dysfunction in skeletal muscle: implications for therapeutic intervention. *Microcirculation, endothelium, and lymphatics* **5**, 277-298 (1988).

227 Shinbo, T. *et al.* Breathing nitric oxide plus hydrogen gas reduces ischemia-reperfusion injury and nitrotyrosine production in murine heart. *American Journal of Physiology-Heart and Circulatory Physiology* **305**, H542-H550 (2013).

228 Dreyer, W. J. *et al.* Neutrophil accumulation in ischemic canine myocardium. Insights into time course, distribution, and mechanism of localization during early reperfusion. *Circulation* **84**, 400-411 (1991).

229 Crawford, M. H. *et al.* Complement and neutrophil activation in the pathogenesis of ischemic myocardial injury. *Circulation* **78**, 1449-1458 (1988).

230 Lucchesi, B. R., Werns, S. W. & Fantone, J. C. The role of the neutrophil and free radicals in ischemic myocardial injury. *Journal of molecular and cellular cardiology* **21**, 1241-1251 (1989).

231 Pearl, J. M., Drinkwater, D. C., Laks, H., Capouya, E. R. & Gates, R. N. Leukocyte-depleted reperfusion of transplanted human hearts: a randomized, double-blind clinical trial. *The Journal of heart and lung transplantation: the official publication of the International Society for Heart Transplantation* **11**, 1082-1092 (1991).

232 Romson, J. L. *et al.* Reduction of the extent of ischemic myocardial injury by neutrophil depletion in the dog. *Circulation* **67**, 1016-1023 (1983).

233 Simpson, P. J. *et al.* Reduction of experimental canine myocardial reperfusion injury by a monoclonal antibody (anti-Mo1, anti-CD11b) that inhibits leukocyte adhesion. *Journal of Clinical Investigation* **81**, 624 (1988).

234 Delgado-Rizo, V. *et al.* Neutrophil extracellular traps and its implications in inflammation: an overview. *Frontiers in immunology* **8**, 81 (2017).

235 Smith, C. K. & Kaplan, M. J. The role of neutrophils in the pathogenesis of systemic lupus erythematosus. *Current opinion in rheumatology* **27**, 448-453 (2015).

236 Khandpur, R. *et al.* NETs are a source of citrullinated autoantigens and stimulate inflammatory responses in rheumatoid arthritis. *Science translational medicine* **5** (2013).

237 Raza, K. *et al.* Synovial fluid leukocyte apoptosis is inhibited in patients with very early rheumatoid arthritis. *Arthritis research & therapy* **8** (2006).

238 Wang, Y. *et al.* Increased neutrophil elastase and proteinase 3 and augmented NETosis are closely associated with β-cell autoimmunity in patients with type 1 diabetes. *Diabetes* **63**, 4239-4248 (2014).

239 Bennike, T. B. *et al.* Neutrophil extracellular traps in ulcerative colitis: a proteome analysis of intestinal biopsies. *Inflammatory bowel diseases* **21**, 2052-2067 (2015).

240 Bratton, D. L. & Henson, P. M. Neutrophil clearance: when the party is over, clean-up begins. *Trends in immunology* **32**, 350-357 (2011).

241 Bournazou, I. *et al.* Apoptotic human cells inhibit migration of granulocytes via release of lactoferrin. *The Journal of clinical investigation* **119**, 20-32 (2009).

242 Frangogiannis, N. G. The immune system and cardiac repair. *Pharmacological Research* **58**, 88-111 (2008).

243 Soehnlein, O. & Lindbom, L. Phagocyte partnership during the onset and resolution of inflammation. *Nature Reviews Immunology* **10**, 427-439 (2010).

244 Clifford, R. L. *et al.* CXCL8 histone H3 acetylation is dysfunctional in airway smooth muscle in asthma: regulation by BET. *American Journal of Physiology-Lung Cellular and Molecular Physiology* **308**, L962-L972 (2015).

245 McElvaney, O. J. *et al.* The effect of the decoy molecule PA401 on CXCL8 levels in bronchoalveolar lavage fluid of patients with cystic fibrosis. *Molecular immunology* **63**, 550-558 (2015).

246 Gilowska, I. CXCL8 (interleukin 8)--the key inflammatory mediator in chronic obstructive pulmonary disease? *Postepy higieny i medycyny doswiadczalnej (Online)* **68**, 842-850 (2014).

247 Mortaz, E. *et al.* Cigarette smoke induces CXCL8 production by human neutrophils via activation of TLR9 receptor. *European Respiratory Journal* **36**, 1143-1154 (2010).

248 Hashemian, S. M. R. *et al.* Elevated CXCL-8 expression in bronchoalveolar lavage correlates with disease severity in patients with acute respiratory distress syndrome resulting from tuberculosis. *Journal of Inflammation* **11**, 21 (2014).

249 Matsumoto, T. *et al.* Elevated serum levels of IL-8 in patients with HIV infection. *Clinical & Experimental Immunology* **93**, 149-151 (1993).

250 Carrol, E. D. *et al.* Chemokine responses are increased in HIV-infected Malawian children with invasive pneumococcal disease. *Journal of acquired immune deficiency syndromes (1999)* **44**, 443 (2007).

251 Zheng, J. C. *et al.* HIV-1-infected and/or immune-activated macrophages regulate astrocyte CXCL8 production through IL-1β and TNF-α: Involvement of mitogen-activated protein kinases and protein kinase R. *Journal of neuroimmunology* **200**, 100-110 (2008).

252 Mamik, M. K. & Ghorpade, A. Src homology-2 domain-containing protein tyrosine phosphatase (SHP) 2 and p38 regulate the expression of chemokine CXCL8 in human astrocytes. *PloS one* **7**, e45596 (2012).

253 K Mamik, M. & Ghorpade, A. CXCL8 as a potential therapeutic target for HIV-associated neurocognitive disorders. *Current drug targets* **17**, 111-121 (2016).

254 Zhang, J. *et al.* CSF multianalyte profile distinguishes Alzheimer and Parkinson diseases. *American journal of clinical pathology* **129**, 526-529 (2008).

255 Corrêa, J. D., Starling, D., Teixeira, A. L., Caramelli, P. & Silva, T. A. Chemokines in CSF of Alzheimer's disease patients. *Arquivos de neuro-psiquiatria* **69**, 455-459 (2011).

256 Bartosik-Psujek, H. & Stelmasiak, Z. The levels of chemokines CXCL8, CCL2 and CCL5 in multiple sclerosis patients are linked to the activity of the disease. *European journal of neurology* **12**, 49-54 (2005).

257 Oz, M. C. *et al.* Ischemia-Induced Interleukin-8 Release After Human Heart Transplantation A Potential Role for Endothelial Cells. *Circulation* **92**, 428-432 (1995).

258 Yu, J. *et al.* Myeloid-derived suppressor cells suppress antitumor immune responses through IDO expression and correlate with lymph node metastasis in patients with breast cancer. *The Journal of Immunology* **190**, 3783-3797 (2013).

259 Srivastava, M. K., Sinha, P., Clements, V. K., Rodriguez, P. & Ostrand-Rosenberg, S. Myeloid-derived suppressor cells inhibit T-cell activation by depleting cystine and cysteine. *Cancer research* **70**, 68-77 (2010).

260 Sparmann, A. & Bar-Sagi, D. Ras-induced interleukin-8 expression plays a critical role in tumor growth and angiogenesis. *Cancer cell* **6**, 447-458 (2004).

261 Alfaro, C. *et al.* Tumor-produced interleukin-8 attracts human myeloid-derived suppressor cells and elicits extrusion of neutrophil extracellular traps (NETs). *Clinical Cancer Research* **22**, 3924-3936 (2016).

262 Cools-Lartigue, J. *et al.* Neutrophil extracellular traps sequester circulating tumor cells and promote metastasis. *The Journal of clinical investigation* **123**, 3446-3458 (2013).

263 Fang, W. *et al.* Tumor-associated macrophages promote the metastatic potential of thyroid papillary cancer by releasing CXCL8. *Carcinogenesis* **35**, 1780-1787 (2014).

264 Tong, H. *et al.* Tumor-associated macrophage-derived CXCL8 could induce ERα suppression via HOXB13 in endometrial cancer. *Cancer letters* **376**, 127-136 (2016).

265 Li, X.-P. *et al.* Co-expression of CXCL8 and HIF-1α is associated with metastasis and poor prognosis in hepatocellular carcinoma. *Oncotarget* **6**, 22880 (2015).

266 Xiao, Y.-C. *et al.* CXCL8, overexpressed in colorectal cancer, enhances the resistance of colorectal cancer cells to anoikis. *Cancer letters* **361**, 22-32 (2015).

267 Liu, Q. *et al.* The CXCL8-CXCR1/2 pathways in cancer. *Cytokine & growth factor reviews* **31**, 61-71 (2016).

268 Ali, S. *et al.* A non-glycosaminoglycan-binding variant of CC chemokine ligand 7 (monocyte chemoattractant protein-3) antagonizes chemokine-mediated inflammation. *The Journal of Immunology* **175**, 1257-1266 (2005).

269 Ades, E. W. *et al.* HMEC-1: establishment of an immortalized human microvascular endothelial cell line. *Journal of Investigative Dermatology* **99**, 683-690 (1992).

270 Davidson, M. M. *et al.* Novel cell lines derived from adult human ventricular cardiomyocytes. *Journal of molecular and cellular cardiology* **39**, 133-147 (2005).

271 England, P. H. *Culture Collection - MCF-7*, <https://www.phe-culturecollections.org.uk/collections/ecacc-cell-line-profiles.aspx> (

272 England, P. H. *Culture Collections - MDA-MB-231*, <https://www.phe-culturecollections.org.uk/collections/ecacc-cell-line-profiles.aspx> (

273 Kuhns, D. B., Priel, D. A. L., Chu, J. & Zarember, K. A. Isolation and functional analysis of human neutrophils. *Current protocols in immunology* **111**, 7.23. 21-27.23. 16 (2015).

274 Adan, A., Alizada, G., Kiraz, Y., Baran, Y. & Nalbant, A. Flow cytometry: basic principles and applications. *Critical reviews in biotechnology* **37**, 163-176 (2017).

275 Laemmli, U. K. Cleavage of structural proteins during the assembly of the head of bacteriophage T4. *nature* **227**, 680 (1970).

276 Meester, I. *et al.* Natural truncation of RANTES abolishes signaling through the CC chemokine receptors CCR1 and CCR3, impairs its chemotactic potency and generates a CC chemokine inhibitor. *European journal of immunology* **28**, 1262-1271 (1998).

277 Trenchevska, O. *et al.* Quantitative mass spectrometric immunoassay for the chemokine RANTES and its variants. *Journal of proteomics* **116**, 15-23 (2015).

278 Grebely, J. *et al.* Plasma interferon-gamma-inducible protein-10 (IP-10) levels during acute hepatitis C virus infection. *Hepatology* **57**, 2124-2134 (2013).

279 Riva, A. *et al.* Truncated CXCL10 is associated with failure to achieve spontaneous clearance of acute hepatitis C infection. *Hepatology* **60**, 487-496 (2014).

280 Proost, P. *et al.* Amino-terminal truncation of CXCR3 agonists impairs receptor signaling and lymphocyte chemotaxis, while preserving antiangiogenic properties. *Blood* **98**, 3554-3561 (2001).

281 Yoshida, K. *et al.* Citrullination of Epithelial Neutrophil–Activating Peptide 78/CXCL5 Results in Conversion From a Non–Monocyte-Recruiting Chemokine to a Monocyte-Recruiting Chemokine. *Arthritis & Rheumatology* **66**, 2716-2727 (2014).

282 Nguyen, H., Park, J., Kang, S. & Kim, M. Surface plasmon resonance: a versatile technique for biosensor applications. *Sensors* **15**, 10481-10510 (2015).

283 El-Aneed, A., Cohen, A. & Banoub, J. Mass spectrometry, review of the basics: electrospray, MALDI, and commonly used mass analyzers. *Applied Spectroscopy Reviews* **44**, 210-230 (2009).

284 Procino, G. *et al.* Extracellular calcium antagonizes forskolin-induced aquaporin 2 trafficking in collecting duct cells. *Kidney international* **66**, 2245-2255 (2004).

285 Armoundas, A. A. Discordant calcium transient and action potential alternans in a canine left-ventricular myocyte. *IEEE Transactions on Biomedical Engineering* **56**, 2340-2344 (2009).

286 Sigma-Aldrich. *Amino Acids Reference Chart* <http://www.sigmaaldrich.com/life-science/metabolomics/learning-center/amino-acid-reference-chart.html> (2016).

287 (NCBI), N. I. o. H. *Amino Acid Explorer*, <http://www.ncbi.nlm.nih.gov/Class/Structure/aa/aa_explorer.cgi> (

288 van der Vliet, A., O'Neill, C. A., Halliwell, B., Cross, C. E. & Kaur, H. Aromatic hydroxylation and nitration of phenylalanine and tyrosine by peroxynitrite. *Febs Letters* **339**, 89-92 (1994).

289 Abello, N., Kerstjens, H. A. M., Postma, D. S. & Bischoff, R. Protein tyrosine nitration: selectivity, physicochemical and biological consequences, denitration, and proteomics methods for the identification of tyrosine-nitrated proteins. *Journal of proteome research* **8**, 3222-3238 (2009).

290 Sawant, K. V. *et al.* Chemokine CXCL1 mediated neutrophil recruitment: Role of glycosaminoglycan interactions. *Scientific reports* **6**, 33123 (2016).

291 Pierzchala, A. W., Kusz, D. J. & Hajduk, G. CXCL8 and CCL5 expression in synovial fluid and blood serum in patients with osteoarthritis of the knee. *Archivum immunologiae et therapiae experimentalis* **59**, 151-155 (2011).

292 Hashemian, S. M. *et al.* Budesonide facilitates weaning from mechanical ventilation in difficult-to-wean very severe COPD patients: Association with inflammatory mediators and cells. *Journal of critical care* **44**, 161-167 (2018).

293 Wang, C. *et al.* CXCL13, CXCL10 and CXCL8 as potential biomarkers for the diagnosis of neurosyphilis patients. *Scientific reports* **6**, 33569 (2016).

294 Rotondi, M., Coperchini, F., Pignatti, P., Magri, F. & Chiovato, L. Metformin reverts the secretion of CXCL8 induced by TNF-α in primary cultures of human thyroid cells: an additional indirect anti-tumor effect of the drug. *The Journal of Clinical Endocrinology & Metabolism* **100**, 427-432 (2015).

295 Coperchini, F. *et al.* Normal human thyroid cells, BCPAP, and TPC-1 thyroid tumor cell lines display different profile in both basal and TNF-α-induced CXCL8 secretion. *Endocrine* **54**, 123-128 (2016).

296 Zhang, Y. *et al.* Enhanced interleukin-8 release and gene expression in macrophages after exposure to Mycobacterium tuberculosis and its components. *The Journal of clinical investigation* **95**, 586-592 (1995).

297 Friedland, J. S., Remick, D. G., Shattock, R. & Griffin, G. E. Secretion of interleukin-8 following phagocytosis of Mycobacterium tuberculosis by human monocyte cell lines. *European journal of immunology* **22**, 1373-1378 (1992).

298 Ooe, H., Maita, C., Maita, H., Iguchi-Ariga, S. M. M. & Ariga, H. Specific cleavage of DJ-1 under an oxidative condition. *Neuroscience letters* **406**, 165-168 (2006).

299 Ho, R. J. Y. *Biotechnology and biopharmaceuticals: transforming proteins and genes into drugs*. (John Wiley & Sons, 2013).

300 Griffin, J. H., Fernandez, J. A., Gale, A. J. & Mosnier, L. O. Activated protein C. *Journal of Thrombosis and Haemostasis* **5**, 73-80 (2007).

301 Vieira, M. & Saraiva, M. J. Transthyretin: a multifaceted protein. *Biomolecular concepts* **5**, 45-54 (2014).

302 Hutchinson, W. L., Hohenester, E. & Pepys, M. B. Human serum amyloid P component is a single uncomplexed pentamer in whole serum. *Molecular Medicine* **6**, 482 (2000).

303 Moser, B., Wolf, M., Walz, A. & Loetscher, P. Chemokines: multiple levels of leukocyte migration control☆. *Trends in immunology* **25**, 75-84 (2004).

304 Lobito, A. A., Gabriel, T. L., Medema, J. P. & Kimberley, F. C. Disease causing mutations in the TNF and TNFR superfamilies: Focus on molecular mechanisms driving disease. *Trends in molecular medicine* **17**, 494-505 (2011).

305 Dinarello, C. A. Immunological and inflammatory functions of the interleukin-1 family. *Annual review of immunology* **27**, 519-550 (2009).

306 Luster, A. D., Unkeless, J. C. & Ravetch, J. V. γ-Interferon transcriptionally regulates an early-response gene containing homology to platelet proteins. *Nature* **315**, 672 (1985).

307 Turner, M. D., Nedjai, B., Hurst, T. & Pennington, D. J. Cytokines and chemokines: at the crossroads of cell signalling and inflammatory disease. *Biochimica et Biophysica Acta (BBA)-Molecular Cell Research* **1843**, 2563-2582 (2014).

308 de Campos Zuccari, D. A. P. *et al.* An immunohistochemical study of interleukin-8 (IL-8) in breast cancer. *Acta histochemica* **114**, 571-576 (2012).

309 Celik, B. *et al.* CXCL8, IL-1β and sCD200 are pro-inflammatory cytokines and their levels increase in the circulation of breast carcinoma patients. *Biomedical reports* **5**, 259-263 (2016).

310 Freund, A. *et al.* IL-8 expression and its possible relationship with estrogen-receptor-negative status of breast cancer cells. *Oncogene* **22**, 256 (2003).

311 Bièche, I. *et al.* CXC chemokines located in the 4q21 region are up-regulated in breast cancer. *Endocrine-related cancer* **14**, 1039-1052 (2007).

312 Ginestier, C. *et al.* CXCR1 blockade selectively targets human breast cancer stem cells in vitro and in xenografts. *The Journal of clinical investigation* **120**, 485-497 (2010).

313 Fleisher, B., Clarke, C. & Ait-Oudhia, S. Current advances in biomarkers for targeted therapy in triple-negative breast cancer. *Breast Cancer: Targets and Therapy* **8**, 183 (2016).

314 Heinecke, J. L. *et al.* Tumor microenvironment-based feed-forward regulation of NOS2 in breast cancer progression. *Proceedings of the National Academy of Sciences* **111**, 6323-6328 (2014).

315 Frangogiannis, N. G. Chemokines in the ischemic myocardium: from inflammation to fibrosis. *Inflammation Research* **53**, 585-595 (2004).

316 Frangogiannis, N. G. & Entman, M. L. Chemokines in myocardial ischemia. *Trends in cardiovascular medicine* **15**, 163-169 (2005).

317 Abe, Y. *et al.* Transient rise in serum interleukin-8 concentration during acute myocardial infarction. *Heart* **70**, 132-134 (1993).

318 Hulthe, J. *et al.* Plasma interleukin (IL)-18 concentrations is elevated in patients with previous myocardial infarction and related to severity of coronary atherosclerosis independently of C-reactive protein and IL-6. *Atherosclerosis* **188**, 450-454 (2006).

319 Herder, C. *et al.* Chemokines and incident coronary heart disease: results from the MONICA/KORA Augsburg case-cohort study, 1984–2002. *Arteriosclerosis, thrombosis, and vascular biology* **26**, 2147-2152 (2006).

320 Kortekaas, K. A. *et al.* No indications for platelet activation in acute clinical myocardial or renal ischemia/reperfusion injury. *American journal of translational research* **10**, 816 (2018).

321 Boyle Jr, E. M. *et al.* Inhibition of interleukin-8 blocks myocardial ischemia-reperfusion injury. *The Journal of thoracic and cardiovascular surgery* **116**, 114-121 (1998).

322 Turner, N. A., Das, A., O'Regan, D. J., Ball, S. G. & Porter, K. E. Human cardiac fibroblasts express ICAM-1, E-selectin and CXC chemokines in response to proinflammatory cytokine stimulation. *The international journal of biochemistry & cell biology* **43**, 1450-1458 (2011).

323 Somasundaram, P. *et al.* Mast cell tryptase may modulate endothelial cell phenotype in healing myocardial infarcts. *The Journal of Pathology: A Journal of the Pathological Society of Great Britain and Ireland* **205**, 102-111 (2005).

324 Apostolopoulos, J., Davenport, P. & Tipping, P. G. Interleukin-8 production by macrophages from atheromatous plaques. *Arteriosclerosis, thrombosis, and vascular biology* **16**, 1007-1012 (1996).

325 Freund, A. *et al.* Mechanisms underlying differential expression of interleukin-8 in breast cancer cells. *Oncogene* **23**, 6105 (2004).

326 Maehata, Y. *et al.* Reactive oxygen species (ROS) reduce the expression of BRAK/CXCL14 in human head and neck squamous cell carcinoma cells. *Free radical research* **44**, 913-924 (2010).

327 Lu, T. & Finkel, T. Free radicals and senescence. *Experimental cell research* **314**, 1918-1922 (2008).

328 Mahalingaiah, P. K. S. & Singh, K. P. Chronic oxidative stress increases growth and tumorigenic potential of MCF-7 breast cancer cells. *PloS one* **9** (2014).

329 Lakshminarayanan, V., Beno, D. W. A., Costa, R. H. & Roebuck, K. A. Differential regulation of interleukin-8 and intercellular adhesion molecule-1 by H2O2 and tumor necrosis factor-α in endothelial and epithelial cells. *Journal of Biological Chemistry* **272**, 32910-32918 (1997).

330 Wiktorowska-Owczarek, A. The effect of diclofenac on proliferation and production of growth factors by endothelial cells (HMEC-1) under hypoxia and inflammatory conditions. *Acta Pharmaceutica* **64**, 131-138 (2014).

331 Wiktorowska-Owczarek, A., Namiecińska, M. & Owczarek, J. The effect of ibuprofen on bFGF, VEGF secretion and cell proliferation in the presence of LPS in HMEC-1 cells. *Acta Poloniae Pharmaceutica. Drug Research* **72**, 889-894 (2015).

332 Prolo, C., Álvarez, M. N. & Radi, R. Peroxynitrite, a potent macrophage-derived oxidizing cytotoxin to combat invading pathogens. *Biofactors* **40**, 215-225 (2014).

333 Haim, K., Weitzenfeld, P., Meshel, T. & Ben-Baruch, A. Epidermal growth factor and estrogen act by independent pathways to additively promote the release of the angiogenic chemokine CXCL8 by breast tumor cells. *Neoplasia* **13**, 230-243 (2011).

334 Kurokawa, Y. K. & George, S. C. Tissue engineering the cardiac microenvironment: Multicellular microphysiological systems for drug screening. *Advanced drug delivery reviews* **96**, 225-233 (2016).

335 Singh, S., Wu, S., Varney, M., Singh, A. P. & Singh, R. K. CXCR1 and CXCR2 silencing modulates CXCL8-dependent endothelial cell proliferation, migration and capillary-like structure formation. *Microvascular research* **82**, 318-325 (2011).

336 Sharma, B., Nawandar, D. M., Nannuru, K. C., Varney, M. L. & Singh, R. K. Targeting CXCR2 enhances chemotherapeutic response, inhibits mammary tumor growth, angiogenesis, and lung metastasis. *Molecular cancer therapeutics* **5**, 799-808 (2013).

337 Tarzami, S. T. Chemokines and inflammation in heart disease: adaptive or maladaptive? *International journal of clinical and experimental medicine* **4**, 74 (2011).

338 Yang, H. *et al.* Toll-like receptor 4 prompts human breast cancer cells invasiveness via lipopolysaccharide stimulation and is overexpressed in patients with lymph node metastasis. *PloS one* **9** (2014).

339 Ashki, N., Hayes, K. C. & Bao, F. The peroxynitrite donor 3-morpholinosydnonimine induces reversible changes in electrophysiological properties of neurons of the guinea-pig spinal cord. *Neuroscience* **156**, 107-117 (2008).

340 Singh, R. J., Hogg, N., Joseph, J., Konorev, E. & Kalyanaraman, B. The peroxynitrite generator, SIN-1, becomes a nitric oxide donor in the presence of electron acceptors. *Archives of biochemistry and biophysics* **361**, 331-339 (1999).

341 Stone, J. R. & Yang, S. Hydrogen peroxide: a signaling messenger. *Antioxidants & redox signaling* **8**, 243-270 (2006).

342 Armbruster, D. A. & Pry, T. Limit of blank, limit of detection and limit of quantitation. *The Clinical Biochemist Reviews* **29**, 49-52 (2008).

343 Magnani, A. *et al.* Inflammatory manifestations in a single-center cohort of patients with chronic granulomatous disease. *Journal of Allergy and Clinical Immunology* **134**, 655-662 (2014).

344 Numanami, H. *et al.* Peroxynitrite enhances interleukin-10 reduction in the release of neutrophil chemotactic activity. *American journal of respiratory cell and molecular biology* **29**, 239-244 (2003).

345 Freels, J. L. *et al.* Enhanced activity of human IL-10 after nitration in reducing human IL-1 production by stimulated peripheral blood mononuclear cells. *The Journal of Immunology* **169**, 4568-4571 (2002).

PUBLICATIONS ARISING FROM THIS STUDY

PUBLISHED:

Thompson S, Martínez-Burgo B, Sepuru KM, et al. Regulation of Chemokine Function: The Roles of GAG-Binding and Post-Translational Nitration. *International Journal of Molecular Sciences*. 2017;18(8):1692. doi:10.3390/ijms18081692.

Barker C.E., **Thompson S**, O'Boyle G, et al. CCL2 nitration is a negative regulator of chemokine-mediated inflammation. *Scientific Reports*. 2017;7:44384. doi:10.1038/srep44384.

Thompson S, Redgrave R, Arthur HM, Kirby JA and Ali S. Modulation of Wound Healing Post-Myocardial Infarction. *In: British Society for Immunology Annual Congress, Immunology*. Brighton, UK: Wiley-Blackwell Publishing, Volume 143, Issue S2 2014, page 130.

UNDER PREPARATION:

Thompson S, et al. Nitration of CXCL8: Implications for Biological Function.
This is currently being prepared for submission.

ORAL AND POSTER PRESENTATIONS:

European Chemokines and Migrating Cells Conference (Cardiff, 6th-9th September 2017) **Research poster: Thompson S**, Sepuru KM*, Rajarathnam* K, Kirby JA, Sheerin NS and Ali, S. "Post-Translational Modification of Chemokines during Transplantation".

Gordon Conference/ Seminar – Chemotactic Cytokines (Girona, Spain, 27th May – 3rd June 2016) **Research poster: Thompson S**, Sepuru KM*, Rajarathnam* K, Kirby JA, Sheerin NS and Ali, S. "Post-Translational Modification of Chemokines during Transplantation".

British Microcirculation Society Conference (Newcastle, 7th-8th April 2016) **Member of the organizing committee and presented a research poster: Thompson S**, Sepuru KM*, Rajarathnam* K, Kirby JA, Sheerin NS and Ali, S. "Post-Translational Modification of Chemokines during Transplantation".

AWARDS:

EMBO Short-Term Fellowship (2018) – €2783.39 awarded to facilitate a collaborative research visit to the laboratory of Professor Paul Proost, Rega Institute, KU Leuven, Belgium.

British Society for Immunology (BSI) Travel Award (2016) – £700 awarded to attend Gordon Conference/ Seminar (Girona, 2016) and present a research poster.